UNIVERSITY OF SOUTHAMPTON

Faculty of Engineering, Science and Mathematics

School of Engineering Sciences

Testing and Characterisation of Large High-Energy Lithium-Ion Batteries for Electric and Hybrid Electric Vehicles

By

Dennis Doerffel

Thesis for the degree of Doctor of Philosophy

March 2007

UNIVERSITY OF SOUTHAMPTON

ABSTRACT

FACULTY OF ENGINEERING, SCIENCE AND MATHEMATICS

SCHOOL OF ENGINEERING SCIENCES

Doctor of Philosophy

TESTING AND CHARACTERISATION OF LARGE HIGH-ENERGY LITHIUM-ION BATTERIES FOR ELECTRIC AND HYBRID ELECTRIC VEHICLES

By **Dennis Doerffel**

This thesis considers the drivetrain and battery system requirements of Hybrid Electric Vehicles. The data herein proves that a series hybrid electric drivetrain with Lithium-ion batteries and plug-in recharge promises to be viable and sustainable. However, for mass production of series HEVs comprehensive performance characteristics and prediction of ageing behaviour of Lithium-ion batteries is essential but currently not available.

The main part of the thesis, following a graphical comparison of different energy storage solutions, is a detailed treatise on large Li-ion batteries. Construction and Li-ion working principles are summarised, together with several effects such as Peukert and memory effects, ageing of Li-ion cells, their temperature dependence and safety, and limits of charging/discharging.

Preliminary performance tests on 50 and 100 Ah Li-ion cells showed the necessity for a careful investigation of suitable reference conditions in order to achieve reproducibly precise results from repeated discharge/charge cycles. Then the main tests result in detailed graphs and tables of the discharge and charge characteristics. These main tests include effects of rate of discharge, energy-efficiency, temperature, resting time between test-cycles, hysteresis, ageing, and degradation. A new testing method that is based on the step response technique is suggested and investigated to whether it gives a meaningful but rapid measure of open circuit voltage and equivalent circuit models of the battery. Statistically significant theoretical models, equations and graphs are included.

The Appendix gives summaries of the author's seven main publications and presentations dealing with Systems Approach and five publications on Large Li-ion batteries, followed by most of these in full.

List of Contents

List of Figures

List of tables

DECLARATION OF AUTHORSHIP

I, Dennis Doerffel declare that the thesis entitled

Testing and Characterisation of

Large High-Energy Lithium-Ion Batteries

for Electric and Hybrid Electric Vehicles

and the work presented in it are my own.

I confirm that:

- this work was done wholly or mainly while in candidature for a research degree at this University;
- where any part of this thesis has previously been submitted for a degree or any other qualification at this University or any other institution, this has been clearly stated;
- where I have consulted the published work of others, this is always clearly attributed;
- where I have quoted from the work of others, the source is always given. With the exception of such quotations, this thesis is entirely my own work;
- I have acknowledged all main sources of help;
- where the thesis is based on work done by myself jointly with others, I have made clear exactly what was done by others and what I have contributed myself;
- none of this work has been published before submission.

Signed: …….

Date: 29.03.2007

ACKNOWLEDGEMENTS

The following people, companies and institutions have contributed significantly to this thesis or supported me throughout the project. I would like to thank

- Stephie for her support, help and endless understanding in all the years,
- my mother, grandmother, father and aunt and their partners for their encouragements, empathy and for enduring the highs and lows,
- my supervisor, Dr. Suleiman Sharkh, for having made this project possible and for his support and patience,
- Simon Barnes from Lewis Industrial Products Ltd. for lending us the Digatron battery tester for several years,
- the ISEA (institute for power electronics and electrical machines) in Aachen, Germany, for letting me use their battery testers,
- Christian Maul for his help and encouragements throughout the years,
- Alan and Honor Ward for all their encouragements and also for proof-reading several publications,
- Brenda for proof-reading this thesis, for teaching me some finer points of the English language and also for her patience,
- Richard Fletcher and my PhD colleagues for stimulating discussions, providing a great time and helping me to get my mind off the batteries,
- all my friends for their support,
- the staff at the School of Engineering Sciences and at the Faculty of Engineering, Science and Mathematics for their help and patience,
- many researchers and other professionals, whom I met at various conferences, seminars and exhibitions for valuable and technical discussions.

Definitions

These definitions are in accordance with British and European Standards [15] unless otherwise specified.

Anode (in an electrochemical cell): The electrode, which is oxidized. This is the negative electrode during discharging or the positive electrode during charging [51][1].

Cathode (in an electrochemical cell): The electrode, which is reduced. This is the positive electrode during discharging or the negative electrode during charging [51][1].

Cell: An electrochemical assembly of electrodes and electrolyte, which constitutes the basic unit of a battery.

Battery: Two or more cells connected together and used for storing electrical energy.

In the following definitions the word "cell" may also stand for the word "battery", where appropriate.

Secondary cell: Rechargeable cell.

Unspillable cell: A cell from which the electrolyte cannot escape whatever its orientation.

Valve regulated (sealed) cell: A cell which is closed under normal conditions but which has an arrangement which allows the escape of gas if the internal pressure exceeds a predetermined value. The cell cannot normally receive addition to the electrolyte.

---

[1] The term "Anode" or "Cathode" cannot be related directly to the positive or negative electrode without knowing whether the battery is charged or discharged. The author is avoiding the terms anode or cathode and he is using the terms positive or negative electrode instead, for this reason.

Gastight sealed cell: A cell which remains closed and does not release either gas or liquid when operated within the limits specified by the manufacturer. The cell may be equipped with a safety device to prevent it from bursting.

Hermetically sealed cell: A gastight sealed cell without pressure release device.

Maintenance-free cell: A cell which during its service needs no maintenance, provided that specified operating conditions are fulfilled.

Positive plate: A plate of a secondary cell which constitutes the cathode during discharge and the anode during charge.

Negative plate: A plate of a secondary cell which constitutes the anode during discharge and the cathode during charge.

Reversal (of a cell): A change in the normal polarity of a cell.

(Cell) capacity: The quantity of electricity or electric charge which a fully charged cell can deliver under specified conditions (rate of discharge, end voltage, temperature). *Note:* The SI unit for electric charge is coulomb but, in practice, battery capacity is usually expressed in ampere-hours (Ah).

Nominal capacity: A suitable approximate quantity of electricity used to identify the capacity of a cell.

Rated capacity: The quantity of electricity, declared by the manufacturer, which a cell or battery can deliver under specified conditions after a full charge.

Energy of a cell: The energy which a fully charged cell can deliver under specified conditions. *Note:* The SI unit for energy is the joule but, in practice, energy of a battery is usually expressed in watt-hours (Wh).

Charge / discharge rate: The current at which a cell is charged / discharged.

"C" Rate (discharge current)[52]**:** A common method for expressing the charge or discharge current, expressed as $I = M \cdot C_n$

where I is the current, expressed in Amperes, M is a multiple or fraction of C_n, C_n is the rated capacity declared by the manufacturer in Ampere-hours, and n is the time in hours for which the rated capacity is declared. A different standard has been developed [16] recently but the above method is still commonly used and will be used [55] throughout this thesis.

Hourly rate: Another method for specifying the current. This is the current at which the battery will discharge for a specified number of hours. [52]

"E" Rate: Similar to the "C" rate but based on energy and power. It specifies a constant power for charging or discharging. [52].

End-of-charge rate (EOCC – end-of-charge current): The value of current during the final stage of charging a cell.

The ***theoretical voltage*** is a function of the anode and the cathode materials, the composition of the electrolyte and the temperature (usually stated at 25 degC) [52]. The ***nominal voltage*** is one that is generally accepted as typical of the operating voltage of the battery [52]. The ***working voltage*** is the typical voltage or range of voltages of a battery during discharge[55]. The ***on-load voltage*** is the voltage between the terminals while delivering current.

Open circuit voltage (OCV): The battery voltage under no-load conditions. It is usually a close approximation of the theoretical voltage [52].

Stabilized OCV (SOCV): The open circuit voltage at equilibrium (OCV_{eq}). After current reaches zero, the OCV will drift for a certain period of time, but will eventually stabilize. The waiting time required for reaching the SOCV can be around 60 minutes for lead-acid (where the drift becomes only minor after 15 minutes) but it can be much longer for other chemistries. This makes it unlikely to reach SOCV in some operating conditions [78].

Voltage efficiency: The ratio of average voltage during discharge to average voltage during recharge under specified conditions of charge and discharge [55].

Cut-off voltage or end-of-discharge voltage (EODV): The specified voltage at which a discharge of a battery is considered finished.

End-of-charge voltage (EOCV): The voltage of a cell during charging at specified conditions when a cell has become completely charged.

Charge factor (charge efficiency): The factor by which the quantity of electricity delivered during discharge is multiplied to determine the minimum quantity required by the battery to recover its fully charged state.

Energy efficiency - here frequently just "efficiency": The ratio of the watt-hours delivered on discharge of a battery to the watt-hours needed to restore it to its original state under specified conditions of charge and discharge.

Apparent internal resistance: The quotient of the change of voltage of a cell to the corresponding change of current under specified conditions.

Constant current charge (CC charge): A charge during which the current is maintained at a constant value and where usually the terminal voltage increases.

Constant voltage charge (CV charge): A charge during which the voltage across the terminals is maintained at a constant value and where usually the charge current decreases.

Modified constant voltage charge: Constant voltage charge with current limitation. This effectively is the same as what is known as a CC-CV charging regime (constant current – constant voltage).

Fully charged state: A state where all the available active material has been reconverted to its fully charged state.

Overcharge: Continued charging after the full charge of a cell or battery.

Self-discharge: Loss of chemical energy due to spontaneous reactions within the battery when not connected to an external circuitry.

Charge retention: The ability of a cell to retain charge on open circuit under specified conditions.

Equalising charge: An extended charge to ensure complete charging of all cells in a battery.

Trickle charge: A continuous charge at a low rate, which compensates for self-discharge and thus maintains the battery in an approximately fully charged state.

Charge acceptance: The ability of a cell to accept charge under specified conditions.

Cycle: A sequence of a discharge followed by a charge or a charge followed by a discharge under specified conditions.

Service life: The period of useful life of a cell under specified conditions.

Endurance: Numerically defined behaviour of a battery during a given test simulating certain conditions of service.

Maximum total capacity: This is the maximum capacity that is practically available from a cell under most advantageous conditions. The maximum total capacity will decrease with ageing of the cell.

Full charge capacity (FCC): This is the maximum stored charge capacity of the battery expressed in Ah. This value varies from cell to cell and decreases over battery lifetime. It is dependant on temperature and rate of discharge and the test conditions need to be specified [78].

Actual or remaining capacity: The capacity that can still be discharged under specified conditions after a partial discharge [78].

State of charge (SOC%): The remaining capacity expressed as a percentage of the full charge capacity [78] $SOC = \frac{AC}{FCC} \cdot 100\%$

Depth of Discharge (DOD): The depth of discharge is the capacity taken from the battery after a full charge.

Depth of Discharge (DOD%): The ratio of the DOD (in Ampere-hours) to the cells rated capacity.

Residual capacity (RC): The residual capacity is the capacity that is left in a battery after an apparent full discharge at a given condition. The RC is the maximum total capacity minus the FCC.

Hybrid electric vehicle (HEV): A vehicle that is powered by two or more energy sources, one of which is electricity. HEVs may combine the engine and fuel system of a conventional vehicle with the batteries and electric motor of an electric vehicle in one drivetrain. There are many different possible types of HEVs and also different ways of categorising them. The types defined below are those that are used in this thesis.

Parallel hybrid electric vehicle: In a parallel hybrid electric vehicle drivetrain, both power systems work in parallel. The electric part of the drivetrain and the other part are both mechanically connected to the wheels and their speed follows the speed of the wheels.

Series hybrid electric vehicle: In a series hybrid electric vehicle, the electric part of the drivetrain is connected to the wheels but the other part is not. The non-electric part serves as an electric power generator.

Power split hybrid electric vehicle: In a power split hybrid electric vehicle, the power required to propel the car can be split to any ratio between the two power systems. Both power systems are still mechanically connected to the wheels but they do not have to follow the wheel speed. Practical implementations (e.g. in Toyota Prius) use a planetary gear.

SLI battery: This is the battery in conventional vehicles powered by combustion engines. It serves the purpose of **S**tarting, **L**ighting and **I**gnition (SLI).

1 Introduction

1.1 Background and Motivation

The world's increasing demand for cars stands in contrast to a backdrop of rising oil prices, recognition of oil dependency and increasing awareness of environmental impacts for example CO_2 emissions and local air pollution. Today's transportation consumes one third of the total energy supply in Europe and the majority of this (three quarters) is for road transportation alone [32; 33].

Electric vehicles significantly reduce the energy consumption and local emissions due to the highly efficient electric machines. However they lack driving range, because the electrical energy storage device – usually a battery – can store only a fraction of the energy if compared with conventional fuel.

An important advance in vehicle technology which could help address some environmental issues whilst meeting the increasing transport demands is the development of the hybrid electric vehicle (HEV). It combines the advantages of the range and freedom of fuel powered vehicles with the environmental benefits of electric drivetrain technology [8; 24; 69; 73].

Storing electrical energy as effectively as possible is the key to the concept of any HEV. Depending on the size and performance of the electrical energy storage device used, it may enable: reducing the engine size; operating the engine only when necessary; providing peak power; capturing energy from braking and re-using it for acceleration (regenerative braking) and propelling the car fully electrically.

Various fundamentally different energy storage technologies are currently under development, ranging from mechanical storage (e.g. flywheels) over electrostatic storage (e.g. super capacitors) to electrochemical storage (e.g. rechargeable batteries). However, this thesis focuses on the electrochemical energy storage using batteries because the characteristics are fundamentally different from other storage technologies. Currently they appear to provide most suitable performance characteristics for storing the electrical energy in the mentioned application.

The conventional vehicle with internal combustion engine (ICE) however is a very mature and accepted technology. It is subject to a significant set of regulations along with established services and structures, so that any significant shift away from this technology is subject to massive barriers and cost [45]. The small battery for starting, lighting and ignition (SLI) in conventional cars already causes a significant percentage of overall vehicle failures. At a time when several carmakers struggle to make profits, moving towards larger electrochemical batteries in cars lies far outside most car manufacturers' expertise and introduces a high risk. It is therefore important to create a better understanding of the working principles of batteries and to generate more expertise on battery behaviour and ageing implications over their life. Modelling, simulating and testing of batteries can achieve this.

Simulation and modelling are widely used methods in research and it is possible to predict behaviour in many fields, for example electronics. This is possible since most manufacturers provide accurate simulation models for their electronic components. Unfortunately, most battery manufacturers do not provide such models. Attempts have been made to derive models directly from chemical and physical manufacturing data. However, such models not only disregard important aspects such as surface films in lithium-ion batteries, but they also do not take into account ageing, which significantly changes the behaviour of batteries over their life [11]. Exact physical and electrochemical processes in new battery designs are usually not fully predictable, due to their complex interactions. Furthermore, such electrochemical models would be very complex and may not be suitable for system level simulations. Testing is and will remain important for characterising, modelling, simulating and understanding batteries on a system level, as well as in the process of developing new battery technologies.

Unfortunately, the behaviour of batteries depends on a wide range of factors, some of which are interdependent. Temperature and current are amongst the variables one may expect but other factors, such as exact conditions of use, both over the battery's lifetime and even its very recent usage are much more difficult to quantify. The previous charge or discharge condition, for example, may significantly influence the behaviour in the subsequent discharge. While such an apparent short-term performance change due to certain charging conditions, for example, may be

reversible, there are also ageing effects, which significantly influence the battery performance irreversibly. This makes it very challenging, time consuming and expensive to exhaustively test batteries. In contrast, while it is possible to exhaustively test and accurately model an electric machine in just a few days, it would take several months or longer to conduct testing on a battery and the results of which would be significantly less meaningful.

This scenario becomes even more challenging, when testing large batteries if compared to small batteries. Usually, several batteries are required and must be tested at the same time using multiple test equipment. Material costs are higher for larger cells and the test equipment is more expensive as well due to the requirement for high currents. Finally, large batteries are expensive to the end-user and this means that it is more important to accurately predict the behaviour and ageing of larger batteries than it normally is for smaller batteries. Additionally, there is currently a rapid development in battery technologies and this means that product cycles are often shorter than the time that is required for exhaustive testing. It should also be mentioned that test results with small cells could not simply be scaled up, because they exhibit different temperature gradients, potential gradients and current distribution within the cell.

1.2 Scope

This work is on investigating a potentially faster, lower-cost and sufficiently exhaustive testing method for large batteries. A comprehensive and generic testing template for a range of applications would not yield such a quick, low-cost testing method. The testing method has to be designed more specifically with an application in mind if it is to be efficient.

However, in order to keep this work as generic and comprehensive as possible, a testing template will be described and also the process of deriving such testing requirements and methods starting from the battery system requirements in the application and based on available information on typical battery characteristics.

The example application chosen here is a particular type of HEV as will be explained in the next chapter. It will be shown that the lithium-ion battery is currently the most

promising candidate for this type of vehicle. At the start of this project, there was hardly any description of characteristics available on large lithium-ion batteries in general and, in particular, there was no information available on the specific type of lithium-ion battery used in this project.

Preliminary tests were designed based on available information on the characteristics of small lithium-ion cells and other battery chemistries and subsequently were conducted on the large cells. The results from these tests were then analysed and it is shown how the information gained was used to derive some specific tests as well as a testing series with the mentioned application in mind.

These tests were then conducted on the lithium-ion battery test specimen, the results are reported and discussed in this thesis, and suggestions for the improvement of testing are provided.

1.3 Research Aims

One aim of this research project is to investigate a range of different hybrid and electric drivetrain configurations in the light of future transportation requirements and energy scenarios. This work is not published in this thesis as it is out of scope for this document. However, the work can be found in [24].

This thesis covers the work towards the second aim of the research project.

This second aim is to investigate more efficient test methods for characterising and understanding the performance behaviour of large lithium-ion batteries in a specific application. This specific application is a series hybrid electric vehicle with recharge facility as investigated in the first part of the project.

2 Specification of Drivetrain and Battery System Requirements of an HEV

2.1 Introduction

It is important to understand the application in order to define the requirements for characterising and the scope for testing the battery that is used in that application. This chapter covers the specification of an HEV drivetrain application and the derivation of the requirements for the battery system in such a drivetrain.

This chapter also covers parts of the process of choosing an innovative HEV drivetrain configuration which appears promising in future scenarios, but was not seriously investigated in the past. This effort was made in order to conduct, not only, original, but also, relevant research.

During this project, the author put significant effort into researching issues such as future fuels, energy resources and other drivetrain alternatives, which is important background information for the process of choosing a particular HEV drivetrain configuration. This material is not included in this thesis, because it is out of the scope of this document. However, it is mentioned at this point due to its increasing relevance and due to the fact that some novel approaches lead to interesting findings. Interested readers can find a reference and a download link to this work in the appendix [24].

2.2 Background on HEV Technologies

Cars have evolved significantly over the last 100 years. They have become more versatile, have better performance and are more comfortable, without significant increases in relative purchasing cost. This has lead to an unprecedented increase in the number of vehicles on the road, especially given recent changes in work practices that require individuals to be increasingly mobile. This increase in the number of vehicles together with rising awareness of their environmental impact and the question of sustainability provided stimulus for current discussion on future mobility [24; 32; 33; 62; 68].

Conventional cars with their internal combustion engines do not meet future requirements regarding noise and emission levels, and energy consumption [82]. On the other hand, electric vehicles, although having far less impact on the environment, do not meet customer requirements regarding range, versatility or cost [80] and fuel-cell vehicles still need considerable development of their technology and refuelling infrastructure [47; 70]. These limitations have led to attention being directed towards development of hybrid electric vehicles and most recent developments have concentrated on the parallel hybrid; the series hybrid electric vehicle, in general, being considered to be inferior to the parallel [39; 44]. However, recent developments in battery technology [19] can make the series hybrid electric vehicle an increasingly interesting alternative.

The importance of a systems design approach and the relevance of simulation and modelling for assessing hybrid electric vehicle drivetrains has been shown earlier [56]. This chapter demonstrates how this approach can be used for making initial choices on innovative or radical drivetrain solutions. As an example a plug-in series hybrid electric vehicle will be evaluated. This is a hybrid electric vehicle which can be recharged from a mains outlet and which is intended mainly for urban and neighbourhood journeys [8]. Firstly, the HEV configuration and the main vehicle specification will be determined so that they meet consumer aspirations. Secondly, the drive train components will be carefully selected based on data from commercial-off-the-shelf (COTS) components in order to make sure the concept is achievable. Finally, the modelling and simulation will be used to assess whether that drivetrain concept ensures peace-of-mind in terms of both environmental impact, compared to a pure electric vehicle, and range and versatility, compared to a conventional car, without sacrificing affordability.

2.3 Drivetrain Configuration

Hybrid electric drivetrains can be configured in various ways. The three main categories are the “series hybrid electric vehicle”, the “parallel hybrid electric vehicle” and the “power split hybrid electric vehicle”. Each vehicle in each of the three categories can be designed with a different grade of hybridisation. The grade of hybridisation refers to the ratio of installed electric power to total power. In other cases, it refers to the extent to which the electrical energy storage device can propel

the vehicle if compared with the energy stored in the fuel. Furthermore, it is possible to distinguish by different types of fuel converters (combustion engines, fuel cells or alternative engines such as Stirling motors or turbines) and different types of electrical energy storage devices or their combinations (super capacitors, different types of batteries, flywheel). Additionally, the type of fuel should be specified as this can have implications on the system design. Most alternative fuels for example require more volume or weight for the same amount of stored energy.

Some hybrid concepts can exhibit a variety of attributes with significant impact on the configuration. Torque addition for example appears to be more sensible in cases where the propulsion is mainly based on the combustion engine and where the electric motor for example adds or subtracts torque for smoothing the engine usage. Speed addition is more sensible where the electric motor is the main player and where a combustion engine is used mainly for achieving higher speeds without requiring additional gear ratios. Force addition is where for example a combustion engine powers the front wheels and the back wheels are powered by electric motors. Finally, it is important to specify whether the electrical energy storage device can be recharged externally (e.g. from the mains).

Specifying the drivetrain configuration is important before researching into the electrical energy storage device technology. Different configurations exhibit significantly different requirements on all the components.

2.4 Vehicle Performance Criteria

It was a substantial part of this project to research background information on different HEV configurations, their advantages and disadvantages, and to assess their potential as a successful future drivetrain configuration in the light of future energy supply scenarios and transportation requirements. This part of the work is covered in the author's transfer thesis and can be found in the appendix.

It identifies the series hybrid electric vehicle with plug-in recharge facility to have significant potential as a future automotive solution. This vehicle is normally charged from electricity, which can be generated from renewable sources and distributed through the existing network. The vehicle operates as an electric vehicle, but has a

small engine-driven generator to extend the range of travel. The electrical energy storage device is a lithium-ion battery, which currently offers the most suitable performance characteristics in terms of size, weight and other attributes. It also promises to meet requirements in terms of cost in volume production. The type of fuel and fuel converter is less important in this drivetrain concept because it is more modular than, for example, the power split hybrid. Fuel converters could be, initially, combustion engines with a generator then be Stirling motors with reduced emission and noise levels and, ultimately, be fuel cells once they are viable. The proposed vehicle specification is based on the following list of considerations.

> These considerations are idealised. Trends, fashions, the desire for speed, power or large cars are not considered in this work. The author realises the importance of such criteria for making a realistically sellable vehicle. The list here should be understood as minimum requirements that serve to evaluate whether this drivetrain configuration might be viable. Performance and other criteria can be improved or added at cost.

Speed: The rated motor power and the smallest gear ratio are determined by the maximum design-speed of the vehicle and the maximum motor speed. The rated battery power is a major cost issue and in a pure EV this is determined by the rated motor power, hence maximum speed. In the proposed series hybrid electric vehicle however, the rated motor power mainly determines the generator and engine power and not the rated battery power. The higher the speed of this type of HEV the larger the four main and costly drivetrain components (power-electronics, motor, generator and engine) need to be. The maximum design speed of the vehicle should therefore be chosen very carefully and should preferably be as low as possible without compromising comfort. The UK as well as many other countries has a speed limit of around 70 mph (112 km/h) and the chosen vehicle should be able to achieve this speed consistently.

Gradeability: The rated motor power is determined by the road gradient and / or the maximum vehicle speed. The maximum road gradient on UK highways is 4%. Assuming the use of a gearbox the maximum gradient determines the highest gear ratio. Most hills exhibit less than 20% gradient and signs do warn before a route with

higher gradients. The vehicle is designed to climb at least 20% while carrying maximum load.

Acceleration: The maximum motor torque and the gear ratio are determined by the acceleration requirements. For the purpose of this research an axial air-gap permanent magnet brushed motor, which is capable of producing constant torque vs speed and with about 50% overload torque capability is chosen. The overload capability of most motors exceeds this. It can be assumed that a motor that achieves the maximum speed at highway gradient is sufficiently powerful for acceptable acceleration in urban areas. However, a simulation will be used later in order to determine acceleration performance of the vehicle.

Driving Range: The envisaged pure electric driving range determines the battery size. Most trips are short trips; about 80% of all travelled distance being shorter than 40 km per trip [32; 33]. To keep the battery in an efficient state of charge range for this distance, the state of charge (SOC) should remain above 20% even when the battery is close to the end of its life (80% of rated capacity). As a result, the vehicle should initially achieve 40 km / (0.8 • 0.8) ≈ 60 km in pure electric mode. An energy management strategy will provide peace of mind by starting the generator automatically in order to extend the driving range to at least 300 km.

Noise: This vehicle is designed for short trips. These trips usually have a low average speed. At low speeds the engine noise of conventional cars is higher than the noise of tyres and air-resistance [76]. The electric motor itself is very quiet and the energy management has a goal to avoid starting the combustion engine when engine noise has major impacts (e.g. inside towns at low speeds or when waiting in traffic jams). The vehicle mass should be kept low to decrease tyre noise at higher speeds.

Pollution: This vehicle is essentially a battery powered electric vehicle that is normally recharged from the mains. This type of vehicle has no local pollution. It has no overall pollution or greenhouse gas emissions if recharged with renewable electricity. The combustion engine will only cut in if necessary to achieve the desired trip distance or the desired power. The energy management strategy will ensure that the engine runs as rarely as possible and in its best efficiency/ lowest pollution region. It also aims to reduce cold starts to keep the level of pollution low.

Vehicle size: Lightweight vehicles keep impacts low in urban driving. A Daewoo Matiz (see Figure 1) is used for the simulations.

Figure 1 Daewoo Matiz

Handling/Comfort: The series hybrid electric drivetrain can enhance the handling as the heavy engine is replaced with a number of components (battery, small engine, generator, etc.), which can be mounted in different places for an optimised weight distribution. As a result of a more even weight distribution between front and back, power steering may not be essential. Unlike a combustion engine, the electric motor produces full torque from zero rpm resulting in less gear changing. Additionally, the electric motor exhibits a small rotational inertia and can be accelerated very fast, especially if supported from dedicated control algorithms in the power electronics - hence making a clutch potentially redundant [49]. Less motor noise and vibrations will increase comfort especially in urban driving with frequent start-stop cycles. Electrically powered air-conditioning can be implemented, which reduces the losses when not in use.

Energy Consumption: The aim is to keep the energy consumption at 1 - 2 L/100km (this is between 140 and 280 British mpg) of petrol equivalent in urban driving. In urban driving the vehicle is purely battery powered and recharged from the mains. The extra-urban consumption is higher due to the higher drag losses at higher velocities. Also, the engine may have to cut in to provide additional power or range. The aim in this scheme is about 3 L/100km (this is about 94 British mpg). This vehicle is mainly designed for short trips and thus, the combined consumption is closer to the urban driving consumption and should be below 2 L/100km (this is about 140 British mpg).

Vehicle Mass: The vehicle mass has major impacts on most of the requirements mentioned above. Keeping the mass low means better gradeability, acceleration and range, with less noise and lower energy consumption. The aim is to keep or, even, reduce the vehicle mass when compared to the original vehicle by selecting the smallest and lightest possible versions of the heaviest of the components, such as the battery and the engine. The motor and generator to be used are permanent magnet motors with very high power/mass ratio (e.g. 1 kW/kg continuous power).

Cost: The purchase cost is targeted to be similar to a conventional vehicle by trying to keep the technology simple and the battery small. The battery is a major cost factor and thus, a battery management strategy ensures the highest possible life expectancy of the battery combined with optimised performance. This is achieved by managing battery temperature and charging as well as utilising closed loop controls during discharging taking several factors into account (e.g. individual cell voltages and temperatures).

2.5 Component Specifications

This paragraph derives the component specifications from the vehicle criteria. The following formula were used to estimate the power requirements:

Rolling resistance: $$P_r(v) = c_r \cdot m_{\max} \cdot g \cdot v \quad (1)$$

Air drag: $$P_{air}(v) = c_d \cdot A_f \cdot \tfrac{1}{2} \cdot \zeta \cdot v^3 \quad (2)$$

Power demand for gradient: $$P_{grad}(gradient, v) = m_{\max} \cdot g \cdot v \cdot \sin(\arctan \tfrac{gradient}{100}) \quad (3)$$

The following constants were used:

Gravitational acceleration: $g = 9.81 \, m/s^2$

Air density at 1 bar and 20 ºC: $\zeta = 1.19 \, kg/m^3$

The total motor power to propel the vehicle at a certain speed (v) and up a certain gradient is:

$$P_{mot}(gradient, v) = \frac{P_r(v) + P_{air}(v) + P_{grad}(gradient, v)}{\overline{\eta_{mech}}} \quad (4)$$

Mechanical drivetrain efficiency (gearbox, differential) is assumed to be on average:

$\overline{\eta_{mech}} \approx 0.9$

The chosen vehicle has the following body attributes:

Air drag coefficient: $c_d = 0.32$ (estimated)

Frontal area: $A_f = 2.01\ m^2$ (estimated)

Tyre rolling coefficient: $c_r = 0.009$ (Advisor file [60])

Mass: $m = 778$ kg (Daewoo Matiz [22])

Maximum mass: $m_{max} = 1153$ kg (Daewoo Matiz)

Figure 2 shows the power requirements to overcome the rolling resistance, the air drag, the gradient of 4 % and the total required motor power versus speed.

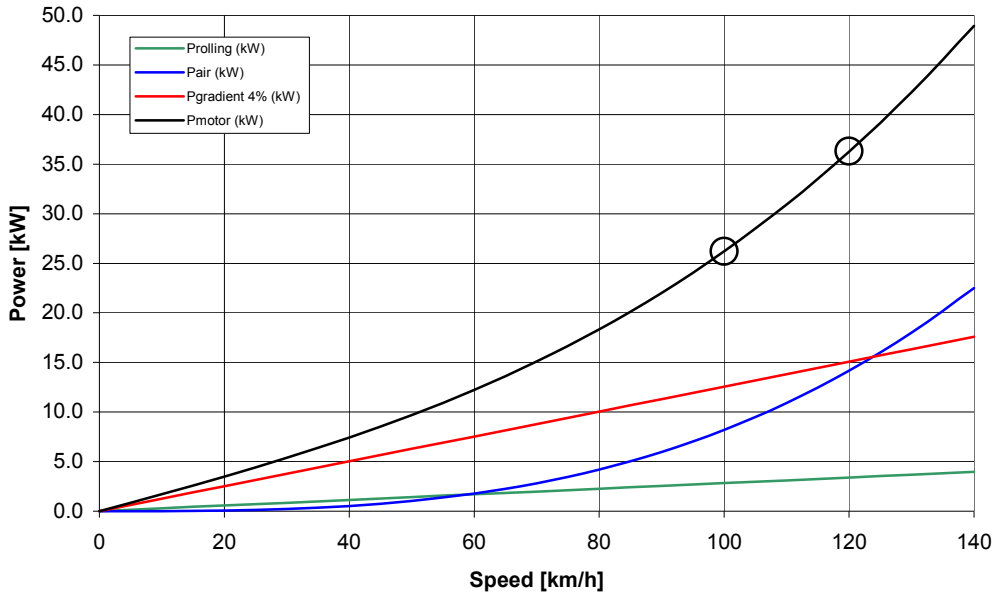

Figure 2 Power requirements over speed for the chosen Vehicle with 4% gradient

Propulsion motor requirements:

The power requirement of the electric propulsion motor is determined by the maximum speed and the maximum gradient at this speed. The maximum gradient on UK highways is 4% = 2.3º. The designed maximum speed is 120 $^{km}/_{h}$. All calculations are undertaken with maximum mass m_{max}. To achieve 120 $^{km}/_{h}$ with 4% gradient, the propulsion motor power requirement is:

$$P_{mot}(4\%, 120\,{}^{km}/_{h}) \approx 36kW \qquad \text{(see Figure 2)}$$

The chosen motor is a permanent magnet motor with axial air gap and pancake design. The purchase cost of this motor type has a strong relation to the motor power due to the speed limitation and the cost of rare-earth magnets.

Motor size and cost may be reduced if the speed demand is relaxed. At a 4% highway grade (this is when a crawling-lane for lorries is implemented), the allowed speed is usually limited to less than 112 $^{km}/_{h}$. If the vehicle is designed to run at 100 $^{km}/_{h}$ with

this 4% gradient it will still meet the requirements, but allow for a smaller propulsion motor: $P_{mot,cont} = P_{mot}(4\%, 100\,{}^{km}/_{h}) \approx 26kW$ (see figure 2)

This power reduction of nearly 30% helps to reduce the cost remarkably. The 26 kW motor is still sufficient to propel the car at a speed of 120 km/h. The overtorque capability of at least 1.5 of this motor type still allows for short duration gradients of 4% at this speed. For longer gradients, the speed needs to be decreased to 100 ${}^{km}/_{h}$ and a higher gear ratio may become necessary to receive maximum power.

In order to use motor specifications that are practically achievable, the modelled motor was scaled up from an existing off-the-shelf motor, the Lynch LM200 [28; 34]. The LM200 produces 10kW continuously. The electric propulsion motor torque is scaled up with a factor of 2.7. The scaled motor produces up to 70 Nm continuous and runs at maximum 3,600 rpm with this load. The type of motor provides very good efficiency (90%) in a wide operating region and a very good power to mass ratio of about 1 kW/kg. High torque and low speed keeps gear losses and noise down. Figure 3 shows the efficiency map for this motor and the operating points in the extra urban driving cycle (EUDC). This simulation result [60] shows that the chosen motor is working within an optimally efficient range. The motor power is suitable for this vehicle.

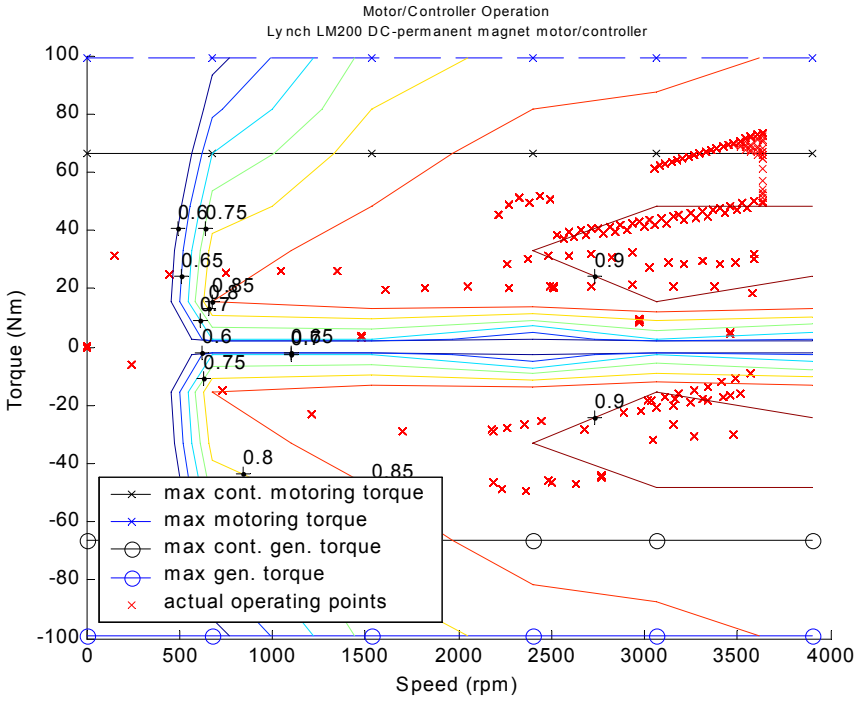

Figure 3 Propulsion Motor/Controller Efficiency Map with Operating Points in EUDC

Engine/generator requirements:

The engine/generator requirements are determined by the average power requirements in this series HEV concept. Cruising at 112 $^{km}/_{h}$, the maximum velocity on UK highways, without gradient is assumed to define the average power in worst case. The continuous generator output power requirement is:

$$P_{gen,cont} = P_{mot}(0\%, 112\,{}^{km}/_{h}) \approx 16.5kW$$

The chosen generator is also a scaled up version of the Lynch LM200 with a scaling factor of 1.7. In this instance, that electric machine is used as a generator. The electric output power is 17 kW with an estimated efficiency of 85% the mechanical input power has to be 20 kW. This is the minimum continuous engine power requirement:

$$P_{engine,cont} \approx 20kW$$

This vehicle concept is designed for urban driving with mainly short trips. The generator and engine increase versatility and peace-of-mind for the driver. There is no requirement for the driver to constantly monitor and evaluate the remaining battery state-of-charge. Thus, the engine is designed to run only rarely and only when noise, vibrations and emissions play a minor role. A low-cost, small, lightweight engine can be chosen. For example, a 350 cc four-stroke engine size is sufficient to produce 20 kW. In this study, the Advisor SI-30 engine is chosen and scaled down to 20 kW for simulation purpose. Figure 4 shows that in this engine, the maximum power point equals the maximum torque point with good efficiency at this point too.

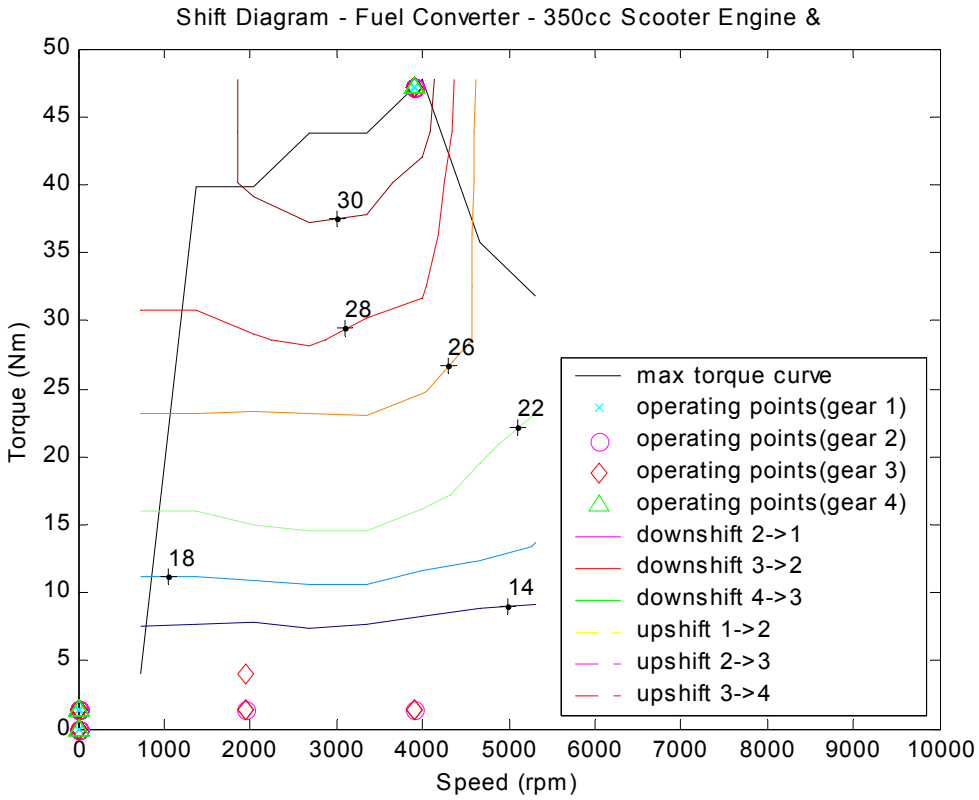

Figure 4 Engine Efficiency Map with Operating Points

Energy storage requirements:

There are two main energy storage requirements: Available energy and maximum power. The available energy should be sufficient for 60 km urban traffic in pure electric driving mode as mentioned above. The average velocity in cities is about 30 $^{km}/_{h}$. In a simplified calculation, an average of 50 $^{km}/_{h}$ it is assumed. This is to take into account that the average speed is based on a higher speed plateau but with frequent starts and stops. The motor power to propel the vehicle at 50 $^{km}/_{h}$ is:

$$P_{mot}(0\%, 50\,{}^{km}/_{h}) \approx 2.7kW$$

Assuming an overall drivetrain efficiency of about 60%, the required energy storage capacity is at least:

$$E_{storage,\min} = \frac{60km}{50\,{}^{km}/_{h}} \cdot \frac{2.7kW}{0.6} \approx 5.4kWh$$

The battery power should be sufficient to boost the propulsion motor to its highest power, when the generator runs. Maximum motor power is 1.5 times continuous motor power.

$$P_{storage,\max} = 1.5 \cdot P_{mot,cont} - P_{gen,cont} \approx 22kW$$

Modern high power lithium-ion batteries are capable of discharging currents that are equal to 5 times the rated capacity. However, in order to achieve full performance even after some degradation or in cold conditions, a maximum discharge of 3C (3 times the rated capacity) was assumed. The energy storage capacity is determined by this requirement, provided it also meets the criteria for pure electric range:

$$E_{storage} = \frac{P_{storage,\max}}{3} \cdot h \approx 7.5kWh$$

A Li-Ion battery (Thunder Sky TS-LP8582B) [77] has been chosen to keep the battery size and mass low. Li-Ion batteries also provide very good efficiency and good cycle life. Purchase cost is becoming competitive (300 to 500 $^{US\$}/_{kWh}$). A comparatively low voltage of 72V, but high capacity of 110Ah, provides the required power and energy in this case for several reasons. One reason is that Li-Ion batteries essentially need single cell monitoring. A smaller cell number in a series connection has fewer problems with cell-imbalances and requires less expensive battery management systems. Figure 5 shows the chosen battery with a mass of 60 kg and a comparable lead-acid battery with about 250 kg in front of the test-bed vehicle.

Figure 5 Li-Ion (right) and comparable Lead-Acid Battery

Gear ratio requirements:

With most motors and also for highly efficient power electronics and low-voltage batteries, it is required to have different gear ratios in order to allow for maximum speed of 120 km/h on the one hand and good gradeability of 20% on the other. Table 1 summarises the gear ratio calculations:

	1st gear	**2nd gear**	**3rd gear**	**4th gear**
Max. speed	36 $^{km}/_{h}$	60 $^{km}/_{h}$	100 $^{km}/_{h}$	120 $^{km}/_{h}$
Max. gradient	20%	11%	4%	1.7%
Total ratio	10.5	6.3	3.8	3.2
Purpose	Hill climbing	Urban driving	Extra-urban	Motorway

Table 1 Gear-ratios and performance

The vehicle can be driven in 2nd gear only, without needing to change gears in an urban driving cycle. This means good acceleration and comfortable, smooth driving. The gearbox loss characteristics are taken from the TX_VW file that was part of the simulation package (ADVISOR 2002 [60]). The wheel information like losses and rolling-radius are taken from the WH_SMCAR file (ADVISOR 2002). Figure 6 shows the gear ratio changing when accelerating from 0 to 120 km/h. The strategy is to shift into next gear when maximum motor speed is nearly reached. The motor is most efficient at high speeds as shown in figure 3 but still remains quiet.

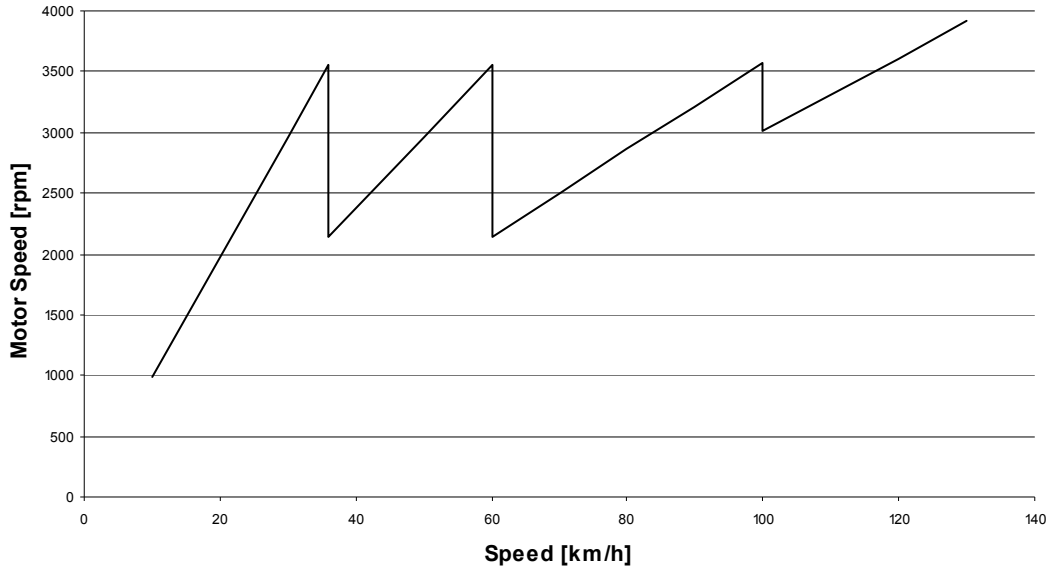

Figure 6 Gear shiflting table: motor speed over vehicle speed

2.6 Simulation

The previous considerations help in estimating initial component specifications. Components and the vehicle were modelled in Advisor2002 package [60] in order to assess whether such a vehicle may meet the requirements. Advisor is a backward-facing vehicle simulation package based on MATLAB/SIMULINK. Vehicle, drivetrain configuration and components can be modelled and run through different standard or purpose-build driving cycles. Different results like loss plots, operating points versus time, operating points in efficiency maps, various model-variables versus time and average values can be visualized.

Simulation results can be summarized as follows:

1. Maximum **velocity** of 120 $^{km}/_{h}$ can be achieved. Average speed of 112 $^{km}/_{h}$ can be achieved sustainable without battery depletion.

2. The **acceleration** results are presented in comparison to the Advisor results for the inbuilt model of the Toyota Prius 1 HEV. The model HEV in this study will undertake this simulation test in full-power hybrid mode with engine/generator switched on.

Test	**Toyota Prius 1**	**Peace-of-Mind HEV**
0 – 50 km/h	5.8 s	5.1 s
50 – 100 km/h	10.4 s	12.4 s
Max. acceleration	3.4 m/s^2	3.6 m/s^2

Table 2 Acceleration results in comparison with Toyota Prius

Table 2 shows that this type of HEV can achieve very good acceleration in urban driving, even better than a Toyota Prius 1. In extra-urban driving the acceleration is worse than in the Prius 1.

3. **Gradients** of 4% can be achieved at 100 $^{km}/_{h}$ with maximum cargo over long duration. 4% at maximum speed for short duration is possible.

4. **Acceleration** in urban driving is sufficient to follow the ECE-15 driving cycle in pure electric mode and in 2nd gear without gear shifting.

5. The **fuel consumption** in 180 km extra urban driving (26 EUDC cycles) is 3.6 $^{l}/_{100km}$ fuel equivalent. In urban driving (ECE-15) the Advisor result is 1.1 $^{l}/_{100km}$ fuel equivalent. With an average charger efficiency of 80% this is less than 1.4 $^{l}/_{100km}$. The

total fuel consumption (20% EUDC 80% ECE) in combined consumption is about 1.8 $^{l}/_{100km}$ compared to the 7.3 $^{l}/_{100km}$ of the same vehicle (Daewoo Matiz) with internal combustion engine.

6. The pure electric **range** in urban driving is 89 km (ECE-15) of which 70 km fall within an optimally efficient range. The hybrid mode range is limited by the fuel tank capacity only.

7. The total vehicle **mass** is 779 kg compared to the 778 kg of the original Daewoo Matiz.

2.7 Summary of Vehicle Drivetrain Characteristics

This chapter shows how some simple initial calculations based on off-the-shelf components and typical vehicle characteristics, together with initial modelling and simulation, can help assessing drivetrains for their potential and suitability. Further and more sophisticated modelling and simulation is subsequently required to provide better estimates of specifications and performance. However, within the broad range of hybrid drivetrain options, it is possible to identify sensible drivetrains in the way demonstrated here.

This chapter also demonstrates that using electric propulsion in vehicles can reduce energy consumption and other impacts like noise or local air-pollution without increasing vehicle mass or decreasing versatility and comfort. The only restriction is a limitation of the maximum speed to a reasonable level, which equals the national speed limits and which does not compromise acceleration. It is shown that the series hybrid electric drivetrain concept can potentially be feasible for such a type of vehicle, where the average power requirement is low. The fuel economy is about four times better than in a comparable vehicle and the comfort is increased without sacrificing performance, versatility, safety or affordability. Environmental impacts like noise and exhaust pipe emissions are decreased.

Nevertheless, during the modelling and simulation work, it became apparent that modelling the battery with sufficient precision was not possible, due to a lack of manufacturer's data. A more sophisticated modelling and simulation approach to the whole vehicle was not justifiable without having a better battery model. Further

research revealed that no battery model was available for large lithium-ion batteries that would meet the level of accuracy of the other vehicle components such as motors and power electronics. An additional challenge is that batteries degrade over time and cycles. There is very little knowledge available on this degradation process and its dependency on battery usage. It was therefore decided to consider the initial results sufficient in order to make the judgement that the chosen drivetrain had significant future potential. The majority of this work is instead focused on the testing and modelling of large lithium-ion batteries with the express view of using them in this drivetrain concept.

2.8 Requirements on the Battery System in this Drivetrain

This chapter has helped to understand the application and its demands on the energy storage solution.

The following requirements on the battery system can be identified:

- It is important to be able to predict the remaining energy or state of charge in the battery at any time during operation. The energy management requires this information in order to make an optimised decision on when to switch the generator on. However, in this application, it would be less critical to accurately determine the remaining energy than it is in a pure electric vehicle, because the generator can always cut in and provide sufficient power for propulsion.
- There are a number of issues that make this prediction of remaining energy very difficult in this application: The battery may be used in a wide operational region, ranging from long durations of idling and self discharge for example during holidays to bursts of high discharge currents. Regenerative braking can provide short intermittent pulses of high charging currents and the temperature range is significant in automotive applications. In essence, the usage profile is very unpredictable. It would be of great advantage if the remaining energy in the chosen battery type was as little dependant on the usage profile as possible.
- The drivetrain examined here provides a plug-in recharge facility. This means that a full charge can usually be expected from time to time. This full charge

can be used as a reference condition for the state of charge determination. However, although the plug-in concept is what makes this drivetrain so energy efficient, it cannot always be expected to be utilised. Some users may choose never to use the plug-in recharge. This means that the state of charge determination method cannot fully rely on these full charge reference points. It is important to investigate whether the chosen battery type allows using methods for state of charge prediction that do not essentially require a full charge reference.

- The battery in the investigated drivetrain is of significant size and cost. It is important to investigate the speed of ageing, so that the over-sizing of the battery can be optimised. The vehicle purchase cost and the battery size exceed what is perceived feasible if the battery was over-sized unnecessarily. However, it would lead to poor customer satisfaction or even warranty problems if it were over-sized too little. The speed of ageing is a substantial part of the running cost of the vehicle and it is therefore crucial for the feasibility of this drivetrain concept. Sudden failures due to unpredictable ageing may even lead to dangerous situations during driving depending on the exact type of failure. Ageing should be as predictable as possible for the chosen battery type.
- The battery is kept as small as possible in the discussed drivetrain. The power capability is the most crucial demand on the battery. This means that the battery may heat up substantially during high rate usage due to its internal impedance. It is important to understand the self-heating mechanisms and characteristics in order to determine whether active cooling is required or what type of cooling may be required for the chosen battery type. It is also important to investigate, how temperature and ageing affects the battery power performance in order to determine whether active heating is required or whether the battery can provide sufficient power levels at low temperatures even after ageing.

The following chapters investigate the mentioned issues for the chosen battery type, starting with a literature review and followed by testing.

3 Large Lithium-Ion Batteries

The previous chapter has helped understanding the application and its requirements on the battery system. This chapter translates these requirements into more specific requirements for testing the battery.

This is achieved by aiming to understand the fundamental working principles and behaviour of lithium-ion batteries. Most of the information available is based on small cells. Other battery chemistries are also covered in this chapter in so far as they appear helpful for identifying certain characteristics that could potentially be relevant for the examined application. This approach helps identifying the gaps in existing knowledge on the characteristics of the chosen battery type and these then translate into the requirements for testing.

3.1 Background Information on Lithium-Ion Batteries

Lithium-ion batteries dominate the market for most portable products such as mobile phones or laptop computers [6]. The success of the lithium-ion battery is mainly due to its significant advantages in terms of performance.

3.1.1 Performance Comparison

Performance has to be assessed in relation to other attributes. A common way for comparing the performance of energy storage solutions is to use the Ragone plot. In such plots, one performance attribute on the first axis is related to another performance attribute on the second axis. The following illustration shows the specific energy in Wh/kg over the energy density in Wh/litre for several different energy storage technologies.

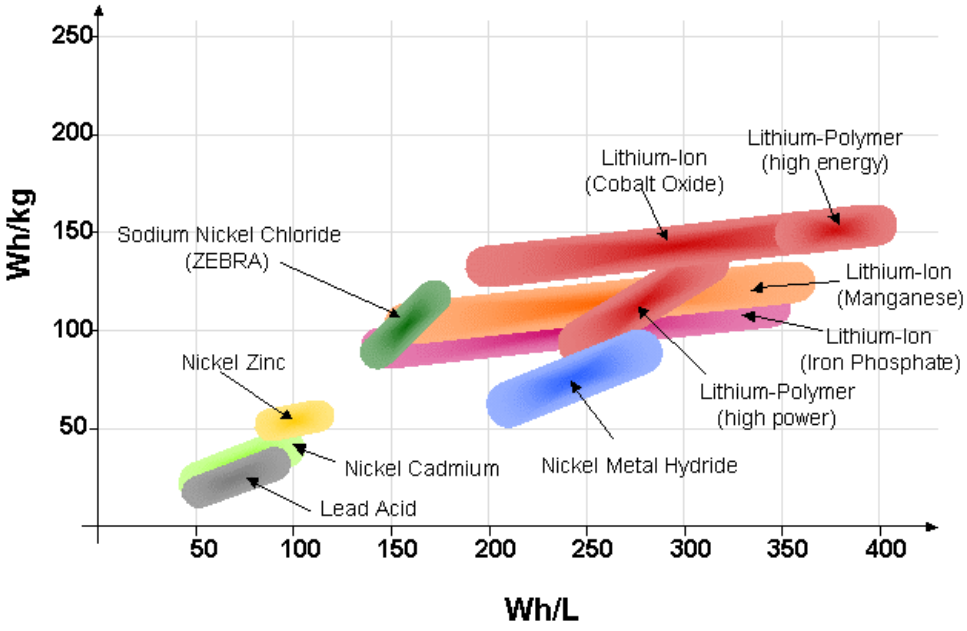

Figure 7 Energy storage performance of different battery technologies (data from manufacturers datasheets and [53]).

Figure 7 shows that lithium-ion cells provide smaller size and lower weight for a given stored energy if compared with other battery technologies. Size and weight can be as little as a quarter, if compared with the lead-acid battery, for example.

In this thesis the term "lithium-ion cell" is used in order to represent the whole family of lithium-ion cells. Terms such as lithium-iron phosphate, lithium-polymer, lithium-manganese, etc. are used to distinguish between different cell constructions and chemistries of lithium-ion cells. The Ragone plot in Figure 7 has revealed that lithium-ion cells have an advantage in terms of storing energy in relation to mass and volume. However, the plot does not provide any information about the power-capabilities of lithium-ion cells. The following Ragone plot shows the specific energy over specific power for several energy storage technologies, including fuel cells and combustion engines.

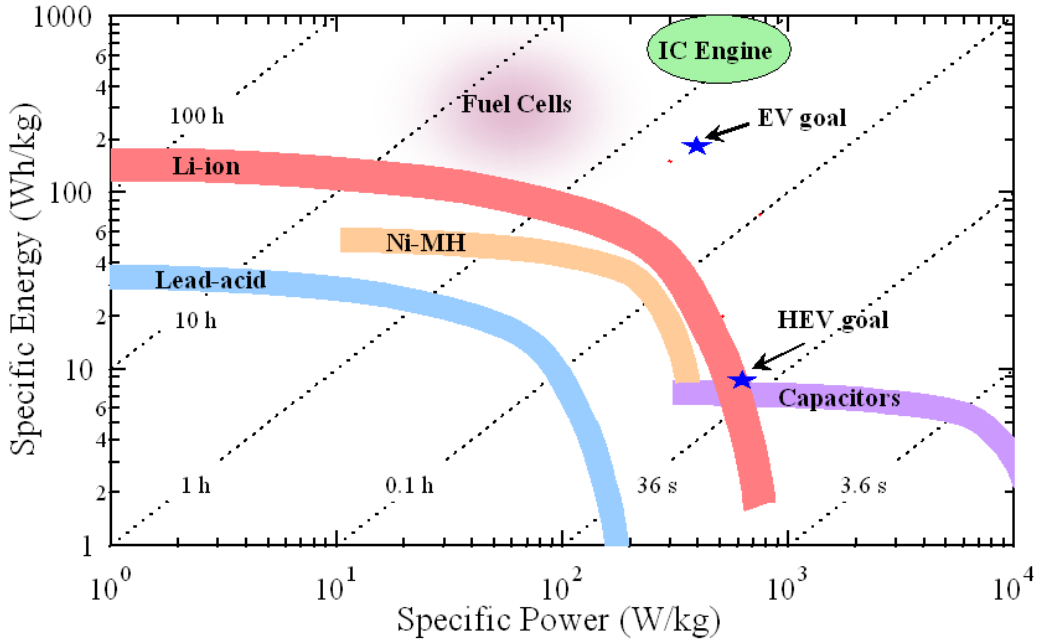

Figure 8 Ragone plot for different energy storage solutions.
With permission from Lawrence Berkeley National Laboratory [72]

It can be seen in Figure 8 that the lithium-ion technology performs better than lead-acid or nickel-metal hydride (NiMH) cells in terms of both energy and power for a given battery weight. This means that lithium-ion cells exhibit very good power performance. It can also be seen that, for very high power requirement, capacitors are more suitable than electrochemical batteries but the energy storage capabilities of capacitors are very limited. However, this graph only compares two attributes. Other attributes, such as volume, cost and "special attributes", have to be considered as well. A discussion of some 'special attributes' will follow in later sections.

The graph in Figure 8 also shows the performance characteristics of fuel cells and combustion engines. However, both of them are energy converters and the energy storage has to be treated separately. In this graph, a typical amount of stored energy (fuel + fuel tank) has been considered for this particular application (e.g. 60 litres of petrol in a car) in order to derive the overall specific energy / specific power performance of the energy storage + converter device. The result varies significantly for other applications and is also dependent on the type of output power requirement (e.g. mechanical or electrical). However, this estimate is adequate for demonstrating that the combustion engines with fuel tank is much better than any type of battery in this comparison. It also demonstrates that fuel cells perform well for storing energy but normally require battery backup or capacitor backup for providing short-term

power. Again, cost, size and other attributes cannot be displayed in such Ragone plots at the same time.

The Ragone plot in Figure 8 shows a typical characteristic of all batteries: The available energy decreases substantially when drawing very high power. This is mainly due to the significant voltage drop and hence power loss when drawing very high currents. This behaviour is in contrast to storing energy in e.g. liquid fuels and hence requires particular attention during testing and implementation of battery systems.

3.1.2 The Construction and Working Principle

The construction of a typical lithium-ion cell can be illustrated as follows:

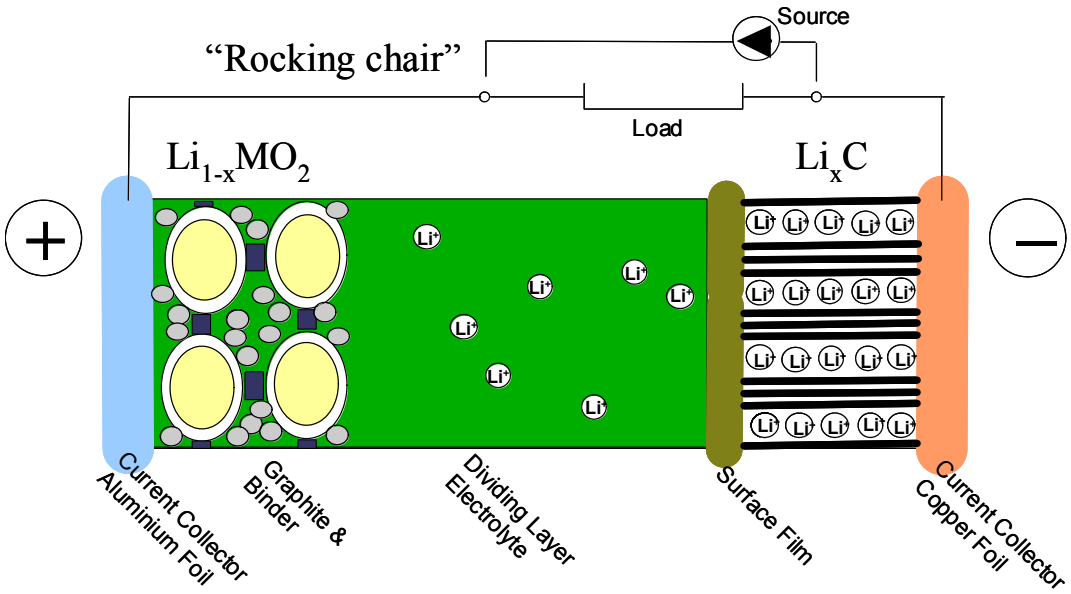

Figure 9 Model of the construction of a lithium-ion cell

Figure 9 shows a model of the most important structural features of a lithium-ion cell. From left to right, one can see the current collector and the active material of the positive electrode, then the electrolyte and dividing layer (separator) and on the right the active material and current collector of the negative electrode.

Due to the high voltage of a lithium-ion cell (nominal 3.6V), the choice of materials for the current collectors is limited to aluminium for the positive electrode and copper for the negative electrode. Usually, the terminal material is the same as the electrode material in order to avoid differences in the voltage potential and risk of corrosion

inside the cells. Establishing reliable and long-lasting connections, especially to the aluminium electrode / terminal, can be challenging and needs to be considered during long-term testing.

The electrolyte is an organic solvent with a lithium-based salt in solution. The electrolyte is electronically non-conductive but it allows transportation of lithium-ions. There is a range of different suitable solvents for lithium-ion cells. Frequently, several different solvents are mixed in various proportions and additives may be added in order to 'engineer' the desired characteristics. Currently, the formulation is optimised for a general broad use. However, the formulation could be optimised for certain applications (e.g. high temperatures in some UPS systems).

During charging, the lithium-ions move through the electrolyte from the positive to the negative electrode; during discharging they move in the opposite direction. They do not form a solid phase of lithium-metal, which then needs to go back into solution. No lithium-metal is formed at any stage during the process. The ions only move back and forth, which gives them the name "rocking-chair" batteries [30]. The reaction kinetics in lithium-ion cells are much faster than in lead-acid batteries, but the mobility of the ions in the electrolyte is comparatively slow and this is why early lithium-ion cells were not very powerful. Nowadays, the paths through the electrolyte are kept very short and, hence, high power is available. This is achieved by utilising a very thin layer of fleece in which the electrolyte is absorbed. Alternatively, the electrolyte is contained in a very thin layer of polymer.

Both electrodes consist of many small particles as shown for the positive electrode in Figure 9. The particles here are a type of lithium-metal-oxide and are 'glued' together and to the current collector using a binder. A conductive filler (e.g. Graphite) is used to increase the conductivity between the particles. The negative electrode is constructed in a similar way, except that the conductive filler is not required because the particles consist of conductive material themselves (e.g. graphite, coke). Controlling the particle size; keeping them small in order to increase the surface area, and reduce the travelling distances for the lithium-ions inside the particles, increases the performance.

The particles on both electrodes are covered with a surface film, which is called solid-electrolyte-interphase (SEI), as indicated on the left-hand side of Figure 9. The right-hand side of Figure 9 shows one of those particles with its SEI magnified, for illustration purposes. Whereas the left hand side shows several of such particles with their surface films, both electrodes, in fact, are constructed in a similar way. During charging / discharging, the lithium-ions travel through the electrolyte, then between the particles, through the SEI into the solid particles. Entering the solid particles is called intercalation. The active material (particles) may contain any number of lithium-ions, within certain limits. They can move inside the layers of the particles. This is why the active material containing intercalated lithium-ions is also called "solid-solution".

3.1.3 Comparison of Specific Behaviour

A few quantifiable battery attributes, such as energy, power, weight, size and cost have already been mentioned. However, most energy storage solutions exhibit a range of "special attributes" which may be specific to a certain technology and which cannot always be quantified. Many of these attributes are very important for the day-to-day use of the energy storage solution and for testing. A few "special attributes" of the most common battery technologies are reviewed in the following paragraphs.

3.1.4 'Peukert Effect'

Most batteries are labelled with their nominal capacity in Ah. Peukert however studied an effect on lead acid batteries in 1899 which showed that the available capacity substantially decreases at higher discharge rates [63]. Usually, the nominal capacity is determined in a five-hour long full discharge with a constant current. In many applications the discharge rate is much higher, in which case the available capacity decreases significantly.

The discharge rate also varies significantly throughout the discharge and there are even short recharge bursts from regenerative braking for the application in this study. Such conditions were not considered during Peukert's tests. Knowing the remaining energy or capacity is very important for this application. This so-called 'Peukert effect' was investigated further by extending his tests using varying currents throughout the discharge.

Initially, a range of tests with lead-acid batteries [26] were conducted which are supposed to be better understood than lithium-ion cells. However, it was found that the 'Peukert effect' is hard to predict during discharges with varying currents, idle times and partial recharge bursts, even for lead-acid batteries. Such conditions are typical in the application considered in this research project and tests were specifically designed and conducted in order to investigate the 'Peukert effect' of lithium-ion cells.

3.1.5 'Memory Effect'

Another probable effect is the 'memory-effect', which is well-known for sealed nickel-cadmium (NiCd) cells [17]. It also moderately applies to NiMH cells [54]. If a NiCd cell is not regularly fully discharged, it appears to 'remember' the lowest state of charge during previous cycles: It cannot provide sufficient power below this state of charge any more. NiCd cells therefore require a full discharge from time to time. This is very user-unfriendly for most applications.

One reason for the success of lithium-ion cells in portable applications is that they do not exhibit this 'memory-effect'. They can be stored or used in any state of charge and they can be recharged when convenient [30]. It was therefore decided not to investigate the 'memory-effect' for the tested specimen.

3.1.6 Ageing Behaviour

Different battery types exhibit different ageing behaviour. The ageing behaviour can usually be derived from an understanding of the fundamental working principles. Possible mechanisms for NiCd and lead-acid batteries in different applications will be reviewed first. Then ageing is discussed for lithium-ion cells.

NiCd batteries suffer from memory effect if they are not frequently fully discharged. This can be related to the ongoing growth of crystals over time. Cycling keeps the crystals smaller and smaller crystals provide higher surface area and hence lower internal impedance and better power

Lead-acid batteries conversely exhibit the opposite behaviour if compared to NiCd batteries. Lead-acid batteries degrade due to sulphation if kept at a low state of

charge. Sulphation even occurs if the battery is not subject to regular full recharges. There is usually not sufficient time to achieve a full recharge in cyclic applications. This undercharge is the main cause for degradation of lead-acid batteries in electric vehicle applications [66]. Charging currents should be as high as practically possible and charging voltages can significantly exceed gassing voltages. Opportunity charges should be applied whenever possible [43].

The ageing behaviour also depends on the type of application. Different applications exhibit different typical usage characteristics. Lead-acid batteries in stand-by applications for example suffer from the opposite problem if compared to traction applications, which were mentioned earlier. In stand-by applications (e.g. un-interruptible power supplies), the battery is kept fully charged at all times. The cells rapidly age due to corrosion or dry-out, which is a result of electrolysis and gassing; in these cases, the charging voltage should not be too high. The optimal charging voltage of lead-acid batteries not only depends on the application but also on the temperature and the ageing status of the cell. Considering that a pack consists of several cells connected in series, charging lead-acid batteries with the correct charging voltage can be very challenging, in particular, in the presence of temperature differences within the pack [48]. The series hybrid electric vehicle application considered in this project requires large battery packs and one key advantage of the specified drivetrain is the possibility to optimise the weight distribution. However, this usually means, that the battery cannot be mounted in one central place and this makes it difficult to keep all the cells at the same temperature.

The working principle of lithium-ion batteries does not permit overcharging and, hence, lithium-ion batteries are not meant to be fully recharged. Apart from lithium-ions moving back and forth, there is no material movement and there are no solution / dissolution processes which could lead to ageing. Ageing mainly occurs due to one or more of the following processes, not considering any abuse conditions:

- Stresses in the electrode material as a result of expansion / contraction due to lithium-ion intercalation during cycling [14].
- The solid electrolyte interphase (SEI) grows and lithium is consumed because the SEI becomes damaged when lithium-ions travel through it. The SEI instantly grows back but increases its thickness at the site of the original

damage. A thickened SEI results in poorer performance. The apparent capacity decrease due to impedance increase may be more significant than the true capacity decrease by consumption of lithium, especially in high-power applications [7; 38; 58].

- Solvent molecules may 'co-intercalate' together with the lithium-ions into the host structure and hence damage the surface structure and prevent further intercalation of lithium-ions. This will result in reduced capacity as well as performance loss due to decreased active surface area [61].
- Electrolyte decomposition [14].
- Lithium deposition and formation of SEI at the negative electrode towards the end of charging [75].

In essence, there is no known ageing process that involves the growth of crystalline structures, which is the cause for sulphation in lead-acid batteries. There is no known reason for why lithium-ion cells should degrade when not kept fully charged and hence no specific tests were conducted here to investigate this issue.

Prolonged float charging as applied in uninterruptible power supply systems (UPS) is likely to cause ageing of lithium-ion cells. The SEI for example will grow more rapidly due to the constantly elevated cell voltage [7; 58]. Prolonged float charging can be avoided in the application considered in this work. Hence, this aspect was not part of the conducted tests.

Up to today, the longevity of the small lithium-ion batteries in most portable applications has not been an issue for manufacturers or suppliers. For large expensive battery packs, ageing and life expectancy however are important issues. Unlike lead-acid batteries, where it is relatively well known how long they last in certain applications, ageing of lithium-ion batteries is still poorly researched [12; 14]. This is mainly due to the fact that large lithium-ion cells have not commonly been available. Only a few manufacturers are able to provide information for certain usage conditions and this information is not based on a huge number of tests. Cell designs change faster than tests can be conducted. A generic 'equation' for predicting the ageing or battery life, taking into account the full range of conditions and also the requirements of a particular application does not exist

The working principle of lead-acid batteries must cause ageing because material goes into solution, is then transported and crystallisation takes place. [66]. In lithium-ion cells there is no such mass transportation and lithium-ions simply move back and forth, travelling through the SEI and intercalate into the electrodes without substantial volume change [38].

The above ageing mechanisms are not very well researched as mentioned earlier, but it would appear that low temperatures and lower terminal voltages will prolong battery life. Furthermore, from the literature review, it appears that the high frequency impedance is affected less by ageing than is the low frequency impedance [50]. Ageing is carefully considered during testing throughout this project and rigorous measures are taken in order to detect and quantify ageing.

3.1.7 Non-Monotone Ageing Behaviour

Some types of batteries suffer from a "sudden death" when reaching their end of life. Flooded lead-acid batteries, for example, can suffer from internal short-circuit after a certain cycle life; they stop working without warning. Lithium-ion cells are subject to a monotonous and predictable ageing. The capacity and the performance decreases slowly over time and cycles [14]. The most important ageing processes are mentioned above. 'Sudden death' is not investigated in this work.

3.1.8 Thermal Management

Many battery types exhibit some issue with heat. They degrade rapidly at elevated temperatures and some heat up significantly during discharging. Substantial heating may occur towards the end of charging due to over-charge side reactions and this may lead to thermal runaway and battery destruction. Effective cooling may be required [20].

Lithium-ion cells are very efficient and they do not generate as much heat. There are no side-reactions by design and hence they do not generate increasingly heat towards the end of charging. In fact, the thermodynamics even make them cool down slightly during charging [30; 67].

On the other hand, lithium-ion cells exhibit small thermal mass, which means that they may heat up more despite generating fewer losses. Additionally, they are sensitive to high temperatures. It is important to consider temperature during testing in order to determine thermal management requirements in the application.

3.1.9 Characteristics at Very Low Temperatures

Batteries with water-based electrolytes may freeze and the battery case may crack at very low temperatures. This is a well-known problem for fully discharged lead-acid batteries with low acid concentration [66]. The organic solvent in lithium-ion cells does not freeze down to temperatures of –40°C or lower depending on the solvent mixture [30].

The performance of some batteries becomes very poor at low temperatures [20]. It is difficult to make general statements about low-temperature performance of lithium-ion cells, but it is possible to design lithium-polymer cells with good performance at low temperatures [46]. It is therefore important to test the low temperature performance of the specific lithium-ion battery to be used.

3.1.10 Emission of Dangerous or Toxic Gases

Lead-acid batteries produce hydrogen gas towards the end of charging. Hydrogen is explosive even in very low concentrations and this is why several regulations and good practices can be found about the ventilation and explosion protection when using lead-acid batteries in various applications [18]. Lithium-ion cells are fully sealed and there is no gassing, therefore, no risk of explosions. Lithium-ion cells require no ventilation so they can be mounted in sealed containers. No specific tests were conducted here in order to investigate gassing.

Lithium-polymer cells are, not only, fully sealed but, also, contain no compressible volume, which means that they can potentially be used under very high pressure. Tests at high hydrostatic pressure for underwater vehicles have been carried out in cooperation with the National Oceanography Centre (NOC) in Southampton. It was confirmed that they can be used under very high pressure without any pressure hull. Also, the cell performance did not change significantly [65] and this could be relevant for the HEV application, because it demonstrates the grade of environmental sealing

of such cells. Water cannot enter such cells and, for example, it would be possible to conduct tests in water baths for temperature control.

3.1.11 Over-Charge and Over-Discharge Behaviour

Lead-acid batteries and NiCd batteries are abuse tolerant and are robust in response to over-charging and deep discharging [17; 54; 66]. Depending on the level and duration of abuse, they may not suffer significantly. Lithium-ion cells are sensitive to abuse conditions. Heavy abuse may cause fire [30]. A battery protection or battery management system is required in order to protect each individual cell in a lithium-ion battery. Degradation or safety under abuse conditions has not been tested in this study.

3.1.12 State of Charge Determination

For some battery types, it is more difficult to determine the remaining capacity during usage than for others. Lead-acid batteries suffer from the 'Peukert-effect' [26; 63] and NiMH batteries exhibit a significant voltage hysteresis between charging and discharging [57]. Furthermore, it is difficult to determine the end-of-charge with NiMH cells [54].

Lithium-ion cells exhibit no significant side-reactions; their coulombic efficiency should therefore be 100% (capacity charged equals capacity discharged) [30]. Simpler and more robust state of charge algorithms could be used. However, there is no "full-charge" reference condition as mentioned earlier and whether they exhibit a hysteresis is controversial [11]. The behaviour in 'Peukert tests', i.e. testing the available capacity with different discharge rates, has not been reported. It is very important in this application to be able to predict the remaining capacity in the battery after certain usage conditions. A series of tests were therefore carried out in order to investigate the available capacity under various conditions, such as current, temperature and ageing.

3.1.13 Safety

Lithium-metal provides a high voltage potential and this is why the lithium-ion cell exhibits such a high terminal voltage of 3.6V. This, in return, is the reason for the high energy density of the cells. The high terminal voltage prohibits the use of water-based electrolytes because electrolysis would occur. An organic solvent is therefore used instead [81].

The above construction characteristics lead to the main disadvantages regarding safety: Lithium metal is highly reactive and cannot be extinguished with water; high energy densities and high power densities usually equate to higher safety risks and the organic solvent is flammable. Fortunately, there are various working principles that make those cells intrinsically safer than it would at first appear.

Firstly, there is no metallic lithium inside lithium-ion batteries. Various lithium-metal batteries have been researched and tried [64] but, for safety reasons, the lithium-ion cell has evolved from those early and sometimes dangerous trials. Since there is no highly reactive lithium-metal inside lithium-ion cells, they are intrinsically much safer than their predecessors. Lithium metal may be plated on the negative electrode only if the cells are being overcharged. However, usually this plated lithium-metal instantly reacts with the electrolyte and increases the SEI layer without compromising the safety. It has to be said however, that in the event of the plating occurring at a high rate (e.g. when overcharging the cell with a high current), this reaction may produce sufficient heat and initiate a thermal runaway.

Fortunately, the separator will exhibit a shut-down behaviour, which means that it stops the lithium-ions from moving through it once the temperature inside the cell rises to a certain level. This will stop the overcharging and hence further reactions [71]. If the process has sufficient thermal momentum and the temperature keeps rising despite the shut-down the separator however will break down. The separator will loose its integrity and may allow the positive and the negative electrode to short-circuit internally [71]. This would cause a rapid and exothermic reaction such that the solvent will ignite, which will lead to more heat generation and even faster reactions. A safety vent will open and prevent the build-up of pressure inside the cell [30]. The

cell will not explode but catch fire and the heat of the fire can be expected to cause adjacent cells to be incinerated as well.

Reversing polarity with high currents can cause a similar scenario. Fortunately, in contrast to burning liquids, the fire will be contained within the battery and not spread.

For the reasons outlined above it is essential to prevent every single cell in a pack from being exposed to any abuse conditions. This is important to bear in mind when designing test equipment and test procedures, as well as when working with the cells during testing. Electronic protection and management in order to monitor individual cells is required in the application or when testing several cells in series connection.

Dangerous abuse conditions may also arise from either mechanical impact, from faulty cells or due to growth of dendrites, which could penetrate the separator and cause local internal short-circuits [71]. However, cell manufacturers and independent institutes conduct various mechanical and electrical tests including abuse conditions in order to assess the safety of the cell design (test specifications: UL1642, UL2054 and SBA G1101). Dendrite growth and separator penetration cannot normally generate sufficient local heat to start a thermal runaway. Low cell voltages or 0V at the cell terminals are indications for internal short-circuits and should not be ignored. Rapid charging should be prohibited in order to prevent sufficient local heat generation inside the cell.

It is possible to use lithium-ion batteries safely, but good system design and electronic protection are essential prerequisites. Finally, the battery industry and research institutes are constantly working to improve the intrinsic safety of batteries. Dedicated safety tests are not within the scope of this work but potential risks were considered during testing.

3.2 Research Objectives

The working principle of lithium-ion batteries is relatively straightforward. Potentially, they are much simpler to use without exhibiting complex behavioural characteristics such as sulphation, 'memory effect', charge-discharge hysteresis or 'Peukert effect'. However, this is not proven and needs to be confirmed.

Objective 1: To assess whether the tested battery specimen exhibits a charge – discharge hysteresis as known from NiMH batteries.

Objective 2: To assess whether the tested specimen exhibits a 'Peukert Effect' or similar effects during discharge.

Objective 3: To assess whether the tested specimen exhibits a 'Memory Effect' as known from NiCd cells.

The state of charge can potentially be determined relatively simply and systems can be designed to be user-friendly in the absence of any of the above effects.

Objective 4: To investigate methods for determining the remaining capacity of large lithium-ion batteries in a specific application and during testing.

Lithium-ion batteries exhibit no over-charge reactions and this means that a true full charge does not exist.

Objective 5: To determine a suitable reference condition during testing and to assess whether this condition would be a suitable reference in the application.

Such a reference condition would be less important if it was possible to use the open circuit voltage for determining the state of charge.

Objective 6: To evaluate to what extent the open circuit voltage can be used for determining the state of charge in practical applications or during testing.

Ageing is a continuous process, which is not interrupted by sudden, unexpected events. However, there is little knowledge of the exact ageing behaviour and therefore meaningful lifetime predictions are currently not possible.

Objective 7: To determine the impacts of cell ageing during testing.

Lithium-ion cells exhibit a low thermal mass and this suggests that they may heat up significantly faster than lead-acid batteries. The self-heating also depends on the internal impedance of the cells. The lithium-ion cells exhibit no side reactions towards the end of charging and this means that they should not heat up as much towards the end of charging as for example NiCd batteries. The low temperature behaviour of lithium-ion cells significantly depends on the construction and the formulation of the organic solvent and the literature reveals relatively little on the temperature behaviour of lithium-ion cells in general.

Objective 8: To characterise the performance of the tested specimen under various conditions for example temperature.

For this, a series of tests is required and it is important to understand the battery characteristics before designing such a time consuming series.

Objective 9: To identify a suitable test series and to assess whether the tested specimen exhibits any other significant behavioural characteristics.

The following objectives were derived from those preliminary tests that were conducted in order to understand the characteristics of the tested specimen.

The true equilibrium open circuit voltage (OCV_{eq}) at various levels of state of charge, temperature and ageing is essential information during testing and for analysing test results. The tested battery specimen exhibited a surprisingly long relaxation time towards reaching such an equilibrium, which results in very long waiting times during tests.

Objective 10: To rapidly determine the true equilibrium open circuit voltage at different states of charge, temperature and ageing.

The long relaxation time of the tested specimen meant that two adjacent test cycles might not be independent from each other. This could be an issue in terms of keeping the overall testing time short whilst still obtaining meaningful results.

Objective 11: To determine an optimised resting time between test cycles.

The step response technique or current pulse interruption technique promises to be cost effective for exhaustively testing large capacity cells. However, this technique has not usually been used or published and it is unclear whether equivalent circuit parameters could be determined easily from such tests.

Objective 12: To evaluate the step-response technique for testing large lithium-ion batteries.

Objective 13: To assess the possibility of directly determining battery parameters from step-response test results.

4 Test Methodology and Preliminary Battery Performance Tests

The approach to testing taken in this work is in many ways novel and alternative to conventional methods. Firstly, the step response technique was employed throughout the whole work. This approach promises to be faster and more cost-effective when compared with more conventional test methods, e.g. impedance spectroscopy.

Secondly, it was investigated, whether it is possible to combine several test objectives into fewer tests. The aim is to characterise the typical behaviour of a production battery, to determine the performance at different temperatures and currents, to measure degradation and to evaluate the test methods at the same time.

Finally, the described test methodology proposes tests conducted on a single cell or using only a small number of cells. It is suggested to obtain statistically meaningful results with a larger number of cells through subsequent tests or through in-situ data logging in field tests or even in sold products.

The manufacturer does not provide any performance data on the tested specimen and general data on the behaviour of large lithium-ion cells was not published either. The previous chapters have identified a substantial gap in knowledge on the characteristics of the chosen cell type. Hence, it appeared not to be feasible to design and conduct a series of tests or specific tests without conducting preliminary test cycles.

Most battery chemistries and designs require some initial cycles, before reaching stable behaviour. These initial cycles were used as preliminary test cycles in order to "get a feel" for the behaviour of the tested cell type. This chapter covers the methodology, results and analysis of these preliminary tests that formed a substantial part of the work carried out during this project. Parts of this work are published in a paper [1]. The findings from these initial test cycles were then used in order to design the tests with specific purposes and the main series of tests, which are discussed in the following chapters.

4.1 Test Apparatus

The tests were carried out on a Digatron UBT universal battery tester (www.digatron.com). The tester can operate in several modes, such as constant current, constant voltage, constant power or constant resistive load. It carries out voltage, current and temperature measurements. A PC was connected through an RS-485 interface. The software "Digatron BTS 600" on the PC allows the defining of the test-procedure and the logging of data, such as, time, current, voltages, power, temperature, watt-hours and ampere-hours. The sampling time and start/stop criteria can be defined. Several limits for the battery can be defined separately, so that the tester can stop for safety reasons in case any of these limits are exceeded. The tester can run and log data independently from the PC but, once connected, the data is uploaded. This ensures a secure data logging, even in case of computer failure. The tester is capable of discharging a single Lithium-ion cell with a current of up to 50A. The charging has to be limited to a current of 30A. The specifications of the tester are as follows:

Maximum discharging current	50 A
Maximum charging current	30 A
Voltage range during charging	1 V … 24 V
Voltage range during discharging	0 V … 24 V
Error – current measurement	± 0.5 % but not better than ± 25 mA
Error – voltage measurement	± 5 mV
Error – temperature measurement	± 0.1 K

Table 3 Specification and errors of the battery tester.

The tested specimen is a high-energy lithium-ion cell (Thunder Sky, China) with a capacity of 50 Ah. The cell size was chosen so that it could be tested up to a 1C rate.

These cells have a thin and lightweight poly-propylene (PP) case that requires external compression in order to maintain good contact between electrodes and electrolyte. This compression was provided to the tested cell by metal plates, aluminium bars and studding. The tested specimen was placed in a temperature-controlled cabinet and tests were carried out between -15°C and 45°C surrounding air temperature. The cell temperature was not kept constant and the cell naturally heated up and cooled down during tests.

Temperature plays an important role for the performance, ageing and safety of lithium-ion cells. Ideally, one would measure the temperature inside the cell but in-situ measurements in sealed cells from a series production are usually not viable. However, it is essential to estimate the temperature inside the cell as accurately as possible. The current collectors are much more thermally conductive than the active material, electrolyte or the PP case of the tested specimen, hence, measuring the temperature at the terminal provides the best approximation to internal temperature. The negative electrode has a higher thermal conductivity than the positive electrode (0.156 cm^2/s instead of 0.116 cm^2/s [71]) and, additionally, dangerous overcharge reactions at high temperature may occur at the negative electrode firstly. For this work the temperature sensor was mounted inside the bolt that screwed into the negative terminal. The temperature was logged during tests together with current and cell voltage.

4.1.1 Test Arrangement During Preliminary Tests

The main tests were carried out at the University of Southampton using the equipment and apparatus described above. However, the preliminary performance tests were carried out on a Digatron tester at the Institute for Power Electronics and Electrical Drives (ISEA) in Aachen. The charge discharge rating of that machine was 100A, as opposed to the 50A of the tester that was used for the main tests. The measurement errors are the same as shown in Table 3, except the error for measuring currents was within ± 50 mA.

The tested lithium-ion cell specimen was a 100Ah cell from the same manufacturer (Thunder Sky) as the 50Ah cell that was used later for the main testing. The cell remained within the battery pack of nine cells during the tests in order to provide the required mechanical compression and in order to simulate a typical in-vehicle configuration. The test arrangement is shown in Figure 10.

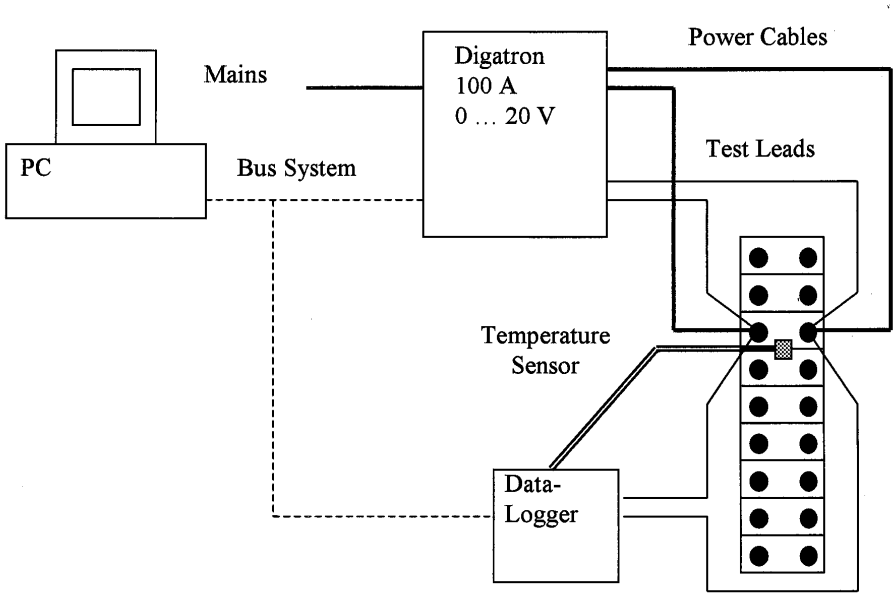

Figure 10 Test arrangement during preliminary tests

One of the cells in the middle of the battery block was chosen for testing because this is the worst case in terms of temperature rise during high-current discharge and charge. The battery was placed on a plastic grid to allow for natural air-cooling and to isolate the battery from the 'ground' heat sink, so that the cell can heat up uniformly during the tests. The ambient temperature was 21°C.

The Digatron battery tester was connected to the cell using cables with a cross-section of 10 mm^2. The test leads for measuring the cell voltage were separate from the power cables in order to eliminate errors due to voltage drop across the cable. A data logger (Digatron DLP 24C) was used for verifying the voltage measurement of the battery tester and for measuring cell temperature. In these preliminary tests, the temperature probe was placed between the cells.

4.2 Test Procedure

For the reasons outlined, the proposed test methodology relies on the step response or current pulse relaxation technique to determine the cell characteristics. The test procedure is designed in order to extract as much information about the cell as possible using a few test cycles only. The following Figure 11 shows the first two out of the three preliminary test cycles that were conducted.

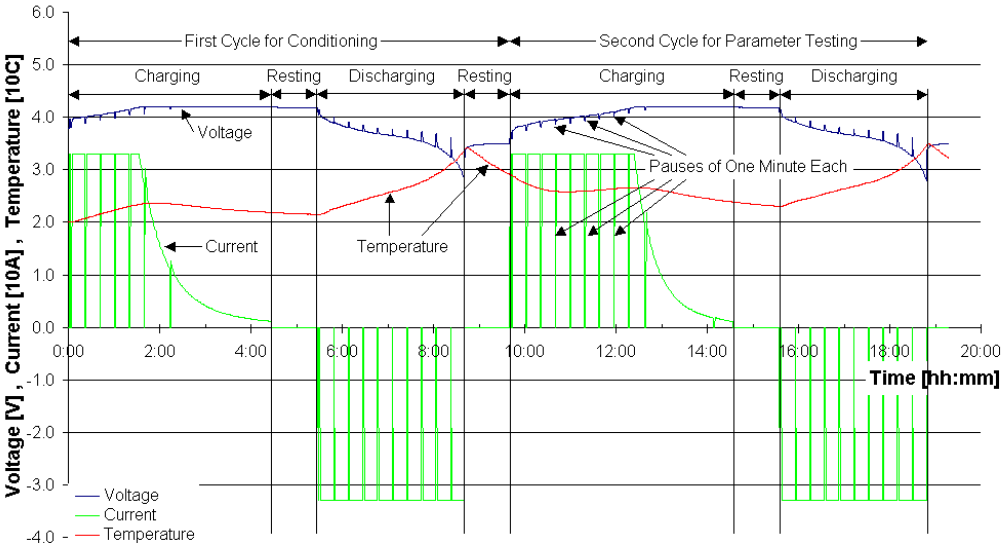

Figure 11 The first two cycles showing the test procedure during the preliminary tests

It shows typical voltage (blue), current (green) and temperature (red) curves. Charging currents are shown as positive and discharging currents are shown as negative values. Temperature and current are scaled with a factor of ten on the y-axis.

Each test cycle started with a pause in order to measure the initial voltage of the cell. Subsequently, the battery was charged with a constant current – constant voltage (CC-CV) charging regime. In this regime, the cell was charged with a constant current till it reached the end-of-charge voltage (EOCV) of for example 4.2V. Charging continues, keeping this voltage constant while the current decreases till it reaches the end-of-charge current (EOCC) of for example 0.01C (0.01C = 1.0 A in case of the 100Ah cell). According to the manufacturer, the cell should be fully charged at that point. After resting for one hour, the battery was then discharged. The discharging was terminated as soon as the cell voltage reached the end of discharge voltage (EODC) of for example 2.8 V.

The main test cycles always started with a fully charged cell, then discharged, then rested, followed by recharging and another resting period before the next test cycle. The preliminary tests however, always started with charging first as indicated in Figure 11. The reasons for this will be discussed in the course of this chapter. The following figure shows the cell voltage, current and temperature during a typical test cycle from the main test series in more detail.

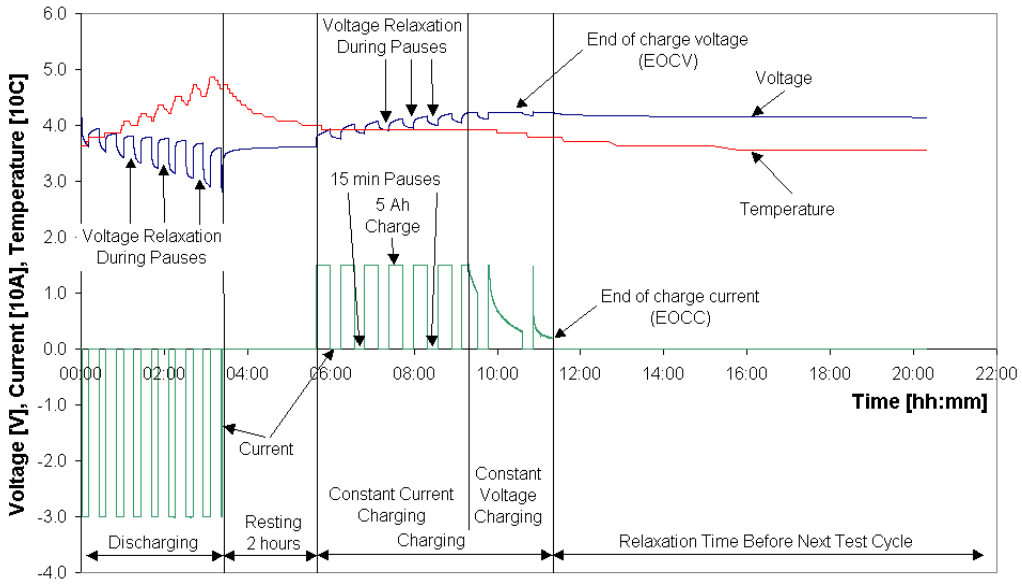

Figure 12 Typical test cycle

Figure 12 shows that each discharging process and each charging process was paused at every 10% change in state of charge. The voltage response during these pauses is later used in order to analyse the dynamic behaviour of the battery at different levels of SOC. A resting time between charging and discharging and between test cycles was used in order to allow the battery to both approach equilibrium and to cool down. The measurements of cell-voltage, current and temperature were recorded. The following accumulated data were also logged throughout each test cycle:

- Ah and Wh in total using balanced counting
- Ah and Wh per step
- Ah and Wh for charging in total
- Ah and Wh for discharging in total

4.3 Preliminary Tests

Several charge / discharge cycles were conducted on a 100Ah large lithium-ion cell (Thunder Sky). The cell voltage, current and temperature during the first two of those cycles is shown in Figure 11. The first cycle was purely for calibrating and forming the cell, so that it was in a known state of charge and performance for future cycles. The second cycle was the first actual test cycle. These first two cycles applied the

recommended charge and discharge current of C/3 (33A). The third cycle followed the same procedure but applied the maximum allowed continuous charging and discharging current of 1C (100A).

The pauses during the preliminary tests were one minute long starting after the first 1 Ah discharged (charged) and then every 10 Ah. A resting time of one hour between charging and discharging was applied. During charging, during discharging and during the long pauses between charging and discharging, measurements were taken once per minute. During short pauses, measurements were taken once per second in order to record the voltage response. The preliminary performance tests are used to generate model parameters. However, the main objective of these preliminary performance tests is to 'get a feel' for the behaviour of the tested specimen. The results of the preliminary tests are presented in the following subsections, as they are important for finalising the test methodology. However, the direct determination of battery model parameters from the preliminary test results is discussed in chapter 5.

4.3.1 Voltages During Preliminary Tests with 33A Charge / Discharge Current

The following Figure 13 shows the cell voltage during the second preliminary test cycle with 33A charge / discharge current. This figure shows the cell voltage as a function of state of charge unlike the previous figures, Figure 11 and Figure 12, where the cell voltage was displayed as a function of time. This allows to directly compare the voltage levels between charging and discharging at the same states of charge.

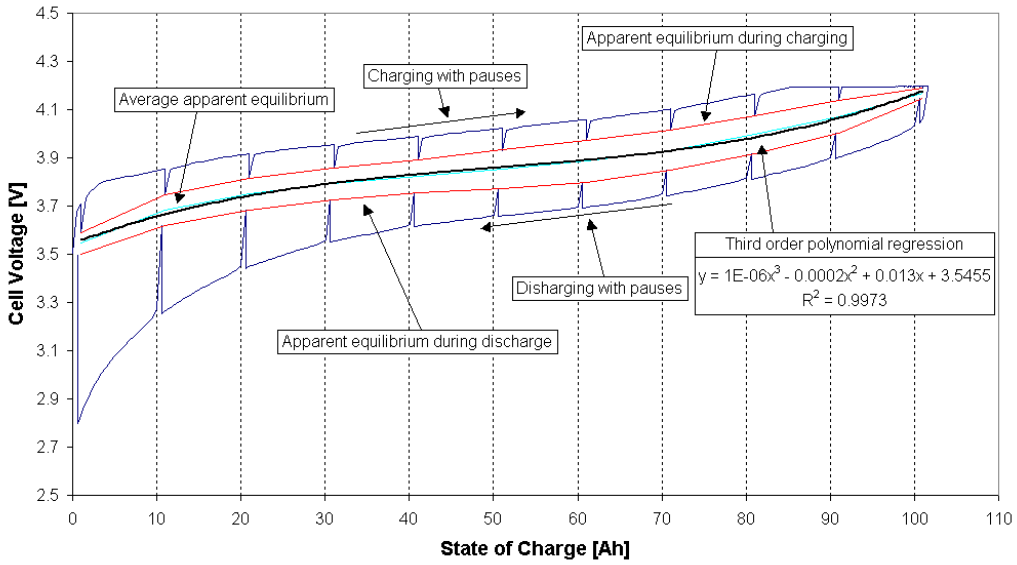

Figure 13 Development of cell voltage during preliminary performance test at 33A charge / discharge current with pauses

The blue curve with the saw-toothed shape in Figure 13 shows the cell voltage during charging and discharging over SOC in measured Ah. The upper curve represents charging and the lower line represents discharging. This representation of cell voltage measurements during the test cycle reveals that the cell does not reach equilibrium at the end of the step response pauses. The equilibrium open circuit voltage cannot directly be measured.

The red curve is an interpolation between the voltage levels at the end of the one-minute long pauses. Initially, it is assumed that the true equilibrium open circuit voltage (OCV_{eq}) lies within an open circuit voltage region, which has these two red curves for charging and for discharging as its boundaries.

The light blue curve in the centre is the mean or average of this region. In some analysis it is assumed that this voltage value represents the OCV_{eq}. The black curve shows the third order polynomial regression of the light blue curve, so that an OCV_{eq} can be calculated at any given SOC.

Specific tests are conducted and discussed in this work in order to investigate whether this suggested method is suitable for reliably determining the OCV_{eq}.

4.3.2 Voltages During Preliminary Tests with 100A Charge / Discharge Current

Figure 14 shows the cell voltage during the second preliminary test cycle with 100A charge / discharge current.

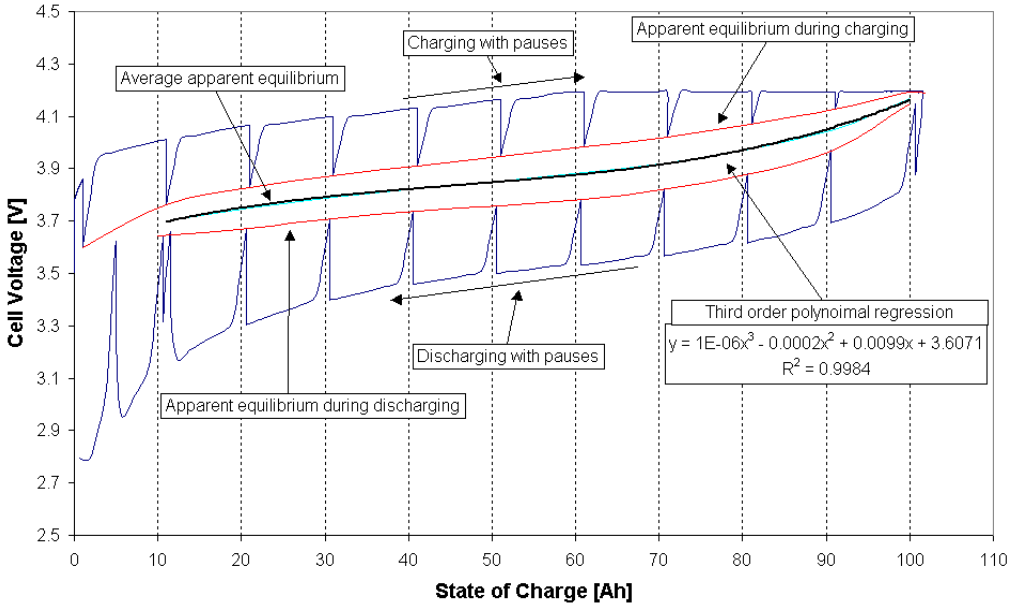

Figure 14 Development of cell voltage during preliminary performance test at 100A charge / discharge current with pauses

The curves in Figure 14 are similar to Figure 13, but were obtained from the test applying the maximum allowed continuous current of 100 A during charging and discharging instead of 33 A.

It can be seen in Figure 14 that the current was interrupted unexpectedly a few times at the end of discharge. This problem when discharging the lithium-ion cell at high currents with the test setup as used during the prelminary tests can be explained as follows. The battery tester is designed for testing lead-acid batteries with a nominal terminal voltage of 12 V. The tested lithium-ion cell however is discharged down to 2.8 V terminal voltage at the end of discharge. The voltage drop across the long high-power cables from the tester to the cell was significant and the battery tester was not able to maintain the 100A through its internal power transistors. Shorter cables with higher cross-section per current were used for all subsequent tests in order to avoid this problem.

4.3.3 Temperature Behaviour During Preliminary Tests

Figure 15 shows the measured cell temperature during the first three preliminary test cycles with different currents.

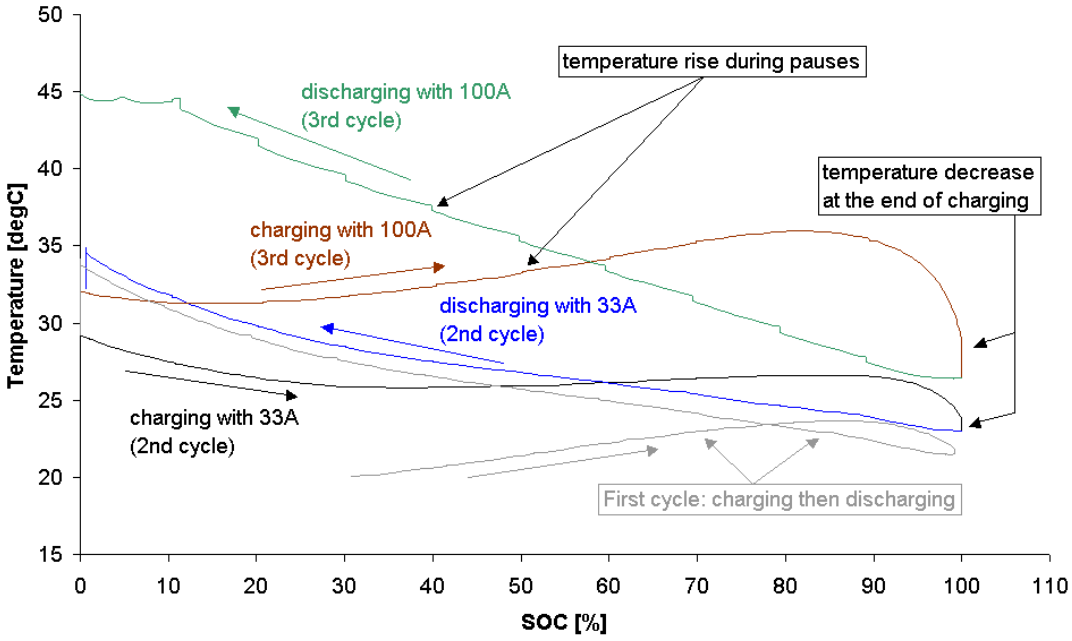

Figure 15 Development of cell temperature as a function of state of charge during preliminary tests at 33A and 100A

Figure 15 shows the temperature behaviour during the preliminary tests as a function of the SOC in %. The SOC is expressed in percentage units unlike in previous figures where it was expressed in Ah. The percentage units are calculated as a ratio of the Ah units divided by the nominal capacity of the tested cell, which is 100Ah in this case. The advantage of using percentage units is that it is simply possible to compare the results with tests undertaken on other cell sizes. The grey curve shows the temperature during the first charge and discharge of the new cell. It starts with charging from a state of charge of about 30% at the ambient temperature of about 20°C. At the end of discharging, the temperature was about 34°C. During the one hour long resting time, the cell cooled down to 29°C before the second cycle commenced with charging. The black curve shows the temperature behaviour during this charging with 33A with increasing state of charge from the left to the right. The blue curve shows the temperature increase during discharging with 33A from the right to the left. The brown and the green curves show the temperature behaviour during charging and discharging with 100A.

The significant decrease in temperature towards the end of charging occurred in the constant-voltage charging regime. The obvious steps in the temperature curves for the 100A tests occurred during the one-minute long pauses.

Figure 15 shows that the temperature wents up during discharging. This self-heating is due to heat from the exothermic reaction and due to losses. A significant temperature rise is apparent during the pauses in the high current (100A) discharge cycle. These steps do not actually represent a higher rate of temperature increase because the figure does not show time, but state of charge. Although time moved on during the pauses, the SOC remained unchanged and hence showing apparently high rate steps. Such steps are still surprising as one might expect the temperature to decrease during the pauses without any current flow. An explanation for the ongoing increase of apparent cell temperature during the pauses is a time delay of the measured temperature, which, although generated inside, is measured outside at the thermally insulating plastic case of the cell. During pauses, the temperature of the outside case still rose. This suggests that the temperature inside the cell was significantly higher than the temperature measured on the outside of the case.

This shows the importance of measuring the internal temperature of the cell, not only, for safety reasons but, also, for determining parameters consistently. The temperature sensor was mounted inside the bolt that screws into the negative terminal during subsequent test cycles in order to improve this temperature measurement.

During charging, the temperature initially went down although the charging current was the same as the discharging current. This can be explained with endothermic reaction cooling during charging and comparatively smaller losses in the beginning of charge. In the middle of the course of charging, the temperature started to rise and this is when the thermodynamic cooling effect becomes smaller than the losses. During the last 10% of charged capacity, the temperature went down again which is due to the decreasing current and hence decreasing losses in the constant voltage phase.

4.4 Step Response Technique

The following paragraphs describe the test methodology that was used to investigate the dynamic behaviour of the cell voltage. The step response technique or current pulse relaxation technique (CPR) was employed throughout.

4.4.1 Typical Voltage Response Behaviour

The charging and discharging was paused for a short time every 10% change of capacity in order to measure and analyse the voltage relaxation.

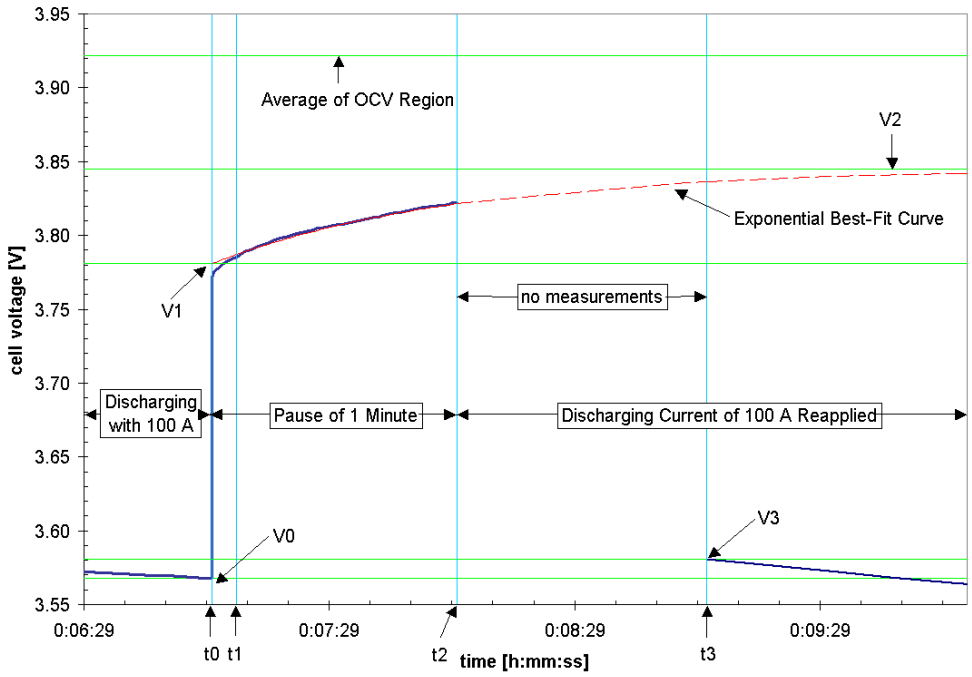

Figure 16 Typical voltage relaxation (step response) during discharging in the preliminary tests

Figure 16 shows a typical cell voltage step response during a discharge pause period. It represents a magnification of one of the step responses as shown in Figure 12. However, this particular voltage response is a section of the voltage curve in the preliminary tests during the discharge with 100A at a state of charge of 71 Ah. This example is used in order to define time values and voltage levels, which will be used in further analysis and discussions.

The time before t_0 in this figure shows the cell being discharged with 100A. During this discharge period, the cell terminal voltage decreased towards the level V_0 with decreasing SOC. The load was switched off at t_0 and the voltage rose almost

immediately to the level V_1. After this voltage step, the cell voltage rose further during the pause of one minute between t_0 and t_2. The discharging current was reapplied at t_2. Unfortunately, due to the specific setup of the battery tester during the preliminary tests, the next measurement was taken one minute later at t_3. At this time, the cell voltage had already dropped down to V_3 and it is not possible to investigate the voltage response to the current being reapplied. The specific settings in the battery tester were improved for the main series of tests, so that continuous measurements could be used to investigate the voltage response where it is most interesting.

Figure 16 also shows how the measured voltage rise during the relaxation is approximated by an exponential best-fit curve. The average of the OCV region, which is shown as a light blue curve in Figure 14 is also indicated in that graph.

4.4.2 Typical Battery Model

Several different models exist for batteries. Electrochemical models and equations are normally used for designing cells, mathematical or equivalent circuit models are used for simulating battery behaviour and thermal models help designing the thermal management and predicting the thermal power limitations. Sometimes a combination of different models is required in order to understand the behaviour. Thermo Analytics Inc. [74] gives a concise and general overview of available models.

An equivalent circuit model type was chosen for the purposes of this research, as electrical system designers can understand this most easily. Such a model can be integrated with other electrical components and simulated using an electronic simulation tools.

A simple equivalent circuit model comprising an electromotive force (EMF), that can be a function of the state of charge, in series with internal resistance, which can be a function of SOC, temperature and history, may not be satisfactory in many applications. Such a model does not represent the dynamic behaviour of the battery, which in many applications is important. A dynamic model of a battery normally contains one RC combination like Randle's model [10] or two RC combinations as suggested by Gao for a Sony Li-Ion cell [37].

More precise models could include for example “Voigt-type” analog (2 – 4 RC combinations in series), which models the surface film impedance. However, this becomes relevant at comparatively high frequencies [7] where precise modelling is not of great importance in the focused application. Another typical element used in more sophisticated models is the Warburg element, which models the solid-state diffusion at low frequencies [7]. The Warburg impedance is not used in this model here, which may lead to significant inaccuracies. However, determining the parameters of the Warburg impedance is complex and would impose additional difficulties when attempting to determine model parameters directly from step response data. It has to be seen whether replacing the Warburg impedance with a more simple RC combination can produce sufficiently accurate results.

Another more sophisticated model element that can be found in the literature is the constant phase element (CPE). CPEs are used to model the depressed semicircles in the high and middle frequency regions that can typically be found in impedance plots of batteries. Although the use of CPEs usually allows fitting the experimental data well, its physical meaning has not been clearly understood. CPEs have been interpreted in terms of phenomena associated with porous electrode structures, overlapping of several semicircles of different relaxation times [36].

The chosen model utilises three simpler RC combinations for characterising the dynamic behaviour of the cell terminal voltage, similar to a model that was suggested for lead-acid batteries [79]. It has to be evaluated whether this simplification is capable of representing the actual cell behaviour or whether it is required to employ more sophisticated model elements.

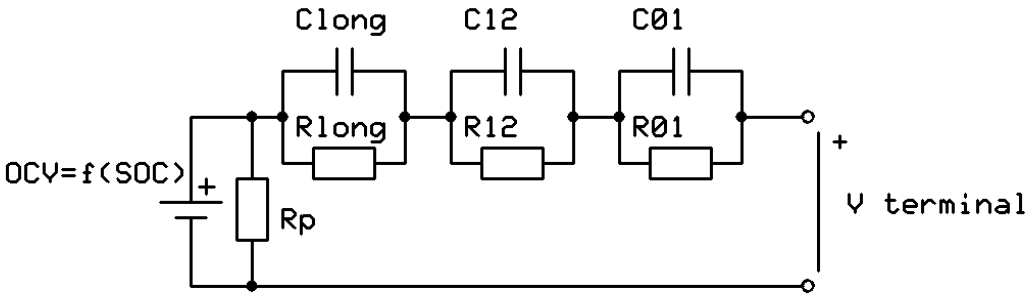

Figure 17 Typical battery model with 3 RC combinations and a resistor R_p for modelling self-discharge.

The resistance R_p models the self-discharge rate, which can be related to the electronic conductivity of the electrolyte. R_p is the only model parameter that cannot be determined from the step response tests. Apart from that, this type of model allows to determine the model parameters directly from the step response results.

The time constants of the three parallel RC combinations exhibit different orders of magnitude and the parameters of each RC combination can be determined individually by analysing the appropriate time window during the step response. However, the appropriate time windows are not yet known, since this would require determining the time constants. This however is one of the objectives of this investigation. Hence, the following analysis is based on an initial guess of suitable time windows.

The initial assumption is that the voltage response which is faster than the sampling rate can be pictured as an 'immediate' voltage response. This 'immediate' voltage response can be related to the ohmic impedance of the cells and is modelled with a resistor in parallel with a capacitor ($R_{01} \parallel C_{01}$). The resistance R_{01} models the magnitude of the voltage jump from V_0 to V_1. The capacitor C_{01} in parallel to it models the behaviour between t_0 and t_1. This capacitor value is important for studying the cell response to high frequencies. An example for this is the simulation of the behaviour when connecting switching converters or inverters. However, the high frequency behaviour is less important for system level simulation. Hence, C_{01} is not determined in this work.

The second assumption is that the voltage relaxation behaviour within the step response pause duration can be characterised with one exponential function, which can be modelled with another RC combination (R_{12} || C_{12}). This RC combination is assumed to represent the charge transfer resistance in parallel to the double-layer capacitance of the cell. The best fitting exponential function is shown as a dashed red curve in Figure 16. It is found using least-mean-squares fitting methodology. The time between t_0 and t_1 (5 seconds) is not taken into account when determining this best fit because the initial behaviour depends on ohmic resistance and surface films. The time constants due to double-layer capacitance and surface films are very different and it is not possible to find a good fit to the measurements by using a single exponential fit function. However, good correspondence between the curve-fit and actual measurement data could be found by omitting these first 5 seconds. The values R_{12} and C_{12} can be determined directly from the fitted exponential curve equation.

The last assumption is that the behaviour with any longer time constants can be described with another single exponential function. Though the voltage apparently approaches level V_2 in this figure, it should actually reach the OCV_{eq} if given an adequate period of time. This long-term behaviour is modelled with R_{long} and C_{long}.

4.5 Determination of SOC During Testing

The model parameters vary with different levels of state of charge. The battery model consists of several sets of model parameters and each set is applicable for a specific state of charge. The state of charge is the therefore the basis for all parameters and it is important to determine the state of charge during testing accurately in order to obtain a meaningful battery model.

4.5.1 Charged / Discharged Capacities During Testing

The preliminary tests are used to investigate the accuracy of state of charge determination during testing.

	33 A Test	**100 A Test**
Charged Capacity	101.6 Ah	101.6 Ah
Discharged Capacity	101.0 Ah	103.2 Ah
Difference	0.6 Ah	- 1.6 Ah

Table 4 Charge / discharge capacities during preliminary performance tests

Table 4 summarises the charged and discharged capacities in the preliminary tests. The first column is for the test cycle with 33 A charge and discharge current and the second column is for the cycle with 100 A. The first row shows the capacity charged into the cell, the second row shows the capacity discharged subsequently and the third row shows the difference between charged and discharged capacity.

For most batteries, one would expect a decrease in the available capacity at higher discharge currents. Peukert studied this in detail for lead-acid batteries [63]. The results of the preliminary tests as shown in Figure 13 and Figure 14 and Table 4 reveal that the tested specimen did not show this behaviour. Surprisingly, the available capacity at 100 A was even slightly higher than the available capacity at 33 A. This may be because the cell heated up much more during the test at a high current as shown in Figure 15. The cell heated up to 35ºC during the test with 33 A discharge current and it heated up to 46ºC during the test with 100 A discharge current. The surrounding temperature was 21ºC in both cases. The differences in temperature are due to self-heating during discharge.

The length of pauses every 10 % of SOC were increased from one minute to 15 minutes for all subsequent test cycles, in order to reduce the overall increase in temperature during a test cycle. The temperature could be controlled more precisely with water-cooling. However this would cause higher temperature gradients inside the large cell. It is important to keep the temperature gradients as low as possible for analysing dependencies on temperature.

The charge factor of lithium-ion batteries is theoretically close to one, because the lithium-ion cell chemistry does not exhibit capacity consuming side reactions. This means that recharging the cell requires the same amount of coulombs which have been previously discharged. Some designs of lithium-ion cell however exhibit capacity-consuming side reactions for improved safety and for keeping the cells balanced. It is essential to understand whether or not the charge factor is one. This is because coulomb counting can be a very precise method for determining the state of charge provided that the charge factor is one and that the coulomb counting is reset at a reference point from time to time. However, having no over-charge reaction means that the cells need to be actively equalised in order to keep them in balance. Coulomb counting is less suitable for cells with capacity-consuming side reactions but those

need no cell equalisation, and single cell voltage observation may not be necessary either.

4.5.2 Investigation of Error Using Balanced Capacity Counting

Table 4 revealed that the differences between discharged and recharged capacities for the tested specimen were very small if compared with the total capacity. The difference was smaller than 1.6 % and, in the second test, with 100 A, the cell actually discharged more capacity than it had been charged with previously. This indicates that capacity consuming side reactions are not significant for this specimen but more tests are required in order to confirm this.

The fact that the cell discharged a higher capacity than it was previously charged with could be due to measurement errors. The capacity was measured by integrating the actual current over time:

$$Q = \int I(t)dt$$

An inaccurate time base cannot produce any difference between the charged and the discharged capacity within one test cycle, because it applies to charging and to discharging and it would cancel itself out. An offset of ΔI in the measured current however would accumulate. The measured capacity during discharge can be expressed as $Q_{measured,discharge} = \int (I(t) + \Delta I)dt$ and, assuming ΔI to be a constant offset error, the measured capacity during charging can be expressed as $Q_{measured,charge} = \int (I(t) - \Delta I)dt$. The measured difference between discharged and recharged capacity becomes:

$$\Delta Q_{measured} = Q_{measured,discharge} - Q_{measured,charge} = \int_{T_{discharge}} \Delta I dt + \int_{T_{charge}} \Delta I dt$$

The specifications of measurement errors of the battery tester suggest a maximum offset error of ΔI = 50 mA. The total time $T_{discharge}$ for discharging was 3 hours but the total time T_{charge} for charging was 4.7 hours due to the decreasing current at the end-of-charge. The times for pauses were subtracted from the above values because

the battery tester measures no current during pauses. The total difference in measured capacity due to offset errors can now be calculated:

$$\Delta Q_{measured} = 3h \cdot 50mA + 4.7h \cdot 50mA = 0.385Ah$$

Hence, measurement errors alone cannot explain this difference of 1.6 Ah between charging and discharging. Other factors, such as differences in the test conditions or using an unsuitable reference condition, have to be considered as causes of this error.

4.6 Investigation of Reference Condition for Test Series

4.6.1 Cycle Definition

During preliminary testing, all cycles started with charging and ended in a discharged state of the battery. Some of the initial tests have shown that this would cause problems during a series of tests, which need to be carried out at different conditions in order to characterize the cell performance. The SOC in the beginning of the actual test is always the same as the SOC at the end of discharging in the previous test. Ideally, this SOC would represent an 'empty' battery but, in fact, this SOC is very dependent on the test conditions, such as temperature and current.

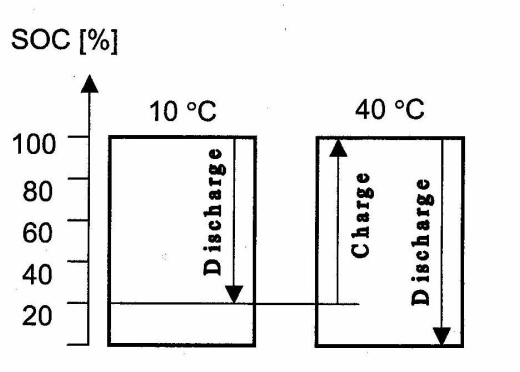

Figure 18 Example of two tests, where both cycles start with charging

Figure 18 shows two successive test cycles. The first test does not fully discharge the cell. A residual SOC of 20% remains in the battery, due to low temperature. The second test starts at this same 20% level of SOC and, thus, this 20% SOC remains untested during charging in the second test cycle.

Another drawback is that all test cycles would have to use the SOC of the previous one as a starting value for counting the coulombs in order to determine the SOC during the test. Unfortunately, one cannot rely on Ah counting for determining the SOC during all subsequent cycles in a series of tests, because the balancing Ah counting drifts with time due to offset errors in the current measurements. Frequent calibrations with a reference state are required in order to overcome this problem.

A full discharge is a poor reference point for most batteries, since the cell usually holds a residual capacity, which depends significantly on the test conditions. The tested 50 Ah specimen showed a difference in residual capacity of 9 Ah (18 %) when discharging at 10 °C if compared with discharging at 40 °C. This would be an unacceptable reference throughout the testing.

4.6.2 End-of-Charge Determination

It is assumed that that a full charge according to the battery manufacturer's recommendations would provide a reference for the state of charge calculation. Ideally, every test cycle should be independent of previous tests and should start in a known condition, and this is why all subsequent tests described in this work start with discharging and end with a charged battery. Every test cycle starts with a fully charged cell regardless of the prevailing test conditions. However, specific preliminary tests were carried out in order to investigate whether this assumption could be made:

The charging procedure used for this investigation was a CC-CV charging. The charging voltage in the constant voltage phase was chosen to be 4.2V (temperature independent). The charging was stopped as soon as the current reached 0.01C (temperature independent).

The following figure shows the charged and discharged capacities in some of those test cycles.

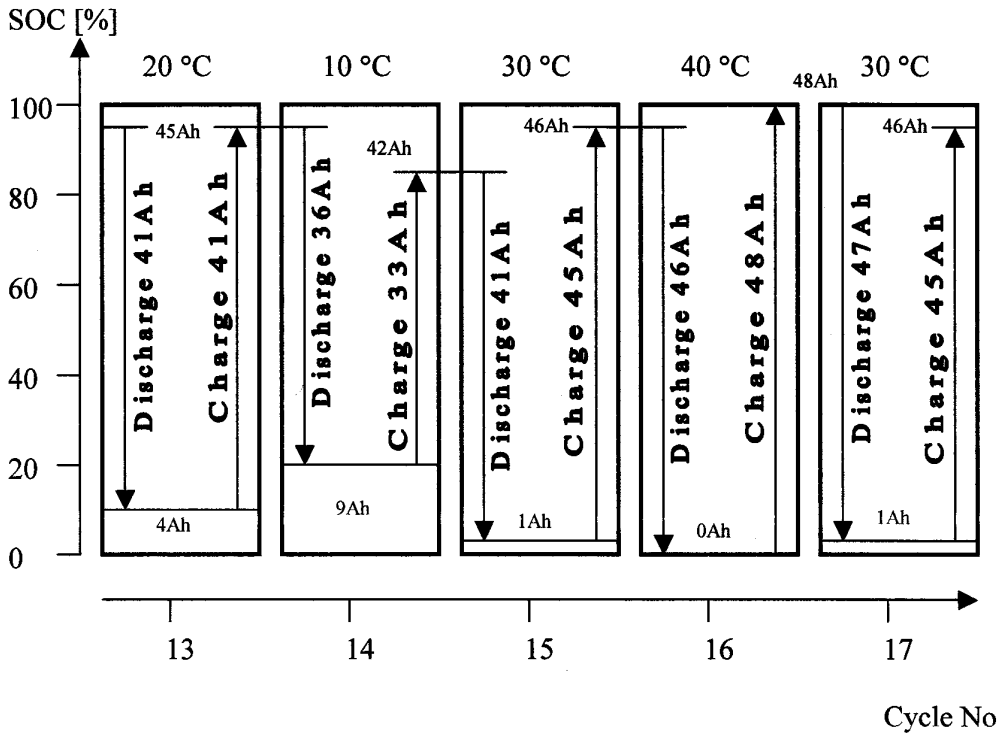

Figure 19 Development of cell capacity during preliminary test cycles without reference point

It can be seen how charged and discharged capacities relate to the state of charge at the end of charge and discharge respectively. It can clearly be seen that the assumption of "fully charged cell" after charging with manufacturer's recommendations cannot be made. Their end-of-charge determination method was insufficient for reaching a consistent state of charge at the end of each test cycle.

The state of the cell at the end of each cycle is dependant on the temperature during that cycle. This is unacceptable for a comprehensive series of test cycles.

Figure 19 shows how the state of charge had to be tracked over the series of tests, at different temperatures, in order to determine the state of charge at any time. Drift will occur due to offset measurement errors when relying purely on such a coulomb counting method and this would lead to significant errors during testing. It has been shown in subsection 4.5.2 that the capacity drift error can be about 0.385 Ah when

testing the 100 Ah cell on the 100A Digatron battery tester. This is 0.385 % per cycle. In the conducting of a series of about 50 tests, this error would accumulate to about 19% if there were no reference points and clearly is an unacceptably high degree of error.

Additional tests were conducted in order to find an end-of-charge determination method as a suitable reference condition, so that the above requirement of independent cycles could be met: These tests are discussed in the following chapters.

4.7 Summary of Preliminary Tests and Design of Experiments

The pause duration for measuring the performance at different SOCs during the preliminary tests was one minute. This time was insufficient for the cell to reach equilibrium. The chosen pause duration is 15 minutes each for the main series of tests in order to determine the OCV more accurately and also to provide more data points for characterising the slow diffusion behaviour of the test specimen. With 15 minute long pauses, each test cycle can still be completed within 24 hours including sufficient resting times between the test cycles.

Whether 15 minute long pauses will significantly improve the determination of the equilibrium open circuit voltage is currently unclear. A novel test is proposed and discussed in the next chapter in order to determine the $OCV_{eq}(SOC)$ curve.

Figure 15 shows that the pauses of one minute are not sufficient to keep the temperature constant during cycling. Longer pauses give the cell more time to cool down, so that the cell temperature stays closer to the controlled temperature in the temperature chamber. The increase in cell temperature during discharging is reduced and this makes it easier to directly compare performance characteristics at different discharge rates, or at different ageing states, because temperature changes as a major influencing factor are reduced.

In the preliminary performance tests, the pauses during discharging were not aligned with the pauses during charging. The discharging was paused at different levels of SOC than the charging. A more sophisticated SOC based test procedure is employed during the main test series. This pauses the charging at the same levels of state of charge where it is paused during the previous discharging within the same test cycle.

This way, the pauses are aligned and this helps determining the true OCV_{eq} more directly by averaging the apparent equilibrium values from charging and discharging. Furthermore, the charge/discharge performance can be compared more directly.

During the preliminary tests, the data logging was configured in such a way that it would take measurements on a time basis (once every second or once a minute). These sampling rates did not seem optimal. Too many redundant data points were logged on some occasions. On others too few were taken. For subsequent tests, the sampling rate was changed to dynamic sampling, where a measurement is triggered if the measured voltage changed by more than 2 mV. Additionally, it is triggered if the measured current changed by more than 0.5 A. With this configuration, the number of measurements is kept small when no changes occur and high sampling rates are achieved when rapid changes take place. It ensures reliable measurements in constant current phases as well as in constant voltage phases.

It also resolves the problem that occurred during the preliminary performance tests as shown in Figure 16 and discussed in subsection 4.4.1. Here, no measurements were taken for some time after reapplying the current, which caused uncertainty as to the behaviour of the cell voltage during that time.

All preliminary test cycles started with charging. This causes problems in a series of tests under different conditions. Test cycles are not independent from each other as discussed in subsection 4.6.1. Ideally, every test would be independent of every other test in a series. And so, every test cycle in the main series of tests starts with discharging, followed by charging after a resting time in order to achieve this.

During preliminary tests, the cell voltage still changed significantly at the end of the one-hour long resting time between the two tests. Potentially, this is because it has not reached equilibrium yet. However, the cell temperature did not reach its ambient temperature within that time either and this may also cause the cell voltage to continue to change. It is important to have a stable cell temperature and voltage in the beginning of each test, so that the cell is in a known state. Ideally it reaches equilibrium in terms of its electro-chemistry as well as thermally. Hence, for the main series of tests, the resting time between all test cycles is increased. On the other hand, resting for too long increases the total time required for testing. A novel test is

proposed and discussed in the next chapter in order to determine, whether a subsequent test cycle can be affected significantly by the previous test cycle and in order to determine an optimum resting time between two test cycles.

Preliminary tests and also the mentioned resting time tests revealed that the tested specimen reaches equilibrium so slowly that it is unclear whether the cells actually exhibit a hysteresis phenomenon as known from NiMH cells. Dedicated tests are proposed and discussed in the following chapter in order to investigate this.

An interesting finding during the preliminary performance tests is that the cell released almost the same capacity regardless whether the discharge current was 33A or 100A. This is in contrast to what is known from lead-acid batteries and to the findings of Peukert [63]. This issue is investigated and discussed separately with dedicated novel tests in the following chapter.

Preliminary tests have revealed, that the end-of-charge determination as suggested by the manufacturer could not provide a suitable reference condition. An accurate end-of-charge determination is important and some dedicated tests are proposed and discussed in the following chapter in order to achieve consistency.

The following design of experiment is used for the main series of tests in order to determine and validate a suitable reference condition at various conditions. One specific condition (charging at 25°C at 15A) is chosen as a reference. Some recharges are based on coulomb counting but this reference charging is used frequently throughout the tests in order to avoid an unnoticed drift in the state of charge.

The type of cell that is used for testing showed degradation during earlier tests [1]. Three different measures are built into the design-of-experiment in order to cope with degradation during the tests:

1. The test conditions are chosen randomly in order to minimise systematic errors.

2. One test condition is chosen as a reference. It is applied from time to time, so that the degradation can be quantified and eliminated during later analysis.

3. The test conditions at the beginning of the series of tests are repeated at the end, so that the degradation elimination method can be verified.

Most batteries show a high performance variation during the first cycles. The tested cell is cycled several times before starting the actual series of tests in order to minimise this problem.

Cycle number		Ambient temperature in temperature chamber [9]						
		-15	**-5**	**5**	**15**	**25**	**35**	**45**
Discharge current [A]	**5**	32	33	34,57	35	36,52	37	38,72
	15		29	28,55	20,49	19,22,43,44,45,51,56,66	21,46	23
	30			31	27,48	26,50	25,47	24
	45				41	30,53	40	39

Table 5 Design-of-experiment.

Table 5 shows the design-of-experiment. The series of test cycles is randomly chosen in order to implement the measures mentioned above. The first 18 cycles are used for reaching stable cell performance and also for some preliminary tests. The cycle numbers that are not shown in the table above are used for other tests, such as, for example, OCV tests. Seven different temperature settings between –15°C and 45°C and four different discharge currents between 5 A and 45 A are chosen. Higher discharge rates are omitted at lower temperatures, as indicated by the grey area in Table 5.

5 Results and Discussions

This chapter presents and discusses the results from the main series of tests and from some specific test.

5.1 Direct Determination of Model Parameters from Preliminary Tests

One objective of this work is to directly determine model parameters from step response test results. A suitable battery model that could facilitate the direct determination of its parameters was chosen and described in subsection 4.4.2. This section here generally refers to the battery model shown in Figure 16. The following subsections describe the process and evaluate the results based on the test data gained from the preliminary tests.

5.1.1 Immediate Voltage Response – Ohmic Resistance

In each pause during charging and discharging, the voltage rises immediately after the current has stopped. This immediate step in voltage is defined as

$$\Delta V_{01} = |V_1 - V_0|$$

It is assumed that this immediate change in voltage can be related to the internal ohmic resistance R_{01} of the battery. The voltage across the RC combinations $R_{long}C_{long}$ and $R_{12}C_{12}$ does not change significantly during this time. This immediate voltage response is in the order of milliseconds, whereas their time-constants are of a different order of magnitude. This aids to calculate the resistance R_{01} for charging and for discharging at various SOC, based on the following equation:

$$R_{01} = \Delta V_{01} / |I|$$

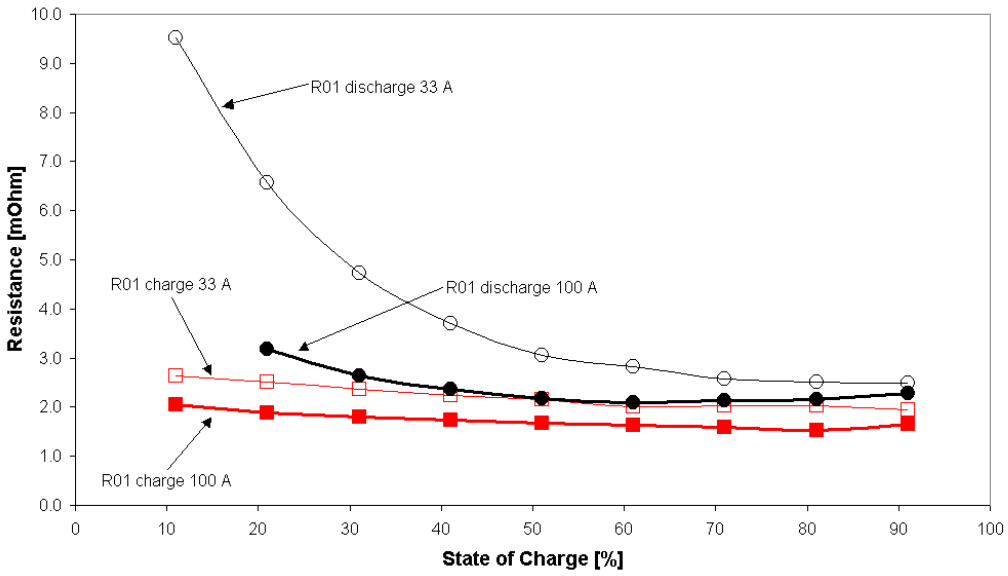

Figure 20 Internal resistance R_{01} as a function of SOC during charging and discharging obtained from different tests (temperature not constant).

Figure 20 shows the result of this analysis. The two top curves show the resistance R_{01} during discharging as a function of SOC. One is obtained from the 33 A test and the other from the 100 A test. The two other curves show the equivalent results for charging.

R_{01} usually models the electronic resistances in the current collectors and terminals and the ionic resistance of the electrolyte. Hence it should be more or less independent on the SOC. However, Figure 20 reveals that this resistance increases substantially at lower SOCs during discharge. This increase is less apparent at a higher discharge current and even less evident but still noticeable during charging.

Considering some typical impedance spectra of lithium-ion cells, the first semi-circle corresponds to the charge-transfer process. The typical time constant of the double layer capacitor in parallel to this charge transfer resistance is in the order of 0.1 ms to 80 ms. The 80ms were derived from C_{dl} = 0.4 F and R_{ct} = 0.2 Ω for a CGR17500 li-ion battery [11] and the 0.1 ms were derived from a typical impedance plot shown in the same reference. Here, in these tests, the first 5 seconds of the step response were taken into account for determining the ohmic resistance of the cell. This suggests that the charge transfer resistance was partly included in the measurement of R_{01}, which was believed to be the ohmic resistance. This could explain why the R_{01} as shown in Figure 20 increases at low state of charge. The ohmic resistance, in theory, is

independent of the SOC, whereas, the charge-transfer resistance does depend on the SOC because it is related to the concentrations of active species.

Additionally, the sampling rate of 1 s^{-1} during the preliminary tests is too slow for determining the electronic resistance of the cell. The maximum possible sampling rate of the battery tester (100 Hz) is used during the main series of tests in order to be able to distinguish between charge transfer resistance and ohmic resistance in the beginning of each voltage relaxation period.

5.1.2 Charge Transfer Resistance and Double Layer Capacitance

Similarly, the resistance R_{12} can be determined using the following equations:

$$\Delta V_{12} = |V_2 - V_1|$$

$$R_{12} = \Delta V_{12} / |I|$$

Again, the voltage across the RC combination $R_{long}C_{long}$ is not changing significantly during this time, because it has a time constant which is at least one order of magnitude higher. The voltage across $R_{01}C_{01}$ however is not changing significantly anymore, because its time constant is much shorter and has reached a stable voltage value already.

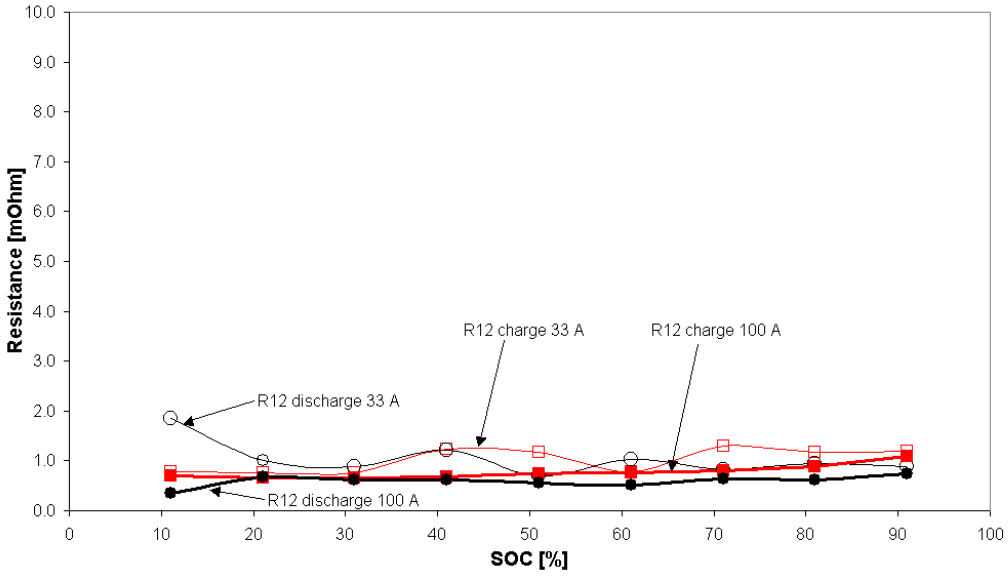

Figure 21 Internal resistance R_{12} as a function of SOC during charging and discharging with 33 A and 100 A (temperature not constant).

Figure 21 shows the resistance R_{12} as a function of SOC during discharging and charging with 33 A and 100 A. The scale on the y-axis is the same as in Figure 20 so that the magnitudes of these two resistances can be compared directly.

The second RC combination in Figure 17 with R_{12} and C_{12} is supposed to model the double-layer capacitance in parallel to the charge transfer resistance. The results shown in Figure 21 show constant resistance over the whole range of SOC and also at different currents. This is surprising because the charge transfer resistance is known to be non-linear with current and it should also be strongly dependant on the state of charge. However, it was revealed in section 5.1.1 that part of the actual transfer resistance was considered to be the ohmic resistance. Taking this into account, the transfer resistance would actually look similar to Figure 20 and not like in Figure 21. This would agree much better with the theory of non-linear charge transfer resistance.

However, the charge transfer resistance during charging seemed higher at low SOC if compared with high SOC though it should be smaller. A possible explanation for the increase of the charge resistance at low SOC is a growth of solid electrolyte interphase (SEI) on the positive electrode surface. It is interesting to note that the voltage drop or rise within the time of 5 seconds to 1 minute after the current step is proportional to the current and independent of temperature and state of charge, as revealed in Figure 21.

5.1.3 Diffusion Impedance

This subsection focuses on the voltage difference between V_2 and the average of the OCV region. The average of the OCV region is called OCV in this section. Though the graph in Figure 16 suggests that the cell voltage approaches level V_2, additional tests have revealed that it actually approaches OCV, if given an adequate period of time. See the section on OCV(SOC) determination, section 5.3.

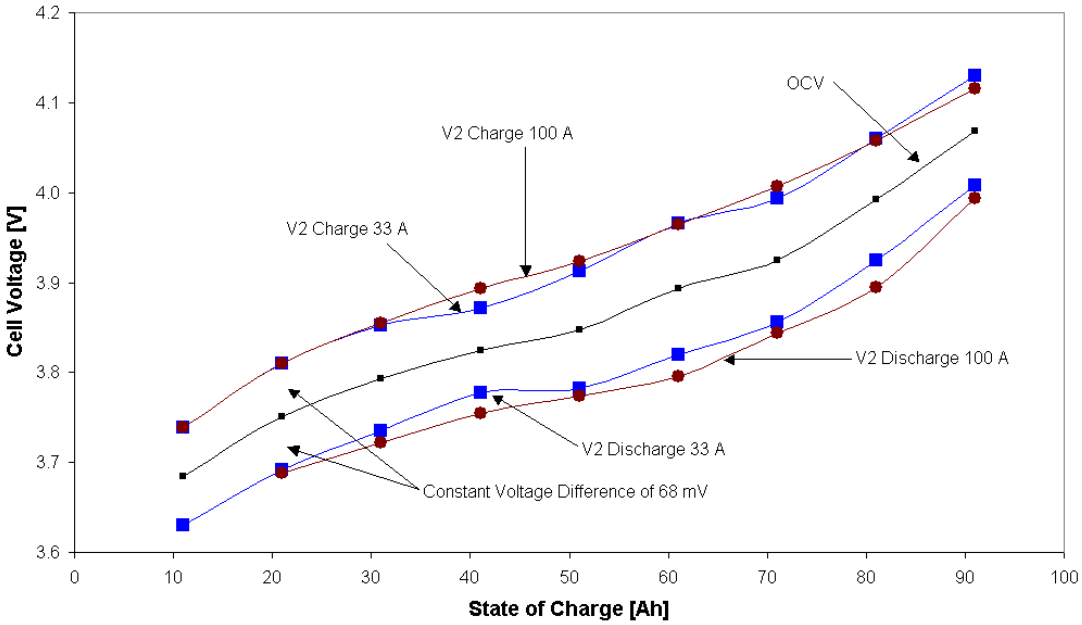

Figure 22 V_2 During charging and discharging at 33 A and at 100 A and OCV over SOC

Figure 22 shows the level V_2 over SOC for charging and discharging, at 33 A and 100 A, and the OCV over SOC. It reveals that the level of V_2 is independent of the current. The difference between V_2 and OCV for SOC levels between 10% and 90% is a constant 68 mV measured with a standard deviation of 12 mV. This difference is the same for charging and discharging. Temperature changes are significant during this test and V_2 shows no relation to the temperature changes either.

5.1.4 Modified Equivalent Circuit Model

The typical battery model as shown in Figure 17 is used as the basis for determining model parameters. However, Figure 22 reveals that the long term voltage relaxation difference $|V_2 - OCV|$ appears to be independent of the current. This difference for SOC levels between 10% and 90% is a constant 68 mV measured with a standard deviation of 12 mV. It is also the same for charging and discharging and it shows no relation to the temperature changes during tests.

This means that this long-term voltage response behaviour can be modelled with a Zener diode instead of using a resistor, because the voltage drop is constant and not proportional to the current. Figure 23 shows the equivalent circuit model that is based on this approach. The OCV or electromotive force (EMF) is modelled as an ideal voltage source that is a function of the SOC.

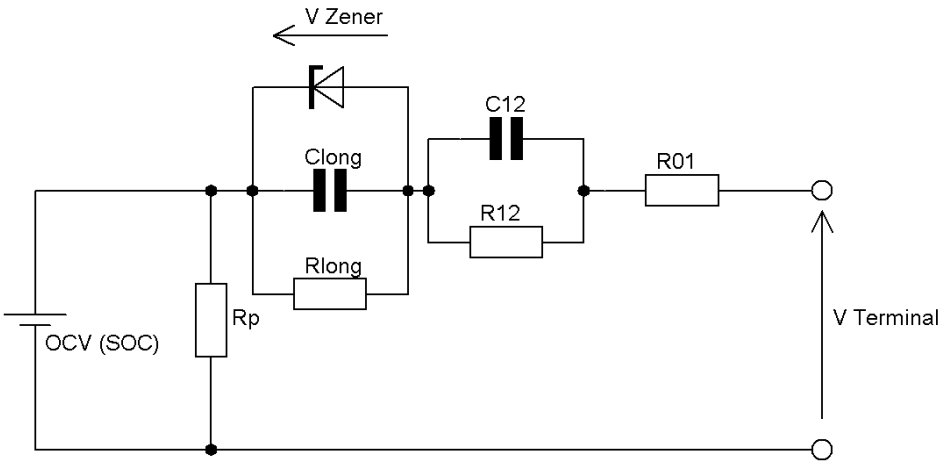

Figure 23 Battery model according to the parameter analysis based on the preliminary test results

However, some tests that are discussed later in the thesis (hysteresis test, conventional OCV test with long resting times) reveal that the long time constant modelled with R_{long} and C_{long} is in the order of several hours and thus longer than the whole test procedure. The above method for determining R_{long} on the other hand assumes that C_{long} is fully charged before every pause, which is clearly not the case. In fact, the current bursts are relatively short if compared with the time constant of R_{long} and C_{long}, so that ignoring R_{long} and just considering the current through C_{long} can model the voltage drop:

$$\left|V_2 - OCV\right| = \sum_{\text{dischargebursts}} \left[\int_{\text{tburst}} Idt \right]$$

In this case, however, the voltage difference goes up during charging and goes down again during discharging. Whether this actually agrees with the practical behaviour cannot be studied without validating the method for true OCV determination first.

5.2 Reference Condition During Testing

This section presents the results and discusses the methodology of the tests that are conducted in order to find an end-of-charge determination that is suitable as a reference point for resetting the coulomb counting. The first subsection is on determining the temperature dependency of the end-of-charge voltage (EOCV), the

second subsection is on determining the temperature dependency of the end-of-charge current (EOCC) and the third subsection is on validating the end-of-charge determination method.

5.2.1 The EOCV as a Function of Temperature

The following test is conducted in order to quantify the EOCV level and its dependency on the temperature. A cell is fully charged and, after a resting time of several hours, the cell temperature is cycled in a temperature control cabinet. The temperature is changed with a rate of 6 K/h. This rate seems reasonably slow for minimising temperature gradients inside the cell but fast enough in order to ignore self-discharge activity and to keep the testing time requirements within acceptable limits. Cycling over each temperature setting several times allows to validate the results. The cell voltage is logged during this process.

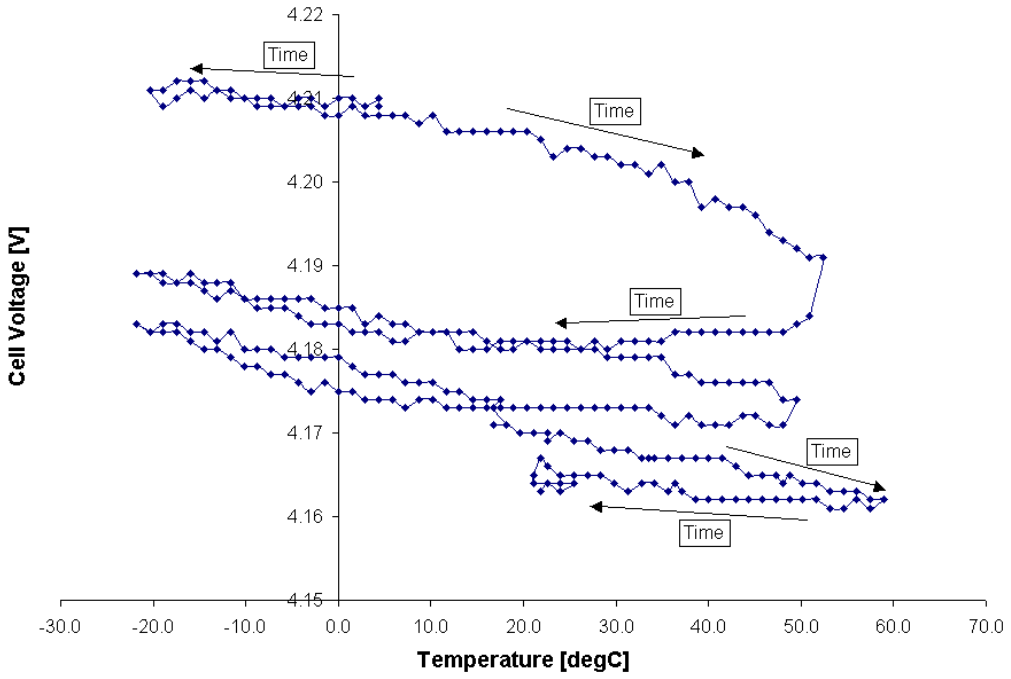

Figure 24 Development of the voltage of a fully charged cell during temperature cycling with an insufficient resting time after the last charging

Figure 24 shows the result of these tests. The cell voltage is plotted over temperature. It can be seen that no consistent cell voltage values are measured during this test. It can be assumed that the cell had not reached equilibrium before starting the test despite a long resting time of several hours. The same test is repeated but with a very long resting time of 20 days after the last charging.

Figure 25 shows the result of the refined test for measuring the open circuit voltage at true equilibrium of a fully charged cell as a function of cell temperature.

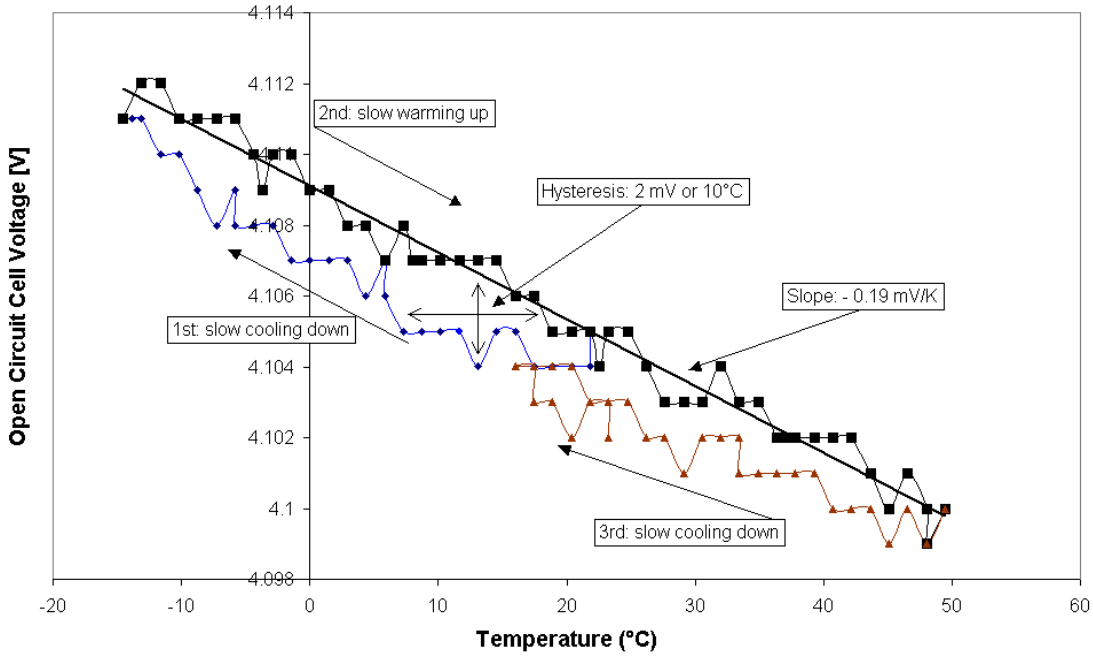

Figure 25 Development of the open circuit voltage during temperature change.

Initially, the cell voltage rises during cooling down (blue part of the curve). The rate of temperature change for this part of the test is -20 K/h. Then the voltage falls during warming up (black part of the curve). The rate of temperature change for this part of the test is 6 K/h. Finally the voltage increases again during cooling down until the starting temperature is reached (brown part of the curve). The rate of temperature change for this last part of the test is -4 K/h. The voltage at the end of the test is approximately the same as at the start of the test. However, a hysteresis of approximately 2 mV or 10°C can be seen. All single measurements are shown in the figure and they are connected with lines in chronological order. The measurements during the continuous warming up (black) are considered for obtaining a best-fit curve.

Figure 25 shows that the temperature dependency of the tested specimen is linear with a slope of -0.19 mV/K. This is a total of 11.4 mV over the whole temperature range during the series of tests. Considering that the error of the voltage measurement is ±5 mV as stated in Table 3, this is a very small voltage change. Also, most practical

battery management systems would experience difficulties trying to utilise this dependency in a significant way.

However, it is interesting to investigate how much this temperature dependency of the EOCV contributed to the inconsistency of the end-of-charge determination method, which was used in the preliminary tests. The slope of the OCV (SOC) for a 50 Ah cell is not more than 0.15 Ah/mV. This means that the difference of 5.7 mV of EOCV between 10 °C and 40 °C equates to not more than 0.855 Ah difference in SOC (1.7 % error in SOC for the 50 Ah tested specimen). The measured difference in the preliminary tests however was 6 Ah. This means, that the temperature dependency of the EOCV contributed only to about 14 % of the whole inconsistency. The remaining 86 % must be accounted for by making the EOCC temperature dependant, and this is discussed in the next subsection.

An interesting phenomenon during temperature cycling is the small hysteresis of about 2 mV that can be seen consistently in Figure 25. On the graph, start and end points join each other, which demonstrates the repeatability of this test. Also, it proves that significant self-discharge did not occur. The temperature is changed very slowly; so that temperature gradients inside the cell cannot contribute to this phenomenon.

One possible explanation is a slow formation and relaxation of concentration gradients but this would require net electrode reactions and ion movement, which seems unlikely. Furthermore, the relaxation is much faster at higher temperatures and one would expect a smaller hysteresis at higher temperatures when compared with the hysteresis at lower temperatures. This could not be observed. It remains fair to say that this temperature-voltage hysteresis phenomenon still is poorly understood.

5.2.2 Temperature Dependency of the EOCC

It is not necessary to reach a *fully* charged state at the end of charging under all test conditions but it is essential to reach the *same* state of charge under all conditions in order to obtain consistent results. The following tests determine the end-of-charge current as a function of temperature so that the SOC is the same regardless of the prevailing temperature during that test

No separate tests are conducted in order to determine the EOCC at various conditions. Instead, this investigation is actually part of the main series of tests for determining performance and degradation as described in section 4.7. This significantly helps reducing the overall time for testing. However, it is important to implement means of validating the results for this particular issue so that the state of charge can be established reliably throughout the tests. The SOC is a key foundation to the testing and later analysis.

The following reference charge cycle is defined for validation and for resetting the coulomb counting. With a surrounding temperature of 25°C, as controlled in the temperature control cabinet, the cell is charged using a CC-CV regime. The charging current during the constant current phase is 15A. The manufacturer recommended at that time a maximum charging voltage of 4.25V per cell, regardless of temperature. The test described earlier revealed that the OCV and, hence, the EOCV, is temperature dependant with a linear relationship of approximately -0.19 mV/K. The minimum temperature considered for testing is -60°C because this is the minimum permitted temperature as specified by the manufacturer at that time (in year 2002). At this temperature, a maximum permitted charging voltage of 4.25V should be applied. The charging voltage at higher temperature has to decrease with the rate mentioned above. Hence, the end-of-charge voltage setting at reference condition (25 °C) is as follows.

$$\mathrm{EOCV}(25°\mathrm{C}) = 4.25\mathrm{V} + \left(-0.19\,\tfrac{\mathrm{mV}}{\mathrm{K}}\right)\cdot\left[25°\mathrm{C} - \left(-60°\mathrm{C}\right)\right] = 4.234\mathrm{V}$$

The cell is considered fully charged under these defined reference conditions when, during the constant voltage phase, the current drops below 0.01C, which equates to 500 mA for the tested 50 Ah cell.

The aim of the investigation described here is to determine the end-of-charge current at other temperatures so that the amount of charge supplied during charging becomes independent of the cell temperature. Coulomb counting is used to determine the end-of-charge at temperatures, other than 25ºC, throughout the series of tests. The charging is stopped after returning as many Ah as had been previously discharged in that cycle. The end-of-charge current I_{EOC} is the current that is reached just before the

charging is switched off. This end-of-charge current is recorded as a function of the temperature setting in that particular test cycle.

Using coulomb counting for fully recharging the cell assumes a charge efficiency of 100%, which can normally be expected for lithium-ion cells, as discussed in the literature review. However, frequent repetitions of reference-cycles and thus reference-charging are conducted in order to verify this assumption. Furthermore, this measure is important in order to prevent or detect any drift in SOC due to systematic errors in current measurements or coulomb counting.

It is found for the tested li-ion specimen that the charging time for recharging the discharged capacity increases dramatically below 15°C. Charging times of up to 18 hours are required in order to fully return the discharged capacity at 15°C. About 22 hours are required at 5 °C in order to recharge only 90% of the capacity. At least additional 33 hours would be required in order to replace the remaining 10% at the final rate of about 150 mA. These waiting times are not acceptable during a series of tests.

The following methodology is applied in order to cut waiting times down at temperatures below 15°C. The charging is stopped before it is complete. The time requirement for this *main charging phase* is between 3 to 22 hours. Subsequently, the cell is heated up to the reference temperature (25°C) and charging continues to the reference EOC determination I_{EOC}(25 °C) = 0.5A (finishing charge). Coulomb counting is used in the following way for validating this procedure. The main charging returns the capacity Q_{cha} and the 'finishing charge' should always return the 'missing capacity' Q_{fin}. The total charge $Q_{tot} = Q_{cha} + Q_{fin}$ should return the previously discharged capacity $Q_{dis,}$ if this method is valid.

The following figure shows the EOCC that is determined as a function of cell temperature.

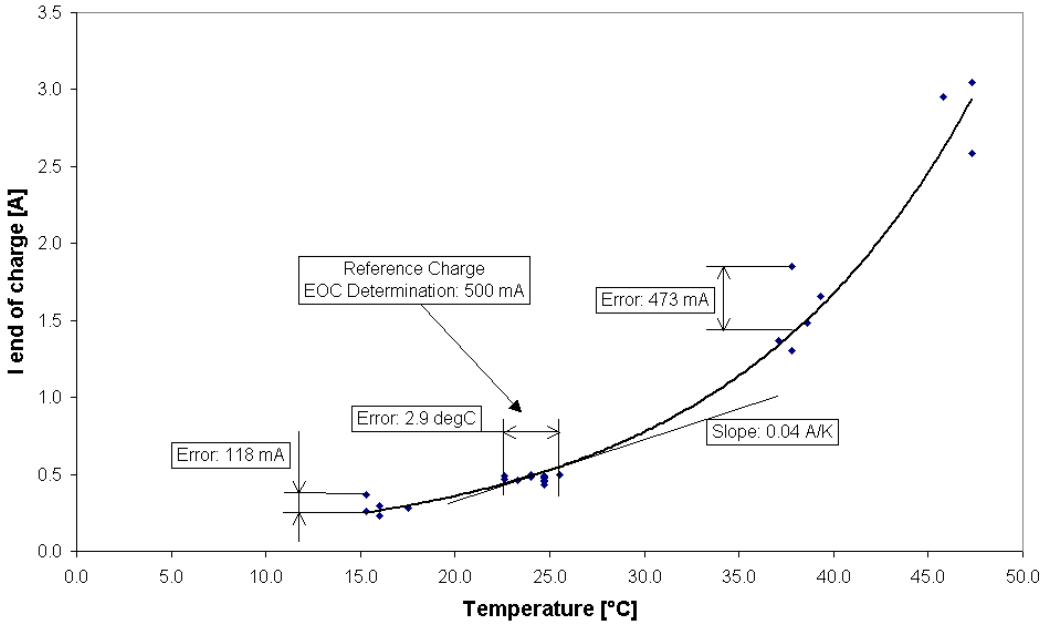

Figure 26 End-of-charge current for reaching a consistent 'full' charge as a function of temperature.

Figure 26 shows the EOCC(T) that is required in order to reach a consistent SOC at the end of each charge during the actual test series. The temperature shown here is the actual cell temperature measured at the end of charging. All measured values are shown as separate points and an exponential best-fit curve is indicated.

25°C is the reference temperature complying with the manufacturer's recommended EOCC(25 °C) = 0.5A. At higher temperatures, the cell reaches the same state of charge much earlier and the current only needs to drop down to about EOCC(35 °C) = 1.5A or EOCC(45 °C) = 2.7A. The charging at lower temperatures takes much longer, and the current has to drop down to lower values, for example, EOCC(15 °C) = 0.3A. At even lower temperatures, the 'full' state of charge cannot be reached within a reasonable amount of time. Hence, no measurements are shown in Figure 26.

5.2.3 Errors During Determination of the EOCC

The error of the temperature setting at reference condition (25 °C) is a total of 2.9 K, as indicated in Figure 26. This is due to offset errors of the temperature-controlled cabinet. The EOCC (temperature) curve has a slope of about 0.04 A/K at 25 °C as can be seen in Figure 26. This means that this temperature error equates to an error of 116 mA in EOCC.

Determining the slope of the EOCC (T) curve is part of this investigation and this slope was unknown before the time of testing. Hence, no adjustments to the EOCC were made during testing. Instead, the EOCC compensation was omitted and this can be translated into a difference in recharged capacity at reference conditions. For further investigation, a typical reference cycle (5th test at 25 °C 15 A) is employed in the following paragraphs.

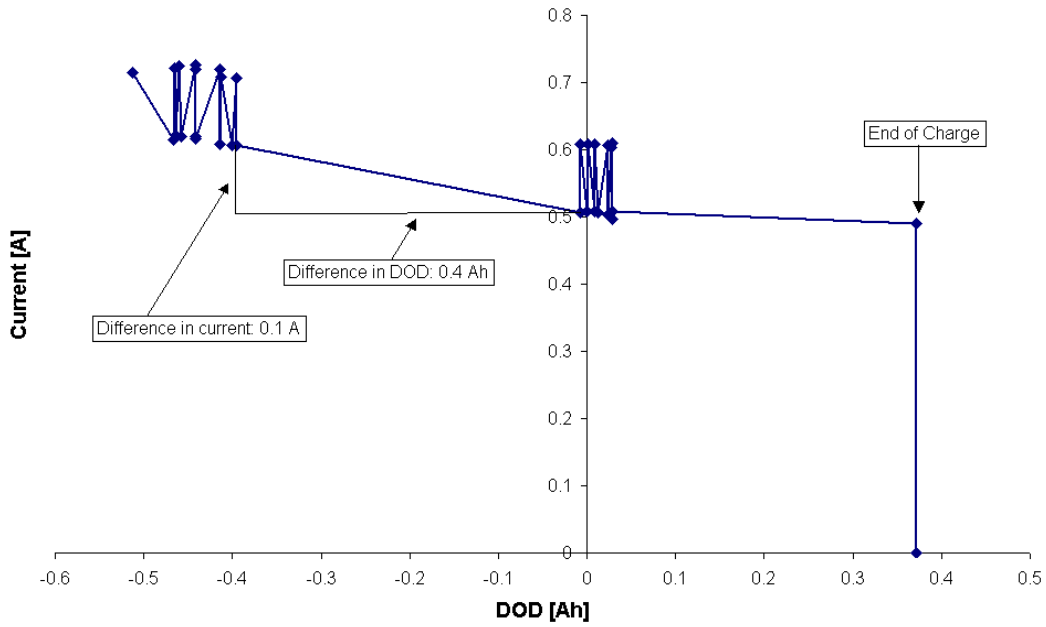

Figure 27 Current over DOD at the end of a typical reference cycle

Figure 27 shows the current over DOD at the end of this reference cycle. It can be seen that the error of 116 mA in the current causes an error of about 0.5 Ah in recharged capacity. Apparently, the current seems to toggle between two values from time to time. This problem is typical for that battery tester at the end of charging. The toggle difference is about 100 mA. This is much larger than the current measurement precision of that tester and, hence, it can be assumed that the toggling is

due to some instability in the closed loop control in the constant voltage charging phase at low currents. However, in a worst-case scenario, the total error of this method for recharging at reference conditions is about 0.5 Ah.

The other interesting question is to investigate how precise this method is at other temperatures. Figure 26 shows the two potentially largest errors in EOCC during the tests. The largest absolute error is 473 mA at a setting of 35°C (about 34% relative error). However, the largest relative error is in a test at 15°C. Here, the absolute error is 118 mA (about 47 % relative error). Using typical cycles at these temperatures, one can obtain the equivalent error in capacity in the same way as shown in Figure 27. The error at 15 °C is about 1.8 Ah (3.6 % of total capacity) and the error at 35 °C is about 0.5 Ah (1.0 % of total capacity). Errors at 45 °C are smaller.

This error in EOCC at temperatures other than the reference temperature stems from various sources. One of the causes is the error in temperature setting at reference conditions, which results in an error in recharged capacity, as discussed earlier.

Another source of error stems from the fact that the charging is paused every 10 % of SOC. Due to the relaxation phenomenon, the determined EOCC is generally higher if this pause is closer to the end-of-charge. This happened, for example, in the test with the highest error (15 °C, 45 A). The charging current over SOC for this test is shown in the following figure.

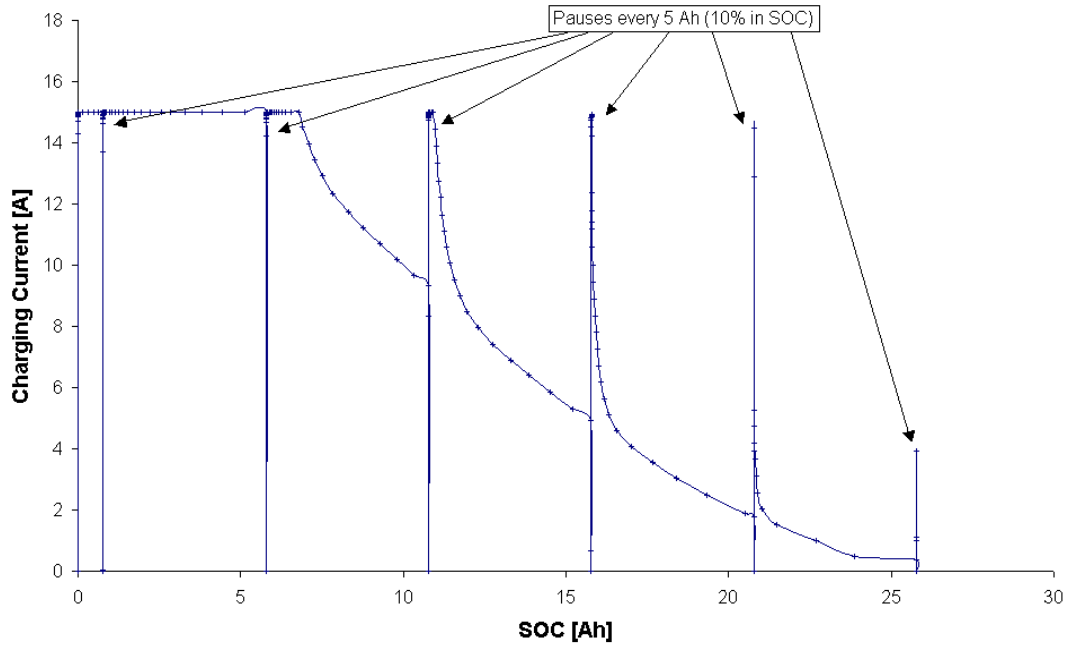

Figure 28 Charging current in a test with the pause right before the end-of-charge

It can be seen that the last pause occurs right before reaching the end of charge. No significant capacity is recharged after this pause. The EOCC for this temperature, determined here in Figure 28, is much higher than it would be if this pause had been suppressed. This is a clear disadvantage of using the normal test cycles with the pauses not only for determining performance parameters, but also for determining the EOCC. However, as a suggestion for future testing, such pauses just before the end of charge should be suppressed. In the case of a reference cycle, this can be achieved by letting the charge finish without any pause once the current has almost reached the EOCC. For other cycles, the pause should be suppressed once the capacity to remain recharged is close to zero. A similar method may be useful towards the end of discharge in order to improve the consistency of results for the available capacity as a function of discharge conditions.

5.2.4 Validation of End-of-Charge Determination Method

The end-of-charge determination was not a stand-alone test. This investigation was part of the series of test cycles that were conducted for determining cell performance characteristics. This validation here is required in order to assess whether significant drift in coulomb counting occurred throughout the series of tests. The reference

charging condition is a full recharge at 25 °C with 0.3C initial current and an EOCC of 0.5 A. This reference charging condition applied at most cycles at reference condition (25 °C) and, additionally, in the 'finishing charge' at all cycles at temperatures below 15 °C, as outlined in subsection 5.2.2. The reference charge provides a defined state of charge and is used to calibrate the coulomb counting between the cycles at different temperatures. The following figure compares the recharged capacities in these reference charges with the discharged capacities in the same cycles, respectively.

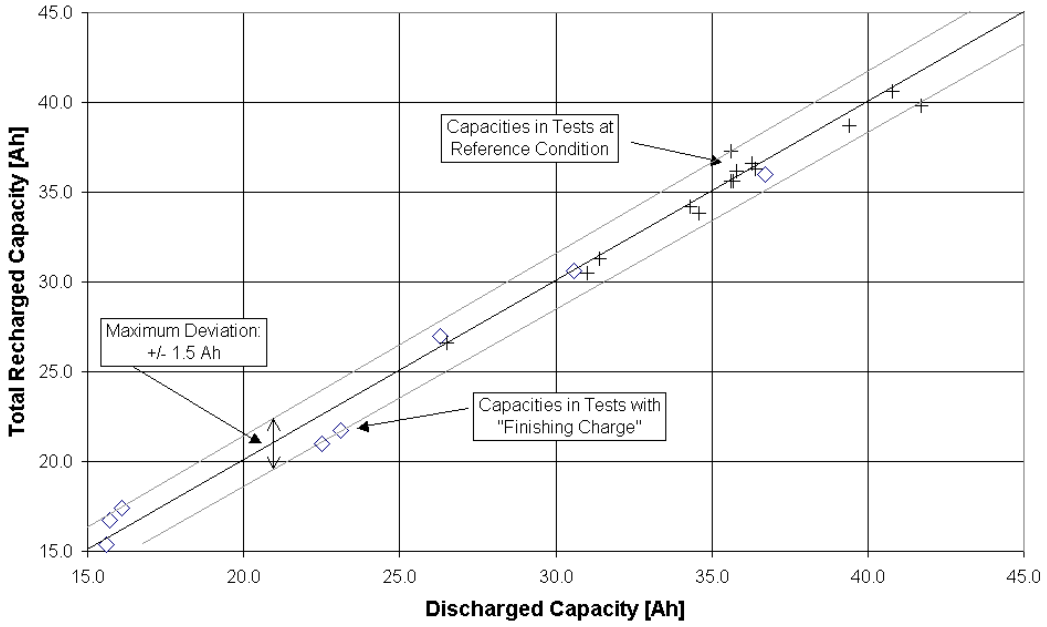

Figure 29 Correlation results of the consistency test

Figure 29 shows the validation results of the described end-of-charge method. The total recharged capacity Q_{tot} in Ah is plotted versus the discharged capacity Q_{dis} in Ah. The crosses represent the individual results from all the tests at reference charging conditions, and the quadrates represent the results from all the tests with 'finishing charge' at reference conditions. The straight line in the middle represents perfect correlation between discharged and recharged capacity.

The correlation between charged and recharged capacities is an indicator for the validity of the suggested method. All measured capacities are close to perfect correlation within an error of ± 1.5 Ah for the tested 50 Ah cell, as can be seen in Figure 29. As mentioned earlier, this error stems from various sources:

- Error due to the temperature control during reference cycles. The resulting error is smaller than 0.5Ah.
- Error due to pauses shortly before the end-of-charge. The resulting errors can be high. An error of up to 1.8Ah was identified for a non-reference charge and the maximum error for reference cycles is 0.5Ah.
- Error due to offset errors in current measurement and the drift in coulomb counting, which results. In subsection 4.5.2 the maximum error due to drift for the tester used in the preliminary tests was calculated. The tester used for the main series of tests exhibits an offset error of 25 mA instead of 50 mA, therefore, the drift is less than 0.188 Ah per test cycle. The maximum number of non-reference cycles between cycles with reference charge is 6, giving a total maximum error of 1.128Ah. Indeed the discharged capacity after these 6 cycles was 35.6 Ah, with 37.3 Ah being returned on recharge. This represents an error of 1.7 Ah, which is in this region.
- Errors due to self-discharge and decreasing capacity. These are also expected to contribute to the total errors.

This reveals that the method for determining the end of charge, as suggested here, is able to determine the end of charge at other temperatures than reference temperature. The error in capacity is smaller than ±1.8 Ah and could be decreased by suppressing the last pause in certain cases.

The EOCC curve, as shown in Figure 26, can be used in any application in order to provide the reference that is required when using coulomb counting methods for determining the SOC. The recharge will usually not be disrupted in such applications and so the error can be expected to be better than ± 3.6 % of the total battery capacity. However, the tested cell was subject to about 72 charge / discharge cycles in total and it is still unclear whether this method is affected by ageing and, if so, how.

The battery temperature can frequently be below 15°C in some applications. This means that the battery would frequently not be fully charged. Even worse, the reference for coulomb counting would be missing, and this means that the SOC calculation slowly drifts and becomes very inaccurate. In such cases, it would be better to accept a lower total available capacity and shift the EOCC curve upwards.

This can either be done analytically or by specifying a different reference point during testing. For example, an EOCC of 1.0A at 25°C would shift the curve up if compared with the 0.5 A, as chosen in these tests. Shifting the curve upwards would return less charge into the battery and there would be less energy available during discharges. However, contrary to lead-acid batteries, the life of lithium-ion batteries is increased by not fully charging them.

The manufacturer of the tested specimen has changed his end-of-charge condition several times in the course of this project and the latest recommendation is a temperature dependant EOCV, as shown in Figure 30.

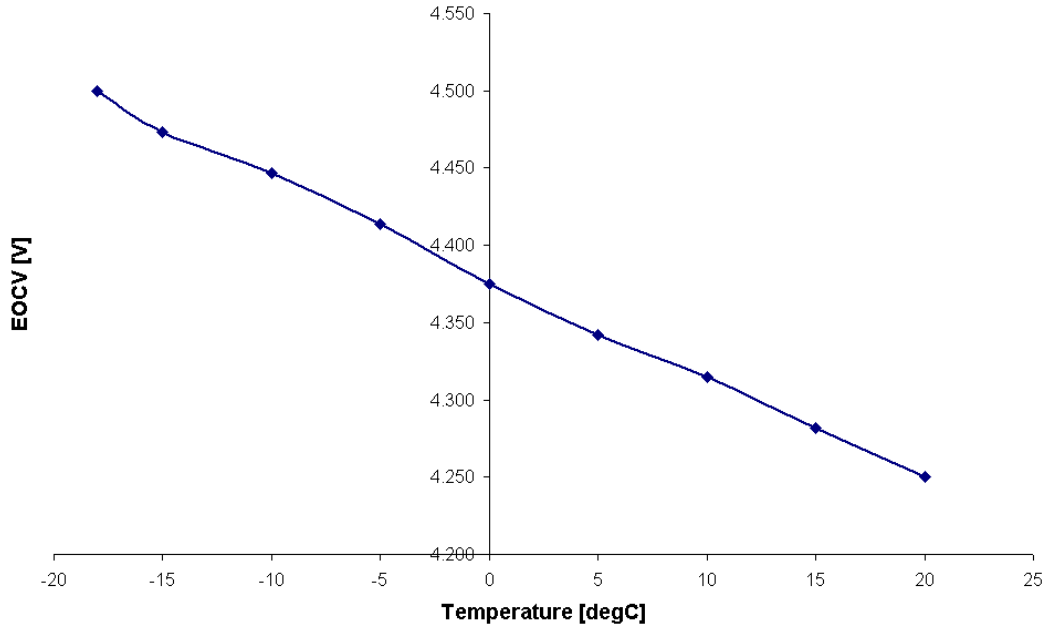

Figure 30 Latest EOCV as a function of temperature recommendation from the manufacturer.

This end-of-charge condition speeds up the recharging process at lower temperatures, especially towards the end of charging. It may or may not provide a consistent state of charge after recharging at different temperatures, even when the EOCC is the same value. This has not been investigated and such high end-of-charge voltages will almost certainly let the cell degrade more rapidly, because side-reactions will occur faster. It is unclear whether these high charging voltages would impose any safety risks.

5.3 Determination of Equilibrium Open Circuit Voltage

The idea behind having an appropriate end-of-charge determination method is to achieve independence between test cycles and to be able to measure cell performance parameters at well-defined and comparable states of charge. The method for this as suggested in the previous section is viable but requires a high level of attention. The OCV is an indicator for the state of charge for some cell chemistries and designs and, hence, making use of this during testing is evaluated for the tested specimen.

Apart from this, the open-circuit voltage (OCV) as a function of state of charge (SOC) is one of the most important parameter-curves of a battery. In a conventional test, this voltage is normally measured as the steady-state open-circuit terminal voltage at different states of charge. However, the preliminary performance tests described earlier indicate that the tested large lithium-ion cell requires more than 24 hours for reaching true equilibrium. The whole test for determining the OCV(SOC) curve would take several days on a single cell. The amount of time increases further if one wanted to determine variations with temperature, variations between different cells and variations during ageing.

Some assumptions have been made when determining the parameters in section 5.1. One of them was that the OCV_{eq} could be determined by average the OCV region. The next sections investigate whether this was a valid assumption. In general, the next sections focus on faster methods for the determination of the OCV_{eq}(SOC) curve.

The following investigation is based on the data from the preliminary performance tests. Figure 31 represents the test data where the voltage during the test procedure was plotted against the SOC of the battery.

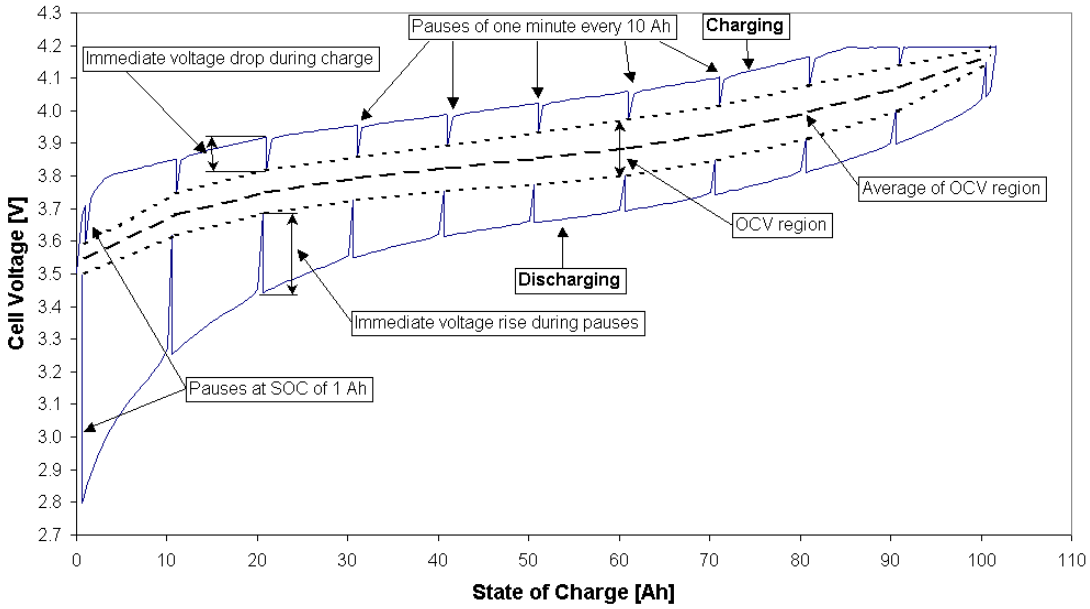

Figure 31 Cell voltage versus SOC during charging and discharging

The voltage drop that can be seen at 1 Ah and every 10 Ah during charging, and the voltage rise during discharging, are caused by the one-minute long pauses, as defined in the test procedure. All voltage over state-of-charge points reached at the end of these pauses during discharging and charging are connected with dotted curves. The top dotted curve is for charging and the bottom one is for discharging. If the pauses were long enough, then, ideally, these two curves should be identical and then they would reflect the OCV_{eq}. However, they are not identical, as can be seen in Figure 31. This is because the cell did not reach true equilibrium during the one-minute long pauses. The OCV_{eq} cannot be measured directly but it is assumed that the area between the two dotted lines is the region where the OCV_{eq} can be 'found'. The dashed line shown in Figure 31 is the mean of the dotted lines.

One objective here is to determine the equilibrium open-circuit voltage as a function of the state of charge $OCV_{eq}(SOC)$. Further objectives are to evaluate faster methods for determining this curve, to evaluate its applicability for state of charge determination during laboratory tests and in applications, and to study possible changes in this curve due to ageing.

5.3.1 Different Methods for Determining $OCV_{eq}(SOC)$

Three different methods were used for determining the $OCV_{eq}(SOC)$:

1. Measuring the OCV immediately after switching off the load / charging current and using the average between the charging / discharging values at each SOC in order to estimate the OCV_{eq}.
2. Measuring the step response after switching off the load / charging current. Applying exponential curve-fitting in order to estimate the OCV that would be approached after infinite waiting time and determine the true OCV_{eq} by averaging the results from charging / discharging at each SOC.
3. Waiting for 12 hours before measuring the OCV at each SOC during charging and during discharging.

The results of different OCV determination methods are presented in Figure 32 for comparison. The cell voltage is plotted versus state of charge in Ah. Two curves represent the results obtained from the first OCV measurement method. One is from the test with 33A charge/discharge current and the second from the test with 100A. The other two curves represent the results from the second OCV test method with 33A and 100A.

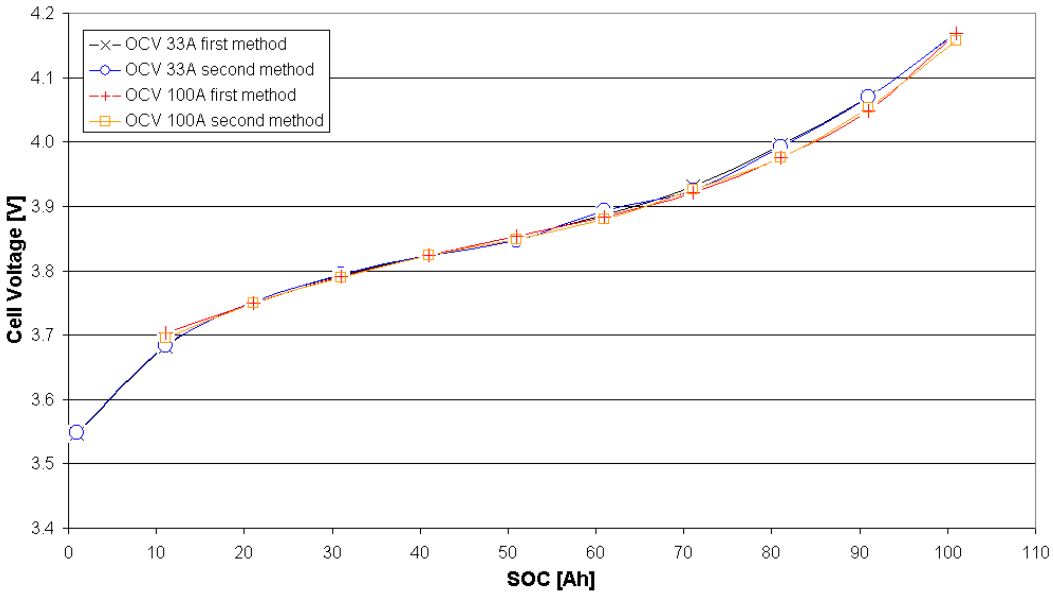

Figure 32 Comparison of OCV results from different test methods and at different charge / discharge currents

Figure 32 shows that the results of the first and the second test method coincide over the full range of SOC. There seem no advantages in using the second method, which takes longer and requires sophisticated processing. Both tests with 100A do not reach down to 0Ah SOC because of residual capacity at high currents. Small differences of about ± 10 mV (± 1.5 % in SOC) can be observed between the tests with 100A and 33A in the SOC region of 70Ah to 90Ah. Apart from these minor differences, the results with both current rates are almost indistinguishable.

However, the tests here always follow the same charge / discharge pattern as suggested in section 4.2. In particular, every discharge burst discharges the same amount of capacity (about 10% of the total capacity) regardless of the current. It remains uncertain whether the OCV results would be the same for different currents if, for example, the burst time was kept constant rather than the discharged capacity.

The following paragraphs compare the OCV results from the rapid method (first method) with results obtained from a conventional test-method (third method) with longer waiting times (12 hours) at each SOC.

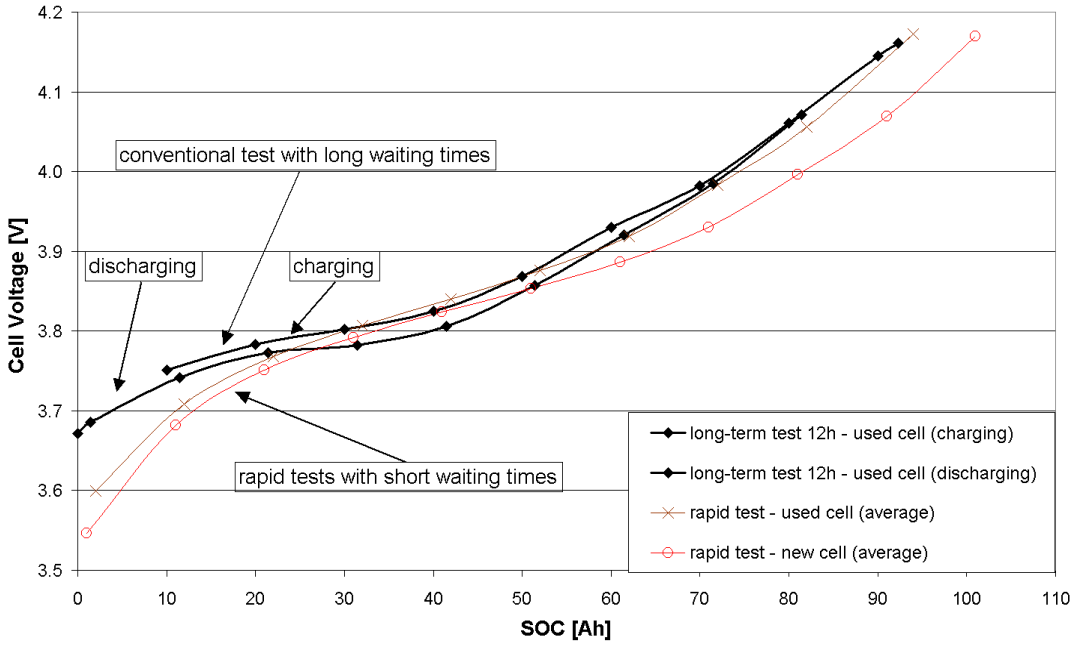

Figure 33 OCV as a function of SOC in Ah obtained with rapid and conventional testing methods for new and aged Lithium-ion cell

Figure 33 shows the OCV as a function of SOC in Ah. The right curve in red represents the results obtained from the rapid test methods described earlier. Only one curve is chosen out of the four because the four curves are very similar, as shown in Figure 32. The two black curves on the left, close to each other represent the OCV results obtained from a conventional OCV determination method with 12 hours waiting time at each SOC (third method). The upper curve is obtained during charging and the lower curve is obtained during discharging. This test was conducted on the same cell but one year and 16 cycles after the rapid OCV methods. The brown curve is obtained at this same ageing status but using the same rapid method (first method) as the red curve.

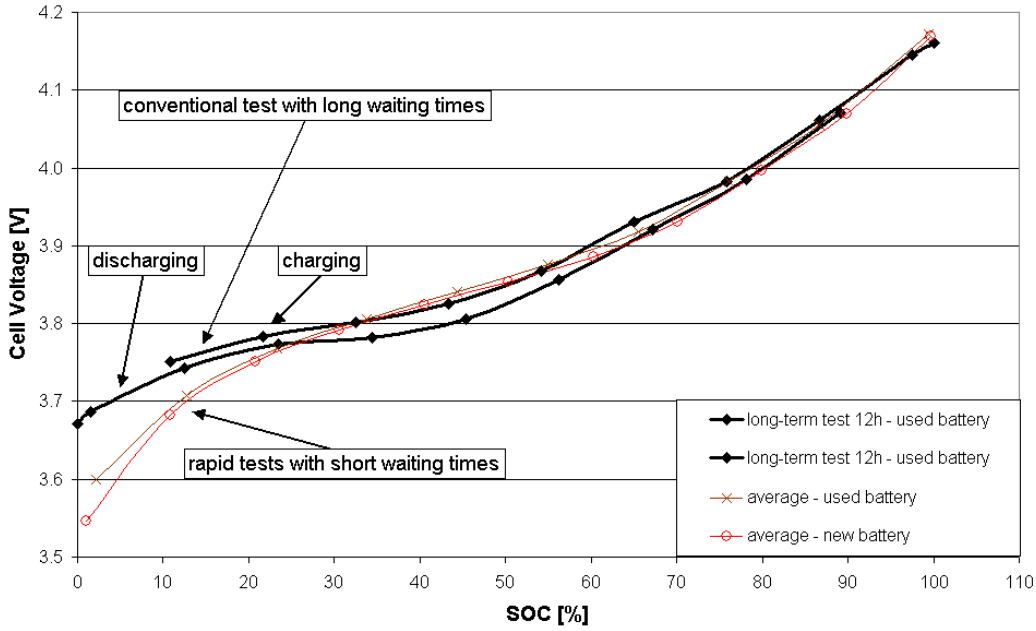

Figure 34 OCV as a function of SOC in % obtained with rapid and conventional testing methods for new and aged Lithium-ion cell

Figure 34 shows the same results as Figure 33 but with an SOC axis in % instead of absolute Ah. By this means, the decrease in total capacity due to ageing is taken into account.

However, the conventional method with long waiting times produces significantly different results at 20% SOC and below, as can be seen in Figure 34. The differences are in the order of up to 200 mV or 10% SOC. This indicates that mass transportation limitations lead to an accumulation of concentration gradients during discharge. These gradients do not relax within a few minutes and are not even reversed with the

waiting time of one hour and the subsequent initial charging process, which commenced after the full discharge. The effect of this slow diffusion behaviour is so significant that one must assume that the resting time between test cycles will have an impact on the cell performance. Section 5.5 presents and discusses the results of some tests that were specifically designed and conducted in order to investigate this issue.

Figure 34 shows that the two curves obtained from the long-term test do not match between charging and discharging. This reveals that, either, a resting time of twelve hours is not sufficient for reaching true equilibrium, or, that the tested specimen exhibits a significant hysteresis between charging and discharging. Section 5.4 presents and discusses the results of a test that investigates whether any charge / discharge hysteresis exists.

The current during charging is always the same as during discharging for the above test cycles. For most Lithium-Ion cell chemistries, however, the maximum allowed discharge current is significantly higher than the maximum allowed charging current. This means that when testing at maximum allowed discharging currents, the following recharging would have to be at a lower current and it remains unclear whether this method would still produce consistent $OCV_{eq}(SOC)$ results.

5.3.2 The Influence of Ageing

Figure 33 shows the OCV as a function of SOC measured in Ah. It can be seen that the total capacity decreases due to ageing. The OCV does not correlate very well with the absolute capacity measured in Ah. However, Figure 34 reveals that the battery age has only marginal influence on the shape of the OCV curves if this was plotted against the SOC expressed in %. This indicates that the tested cell has suffered from a net loss of capacity rather than an apparent capacity loss due to impedance increase.

5.3.3 The Applicability of the OCV for SOC Determination

This section has so far shown, that the proposed rapid method is suitable for determining the OCV_{eq} between 20% SOC and 100% SOC. It is sufficient to let the cell voltage relax for one minute or less and then determine the OCV_{eq} by averaging the cell voltage during charge and discharge at this point. The magnitude of current

does not affect the results of the proposed method and the effects of ageing can be eliminated.

However, in typical applications, one would have to use the OCV directly in order to predict the OCV_{eq}. Averaging between the OCV during charging and discharging is generally not possible. Unfortunately, the OCV differs significantly from the true equilibrium OCV_{eq}. The OCV depends on the discharging / charging history. The time required for reaching true equilibrium depends significantly on the temperature and, possibly, also on the age of the cell. Hence, it can be concluded that the apparent OCV is not suitable for determining the SOC neither during testing nor in real-world applications. Currently, methods based on coulomb counting using a suitable reference such as full charge / full discharge are more appropriate.

5.4 Hysteresis Test

The tests above have revealed that the apparent equilibrium voltage during charging is higher than the apparent equilibrium voltage during discharging, even when using the conventional test with very long waiting times (see subsection 5.3.1). This suggests that there might be a hysteresis even in the true equilibrium voltage, as has been found for NiMH cells [57] and is also suggested for some lithium-ion cells [11]. It is important to investigate whether there is any hysteresis and also to quantify it, because any significant hysteresis would make the determination of SOC from the OCV very difficult, especially if the OCV(SOC) curve is very flat.

The following test is conducted in order to investigate and measure the hysteresis. A fully charged cell is discharged to about 50% SOC and left to rest for 48 hours. 50% SOC is chosen because the preliminary tests revealed that the OCV(SOC) is most flat around this state and any hysteresis would have the most significant impact on the SOC determination. After the 48-hour rest, the discharge is continued until the cell reaches its end-of-discharge voltage. Then the cell is recharged to the same state of charge where the waiting time was applied during the discharge and left to rest for 48 hours again. Finally, the cell is fully recharged. This test is conducted at 35 ºC.

The same test is repeated at a lower temperature of only 5 ºC but with a longer resting time of 96 hours, in order to investigate the dependency on temperature and resting time.

The following figure presents the result from the hysteresis test at 5ºC and with a resting time of 96 hours.

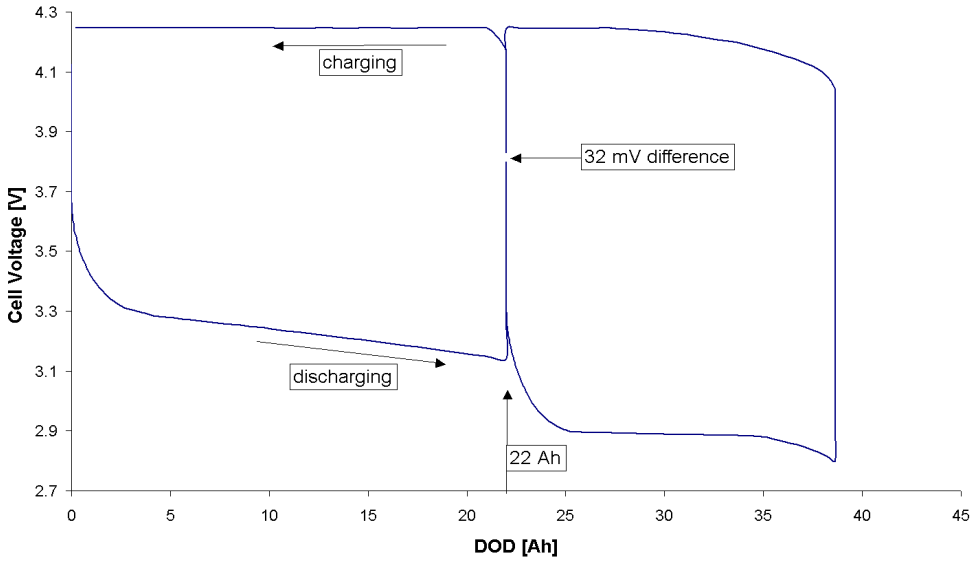

Figure 35 Cell voltage during hysteresis test at 5°C and with 96 hours resting time.

Figure 35 shows the cell voltage over DOD during the hysteresis test. The bottom curve shows the decreasing cell voltage with increasing DOD during discharging. At a DOD of 22 Ah, the discharging is stopped for 96 hours and the open circuit voltage rises to 3.799 V. Subsequently, the discharging continues until the cut-off voltage of 2.8 V is reached at a DOD of 38.7 Ah. The cell voltage rises in the subsequent pause of 5 hours without a change of DOD. The top curve shows the increasing cell voltage with decreasing DOD during the subsequent recharging. The charging is stopped for 96 hours at a DOD of 22 Ah and the cell voltage drops down to 3.831 V at the end of this pause. The majority of the subsequent recharge of the remaining 22 Ah occurs in a constant-voltage charging regime.

The difference of the open circuit voltages at the end of the 96 hour-long pauses is 32 mV between charging and discharging.

Figure 36 shows the cell voltage over DOD during the hysteresis test at 35 ºC with 48 hours resting times.

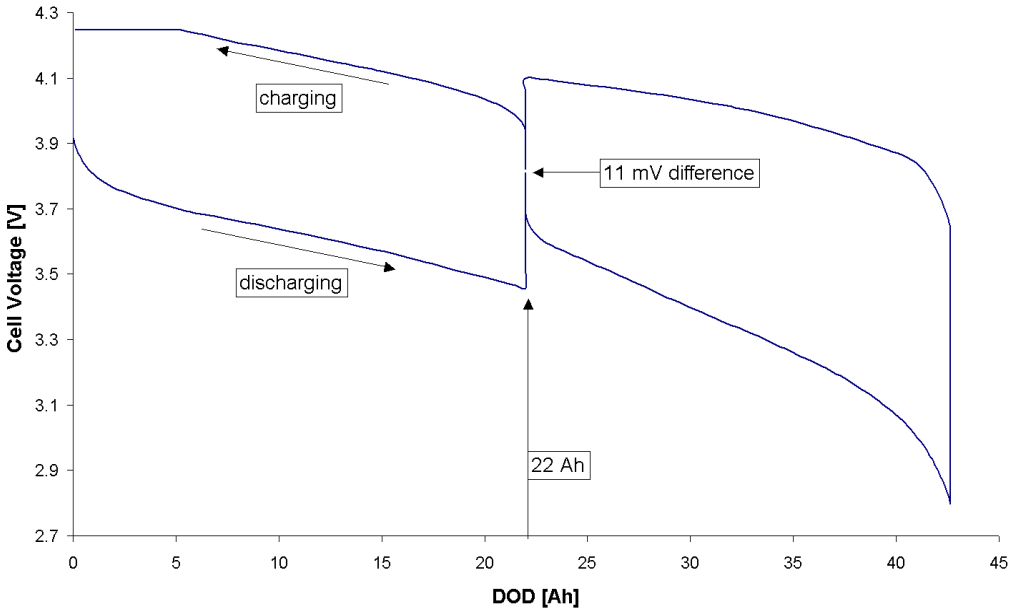

Figure 36 Cell voltage during hysteresis test at 35°C and with 48 hours resting time

Table 6 summarises the results from this test and compares them with the results at different test conditions.

Test condition	5 ºC, 96 hours	35 ºC, 48 hours
Apparent equilibrium during discharge	3.799 V	3.810 V
Apparent equilibrium during charge	3.831 V	3.821 V
Apparent hysteresis	32 mV	11 mV
OCV (average apparent equilibrium)	3.815 V	3.8155 V
Discharged capacity	38.7 Ah	42.6 Ah

Table 6 Results of two hysteresis tests conducted under different conditions.

The hysteresis test shown in Figure 35 was at a low temperature (5ºC) and the resting time was 96 hours. This test shows a cell voltage difference of 32 mV between charging and discharging, measured at the end of these resting times. This difference is measured at a DOD of 22 Ah, which is about half of the total available capacity. The second hysteresis test shown in Figure 36 is at a higher temperature (35 ºC) and the measured difference is only 11 mV at the same DOD, although the resting time is reduced to 48 hours only. This shows that the temperature plays a very important role in the case of the tested specimen. It could be that either the hysteresis is much more significant at lower temperatures or that the cell needs much longer for reaching true equilibrium.

The question of whether the measured differences are actually due to hysteresis or due to very slow relaxation is very difficult to investigate. The resting times in the two tests were already so long that the voltage slopes were so small that the resting time would have to be increased to another order of magnitude in order to make a significant improvement to the measurement. However, this would not only increase the time required for testing, but also, self discharge might significantly influence the measurement by reducing the cell voltage.

Assuming that the true equilibrium OCV_{eq} is the average of the values during charging and during discharging, the first test would yield an OCV_{eq} of (3.799 V + 3.831 V) / 2 = 3.8150 V. For the second test it would be (3.810 V + 3.821 V) / 2 = 3.8155 V. Considering that the measurement error of the battery tester is ±5 mV, this can be regarded as the same result.

The difference of 32 mV is relatively small if compared with the total voltage swing of about 1100 mV at that DOD. Furthermore, it is considerably smaller than the total voltage difference of 2· 68 mV = 136 mV, which was apparently observed during the preliminary tests. Unfortunately, the slope of the OCV(DOD) curve is shallow for the tested specimen. At a DOD of 22 Ah, the slope is about 0.15 Ah/mV for a 50 Ah cell. A measured voltage difference or hysteresis of 11 mV equates to a difference of 1.7 Ah (3.3%) and the 32 mV measured at 5ºC equates to a difference of 4.8 Ah (9.6%). This means that the apparent equilibrium voltage values are not suitable for determining the SOC very precisely, especially at low temperatures. Considering that the resting times in most applications are well below 48 hours, one can expect errors of more than 10% if one had to rely on voltage measurements for SOC determination. This is why the series of tests conducted in this work bases their SOC determination on coulomb counting with a suitable reference at full charge.

Assuming that the measured voltage differences are due to the slow relaxation and not to hysteresis, it seems also important to investigate whether the time between two subsequent tests may influence the performance of the second test cycle. This question is investigated and the results are presented and discussed in the following section 5.5.

The hysteresis tests revealed an interesting phenomenon of the tested specimen. In the hysteresis test under warm conditions, as shown in Figure 36, the performance of the cell during discharge after the resting time is significantly higher than it would have been without the resting time. This is due to the relaxation of concentration gradients during the resting time. However, the hysteresis test at low temperature revealed the opposite behaviour where the performance is worse after the resting time. This is due to substantial cooling down during that resting time.

Temperature plays an important role for the performance of these cells. The hysteresis tests, in particular, showed that the available energy depends significantly on the usage profile. Long pauses can improve the performance at high temperatures but at low ambient temperatures, the performance might decrease. However, thermal insulation can improve the performance in cold conditions. This observation is important to understand, because it means that the test pattern and the type of cooling/insulation should be as close as possible to the actual condition in the target application.

5.5 Resting Time Between Test Cycles

The hysteresis tests have revealed that the resting time can significantly affect the performance of a cell. It is important that the preceding test cycle in a series of test cycles does not influence the behaviour of the following test cycle. Hence, the resting time should be as long as possible in order to approach true equilibrium. However, the tests above have revealed that this can take several days [1] and such long waiting times are unacceptable for rapid testing.

Keeping the resting short but always the same during a series of test cycles would help to obtain consistent results. However, the time for relaxation depends on temperature, and this varies significantly between test cycles. Additionally, it is difficult to keep the time between test cycles constant, for practical reasons.

Three typical test cycles are conducted with three different resting times between each cycle in order to determine suitable resting time ranges rather than one optimal resting time. The shortest resting time is 1 hour, the medium resting time is 5.5 hours and the maximum resting time is 26.5 hours. The current is 15A (0.3C for the 50Ah cell) and

a low temperature of 0ºC is chosen, because this presents a worst-case scenario. Ion movements are slow at low temperatures and higher temperatures require shorter resting times. A resting time that is sufficient for low temperatures also will be sufficient for higher temperatures.

The test pattern for this resting time test is as follows:

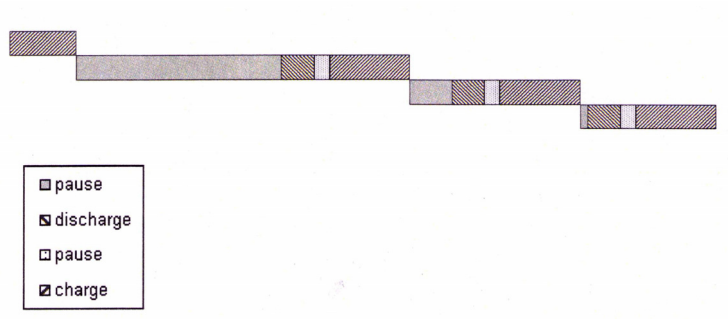

Figure 37 Test for finding the optimal resting time between test cycles.

The following figure shows the results from these resting time tests.

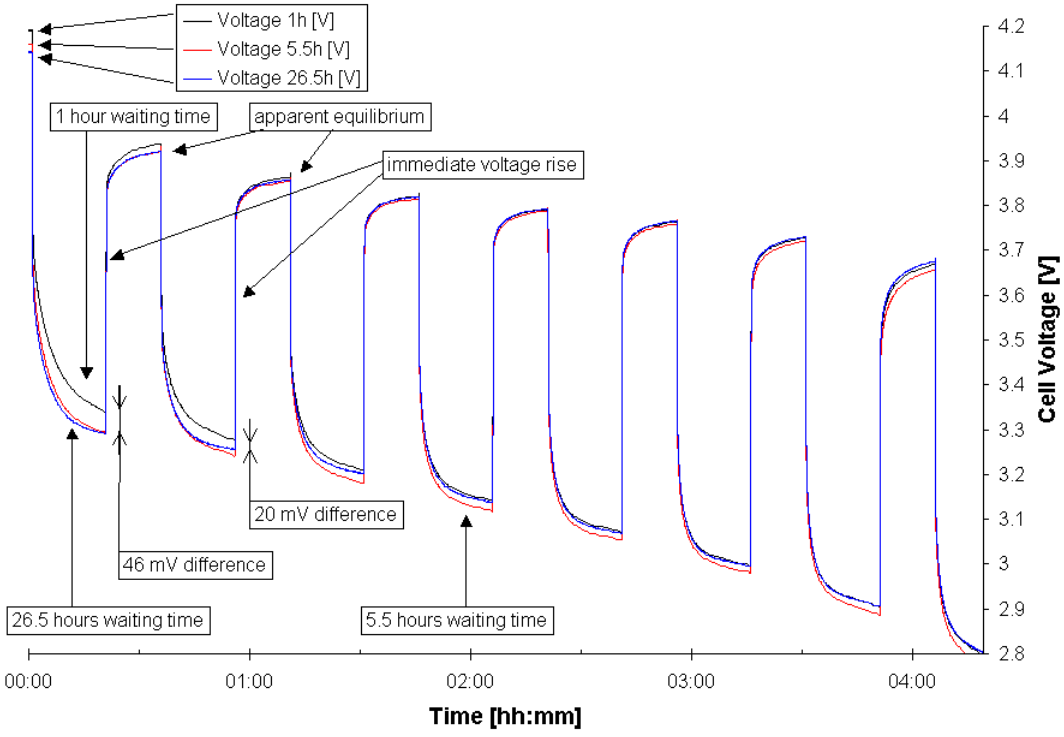

Figure 38 Cell voltage during resting time test.

In Figure 38, the cell voltage is plotted over discharge time for three different test cycles under the same conditions (0°C, 15A). Each discharge step discharges 5Ah and takes 20 minutes. The pauses after each discharge step are 15 minutes. The voltage relaxation during these pauses can be seen in Figure 38.

The only difference between the three test cycles is the resting time between the preceding charge and the start of the actual test cycle. The shortest resting time is 1 hour. The two other resting times are 5.5 hours and 26.5 hours. These different resting times lead to different apparent equilibrium voltages at the very beginning of the test as can be seen on the left side of the figure. However, in the course of the discharge test, the two curves with the longer resting times show no significant differences in their voltages. Only the curve with the shortest resting time of one hour exhibits significantly higher cell voltage levels during the first two discharge phases. No significant cell voltage differences can be observed in the remaining discharge phases and relaxation times.

	At the end of 1st discharge	**Immediately after the 1st discharge**	**At the end of the 1st pause**	**At the end of 2nd discharge**	**Immediately after the 2nd discharge**	**At the end of the 2nd pause**
After 26.5h resting time	3.293 V	3.437 V	3.920 V	3.256 V	3.391 V	3.856 V
After 5.5h resting time	3.294 V	3.434 V	3.920 V	3.243 V	3.369 V	3.853 V
After 1h resting time	3.340 V	3.479 V	3.937 V	3.276 V	3.410 V	3.862 V

Table 7 Voltages of interest during the resting time test.

Table 7 summarises the voltages that are of interest during the resting time test. From left to right, it shows the cell voltage at the end of the first discharge burst, then the voltage immediately after stopping the current, then the voltage at the end of the first

pause (apparent OCV), then the voltage at the end of the second discharge burst, then the voltage immediately after the following discharge step and, finally, the voltage at the end of the second pause (apparent OCV). From top to bottom, the table shows the voltages during the test after a long resting time, after a medium resting time and after a short resting time.

With the short resting time, the voltage at the end of the first discharge burst is 46 mV higher when compared with the longer resting times. At the second burst, it is still 20 mV higher. The significantly higher voltages at the end of the first and second discharge bursts increase the available power of the cell.

The test results reveal that the long relaxation times of the tested specimen could cause dependencies between two test cycles. The performance during the first 20 % of discharge, for example, is significantly increased when the resting time after the previous recharge is only one hour. This test result shows that the cell performance significantly depends on the resting time. Consequently, the usage profile up to several hours previous influences the cell's behaviour. The cell exhibits some kind of 'memory', which seems to last for several hours. The tested cell uses comparatively thick materials for electrodes and separators [19], which does explain why the diffusion takes more time to equilibrate concentration gradients.

This 'memory' is important to consider, for various reasons:

- The actual cell performance depends significantly on the previous usage and, hence, performance predictions that are required for some applications will be complex to derive.
- The resting time between tests needs to be optimised and kept similar in order to obtain consistent results from the tests.
- It is difficult to characterise the performance of the cell, because it significantly depends on the usage pattern and, therefore, on the application.
- The performance measured or the step response measured in any test does not necessarily reflect the behaviour in different conditions.

For the test series, it is important to gain consistent results and so, this 'resting time test' is used to define a suitable resting time between test cycles. For the main series

of tests, it is ensured that the resting time between two subsequent test cycles is between 6 hours and 26 hours. This seems to provide consistent results for the tests.

The slow diffusion behaviour not only influences the available performance but it also affects determining battery parameters and state of charge calculations, which will be discussed in more detail in the following two subsections.

5.5.1 The Influence on Determining Battery Parameters

During testing, the voltage relaxation is used for determining battery parameters as described in section 5.1. The immediate voltage rise after the first and second discharge burst is summarised in Table 8.

	Immediate rise 1	**Total potential rise 1**	**Immediate rise 2**	**Total potential rise 2**
Test after 26.5h resting time	144 mV	768 mV	135 mV	727 mV
Test after 5.5h resting time	140 mV	767 mV	126 mV	740 mV
Test after 1h resting time	139 mV	721 mV	134 mV	707 mV

Table 8 Immediate voltage-rise after the first and second discharge burst in the resting time test.

Table 8 shows the immediate voltage rise at the end of the first and the second discharge burst for the three cycles, with three different resting times. Taking the total variation of the different voltage rises into account, the immediate voltage rise does not seem to be affected significantly by the different resting times.

It is assumed that the true equilibrium voltage is the same for all three test-cycles for a given state of charge. Section 5.3 has shown that the true equilibrium voltage of this cell type at a DOD of 5 Ah (12 % DOD for cell with 41.7 Ah total capacity under reference condition) is about 4.061 V and at 10 Ah it is about 3.983 V. The total difference in potential voltage rise can be calculated and is also shown in Table 8. This total rise in cell voltage potential significantly depends on the resting time.

The findings are as expected because the immediate voltage rise can be related to ohmic resistance and charge transfer resistance, which are not dependant on the resting time. Whereas the total rise in cell voltage potential additionally is related to the relaxation of concentration gradients. Concentration gradients, however, depend

on the resting time between tests, because true equilibrium is not reached within those times.

It can be assumed that the performance differences discovered during this resting time test are due to differences in concentration gradients. These should become visible in different diffusion over-potentials (V_{diff}). The diffusion over-potential can be estimated by subtracting the immediate voltage rise from the total potential voltage rise.

The results for the different test situations are shown in Table 9.

	Diffusion Over-Potential 1st step response	**Diffusion Over-Potential 2nd step response**
Test after 26.5h resting time	624 mV	592 mV
Test after 5.5h resting time	627 mV	614 mV
Test after 1h resting time	582 mV	573 mV

Table 9 Diffusion over-potentials during the resting time test.

Table 9 reveals that the over-potential due to diffusion shows significant differences depending on the resting time between two subsequent test cycles.

The results from the tests with medium and long resting times (5.5 hours and 26.5 hours) are very similar at the first step response. However, strangely, the diffusion over-potential with the medium resting time appears to be inconsistent at the second step response. Looking at Figure 38 one can see that the cell voltage in the test after a medium resting time started dropping more rapidly toward the end of discharge. This suggests that the cell was already more depleted than in the two other tests, which indicates that the state of charge may have been slightly lower during that test than during the two other tests. This may be due to various errors during these tests, such as temperature control, state of charge termination, end-of-charge termination, etc.

However, significantly and consistently, the over-voltage potential is smaller for the test with short resting times (1 hour). Here, in the worst-case scenario (comparing the medium resting time with the short resting time), the difference is 45 mV (7.2 %) and 41 mV (6.7 %) for the first and the second discharge burst respectively. These differences would cause significant errors when determining battery parameters based on these step responses.

5.5.2 Determination of SOC from Apparent Equilibrium

The fact that the difference between the apparent equilibrium voltage and the true equilibrium voltage seemed to be constant over the whole range of SOC, discharge current and temperature, as indicated in subsection 5.1.4 suggests, that the apparent equilibrium voltage after a defined time could be useful for determining the state of charge of the cell. This resting time test, however, reveals that the apparent equilibrium voltage after a defined time significantly depends on the charge/discharge history. The voltage differences in apparent equilibrium voltage found here were up to 17 mV at 12 % DOD. Using the apparent equilibrium voltage as a measure of SOC would have lead to an error of more than 2 % in SOC prediction. This would be an acceptable error in practical applications. However, these tests were very similar and the resting times were already long. In practical applications, the variations will be much higher causing larger errors.

5.6 Investigation of Available Capacity at Different Discharge Rates

It is known for many battery types that the available capacity significantly depends on the discharging rate and profile [26]. This section introduces a test methodology that helps understanding the fundamental reasons for that particular behaviour so that accurate state of charge algorithms for varying loads can be developed.

The test procedure for investigating the decrease in capacity at higher discharge currents is as follows:

- A fully charged cell is discharged with a low current I_L = 5A (0.1C) until 2.8V cell voltage is reached.
- The cell is recharged.
- A 6-hour period is allowed to elapse as a resting time, according to the findings from the resting time test. See section 5.5.
- The fully charged cell is discharged with a high current I_H = 50A (1C) until 2.8V cell voltage is reached.
- A period of time is allowed to elapse so that the total discharge time is similar

to the discharge time in the first test cycle, which had a low discharge current (5A).

- The cell is further discharged, but now with a lower rate I_L = 5A (0.1C) until a cell voltage of 2.8V is reached.
- The cell is recharged.
- The time specified in the results from the resting time test is allowed to elapse.
- The whole test cycle is repeated three times.

All tests are carried out under reference conditions (25°C). The charging follows the normal charging procedure as recommended by the manufacturer except that the charging voltage is reduced according to subsection 5.2.1. This means charging current of 15A, a charging voltage of 4.234V and an end-of-charge determination of 0.5A. Coulombs are counted during all tests, and temperature, cell voltage and current are logged.

The first results presented in Figure 39 and Figure 40 are the outcome of a series of tests with two different discharge rates being conducted with an aged 50Ah lithium-ion cells (ThunderSky).

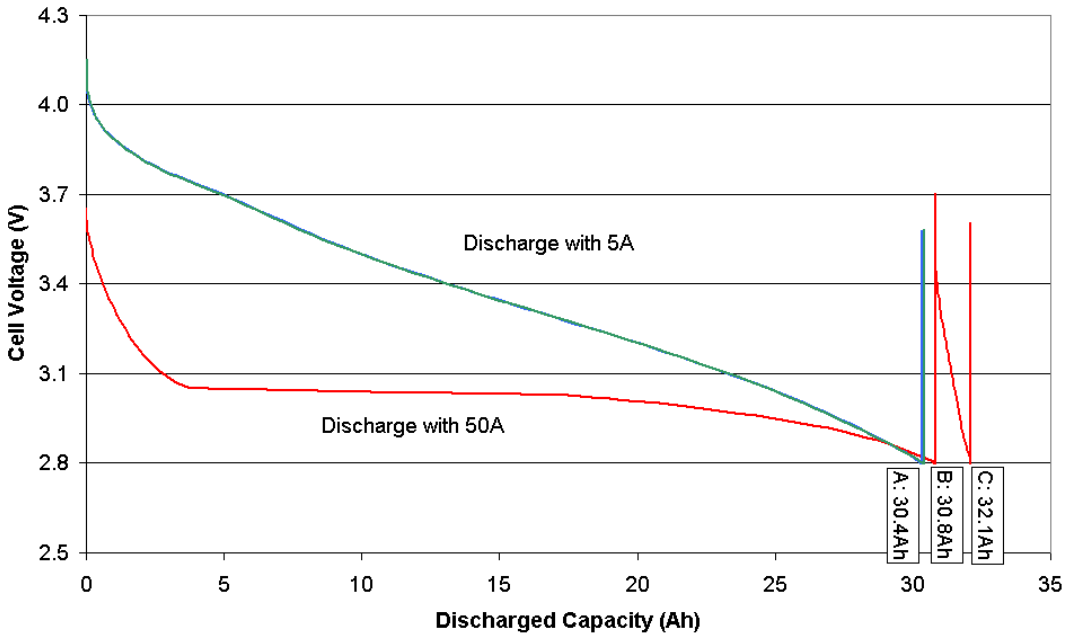

Figure 39 Capacity tests with the Lithium-Ion test specimen – voltage behaviour

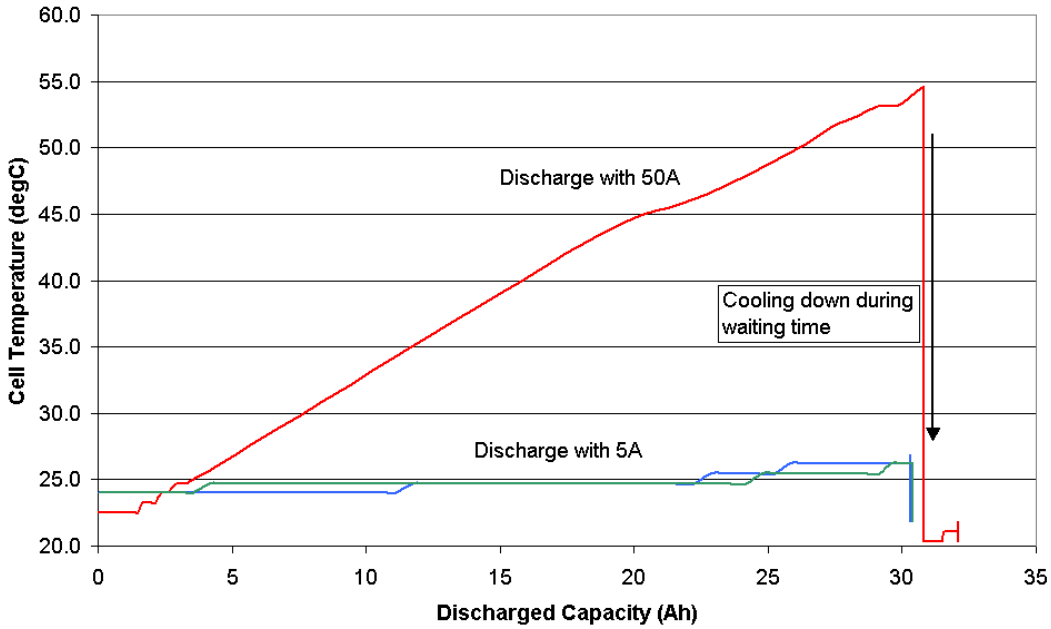

Figure 40 Capacity tests with the Lithium-Ion test specimen – temperature behaviour

Figure 39 shows the cell voltage versus depth of discharge. The bottom curve in this figure shows the discharge with a high rate of 50A until the cut-off voltage of 2.8V is reached at point B. After a resting time of six hours, the cell is further discharged with a small current of 5 A until the cut-off voltage is reached at point C. The top curve represents the discharge at the lower current of 5 A from the beginning until the cut-off voltage is reached in point A. In fact, the top curve consists of two identical curves. These represent repetitions of the same test, revealing the excellent repeatability. Figure 40 shows the cell temperatures during the different tests.

Figure 39 reveals that for the tested large, high-energy Lithium-Ion cell, the dischargeable capacities are between 30 Ah and 32 Ah regardless of the discharge rate. The cell's available capacity at high rate without further discharging at low rate is the same as the available capacity at a low rate from the beginning. The dischargeable capacity in the subsequent discharge at low rate after discharging at high rate is only very small. This observation is unexpected, because most other chemistries provide significantly smaller capacities at high rate discharging. Peukert was the first to investigate this for lead-acid cells [63]. It was found in his study that the available capacity of lead-acid cells decreases after discharging with high currents within the same discharge cycle, even when changing to smaller currents [26]. This

‘passivation’ is not permanent; and is reversed with the next full charging. The lithium-ion cell however does not show this behaviour.

The unexpected behaviour of the tested lithium-ion specimen can be explained by the significant cell-heating during the high-rate discharge, as can be seen in Figure 40. A closer investigation of the voltage curve at high rate discharging in Figure 39 reveals that the voltage drops quickly for the first 5Ah of discharge but then remains almost constant until it starts falling slowly towards the end of discharge voltage. This occurs despite the significant slope in the OCV_{eq} over SOC curve, as shown in Figure 34 and despite the significant slope in the discharge curve at 5A as shown in Figure 39. This means that the internal over-potential required for providing the current decreases significantly during discharging at high currents. This can be explained with the fast rise in cell temperature during the discharge at 50 A, as shown in Figure 40. The temperature rose from less than 25°C to 55°C, whereas, in the discharge at 5A, it stayed at about 25°C. Both reaction kinetics and mass transportation are enhanced at higher temperatures, leading to smaller over-potential.

If cell heating was the reason behind the unexpected behaviour, then performing the same test at higher temperatures from the beginning should show an impact on the results. The losses during discharge are reduced at higher temperatures. This means that, at higher temperatures, the heating at high discharge rates is reduced and the cell may actually provide different capacities at different discharge rates, as originally expected. The above tests are repeated at 40°C ambient temperature, rather than 25°C, in order to investigate this.

			Cycle 1	Cycle 2	Cycle 3
First Test	Discharge @ 5A	Discharged capacity	37.5 Ah	36.5 Ah	37.2 Ah
		Temperature at end of discharge	42.9 ºC	42.9 ºC	43.7 ºC
	Recharge	Recharged capacity	36.5 Ah	37.2 Ah	37.6 Ah
		Temperature at end of charge	40.0 ºC	40.0 ºC	40.7 ºC
Second Test	Discharge @ 50A	Discharged capacity	34.3 Ah	35.0 Ah	35.7 Ah
		Temperature at end of discharge	64.7 ºC	64.7 ºC	66.2 ºC
	Subsequent Discharge @ 5A	Subsequent capacity	2.3 Ah	2.2 Ah	2.1 Ah
		Temperature at end of discharge	41.5 ºC	41.5 ºC	42.2 ºC
	Total discharged capacity		36.6 Ah	37.2 Ah	37.8 Ah
	Recharge	Recharged capacity	37.1 Ah	37.7 Ah	37.8 Ah
		Temperature at end-of-charge	40.0 ºC	40.7 ºC	40.0 ºC

Table 10 Capacities and temperatures during passivation test at 40 °C.

Table 10 shows the charged and discharged capacities as well as the temperatures in these tests. Each test cycle consists of two tests, the first of which is a discharge at low current from the beginning of the test and the second of which is a discharge at first at a high current, followed by discharging at a low current. All three repetitions are shown in chronological order from the left to the right. From top to bottom, the table shows the discharged capacities at low current and the discharged capacities at high current, followed by a discharge with low current. All recharged capacities are shown, as well as the temperature at the end of each test step.

Table 10 reveals that the temperature during discharge at 50A goes up by only 25K rather than 30K, as in the previous test at 25°C. The available capacities at 5 A are about 6% higher than at 50 A. This is a small difference only. However, it cannot be inferred, that the available capacity is almost constant and independent of the discharge rate. The above tests discharged the cell at a constant rate, whereas, in many applications, the discharge varies. Pauses during the discharge will limit

beneficial heating and therefore performance may suffer. High discharge rates may not be possible at lower SOC after long resting times, due to the cooling down during the resting time.

Another similar test is carried out but with pauses during discharging in order to investigate the behaviour under such conditions. The cycle is similar to that used for the performance testing. Two different testing conditions are chosen; one is very demanding on the tested battery and the other one is only moderately demanding. The demanding condition is a discharge with a high current of 50 A at a low ambient temperature of 5ºC. Under the very low demanding condition, the cell is discharged with a current of 5 A at an ambient temperature of about 40 ºC.

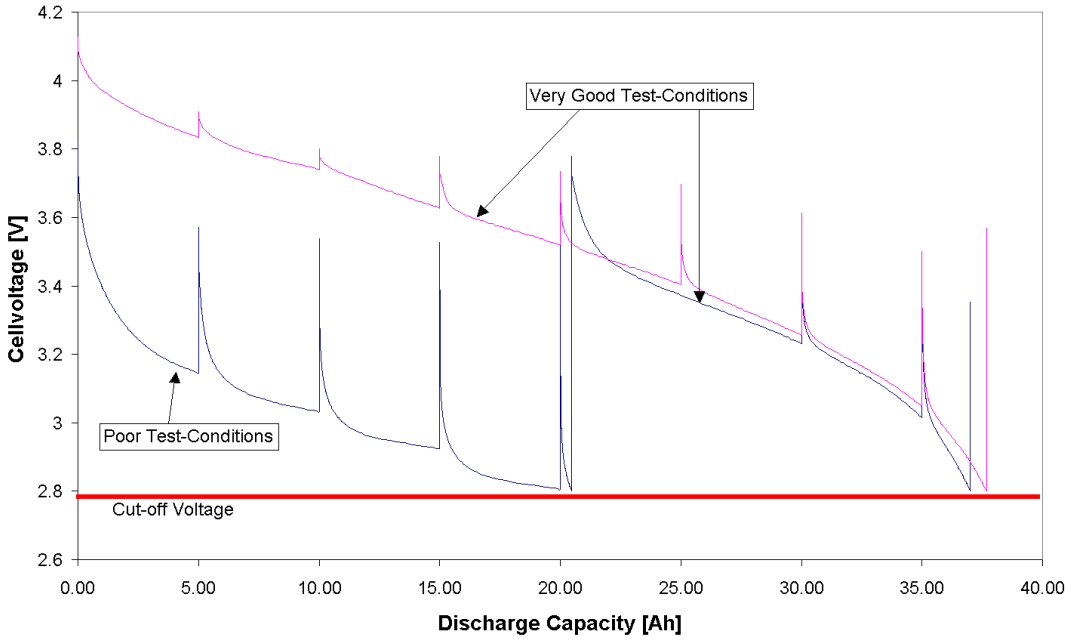

Figure 41 Capacity tests with pauses every 5Ah of discharge – voltage behaviour

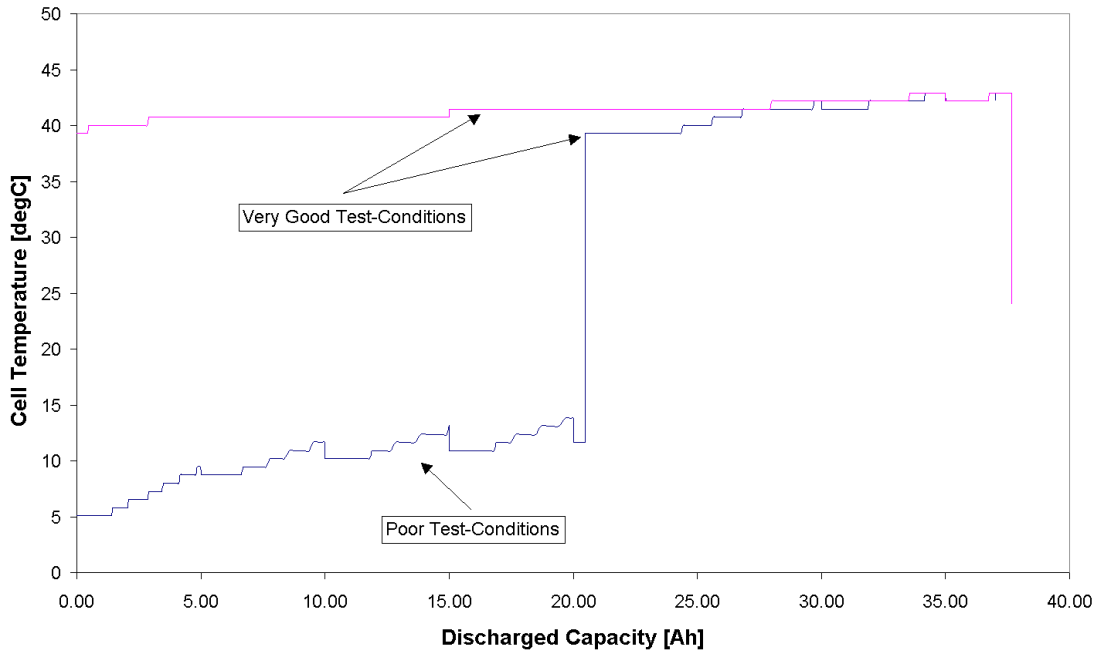

Figure 42 Capacity tests with pauses every 5Ah of discharge – temperature behaviour

Figure 41 and Figure 42 show the results from these test cycles with the pauses. Figure 41 shows the cell voltages versus depth of discharge. The bottom curve in blue shows the discharge under the demanding condition, which is followed by a resting time of 18 hours and a subsequent discharge under the less demanding condition. The top curve in red shows the discharge at the low demanding condition from the beginning of the test. Figure 42 shows the cell temperatures during the same tests. The top curve in red shows the development of cell temperature during the test at less demanding condition and the bottom curve in blue shows the development at demanding conditions, followed by the pause and the subsequent discharge at less demanding conditions.

		CHA0	DCH1a	DCH1b	CHA1	DCH2	CHA2
Time before discharge [h]		-	6.90	18.05	-	7.08	-
Charge / discharge capacity [Ah]		-	20.5	16.5	38.2	37.7	38.8
		-	37.0				
Discharge time [h]		-	2.37	3.82	-	9.30	-
			6.19				
Conditions	**Voltage [V]**	4.237	2.8	2.8	4.237	2.8	4.237
	Current [A]	0.474	15.0	5.0	0.482	5.0	0.490
	Temperature [°C]	21.1	11.6	42.9	24.7	42.9	24.7

Table 11 Results of the passivation test based on a typical test cycle.

Table 11 summarises the result of these test cycles. The series of charge and discharge procedures is presented in chronological order from the left to the right. CHA0 is the last charge before the actual tests. DCH1a and DCH1b are the discharges with changing conditions. Discharging starts under poor conditions (DCH1a) and continues after a pause with DCH1b under good conditions (low current and higher temperature). CHA1 is recharging the capacity under reference conditions as defined in section 5.2. DCH2 is the discharge under good conditions from the beginning and CHA2 is recharging the capacity under reference conditions as defined in section 5.2.

The first row shows the time elapsed before the actual discharge starts. The second and third rows show the charged or discharged capacities. Rows 4 and 5 show the discharge time including the 15 minutes-long intermittencies, and the last three rows show the charge / discharge conditions at the end of charging / discharging.

Figure 42 and Table 11 reveal that, unlike in the first or in the second capacity test, the tested cell does not warm up as much because of the pauses during discharge. The cell heats up by about 5K only and reaches the end of discharge voltage before it has the opportunity to heat up any further. Hence, the obtained capacity under poor conditions (low temperature and high discharge rate) is significantly lower than under more favourable conditions. However, changing to more favourable conditions after discharging under poor conditions allows discharging almost the same amount of total capacity as in the test under favourable conditions from the beginning.

This shows that lithium-ion cells behave fundamentally differently if compared with lead-acid batteries. In [26] it was shown that lead-acid batteries exhibit reduced capacity after discharging at high rates. This is because less conductive reaction products are formed close to the current collectors when discharging at high rates. Active mass is then ‘electrically disconnected’ from the current collectors, resulting in reduced capacity. The capacity is still available but it is ‘connected’ with higher impedance and, hence, is only accessible at much lower currents. It emerged that it was important to understand the fundamental mechanisms behind the reduced capacity during and after discharging at high rates for lead-acid batteries. The fundamental reasons for the behaviour of the tested lithium-ion cell will be discussed in the following paragraphs.

Figure 41 shows that the voltage slope is still small when reaching the cut-off voltage during discharge under poor conditions. This means that further discharging to a lower cut-off voltage would have provided additional capacity. The fact that the dischargeable capacity significantly depends on the conditions solely stems from differences in voltage droop. The end of discharge voltage of, in this case, 2.8 V per cell (VPC) is reached earlier at higher currents or lower temperatures, so that the discharging has to be stopped and the cell appears to be depleted.

The most important parameter for predicting the lithium-ion cell performance is temperature. Low temperatures require higher over-potentials in order to drive the reaction at the desired rate. During charging, this can mean that the charging process takes extremely long or will never return full capacity without exceeding safe charging voltages. During discharging, this can mean that the available capacity at a given performance requirement is lower, or, that the performance is reduced at lower states of charge without falling below a safe or 'healthy' cell voltage level.

This means that the cell performance depends significantly on the cell temperature. However, the cell temperature depends on the usage profile, which, in turn may depend on the cell performance. Furthermore, the cell temperature depends on other factors, such as cooling. Ageing is another significant factor. The SEI increases with ageing, which adds to the internal impedance and decreases performance. The SEI impedance significantly depends on temperature.

Cell heating or cell insulation may improve cell performance drastically. However, ageing is accelerated at elevated temperatures and, after only a few cycles, the improvements that are due to the higher temperatures may be negated by the increasing SEI impedance which is due to ageing. Due to these complex interdependencies, it is very difficult to make general statements or predictions about cell performance. Managing the cell temperature in such a way that they are kept at a constant temperature would significantly help in predicting the cell performance.

During the course of this project, the manufacturer has accounted for this performance decrease at lower temperatures by suggesting an end of discharge voltage which is temperature dependant. Other manufacturers additionally suggest end of discharge voltages that are dependant on the discharge rate. However, such suggestions require

more sophisticated closed-loop type control rather than simple hardware protection incorporated in battery management systems. In addition, these approaches lead to questions of whether such schemes of lowering the allowed cell voltage will accelerate ageing and subsequently affect cell life or cell performance. Investigating this question is not within the scope of this thesis. Significant research is required in this area, in order to optimise the implementation and management of lithium-ion cells. For future research, it is suggested that these questions could, either, be investigated by field-testing with statistical analysis, or, by investigating the effects of the electric field distribution across the cell. The latter would give an insight into possible side-reactions under different conditions.

5.7 Degradation During Main Test Series

One objective is to quantify the degradation. It is assumed that two different kinds of degradation may occur in general:

- A decrease of available capacity due to lithium consumption, pore clogging, electrolyte drying out or structural changes in the electrode material.
- A decrease in performance / impedance increase due to growth of SEI, changes in electrolyte composition or structural changes in the electrode material.

5.7.1 Apparent Capacity Degradation

Figure 43 shows the discharged capacities in Ah for all test cycles.

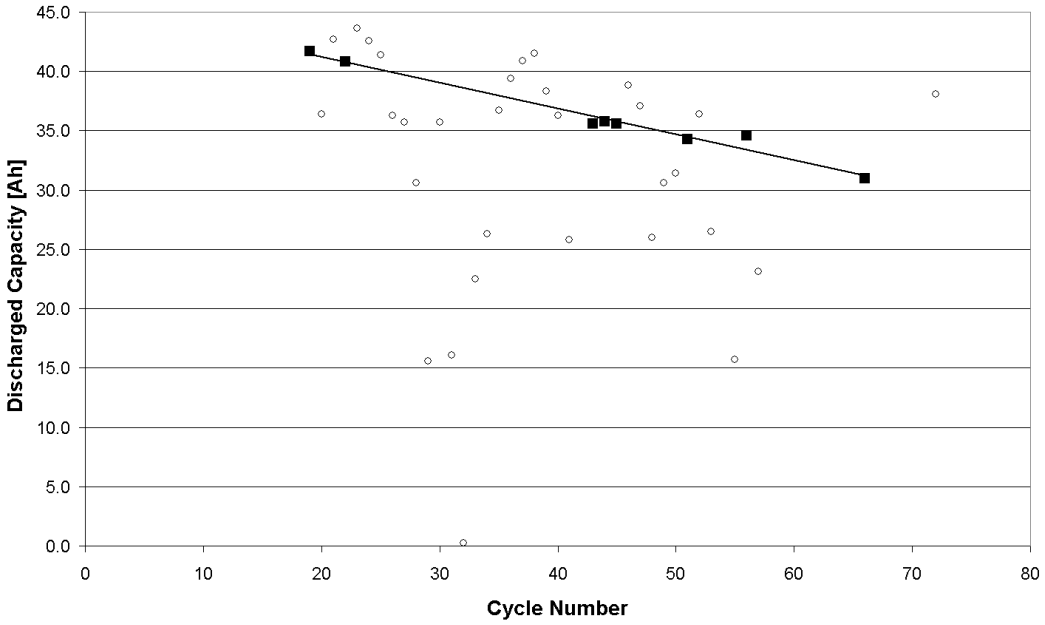

Figure 43 Discharged capacities in subsequent test cycles at different conditions

The discharged capacities depend on the test conditions. The solid squares represent the reference cycles and the small circles represent the results of the other tests as defined in section 4.7. A linear interpolation line is drawn through the points of the reference tests in order to indicate the degradation. This decrease in dischargeable capacity at reference conditions can be represented by the following formula:

$$Q_{dis,ref}(N) = 45.529\text{Ah} - N \cdot 0.2163\text{Ah}$$

The decrease in capacity at reference conditions (25 ºC), as shown in Figure 43, is the apparent decrease in capacity. It represents a combination of decrease in true capacity and increase in internal impedance.

5.7.2 Internal Impedance Degradation

One way of determining whether the cell suffers from an impedance deterioration, which becomes visible as an increase in voltage droop, is to calculate the mean cell

voltage for all reference cycles during the series of tests. The mean cell voltage can be derived as follows.

The discharged energy E in Wh and the discharged capacity C in Ah were logged during the tests:

$$E = \int V_{cell}(t) \cdot I(t)dt \qquad C = \int I(t)dt$$

The discharge rate is a constant current I_0 but with pauses. With T_{net} being the net time with I_0 actually applied, these equations can be simplified to:

$$E = I_0 \cdot \int_{T_{net}} V_{cell}(t)dt \qquad C = I_0 \cdot T_{net}$$

Dividing the energy content E by the capacity C reveals the mean cell voltage during discharging periods:

$$\overline{V_{net}} = \frac{E}{C} = \frac{\int_{T_{net}} V_{cell}(t)dt}{T_{net}}$$

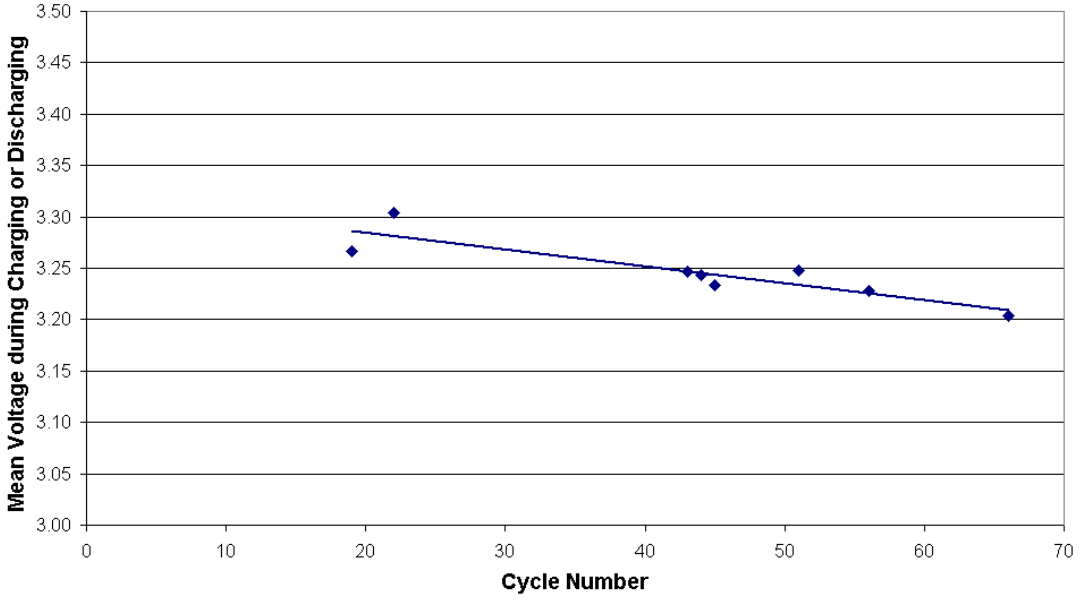

Figure 44 Development of mean discharging voltage over test cycles as an indicator for the decrease in performance

Figure 44 shows the development of this mean cell voltage degradation during discharge over the number of test cycles. Each solid square represents the mean discharge voltage for one test cycle at reference condition. The solid line is a linear regression line through these points.

A clear increase in impedance can be seen. This contributes to the apparent decrease in capacity at reference conditions.

Figure 43 and Figure 44 clearly show that significant cell degradation occurred during testing. The degradation became apparent in decreasing available capacity, as shown in Figure 43 and in a loss of performance, as shown in Figure 44. The tested specimen degraded particularly quickly, as it lost more than 20% of its available capacity within 50 cycles. However, this provides the opportunity for analysing and discussing the effects of degradation during testing, even though only a small number of tests cycles were conducted. This understanding can help when testing higher quality cells, which degrade much more slowly but, also, significantly if many test cycles were conducted. It emphasizes the importance of repeating cycles under the same conditions and also frequently repeating cycles under a chosen reference condition.

5.7.3 True Capacity Degradation

The decrease in capacity can be described with the loss in capacity per cycle or per time. One cell was used for the preliminary tests and then tested again about one year and 16 cycles later. The capacity decreased by about 10 % in this time. Several cells were stored for about one year before being tested and their capacity was similar to that of new cells. The specimen that was used for the series of tests lost about 25 % capacity within 50 cycles and only 4 months. This indicates that for the tested cell type, cycling has a higher impact on capacity loss than time.

As discussed in the chapter 3, ageing mechanisms seem not to be well understood. Up to today, modelling or predicting ageing for a new cell design is highly speculative [14]. However, conclusions can be made from the work described in literature:

- The ageing mechanisms in lithium-ion cells are monotonous, with minimal risk of sudden failure.

- Capacity loss can be modelled through a parabolic equation in time, following the Arrhenius law with temperature.
- Capacity loss can also be modelled as a function of cycles.
- A linear equation for modelling ageing can be used instead of the parabolic equation and this can often produce better extrapolation results. However, no fundamental explanation is currently offered for this.

Hence, it can be assumed that the linear model of capacity degradation over cycles is a suitable approach for investigating capacity degradation.

The approach in subsection 5.7.1 for quantifying the decrease in capacity is to use all of the eight reference test cycles during the series of tests, as shown in Figure 43. The linear regression reveals that the apparent capacity decreases with a rate of 0.2163 Ah per cycle. However, the reference cycle is at 25 °C and at a rate of 15 A discharge. Performance degradation results in higher voltage drop and, hence, the end-of-discharge voltage is reached sooner. Using more favourable conditions (i.e. smaller discharge rates and higher temperatures) is more suitable for determining the true degradation in capacity. This is because using more favourable conditions means that the voltage drop across the internal impedance is smaller and thus the impedance degradation has a smaller effect.

One approach for determining the true decrease in capacity is to analyse the test results under the most advantageous conditions (5A, 45 ºC) where the performance decrease shows the smallest effect. Two tests are conducted under these conditions. The results of these test cycles (cycle number 38 and 72) are:

$$Q_{dis,max}(N=38) = 41.5 \text{ Ah and } Q_{dis,max}(N=72) = 38.1 \text{ Ah}$$

Assuming a linear capacity degradation, this reveals the following relationship:

$$Q_{dis,max}(N) = 45.3\text{Ah} - N \cdot 0.1\text{Ah} \qquad (5)$$

The results under this test condition revealed that the capacity degraded at a rate of only 0.1 Ah per cycle rather than 0.2163 Ah as in subsection 5.7.1. Only two test cycles were conducted under the favourable conditions and this may cause significant

errors. The 15-minute pauses every 10 % of discharged capacity can cause errors similar to those discussed in subsection 5.2.3 for charging. The first test cycle delivered 41.5 Ah, which was shortly after such a pause where the cell had the chance to relax concentration gradients. The second test under the same conditions delivered 38.1 Ah, which was shortly before such a pause. In a worst-case scenario, the cell would have delivered only just above 40.0 Ah in the first test, so that the additional 1.5 Ah could be discharged only due to the previous relaxation of concentration gradients. This means that the capacity degradation would only have been approximately 0.056 Ah/cycle. It can be concluded that the true capacity degradation was between 0.05 Ah/cycle and 0.10 Ah/cycle.

However, it is obvious that the increase of internal impedance was significant and added substantially to the apparent capacity degradation under reference conditions. This is in contrast to the conclusions in subsection 5.3.2, where it seemed that the main degradation was true capacity degradation. However, the results discussed in subsection 5.3.2 were not accurate because those tests were conducted as part of the preliminary tests as defined in chapter 4, which lacked the sophistication of the tests leading to the above results.

5.8 Performance Results

The main series of tests is designed in order to investigate the performance of the lithium-ion cell under various conditions. The first measure of performance to be presented here is the available capacity under different conditions.

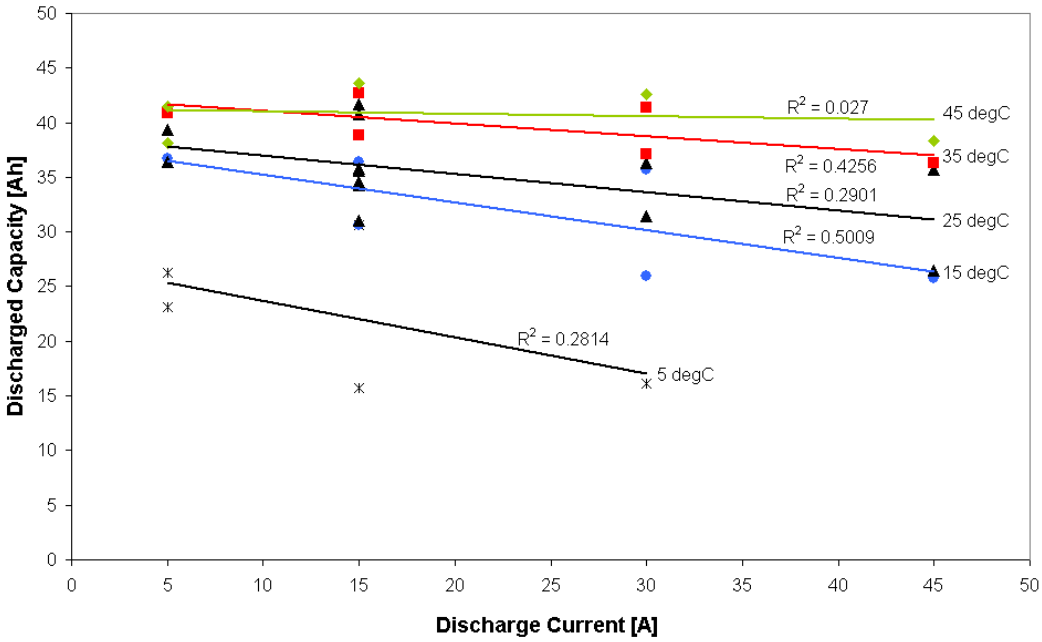

Figure 45 Discharged capacities at different currents and temperatures with trend lines for each temperature

Figure 45 shows the discharged capacity for each test cycle as a function of discharge current. A trend-line is added for each temperature setting. The bottom line is for 5 ºC, the three lines above that are for 15ºC, 25ºC, 35ºC and the top line is for 45ºC.

Figure 45 reveals that there is poor correlation between the interpolated regression line and the measurement points. This is because of cell degradation which occurred during the series of tests which are discussed in section 5.7. The following figure shows the same results but with an attempt to compensate for this cell degradation using the equation (3) from section 5.7.

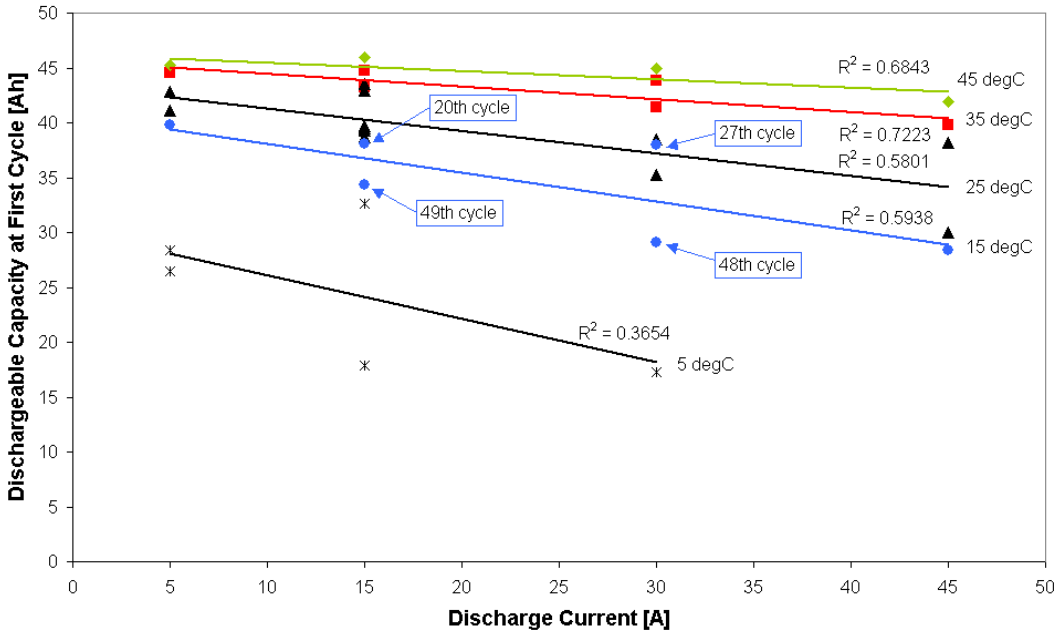

Figure 46 Discharged capacities at different currents and temperatures with compensation for cell degradation during testing

Figure 46 shows the discharged capacities corrected in such a way that they represent the performance as if it was the first test cycle. The capacity is presented as a function of the discharge current. Temperature is the parameter for the five curves. In Figure 46 it can be seen that, although improved, the correlation is still not very good.

However, as already discussed earlier, not only capacity degradation occurred but, also, performance degradation. This can be seen as a consistent type of error in Figure 46. The performance degradation results in a higher voltage drop which, in turn, causes the discharge to reach the cut-off voltage earlier than expected, especially at less favourable conditions (higher current, lower temperature). The corrected capacities are consistently higher during earlier cycles than those during later cycles and this is more apparent at lower temperatures. Some test cycle numbers are pointed out in Figure 46 in order to demonstrate the consistency of this error. It can also be seen that the degradation correction suggested in chapter 5.7 works well for high temperatures where the increase in impedance has little effect on the available capacity.

For gaining better predictions at lower temperatures, one would need to derive a method that takes impedance degradation into account for determining the apparent

capacity degradation at different temperatures and at different discharge rates. However, little is to be gained in practical terms because the apparent capacity significantly depends on cell heating during discharge and also depends on times for relaxation, as already discussed in section 5.5. Knowing the capacity and the apparent capacity degradation for the employed test pattern tells one very little about available capacity and apparent capacity degradation under other conditions. And so, no further investigation was undertaken to improve the correlation of the degradation predictions.

The key to this problem is to describe and quantify the performance degradation in such a way that the performance, the apparent capacity and the available energy can be predicted by simulation. This requires determining the cell parameters and their changes over cycling.

An alternative way is to design the test cycles in such a way that they are similar to the discharge profile in the target application. However, this would require several different tests for different applications and, even then, the discharge profile cannot always be predicted sufficiently accurately.

A third alternative is to insulate or heat the cells, because warm cells are not affected significantly by performance degradation. This means that the pure capacity degradation can be predicted and described more easily, as shown above. However, as warm cells degrade more quickly, a sophisticated temperature heating/cooling strategy might be required in order to optimise the balance between long-life, good performance and accurate performance prediction.

6 CONCLUSIONS

The first major contribution of this work was to holistically derive a hybrid electric vehicle drivetrain concept and specification that is viable and sustainable. For the first time, a series hybrid electric vehicle drivetrain with plug-in recharge facility using modern lithium-ion batteries was investigated and assessed in a future scenario. Previous research concluded this drivetrain concept to be non-viable. To some extent, this was due to employing inferior battery technologies. Partly, this conclusion was due to an assessment based on either the current scenario or based on non-holistically derived future scenarios. The approach presented here however, concluded that this drivetrain has a significant potential to be the short to medium term future solution for individual transportation needs.

It emerged that there was insufficient information on the battery system technology, which is a key component in such a vehicle. Substantial testing is required so that the battery can be modelled and understood sufficiently in order to answer relevant questions. Questions for example, regarding battery life, available performance or electric range under certain conditions. The required information is substantially complex so that using ordinary test methods is very time consuming and expensive.

Conventional test methods usually comprise one or more approaches. One can conduct extensive impedance spectroscopy tests in order to build equivalent circuit models of the test specimen. However, such tests are extremely time consuming and require expensive equipment for testing large cells at high currents. Furthermore, such tests could not determine all performance characteristics such as available capacity or energy under various conditions. They can also not be used for determining specific behaviour patterns such as, for example, charge-discharge hysteresis.

Another conventional test method for determining available energy and for predicting ageing behaviour is to conduct a series of test cycles with several cells under various conditions. Again, such tests are very time consuming and expensive. Furthermore, they do not generate a fundamental understanding or battery model and they have to be designed specifically for an application in order to produce meaningful results.

The other common approaches are fleet and laboratory testing. The design of fleet testing is very demanding and is open to the risk of generating irrelevant data contained in a huge amount of data, and it provides no guarantee of producing adequate relevant data. The same can be said of cycling tests in a laboratory.

The above approaches are very time consuming and expensive and all of them exhibit the significant risk that they generate data that is meaningless or too complex. This means that the test data cannot easily be analysed and, subsequently, it might not be recognised that the data is meaningless. It was possible to show in experiments conducted here that the lack of a suitable full-charge reference point for example could have caused data to be meaningless if no measures had been taken.

The work described here was based on the following approach. At first, an understanding of the application was gained in order to determine the requirements for testing. Then, typical characteristics of the employed battery type were researched as well as relevant characteristics of other battery types; this then helped further to narrow down test requirements. Following this initial work, several preliminary test cycles were conducted and the great importance of conducting this preliminary work became evident. Following that, a few specific tests were designed and conducted based on the outcome from the preliminary tests. Based on the information generated by the preliminary tests, a more meaningful series of test cycles was designed and conducted. The aim of this design was to be able to extract information on a comprehensive range of characteristics under various different conditions from a minimum number of test cycles. Such characteristics included: Ageing behaviour, parameters for modelling, information on available energy, battery capacity and battery efficiency. All tests were conducted with just one test specimen and it is suggested to obtain statistically meaningful results by employing data logging in field tests.

All tests were based on the step response or current interruption technique, which promises to be more cost efficient and faster than traditional approaches such as impedance spectroscopy. For the first time, an attempt was undertaken to derive equivalent circuit model parameters directly from such step response technique. This is considered to be the unique advantage of impedance spectroscopy.

The tests as suggested in this work have been carried out on a large, low-cost, high-energy lithium-ion cell and several relevant findings have been made. The tested specimen for example does not exhibit a consistent reduction of available capacity with higher discharge currents, as observed in lead-acid batteries ("Peukert-behaviour"). It is possible to discharge the same capacity regardless of the discharge current. However, this changes significantly depending on the discharge scenario. The available capacity decreases significantly at higher currents if the cell has sufficient time to cool down during the discharge. This scenario is very likely in any electric vehicle where, for example, the vehicle is driven to work, parked for eight hours, letting the battery cool down, and then driven back home. Suggestions for further work in this area in order to predict the remaining capacity and the performance in a production vehicle can be made. Further tests should be conducted in order to optimise the lower voltage cut-off for the individual cells and the thermal management, so that the life, performance and cost of the battery system can be optimised.

In the course of the work mentioned above, the applicability of the Peukert equation to lead-acid batteries when used in this application was also investigated. It was discovered that the Peukert equation is not relevant and cannot be used in applications with varying currents like ours. This work is not included in this thesis as it was focusing on lead-acid batteries and hence is not directly relevant. However, the investigations produced some interesting results, which were published in a journal and can be found in the appendix.

The test specimen did not exhibit a significant charge-discharge hysteresis if compared with its substantially long relaxation behaviour. This study was able to develop and assess an alternative method for measuring the OCV_{eq}. This method provides results rapidly and during the normal test cycles despite the long relaxation times. $OCV_{eq}(SOC)$ curves were obtained at different temperatures and at different stages of ageing. It was found that these curves were almost independent of ageing, provided that SOC was measured in percentage. This indicates significant consumption of active species to be the main reason for ageing. However, the investigation into ageing suggested that impedance increase was the main reason for ageing throughout the tests. This is an interesting contradiction and it is in line with

the current lack of understanding of ageing in lithium-ion cells. These findings provide an interesting entry point for future research into ageing.

The long relaxation behaviour of the test specimen makes it difficult to measure the OCV_{eq} in the application and during testing. It cannot be used for instant SOC prediction or as a reference during normal operation. Specific tests were designed and conducted in order to determine a suitable reference point. This reference point was successfully assessed with specifically designed measures throughout the test series. The reference condition can be used during testing and also in the application in order to reset coulomb counting for SOC determination. However, it is possible that ageing has a significant effect on this reference condition and this point should be considered and investigated in future research.

It was demonstrated that simple preliminary tests with just one cell are essential before conducting exhaustive tests with several cells. The investigation into an optimum resting time between tests and also the determination of a suitable reference condition are two very important examples. Further work could be done here in order to work out a template for designing and conducting such preliminary test cycles.

The suggested tests were able to detect ageing throughout the test series as well as to measure $OCV_{eq}(SOC)$ curves, model parameters and other relevant characteristics such as capacity. The tested specimen showed substantial ageing during the test cycles and this type of cell can be classified as not suitable for this application. However, the rapid ageing helped to investigate the suitability of the proposed test. Ageing was detected successfully but it appeared difficult to separate capacity degradation from impedance increase. Suggestions for further work can be made in this area in order to obtain more coherent information (e.g. available capacity as a function of temperature and current). It is suggested to determine model parameters for each set of tests and to study the change of those parameters during ageing.

The attempt to directly determine equivalent circuit model parameters from the step response technique proved to be a comparably fast method. However, occasionally, it was difficult to draw suitable lines between the different time constants. This method is very promising and it is suggested to improve the method and the model by employing some initial impedance spectroscopy in order to characterise the model

first and then to employ this method in order to determine parameters during testing. Further research should be carried out in order to validate this method by comparing the results with results from impedance spectroscopy.

Some specific characteristics have been investigated, analysed and described in detail. The recent paper on the Peukert effect as published in the Journal of Power Sources [26] is, for example, already cited in Wikipedia[2] as the only other reference next to the original Peukert paper [63].

In summary, this study has made an important step towards more efficient, more meaningful and also lower-cost testing of electrochemical energy storage devices. Interesting findings have been described and several paths for future research have been opened.

[2] See http://en.wikipedia.org/wiki/Peukert's_Law .

7 Appendix A: Publications and Contributions

The submitted work has been grouped into two main sections. The first section consists of a broader, more holistic systems approach on future individual transportation solutions with vehicles. The second section consists of an in-depth research into the testing and characterisation of large lithium-ion batteries for such transportation solutions and for other applications.

7.1 Section One: Systems Approach

The author's first publication was:

A1: "Peace of Mind Drivetrain for Hybrid Electric Vehicles", a "Special Presentation" in December 2002 by "Britain's Younger Engineers at the House of Commons" [23].

This first publication is in the form of a leaflet and a poster presentation, which were produced for an event at the House of Commons [in 2002]. Claire Curtis-Thomas MP, who was the only MP with an engineering background at that time, organized the event which was intended to raise awareness among MPs and Members of the House of Lords of the importance of British Engineering and provide an opportunity of learning about some state-of-the-art engineering projects. The organiser invited all Universities in Britain to suggest young researchers to present their projects at this event and the author's work in its early stage was one of those selected by the University of Southampton.

This presentation was tailored to its particular audience of non-engineers and was delivered in an accessible format without the usual highly technical details and not in the depth the subject would normally require for a full exposition. However, the presentation is included with this thesis as a suitable entry point for systems engineering towards more sustainable vehicle solutions. It documents the start of the author's work and his ambition to think 'outside the box' and to set his in-depth engineering work, which is reported in more detail in other publications, within the context of a broader view. The poster presentation is included in this appendix.

A2: "Performance Evaluation of a Low Cost Series Hybrid Electric Vehicle", paper presented at the EVS-19 (annual international Electric Vehicle Symposium) 2002 in Busan, South Korea [28].

The second paper included here expands on the work presented in the first publication. A more detailed and more technical discussion on vehicle requirements and impacts can be found, as well as the methodology and the results from modelling and simulating hybrid vehicle drivetrains.

A major contribution of this work was to revisit the series hybrid electric vehicle drivetrain concept to look at its viability in mass-produced cars. Several years earlier, electric vehicles and the hybrid electric vehicle were pronounced "dead" after some trials with small-series production prototypes (e.g. "Audi Duo"). These trials were launched during a major oil crisis but work on these ideas slowed down and eventually stopped when the crisis ended. Even in the beginning of the author's work in 2001, hybrid electric vehicles (HEV) were said to be non-viable due to their "high cost", "technical complexity", "insignificant fuel-saving potential" and "unpredictability of the battery" [21; 44; 59; 70; 73]. Unlike their European and American competitors, the Japanese carmakers Toyota and Honda kept their Reasearch & Development on HEVs ongoing, driven by their vision and by the technological challenge to make these concepts viable. Due to constantly increasing petrol prices and rising awareness of the dependency on oil, as well as technological advances, Toyota and Honda now manage to sell their HEVs very well in the American market and there is rising interest in other major markets. The demand is so significant that all major carmakers are now trying to catch up on 10 years of Research &Development in order to be able to offer HEV solutions to an increasingly aware customer base.

While all current HEVs on the market are parallel or power split HEVs, the series HEV drivetrain is still not seriously considered by any of the major carmakers. This is because of its reputed “higher cost”, “lower efficiency”, and “higher dependency on the battery” [39; 44].

However, many circumstances have changed and still are changing since the carmakers considered series HEV drivetrains. Cost for liquid fuels are consistently rising and this trend is likely to get worse. The number of cars on the roads is steadily increasing, causing more pollution and more traffic congestion [32; 68]. The average traveller uses the car on mostly short journeys at low average speeds [32]. Governments and Local Authorities are increasingly introducing incentives towards alternative cars. Technology is advancing, leading to smaller and more efficient motors, power electronics, cheaper and more powerful microprocessors and, most importantly, much smaller and lighter batteries. Finally, managing the battery in a series hybrid electric vehicle with plug-in facility is considered easier than managing one in a parallel or power split, due to less dynamic usage and more frequent ‘full-charge’ calibration [42].

These changes are in favour of the series HEV and inspired the author to revisit this drivetrain concept as early as in 2002. The work is based on four important ‘pillars': Innovative battery technology using lightweight large lithium-ion cells, which will be subject of the author’s following more in-depth work; the facility to recharge the battery from the mains (plug-in HEV); an intelligent energy management and optimised selection and sizing of drivetrain components based on vehicle performance criteria.

The paper presented at the EVS-19 [28] has stimulated several other researchers around the world to revisit the series HEV, and they have contacted the author in order to obtain the MATLAB modelling files. Lecturers have used the paper for student competitions, asking them to optimise the vehicle concept and the author is giving regular lectures on HEV drivetrains at the University of Southampton.

The author implemented parts of the specified drivetrain into a compact size car in order to validate the simulation results. This task required the design and build of an electronic battery protection system and charging system for the large lithium-ion battery, which was not commercially available at that time. The author has now founded REAPsystems Ltd, a company specialising in the design of battery management systems for large lithium-ion batteries. REAPsystems Ltd. now offers an off-the-shelf product as well as customised solutions for protecting and also managing such batteries[3].

The encouraging simulation results regarding energy consumption and performance, as well as the availability of a functional electric vehicle demonstrator with the lightweight battery attracted a lot of coverage including two spots on both television and radio, an article in the Financial Times, a leading article in the Auto Express and also several articles appearing in various internet magazines and forums.

Nowadays, a few companies have started implementing a series HEV drivetrain into demonstrators and show cars [13]. Commercial companies now offer refitting of the Toyota Prius HEV with larger batteries and a plug-in facility[4] and Toyota has recently announced offering the plug-in facility in future models.

The author's entire body of work up to 2003 has been published in:

A3: Transfer Thesis in 2003 [24].

This thesis covers electronic battery protection circuitry, vehicle integration and holistic vehicle performance requirements. This thesis also contains vehicle impact assessment, which includes well-to-wheel analysis for the energy, technology review, drivetrain modelling and simulation work, as well as derived goals for the energy management of such a series HEV.

---

[3] For more information, see www.reapsystems.co.uk

[4] See EDRIVE (http://www.edrivesystems.com/), going green (http://www.goingreen.co.uk/), Amberjac projects (http://www.amberjac-projects.co.uk/).

The author has been invited to be a co-author of the following two papers, where he was responsible for collecting the data and writing some sections:

A4: "Life Cycle Impacts and Sustainability Considerations for Alternative and Conventional Vehicles", paper for SAE 2003 World Congress & Exhibition [40].

A5: "Sustainable Future Transportation", paper for SAE International Future Transportation Technology Conference, Costa Mesa, California USA [41].

The author took part in a research project on sustainable innovation at the Imperial College in London. He was invited as the stakeholder for the inventors and sustainable innovators. The final report is not the author's publication, but contributions have been made through actively attending all workshops:

A6: "Transforming Policy Processes to promote sustainable innovation: some guiding principles" [35].

The fact that there have been these achievements and requests to make contributions to other authors' work as listed above would support the view that the author's broad-based and holistic approach is considered to be relevant. The author was encouraged to believe that holistic thinking is a very powerful tool capable of assessing ideas and generating forward-looking and far-reaching visions. This is what made the author present a paper, with this focus, at the Vehicular Propulsion and Power Conference (VPPC) 2006:

A7: "System Modelling and Simulation as a Tool for Developing a Vision for Future Hybrid Electric Vehicle Drivetrain Configurations", paper presented at the VPPC 2006 organised by the Power Electronics Society (PELS) and IEEE in Windsor, UK [29].

Whilst the paper is technically based, the presentation focussed more on holistic and "system thinking". The presentation sparked some interesting discussions among the audience, and Prof. Mark Ehsani[5] found that the key objectives were very similar to

[5] Professor Mehrdad (Mark) Ehsani, Texas A&M University (USA), Chair of VPPC Steering Committee & Joint VTS/PELS VPPC Committee.

those which he was going to present in a later keynote presentation [31]. In fact, the author found that the key message of his own presentation found a lot of common ground with several of the keynote speakers. The key message was that "we are very good at researching small problems in great depth but we have to learn to think and research more laterally and to understand how the 'small problems' integrate with the 'bigger problems'".

7.2 Section Two: Large Lithium-Ion Batteries

The first part of the work revealed that the series HEV is a potentially viable vehicle drivetrain concept. However, it was clear at the outset that the energy storage device (battery) is the key component of any HEV drivetrain, and the series HEV in particular. The battery is frequently blamed as being the weakest component in hybrid and electric vehicles but it has been shown that this situation can be improved by effectively managing the battery [5]. This second part of the author's work is concerned with the research on large lithium-ion batteries, their management requirements, testing and characterisation.

The author employed an innovative large lithium-ion battery in the research vehicle. In 2002, as part of the University of Southampton, he was, in fact, the first European customer of a new Chinese company offering such innovative large lithium-ion cells at an affordable price. The author tested the cells at the Institute of Power Electronics and Electrical Machines (ISEA) in Aachen, Germany in 2002 and he published the very promising results for the University of Southampton on the World Wide Web[6]. The electric vehicle with these batteries was exhibited on various occasions.

The public and commercial interest was significant and the author organised two of his own seminars on large lithium-ion batteries, was invited to give presentations at various other seminars and founded his own company in 2003 in order to be able to respond to the commercial enquiries. The recent invited paper presentation as part of the electric vehicle exhibition and seminar at the University of Aschaffenburg,

[6] See http://www.soton.ac.uk/~dad1.htm

Germany gives a very good overview of the opportunities and challenges for using large lithium-ion batteries, and is therefore included in this work:

B1: "Large Lithium-Ion Batteries: a Review", paper presented at the EMA2006, Exhibition and Conference at the University of Aschaffenburg, Germany [27].

The work on modelling and simulating vehicle drivetrains described earlier revealed that modelling the battery exhibits a major challenge. Testing motors, power electronics, engines and gearboxes is a fairly straightforward and fast process. Modelling these components, as well as the vehicle dynamics, is a task that is well understood and which generates sufficiently accurate results, at least for the purpose of modelling a complete drivetrain. Modelling the battery, however, is very challenging and any battery model is prone to produce potentially very misleading results, with inaccuracies far beyond the 10% level. This inaccuracy is due to the many dependencies of the electrochemical process as described in several of the author's publications.

A further complication in modelling the innovative large lithium-ion batteries was that they were new on the market at the time of this work. Characteristics, behaviour, performance and test results were not publicly available and the manufacturers had no test data available whatsoever. The author conducted some preliminary tests, developed a preliminary battery model, described the most significant characteristics and suggested suitable test algorithms. This novel work was published in a journal paper in 2004:

B2: "Rapid Test and Non-linear Model Characterisation of Solid State Lithium-Ion Batteries", Journal of Power Sources 2004 [1].

The author was then involved in testing a different type of lithium-ion cell (high power lithium-polymer cell) with and without high hydrostatic pressure. The cells were tested and characterised under various conditions using the test procedures suggested by the author in the publication mentioned above. The analysis revealed that some characteristics deviated significantly from the results with the first lithium-ion test candidates. The tests, analysis, results and interpretation were published in two papers at two conferences.

B3: "Performance of Lithium Polymer Cells at High Hydrostatic Pressure", paper presented at the 14th UUST (Unmanned Underwater Systems Technology) Conference, 2005 [65].

This paper won the "Best Student's Paper" award at that conference. It is included here because it shows the deviation of characteristics of a different cell type, as well as the applicability of the suggested test procedures for characterising batteries. The author of this thesis was mainly involved in the testing section covered in this paper as well as the interpretation of the results.

However, the author found that the preliminary battery model and characterisation was not fully comprehensive and that much more testing would be required. It became clear that testing itself is a major challenge with large cells, due to the cost of the cells and also due to the cost of the testing equipment. The importance of rapid but comprehensive testing cannot be overemphasized, especially in the light of continuous and rapidly progressing battery research and improvements. Developments are so rapid (or testing takes so much time) that manufacturers nowadays have improved the cell chemistry and cell construction and, hence, have changed cell performance and characteristics by the time the cell testing is completed. For these reasons the author has focussed his research on cell testing towards the end of his project.

All tests are based on the step response or current interruption technique. This technique analyses the voltage response of a cell to interruption of the charge or discharge current. Such interruptions naturally occur during normal use of most batteries or can be stimulated in almost any application without significant additional cost for test apparatus. This technique enables less time-consuming laboratory testing using lower cost equipment when compared with conventional test techniques, such as impedance spectroscopy. A concise summary of the author's work on testing large lithium-ion batteries was presented at the AABC (international Advanced Automotive Battery Conference) in 2005:

B4: "Efficient Testing and Evaluation Methods for Faster Market Introduction of Large Lithium-Ion Batteries", paper presented at the AABC 2005 in Honolulu, Hawaii [25].

This paper firstly presents a solid groundwork towards developing a testing template for testing rapidly but comprehensively and for characterising the performance of new battery chemistries and cell constructions. It is especially dedicated to large cells and an example is given for a high-energy lithium-ion cell.

During the project, the author discovered many performance characteristics that were unexpected and unknown in other battery types. However, the most surprising characteristic of the tested high-energy lithium-ion cell was its ability to provide same or even higher capacity during discharge at high rates when compared to discharge with a lower current under certain circumstances. The so-called Peukert effect, which states that the available capacity is lower at high discharge rates if compared with low rates, [63] is well known in lead-acid batteries but doesn't seem to apply to the tested specimen at all. The author has taken this surprising finding as an opportunity to investigate this so called Peukert effect for lithium-ion batteries, as well as for lead-acid batteries. The Peukert effect is important for designing battery fuel gauges, and several patents have been reviewed. This part of the work has been published in the Journal of Power Sources in 2006 and is included here as an example of the author's in-depth research:

B5: "A critical review of using the Peukert equation for determining the remaining capacity of lead-acid and lithium-ion batteries", Journal of Power Sources 2006 [26].

A1:

"Peace of Mind Drivetrain for Hybrid Electric Vehicles"

"Britain's Younger Engineers at the House of Commons"

[23]

Poster presentation – flyer included here

When will this technology be available?
The proposed drivetrain concept is based on existing technology and existing components like electric motors, Li-Ion battery and motor controller. Infrastructure for fuel and electricity is available. Vehicles comprising this proposed drivetrain can be on the market in the near future.

Our work:
We have specified the drivetrain components by taking into account all mentioned issues. The resulting vehicle has been simulated and assessed against the aims.
We are implementing this drivetrain into a vehicle and will compare real-life results with simulation results. The drivetrain management will be developed.

We are currently searching for partners and for funding.
You are welcome to contact us for further details!

University Of Southampton

www.soton.ac.uk/~dad1

Suleiman Abu-Sharkh
School of Engineering Sciences
University of Southampton
Phone: 023 8059 3397
Fax: 023 8059 3053
S.M.Abu-Sharkh@soton.ac.uk

Dennis Doerffel
School of Engineering Sciences
University of Southampton
Phone: 023 8059 2698
Fax: 023 8059 3230
ddoerffel@ses.soton.ac.uk

www.ses.soton.ac.uk

Peace of Mind Drivetrain for Hybrid Electric Vehicles

The escalating number of vehicles on the road and the dependency on resources has raised awareness to vehicular environmental impacts and sustainability. Future vehicles will need to have less impacts on the environment and significant lower energy consumption. The dream of fuel-cell cars and a sustainable hydrogen economy may be achieved within the next thirty to fifty years.

In the meanwhile the hybrid electric vehicle (HEV) can represent an intermediate step forward. The challenge is finding that drivetrain - among all the uncountable options – that has significant societal advantages, leads the way forward to the hydrogen economy and meets consumer expectations.

Issues

Several aspects have to be considered when searching for suitable future drivetrains:

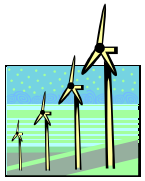

Low Energy Consumption is essential for defeating global warming, decreasing oil-dependency, introducing more expensive renewable energy sources and fuels.

HEV's are a new technology compared to combustion engine cars and they comprise more components. This leads to increased purchase cost. But **affordability** is a key issue for customer acceptance and fast market introduction.

Modern cars are a very sophisticated and versatile product. Alternative drivetrains must be competitive in **versatility and fun** to meet customer expectations.

The **impacts** of cars like noise, pollution and the compatibility with cyclists and pedestrians is what public is getting more and more aware of. They decrease quality of life for everybody.

Added value is the main motivation that makes people buy a new car. The drivetrain needs some sellable features.

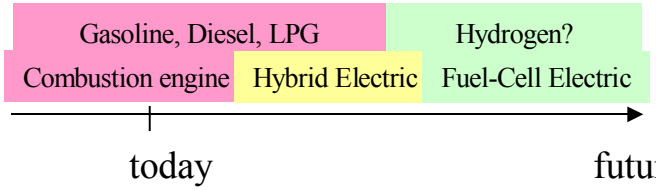

The fuel cell and a hydrogen economy might be the ultimate solution. HEV drivetrains that are introduced soon must be **compatible** with existing fuels and must **prepare** the introduction of fuel cells.

Proposed Drivetrain

Our proposal is a series HEV (SHEV) drivetrain.The vehicle has a pure electric range of 50 miles. This is sufficient for more than 90% of all journeys. Efficient components and recharging from the mains assure highest possible energy economy. A small engine/generator cuts in automatically if additional power or range is required. The engine/generator can be replaced by a fuel-cell when available.
The type and power of components is a key. They have been specified to assure affordability, low weight and small space. Simulation results have shown a fuel economy of up to 250 mpg – four times better than comparable vehicles with combustion engine.
The drivetrain management is an essential part of this concept. It controls the charging of the Li-Ion battery and deals with the cell-management. It runs the engine as rarely as possible, assures proper use of motor and battery but it also provides as much performance as possible. Driver demands, battery state of charge, remaining distance and topography are taken into account.

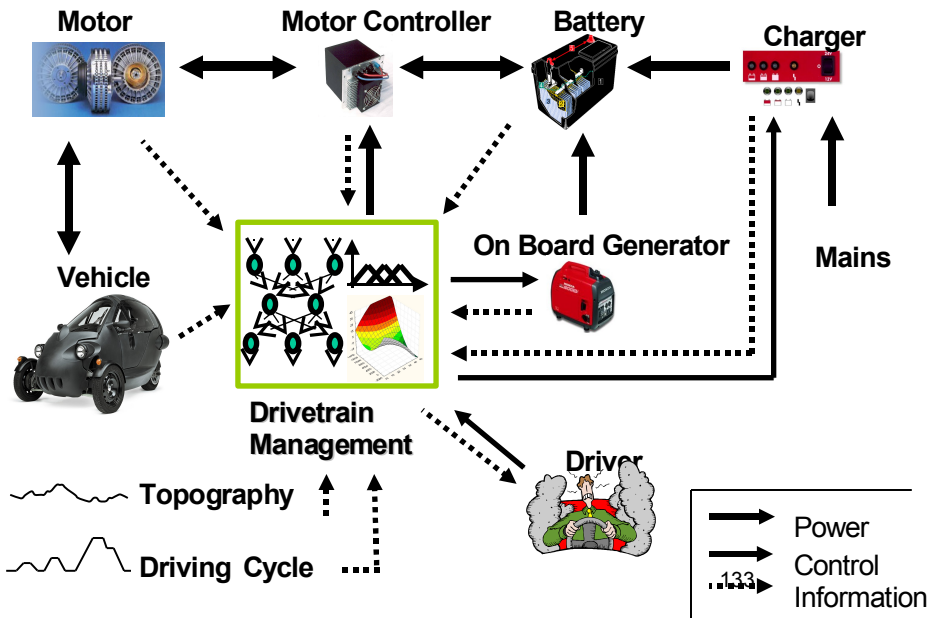

A2:

"Performance Evaluation of a
Low Cost Series Hybrid Electric Vehicle"

EVS-19 (annual international Electric Vehicle Symposium)
in Busan, South Korea

[28]

Conference paper

Performance Evaluation of a Low Cost Series Hybrid Electric Vehicle

Dennis Doerffel, Suleiman Abu-Sharkh

Abstract

The escalating amount of vehicles on the road has raised awareness to vehicular environmental impacts and sustainability; this has provided a stimulus for future mobility considerations. The conventional car may not meet future requirements regarding noise, emissions and energy consumption. There is a distinct lack of short-term alternative solutions that meet consumer requirements and has a potential for mass production. Furthermore, the internal combustion engine has been developed over 100 years and there may be some risk that the automotive companies choose to invest into the "wrong" alternative.

This paper presents a development process in an attempt to find answer this dilemma. The first consideration is the vehicle performance criteria that take into account consumer expectations and operational/regulatory/environmental factors. Secondly, the drive train components are identified, most are commercially available, and are particular to these factors. Finally, a computer simulation is used to assess the performance of the vehicle, in comparison with the factors.

The result of these investigations is a series hybrid electric vehicle that is recharged from the mains. The fuel consumption is four times better than that of a comparable car, but vehicle mass and cost have not increased significantly. The driving range of this vehicle is not limited to the battery-capacity.

This vehicle meets the consumer expectations as well as environmental issues and benefits with added driver comfort. Still being low-cost, it provides the potential for mass-production and thus reducing overall impacts on the environment.

Keywords: HEV, lithium-ion, energy consumption, vehicle performance, cost

1. Introduction

Cars have improved significantly over the last 100 years. They became more versatile, better in performance and more comfortable without increasing the purchase cost, which has lead to unprecedented increase in the number of vehicles on the road, especially given recent changes in work practices that require increase individual mobility. This increase in the number of vehicles together with rising awareness of their environmental impacts and sustainability provided stimulus for current discussion on future mobility.

Conventional cars with internal combustion engine do not meet future requirements regarding noise, emission and energy consumption. On the other hand, electric vehicles, which have far less impact on the environment, do not meet customer requirements regarding range, versatility or cost. Exisiting, mostly parallel, hybrid electric vehicles are too expensive and fuel-cell vehicles still need considerable development of the technology and infrastructure [1] [2]. All recent developments on hybrid electric vehicles have concentrated on the parallel hybrid. The series hybrid electric vehicle has in general been considered to be inferior to the parallel [3].

This paper is concerned with an evaluation of a plug-in series hybrid electric vehicle (mainly for urban and extra urban driving), which design is based on 1) a careful evaluation of vehicle specifications that meet consumer aspirations, and 2) a careful selection of drive train components. The proposed drivetrain concept ensures peace-of-mind concerning environmental impacts like in a pure electric

vehicle and peace-of-mind concerning range and versatility like in a conventional car without sacrificing the affordability.

The paper firstly discusses vehicle performance criteria taking into account consumer expectations and operational/regulatory/environmental factors. Secondly, the drive train components, mostly commercially available, are specified in the light of these specifications. Finally, computer simulation is used to assess the performance of the vehicle in comparison with the specifications.

2. Vehicle Performance Criteria

The proposed vehicle specification is based on the following considerations:

Speed: The maximum design speed of the vehicle determines the rated motor power and the smallest gear ratio at a given maximum motor speed. The rated motor power in a pure EV determines the battery power and this is known as a major cost issue. In the proposed vehicle, the rated motor power determines the generator and engine power as well.

To achieve higher speeds in this type of HEV, the five main and costly components (battery, power-electronics, motor, generator and engine) need to be more powerful and as a result bigger, heavier and more expensive. The maximum design speed of the vehicle should be chosen carefully and preferably as small as possible without compromising comfort. The UK has a speed limit of 70 mph (112 km/h) and our vehicle is designed for this speed.

Gradeability: The road gradient on highways together with the maximum speed determines the rated power requirement of the motor. Maximum road grade on UK highways is 4%. The maximum gradient in general determines the highest gear ratio. Most hills have less than 20% gradient and signs will warn before choosing a route with higher gradients. The vehicle is designed to climb at least 20% with maximum mass to make it versatile.

Acceleration: The acceleration determines the maximum motor torque and the gear ratios layout. We use axial air-gap permanent magnet brushed DC motors, which are capable of producing constant torque over their speed range, with about 50% overload torque capability.

It is assumed that the chosen motor that can achieve the maximum speed at highway gradient is powerful enough for moderate acceleration in urban areas. The simulation results presented later in this paper show that the acceleration performance is satisfactory.

Driving Range: Most trips are short trips: about 80% of all travelled distance is less than 40 km each trip [4] [5]. To keep the battery in an efficient range for this distance, the state of charge (SOC) should remain above 20% even when the battery is close to its end of life (80% of rated capacity). As a result, the vehicle should at least manage to achieve 40 km / (0.8 · 0.8) ≈ 60 km in pure electric mode. The Peace-of-Mind energy management will start the generator automatically to extend the driving range to at least 300 km.

Noise: This vehicle is designed for short trips. These trips usually have a low average speed. At low speeds the engine noise of conventional cars is much higher than the noise of tyres and air-resistance [6]. The electric motor itself is very quiet and the Peace-of-Mind energy management will ensure that the combustion engine does not run when engine noise has major impacts. The vehicle mass will be kept small to decrease tyre noise at higher speeds as well. Thus, this vehicle has very low noise impacts.

Pollution: This vehicle is basically an electric vehicle, powered by a battery. This type of vehicle has no local pollution and no pollution in general if powered with green electricity. The combustion engine will only cut in if necessary to achieve the desired trip distance or the desired power. The

Peace-of-Mind energy management will also assure the engine to run as rarely as possible and in its best efficiency/pollution region. It also avoids cold starts to keep the level of pollution low.

Vehicle size: Though a smaller vehicle keeps impacts low in urban driving and seems to be satisfying for short trips, we use a Daewoo Matiz (see figure 1) for better comparison with actual products.

Figure 1: Daewoo Matiz

Handling/Comfort: We propose to convert a vehicle similar to the Daewoo Matiz and thus the handling and comfort will be at least to the same standard. The conversion will enhance the handling through a better weight distribution. As a result, power steering is not essential any more. Less gear changing, no clutch, less motor noise and vibrations will increase comfort especially in urban driving with many start-stop procedures. Air-conditioning will not be implemented due to its high energy-consumption. Most "eco-cars" like VW Lupo 3l or GM Corsa Eco do not provide this feature either. Nevertheless, it could be implemented with a switch-off facility and powered by gas or even from a larger battery.

Energy Consumption: The aim is to keep the energy consumption between 1 … 2 $^{l}/_{100km}$ of fuel equivalent in urban driving. The vehicle will be purely battery powered and recharged from the mains in this scheme. The extra urban consumption will be higher due to the higher drag losses at higher velocities and because the engine will cut in to provide the power or range. The aim in this scheme is about 3 $^{l}/_{100km}$. This vehicle is designed for mainly short trips and thus, the combined consumption is near to the urban driving consumption and will be below 2 $^{l}/_{100km}$.

Vehicle Mass: The vehicle mass has major impacts on most requirements mentioned above. Keeping the mass low means better gradeability, acceleration, range, less noise and less energy consumption. The aim is to keep or even reduce the vehicle mass, when compared to the original by choosing the heaviest components such as battery and engine as small and light as possible. The motor and generator to be used are permanent magnet DC motors with very high power/mass ratio.

Cost: The purchase cost is targeted to be similar to a conventional vehicle by trying to keep the technology simple and the battery small. The battery is the major cost factor and thus, the battery management ensures highest possible life expectancy of the battery.

In conclusion: The task is to design a mainly battery powered vehicle with very low energy-consumption, pollution and noise but for a competitive purchase price and with high driving range and acceptable performance.

3. Component Specifications

This paragraph derives the component specifications from the vehicle criteria. The following formula are used to estimate the power requirements:

Rolling resistance: $$P_r(v) = c_r \cdot m_{\max} \cdot g \cdot v \quad (1)$$

Air drag: $$P_{air}(v) = c_d \cdot A_f \cdot \tfrac{1}{2} \cdot \zeta \cdot v^3 \quad (2)$$

Gradient demand: $$P_{grad}(gradient, v) = m_{\max} \cdot g \cdot v \cdot \sin(\arctan \tfrac{gradient}{100}) \quad (3)$$

The following constants have been used:

Gravitational acceleration: $g = 9.81 \, {}^{m}/_{s^2}$

Air density at 1 bar and 20 ºC: $\zeta = 1.19 \, {}^{kg}/_{m^3}$

The total motor power to propel the vehicle at a certain speed v and a gradient is:

$$P_{mot}(gradient, v) = \frac{P_r(v) + P_{air}(v) + P_{grad}(gradient, v)}{\overline{\eta_{mech}}} \tag{4}$$

Mechanical drivetrain efficiency is assumed to be on average: $\overline{\eta_{mech}} \approx 0.9$

The chosen vehicle is similar to a Daewoo Matiz [7] with its small mass. The vehicle body attributes are:

Air drag coefficient:	$c_d = 0.32$ (estimated)
Frontal area:	$A_f = 2.01$ m^2 (estimated)
Tyre rolling coefficient:	$c_r = 0.009$ (Advisor file [8])
Mass:	m = 778 kg (Daewoo Matiz)
Maximum mass:	m_{max} = 1153 kg (Daewoo Matiz)

Figure 2 shows the power requirements to overcome the rolling resistance, the air drag, the gradient of 4 % and the total required motor power over speed.

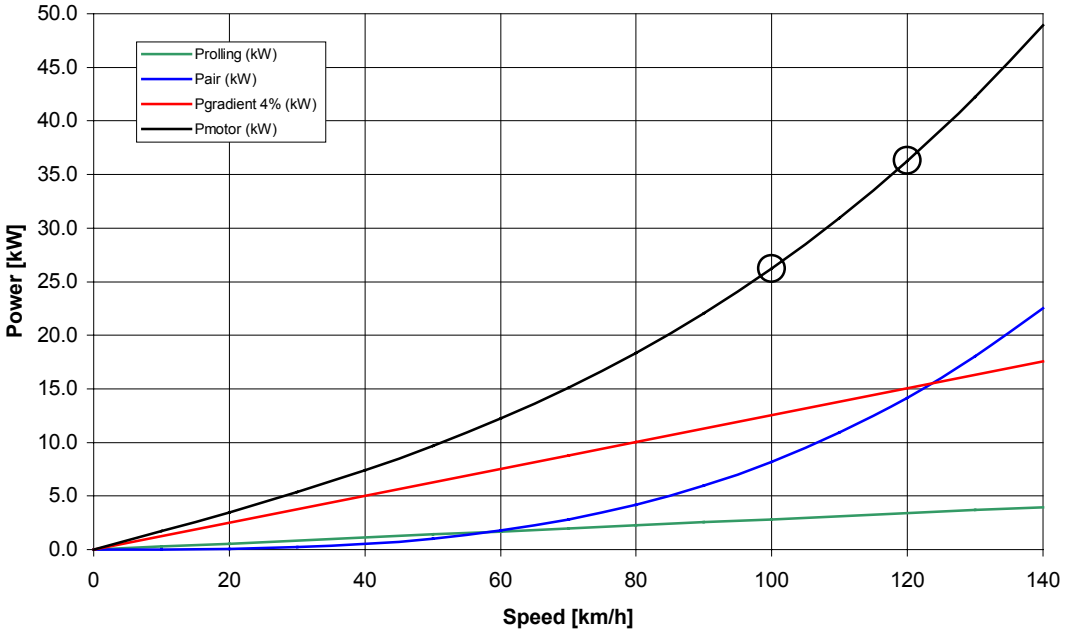

Figure 2: Power Requirements over Speed for the chosen Vehicle with 4% gradient

Propulsion motor requirements:
The power requirement of the electric propulsion motor is determined by the maximum speed and the maximum gradient at this speed. The maximum gradient on UK highways is 4 % = 2.3º. The designed maximum speed is 120 ${}^{km}/_{h}$. All calculations are undertaken with maximum mass m_{max}. To achieve 120 ${}^{km}/_{h}$ with 4% gradient, the propulsion motor power requirement is:

$$P_{mot}(4\%,120\,{}^{km}/_{h}) \approx 36kW \text{ (see figure 2)}$$

The chosen motor is a permanent magnet motor with axial air gap and pancake design. The purchase cost of this motor type has a strong relation to the motor power due to the speed limitation and the cost of rare-earth magnets.

Motor size and cost may be reduced if the speed demand is relaxed. At a 4% highway grade a crawling-lane for lorries will be implemented, the average speed is limited to less than 112 $^{km}/_{h}$. If the vehicle is designed to run 100 $^{km}/_{h}$ with this 4% gradient it will still meet the requirements, but allow for a smaller propulsion motor:

$$P_{mot,cont} = P_{mot}(4\%,100\,{}^{km}/_{h}) \approx 26kW \text{ (see figure 2)}$$

This power reduction of nearly 30% helps to reduce the cost remarkably. The 26 kW motor is still sufficient to propel the car at a speed of 120 $^{km}/_{h}$. The overtorque capability of about 1.5 of this motor type still allows for short duration gradients of 4% at this speed. For longer gradients, the speed needs to be decrease to 100 $^{km}/_{h}$ and a higher gear ratio is necessary to receive maximum power.

The chosen motor is a scaled up version of the Lynch LM200 [9] [10]. The LM200 produces 10kW. The propulsion motor torque is scaled up with a factor of 2.7.The scaled motor produces up to 70 Nm continuous and runs at maximum 3,600 rpm with this load. The brushed DC motor is reliable and control is accurate and simple. The Lynch motor provides very good efficiency (90%) in wide operating region and a very good power/mass ratio of about $1^{kW}/_{kg}$. High torque and low speed keeps gear losses and noise down. Figure 3 shows the efficiency map for this motor and the operating points in the extra urban driving cycle (EUDC). This simulation result [8] shows that the chosen motor is used in a very good efficiency region. The motor power is suitable for this vehicle.

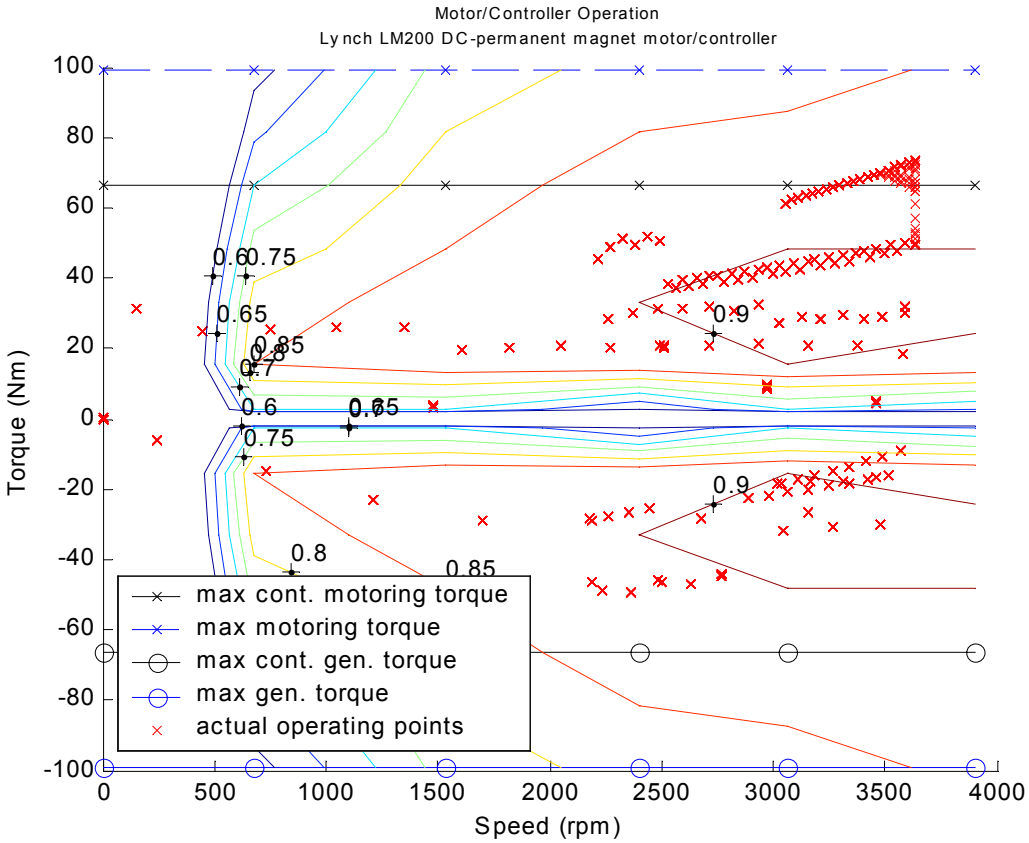

Figure 3: Propulsion Motor/Controller Efficiency Map with Operating Points in EUDC

Engine/generator requirements:
The average power determines the engine/generator power requirement in this series HEV concept. Cruising at 112 $^{km}/_{h}$, the maximum velocity on UK highways, without gradient is assumed to define the average power. The continuous generator output power requirement is:

$$P_{gen,cont} = P_{mot}(0\%,112\,{}^{km}/_{h}) \approx 16.5kW$$

The chosen electric motor, used as a generator is also a scaled up version of the Lynch LM200 with a scaling factor of 1.7. The electric output power is 17 kW with an estimated efficiency of 85% the mechanical input power is 20 kW. This is the minimum continuous engine power requirement.

$$P_{engine,cont} \approx 20kW$$

This vehicle concept is designed for urban driving with mainly short trips. The generator and engine aim to increase versatility and Peace-of-Mind for the driver: no need to think and worry about battery state-of-charge. Thus, the engine is designed to run only rarely and only when noise, vibrations and emissions play a minor role. A cheap, small, lightweight engine can be chosen. For example, a 350 cc four-stroke scooter engine size is sufficient to produce 20 kW. But in this study, the Advisor SI-30 engine is chosen and scaled down to 20 kW for simulation purpose. Figure 4 shows that in this engine, the maximum power point equals to the maximum torque point with good efficiency at this point as well.

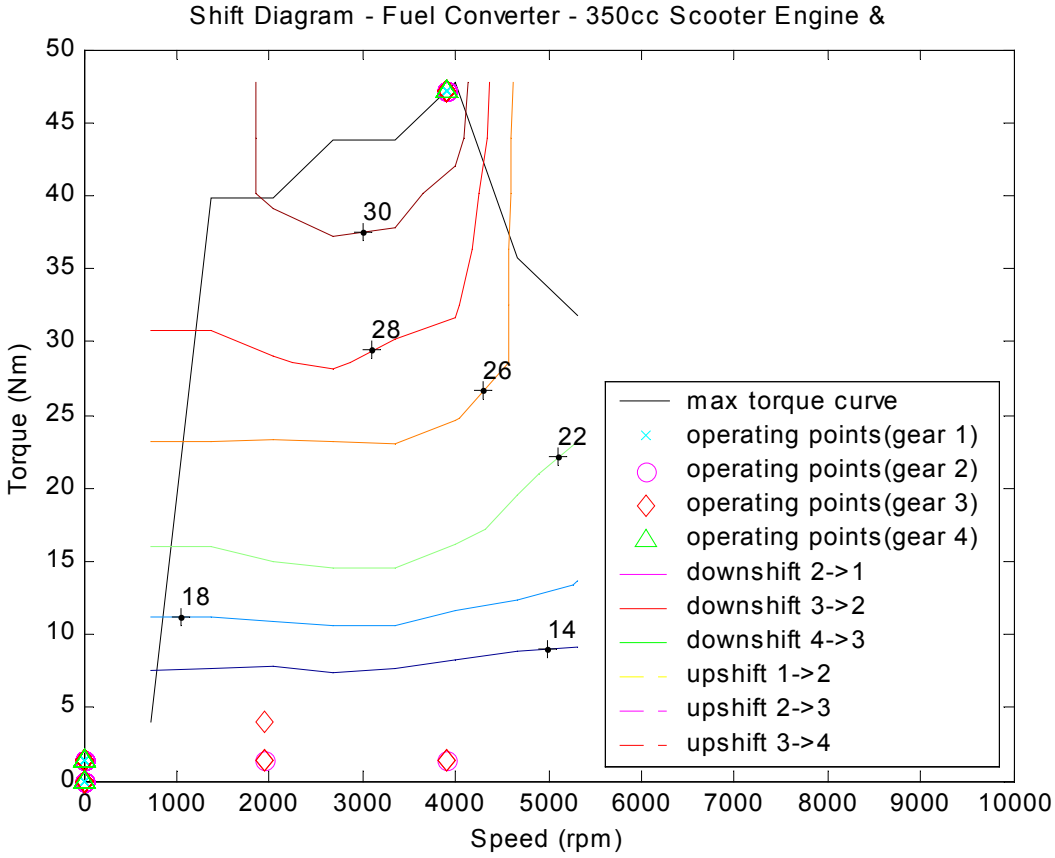

Figure 4: Engine Efficiency Map with Operating Point

Energy storage requirements:
There are two main energy storage requirements: Energy capacity and maximum power. The energy capacity should be sufficient for 60 km urban traffic in pure electric driving mode. The average velocity in cities is about 30 $^{km}/_{h}$. In simplified calculation, we assume an average of 50 $^{km}/_{h}$ for taking the frequent starts and stops into account. The motor power to propel the vehicle at this speed is:

$$P_{mot}(0\%,50\,{}^{km}/_{h}) \approx 2.7kW$$

Assuming a motor/battery efficiency of about 60%, the required energy storage capacity is at least:

$$E_{storage,\min} = \frac{60km}{50\,{}^{km}/_{h}} \cdot \frac{2.7kW}{0.6} \approx 5.4kWh$$

The battery power should be sufficient to boost the propulsion motor to its highest power, when the generator runs. Maximum motor power is 1.5 times continuous motor power.

$$P_{storage,\max} = 1.5 \cdot P_{mot,cont} - P_{gen,cont} \approx 22kW$$

The chosen battery type (Li-Ion) is capable of discharging currents that equal to 3 times the rated capacity. The energy storage capacity is determined by this requirement:

$$E_{storage} = \frac{P_{storage,\max}}{3} \cdot h \approx 7.5kWh$$

A modern Li-Ion battery (Thunder Sky TS-LP8582B) [11] has been chosen to keep the battery size and mass low. Li-Ion batteries also provide very good efficiency and good cycle life. Purchase cost has recently become competitive (400 $^{US\$}/_{kWh}$). A comparatively small voltage of 72V, but high capacity of 110Ah provides the required power and energy. Li-Ion batteries essentially need single cell observation. A smaller cell number in a series connection has fewer problems with cell-imbalances and expensive battery management systems. Figure 5 shows the chosen battery with a mass of 60 kg and a comparable lead-acid battery with about 250 kg in front of our current test-bed vehicle.

Figure 5: Li-Ion and comparable Lead-Acid Battery

Gear ratio requirements:
Different gear ratios will be necessary to allow for maximum speed of 120 $^{km}/_{h}$ on one hand and good gradeability of 20% on the other. Table 1 draws the conclusion of the gear ratio calculations:

	1st gear	2nd gear	3rd gear	4th gear
Max. speed	36 $^{km}/_{h}$	60 $^{km}/_{h}$	100 $^{km}/_{h}$	120 $^{km}/_{h}$
Max. grade	20%	11%	4%	1.7%
Total ratio	10.5	6.3	3.8	3.2
Purpose	Hill climbing	Urban driving	Extra-urban	Motorway

Table 1: Gear-ratios and Performance

The vehicle can be driven in 2nd gear only without changing gears in urban driving cycle. This means good acceleration and comfortable, smooth driving. The gearbox loss characteristics are taken from TX_VW Advisor file. The wheel information like losses and rolling-radius are taken from WH_SMCAR Advisor file. Figure 6 shows the gear ratio changing when accelerating from 0 … 120 $^{km}/_{h}$. The strategy is to shift into next gear when maximum motor speed is nearly reached. The motor is most efficient at high speeds as shown in figure 3 and remains quiet.

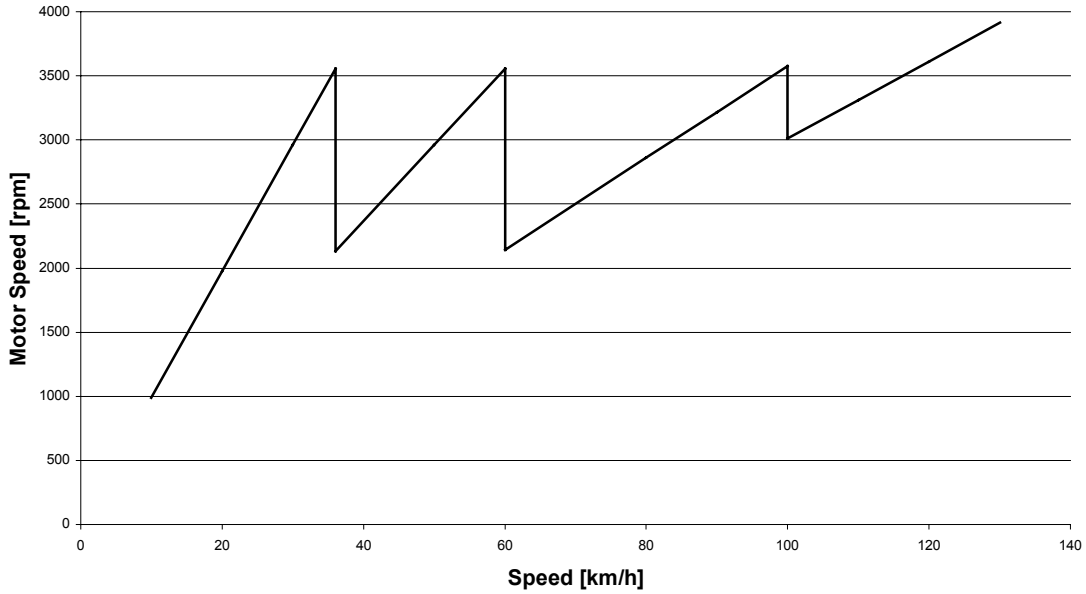

Figure 6: Gear-shifting table: Motor Speed over Vehicle Speed

4. Advisor Simulation

The above calculations helped estimating component specifications. Components and the vehicle have been modeled in Advisor2002 [8] to show that the vehicle meets the requirements. Advisor is a backward-looking Matlab based vehicle simulation program. Vehicle, drivetrain configuration and components can be modeled and run through different standard driving cycles. Different results like loss plots, operating points versus time, operating points in efficiency maps, all sorts of model-variables versus time and average values can be visualized.

Simulation results can be summarized as follows:
1. Maximum **velocity** of 120 $^{km}/_{h}$ can be achieved. Average speed of 112 $^{km}/_{h}$ can be achieved without battery depletion.

2. The **acceleration** results are presented in comparison to the Advisor results for the inbuilt model of th Toyota Prius HEV. The Peace-of-Mind HEV will undertake this simulation test in full-power hybrid mode with engine/generator switched on.

Test	Toyota Prius	Peace-of-Mind HEV
0 – 50 km/h	5.8 s	5.1 s
50 – 100 km/h	10.4 s	12.4 s
Max. acceleration	3.4 m/s^2	3.6 m/s^2

Table 2: Acceleration results in comparison with Toyota Prius results

Table 2 shows, that Peace-of-Mind HEV can achieve very good acceleration in urban driving, even better than a Toyota Prius. In extra urban driving, the acceleration is still acceptable.

3. **Gradients** of 4% can be achieved at 100 $^{km}/_{h}$ with maximum cargo over long duration. 4% at maximum speed for short duration is possible.

4. **Acceleration** in urban driving is sufficient to follow ECE-15 driving cycle in pure electric mode and in 2nd gear without gear shifting.

5. The **fuel consumption** in 180 km extra urban driving (26 EUDC cycles) is 3.6 $^{l}/_{100km}$ fuel equivalent. In urban driving (ECE-15) the Advisor result is 1.1 $^{l}/_{100km}$ fuel equivalent. With an average charger efficiency of 80% this is less than 1.4 $^{l}/_{100km}$. The total fuel consumption (20% EUDC 80% ECE) in combined consumption is about 1.8 $^{l}/_{100km}$ compared to the 7.3 $^{l}/_{100km}$ of the Daewoo Matiz.

6. The pure electric **range** in urban driving is 89 km (ECE-15) and about 70 km in a very good battery efficiency region. The hybrid mode range is limited to the fuel tank capacity only.

7. The total vehicle **mass** is 779 kg compared to the 778 kg of the original Daewoo Matiz.

8. **Cost** has not been modeled and simulated, but the concept tries to keep it as low as possible. The extra urban driving cycle (EUDC) showed that average power need is only about 7 kW. Reducing the engine/generator power to a level of about 10 kW could further decrease cost and extra urban fuel consumption, but will lead to battery depletion mode when running at full speed over long periods of time.

5. Conclusion

This paper demonstrates that using electric propulsion in vehicles can reduce energy consumption and other impacts like noise or local air-pollution without increasing vehicle mass or decreasing versatility and comfort. The only contribution is limiting the maximum speed to a reasonable value that equals to national speed limits in most cases. The series hybrid electric drivetrain concept makes sense in this type of vehicle, where the average power requirement is low. The fuel economy is about 4 times better than in a comparable vehicle without sacrificing performance, comfort, versatility, safety or affordability. Other impacts like noise and emissions are decreased.
The discussed peace of-mind-vehicle concept is implemented in our test vehicle and the energymanagement will be developed. Real world tests and driving will be compared to the simulation results.

6. References

[1] Spiegel, *Brennstoff-Delle: Wie fahren wir in Zukunft?*, in *Spiegel-Online*, 2002, http://www.spiegel.de/auto/news/0,1518,177662,00.html

[2] Thomas Kroher, *Alternativen zum teuren BENZIN (alternatives to the expensive gasoline)*, in *ADAC Motorwelt (German automobile association magazine)*, 2000, p. 18 - 20

[3] Adolf Kalberlah, *Elektro-Hybridantriebe fuer Strassenfahrzeuge*, in *Elektrische Strassenfahrzeuge*. 1994, expert Verlag: Berlin. p. 133 - 149.

[4] eurostat, *Panorama of transport*. 1999 ed. 1999. ISBN: 92-828-7149-5.

[5] eurostat, *Transport and environment*. 2001 ed. 2001. ISBN: 92-894-1190-2.

[6] DJ Thompson, *N3. The drive-by test*, in *Automotive Engineering II*, 2002, University of Southampton.

[7] Daewoo, *Matiz*, in 2002, www.daewoo-cars.co.uk.

[8] National Renewable Energy Laboratory NREL, *ADVISOR (Advanced Vehicle Simulator),* Ver: 2002, www.ctts.nrel.gov/analysis.

[9] Richard Fletcher, *LYNCH electric motor*, 2001, Lynch Motor Company Ltd., http://www.lynchmotor.com/Default.htm.

[10] SM Abu-Sharkh and MTN Mohammad, *Finite Elemente Analysis of an Axial-gap Permanent Magnet DC Motor*, in *Fourth International Conference on Computation in Electromagnetics*, 2002, Bournemouth, UK.

[11] ThunderSky, *Li-Ion Batteries*, 2002, http://www.thunder-sky.com/Gsjj(En).htm.

7. Affiliation

Dipl.-Ing. Dennis Doerffel
University of Southampton, School of Engineering Sciences, Southampton SO17 1BJ
Tel: +44-2380-59-2698 Fax: +44-2380-59-3230 E-mail: ddoerffel@ses.soton.ac.uk
URL: http://www.soton.ac.uk/~dad1
Dennis Doerffel obtained his Dipl-Ing. degree from the University of the German Forces, Hamburg in 1995.
Since 2001 he is a postgraduate student with the University of Southampton.
His research is about the energy management of hybrid electric vehicles.

Dr. Suleiman Abu-Sharkh
University of Southampton, School of Engineering Sciences, Southampton SO17 1BJ
Tel: +44-2380-59-3397 Fax: +44-2380-59-3053 E-mail: S.M.Abu-Sharkh@soton.ac.uk
URL: http://www.soton.ac.uk/~suleiman
Dr. Abu-Sharkh obtained his Beng and PhD degrees from the University of Southampton in 1990 and 1994.
He is a lecturer in Control Engineering, Electric Machines Power Electronics and Electrical Systems.

A3:

Transfer Thesis in 2003

[24]

This thesis is not included in the appendix. It is available from http://eprints.soton.ac.uk/5005/

A4:

"Life Cycle Impacts and Sustainability Considerations for Alternative and Conventional Vehicles"

SAE 2003 World Congress & Exhibition

[40]

This conference paper is not included in the appendix.

A5:

"Sustainable Future Transportation"

SAE International Future Transportation Technology Conference,
Costa Mesa, California USA

[41]

This conference paper is not included in the appendix.

A6:

"Transforming Policy Processes to promote sustainable innovation: some guiding principles"

[35]

This report is not included in the appendix.

It is available from

http://www.sustainabletechnologies.ac.uk

A7:

"System Modelling and Simulation as a Tool for Developing a Vision for Future Hybrid Electric Vehicle Drivetrain Configurations"

VPPC 2006 by the Power Electronics Society (PELS)
and IEEE in Windsor, UK

[29]

Conference paper

System Modeling and Simulation as a Tool for Developing a Vision for Future Hybrid Electric Vehicle Drivetrain Configurations

Dennis Doerffel[1], Suleiman Abu Sharkh[2]

[1]REAPsystems Ltd, 61A Ivy Road, Southampton SO17 2JP, UK.
dennis@reapsystems.co.uk , Tel/Fax: +44-2380-556516 (Corresponding Author)

[2]University of Southampton, SES, Highfield, Southampton SO17 1BJ, UK.
suleiman@soton.ac.uk , Tel: +44-2380-59-3397

***Abstract* - The escalating number of vehicles on the road has raised awareness to their environmental impacts and sustainability; this has provided a stimulus for future mobility considerations. The conventional car may not meet future requirements regarding noise, emissions and energy consumption. There is a distinct lack of short-term alternative solutions that meet consumer requirements and have a potential for mass production. Furthermore, the internal combustion engine has been developed over 100 years and there may be some risk that the automotive companies choose to invest into the "wrong" alternative. However, industry has to accept some responsibility for providing future solutions for the products they introduced and created the demand for in first place. Starting with a vision several years ago, Japanese car companies have now taken the lead with certain types of hybrid electric vehicles. These vehicles exhibit significantly reduced energy consumption, noise emission, exhaust emissions, and yet also have improved comfort and performance. They now thrive in the USA with seemingly unexpected popularity due to rocketing oil prices and increasing awareness of the risk of oil dependency.**

Many car companies now follow this lead. However, there are a vast variety of possible hybrid drivetrain configurations. Modelling and simulation can help in the development and assessment of future drivetrain solutions. This paper focuses on this task using a commercially available modelling and simulation package. A drivetrain design is developed going through some initial considerations based on vehicle performance criteria that take into account consumer expectations and operational/ regulatory/ environmental factors. Based on simulation studies the drive train components are identified, mostly from the available range. Finally, a computer simulation is used to assess the performance of the vehicle.

The result of these investigations is a series hybrid electric vehicle that is recharged from the mains. The fuel consumption is four times better than that of a comparable car, but vehicle mass and cost have not increased significantly. The driving range of this vehicle is not limited by battery capacity. Such a vehicle can meet consumer expectations as well as environmental requirements with added driver comfort. Still being low-cost, it provides the potential for mass-production thus reducing overall impacts on the environment.

***Index Terms* - lithium-ion battery, energy consumption, vehicle performance, cost, hybrid electric vehicle**

I. Introduction

Cars have improved significantly over the last 100 years. They became more versatile, have better performance and are more comfortable without increasing the purchase cost, which has lead to unprecedented increase in the number of vehicles on the road, especially given recent changes in work practices that require an increased individual mobility. This increase in the number of vehicles together with rising awareness of their environmental impacts and sustainability provided stimulus for current discussion on future mobility [1, 2, 3, 4, 5].

Conventional cars with internal combustion engine do not meet future requirements regarding noise, emission and energy consumption [6]. On the other hand, electric vehicles, which have far less impact on the environment, do not meet customer requirements regarding range, versatility or cost [7] and fuel-cell vehicles still need considerable development of the technology and infrastructure [8, 9]. Most recent developments on hybrid electric vehicles have concentrated on the parallel hybrid. The series hybrid electric vehicle has in general been considered to be inferior to the parallel [10, 11]. However, recent developments in battery technology [12] can make the series hybrid electric vehicle an interesting alternative.

The importance of a systems design approach and the relevance of simulation and modelling for assessing hybrid electric vehicle drivetrains has been shown earlier [13]. This paper demonstrates how this approach can be used for making initial choices on innovative or radical drivetrain solutions. As an example we will be evaluating a plug-in series hybrid electric vehicle. This is a hybrid electric vehicle which can be recharged from a mains outlet and which is intended mainly for urban and neighbourhood journeys [14]. Firstly, we will be determining the main vehicle specifications so that they meet consumer aspirations. Secondly, we will be carefully selecting the drive train components based on data from commercial-off-the-shelve (COTS) components in order to make sure the concept is achievable. Finally, the modelling and simulation

will be used to assess whether that drivetrain concept ensures peace-of-mind in terms of both, environmental impacts compared to a pure electric vehicle and range and versatility compared to a conventional car without sacrificing the affordability.

II. Vehicle Performance Criteria

The basic configuration of the vehicle here is a series hybrid that is normally charged from green sources and operates as an electric vehicle, but has a small engine to extend the range of travel. The proposed vehicle specification is based on the following considerations:

Speed: The maximum design speed of the vehicle determines the rated motor power and the smallest gear ratio at a given maximum motor speed. The rated motor power in a pure EV determines the battery power and this is known to be a major cost issue. In the proposed vehicle, the rated motor power mainly determines the generator and engine power. The higher the speed of this type of HEV the larger the four main and costly drivetrain components (power-electronics, motor, generator and engine) need to be. The maximum design speed of the vehicle should be therefore chosen very carefully and preferably as low as possible without compromising comfort. The UK and many other countries have a speed limit of around 70 mph (112 km/h) and our vehicle should be able to achieve this speed consistently.

Gradeability: The road gradient on highways together with the maximum speed determines the rated power requirement of the motor. E.g. the maximum road gradient on UK highways is 4%. Here, we assume the use of a gearbox where the maximum gradient determines the highest gear ratio. Most hills exhibit less than 20% gradient and signs will warn before choosing a route with higher gradients. The vehicle is designed to climb at least 20% carrying maximum load.

Acceleration: The acceleration determines the maximum motor torque and the gear ratio. We assume using an axial air-gap permanent magnet brushed motor, which is capable of producing constant torque vs speed; with about 50% overload torque capability. The overload capability of most motors exceeds this. It can be assumed that a motor that achieves the maximum speed at highway gradient is sufficiently powerful for moderate acceleration in urban areas. However, the simulation will be used in order to determine acceleration performance of the vehicle.

Driving Range: Most trips are short trips: about 80% of all travelled distance is less than 40 km each trip [4, 5]. To keep the battery in an efficient state of charge range for this distance, the state of charge (SOC) should remain above 20% even when the battery is close to its end of life (80% of rated capacity). As a result, the vehicle should initially achieve 40 km / (0.8 · 0.8) ≈ 60 km in pure electric mode. An energy management will provide peace of mind by starting this generator automatically in order to extend the driving range to at least 300 km.

Noise: This vehicle is designed for short trips. These trips usually have a low average speed. At low speeds the engine noise of conventional cars is higher than the noise of tyres and air-resistance [15]. The electric motor itself is very quiet and the energy management will try to prevent starting the combustion engine when engine noise has major impacts (e.g. inside towns at low speeds or when waiting in traffic jams). The vehicle mass will be kept low to decrease tyre noise at higher speeds as well. Thus, this vehicle has very low noise impacts.

Pollution: This vehicle is essentially a battery powered electric vehicle that is normally recharged from the mains. This type of vehicle has no local pollution. It has no overall pollution or greenhouse gas emissions if recharged with renewable electricity. The combustion engine will only cut in if necessary to achieve the desired trip distance or the desired power. The energy management will also ensure the engine will run as rarely as possible and in its best efficiency/ lowest pollution region. It also aims to reduce cold starts to keep the level of pollution low.

Vehicle size: Lightweight vehicles keep impacts low in urban driving. We use the data from a Daewoo Matiz (see Fig. 1) for our simulations.

Fig. 1 Typical Small Vehicle

Handling/Comfort: The series hybrid electric drivetrain can enhance the handling: the heavy engine is replaced with a number of lighter components (battery, small engine, generator, etc.), which can be mounted in different places for an optimised weight distribution. As a result of a more even weight distribution between front and back, power steering may not be essential any more. Unlike a combustion engine, the electric motor produces full torque from zero rpm resulting in less gear changing. Additionally, the electric motor exhibits a small rotational inertia and can be accelerated very fast, especially if supported from dedicated control algorithms in the power electronics hence making a clutch potentially redundant [16]. Less motor noise and vibrations will increase comfort especially in urban driving with many start-stop procedures. Electrically powered air-conditioning can be implemented.

Energy Consumption: The aim is to keep the energy consumption between 1 - 2 $^{L}/_{100km}$ (this is between 140 and 280

British mpg[1]) of petrol equivalent in urban driving[2]. The vehicle will be purely battery powered and recharged from the mains in this scheme. The extra-urban consumption will be higher due to the higher drag losses at higher velocities. Also, the engine will cut in to provide additional power or range. The aim in this scheme is about 3 $^{L}/_{100km}$(this is about 94 British mpg). This vehicle is designed for mainly short trips and thus, the combined consumption is near to the urban driving consumption and should be below 2 $^{L}/_{100km}$ (this is about 140 British mpg).

Vehicle Mass: The vehicle mass has major impacts on most of the requirements mentioned above. Keeping the mass low means better gradeability, acceleration, range, less noise and lower energy consumption. The aim is to keep or even reduce the vehicle mass, when compared to the original vehicle by choosing the heaviest components such as battery and engine as small and light as possible. The motor and generator to be used are permanent magnet DC motors with very high power/mass ratio (e.g. 1 kW/kg continuous power).

Cost: The purchase cost is targeted to be similar to a conventional vehicle by trying to keep the technology simple and the battery small. The battery is a major cost factor and thus, a battery management ensures highest possible life expectancy of the battery combined with optimised performance. This is achieved by managing battery temperature and charging as well as utilising closed loop controls during discharging taking several factors into account (e.g. individual cell voltages and temperatures).

In conclusion: The task is to evaluate whether it may be possible to design an essentially battery powered vehicle with range extender so that it exhibits very low energy-consumption, pollution and noise but keeping a competitive purchase price and with high driving range and acceptable performance .

III. Component Specifications

This paragraph derives the component specifications from the vehicle criteria. The following formula are used to estimate the power requirements:

Rolling resistance: $P_r(v) = c_r \cdot m_{\max} \cdot g \cdot v$ (1)

Air drag: $P_{air}(v) = c_d \cdot A_f \cdot \frac{1}{2} \cdot \zeta \cdot v^3$ (2)

Power demand for gradient: (3)

$$P_{grad}(gradient, v) = m_{\max} \cdot g \cdot v \cdot \sin(\arctan \frac{gradient}{100})$$

The following constants have been used:

Gravitational acceleration: $g = 9.81\,^{m}/_{s}2$

Air density at 1 bar and 20 ºC: $\zeta = 1.19\,^{kg}/_{m}3$

The total motor power to propel the vehicle at a certain speed (v) and up a certain gradient (grad) is

$$P_{mot}(grad, v) = \frac{P_r(v) + P_{air}(v) + P_{grad}(grad, v)}{\overline{\eta_{mech}}} \quad (4)$$

Mechanical drivetrain efficiency is assumed to be on average $\overline{\eta_{mech}} \approx 0.9$.

The chosen vehicle has the following body attributes:

Air drag coefficient:	$c_d = 0.32$	(estimated)
Frontal area:	$A_f = 2.01$ m²	(estimated)
Tyre rolling coefficient:	$c_r = 0.009$	(Advisor file)
Mass:	m = 778 kg	(Daewoo Matiz)
Maximum mass:	m_{max} = 1153 kg	(Daewoo Matiz)

Fig. 2 shows the power requirements to overcome the rolling resistance, the air drag, the gradient of 4 % and the total required motor power versus speed.

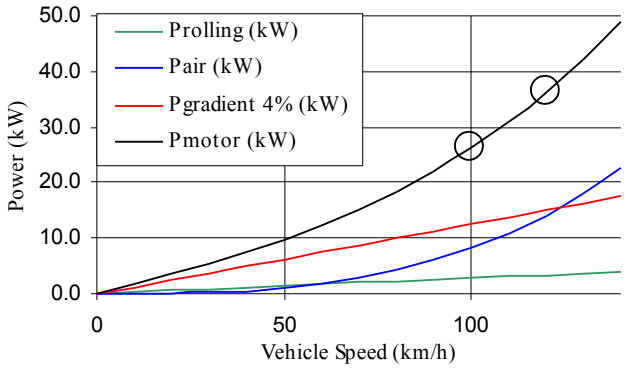

Fig. 2 Power requirements over speed for the chosen vehicle with 4% gradient

Propulsion motor requirements:
The power requirement of the electric propulsion motor is determined by the maximum speed and the maximum gradient at this speed. The maximum gradient on UK highways is 4 % = 2.3º. The designed maximum speed is 120 $^{km}/_{h}$. All calculations are undertaken with maximum mass m_{max}. To achieve 120 $^{km}/_{h}$ with 4% gradient, the propulsion motor power requirement is

$P_{mot}(4\%, 120\,^{km}/_{h}) \approx 36kW$ (see fig. 2).

The chosen motor is a permanent magnet motor with axial air gap and pancake design. The purchase cost of this motor type has a strong relation to the motor power due to the speed limitation and the cost of rare-earth magnets.

1 1 British gallon = 4.546 litres = 1.201 US gallons
2 8.866 kWh of electricity have a petrol equivalent of 1 litre.

Motor size and cost may be reduced if the speed demand is relaxed. At a 4% highway grade (this is when a crawling-lane for lorries is implemented), the allowed speed is limited to less than 112 $^{km}/_{h}$. If the vehicle is designed to run at say 100 $^{km}/_{h}$ with this 4% gradient it will still meet the requirements, but allow for a smaller propulsion motor:

$$P_{mot,cont} = P_{mot}(4\%,100\,{}^{km}/_{h}) \approx 26kW \quad \text{(see fig. 2)}$$

This power reduction of nearly 30% helps to reduce the cost remarkably. The 26 kW motor is still sufficient to propel the car at a speed of 120 $^{km}/_{h}$. The over-torque capability of at least 1.5 of this motor type still allows for short duration gradients of 4% at this speed. For longer gradients, the speed needs to dynamically decrease to 100 $^{km}/_{h}$ and a higher gear ratio may become necessary.

In order to use practically possible motor data, the modelled motor is a scaled up version of the Lynch LM200. The LM200 produces 10kW. The propulsion motor torque is scaled up with a factor of 2.7.The scaled motor produces up to 70 Nm continuous and runs at maximum 3,600 rpm with this load. The type of motor provides very good efficiency (90%) in wide operating region and a very good power/mass ratio of about $1^{kW}/_{kg}$. High torque and low speed keep gear losses and noise down. Fig. 3 shows the efficiency map for this motor and the operating points in the extra-urban driving cycle (EUDC). This simulation result shows that the chosen motor is used in a very good efficiency region. The motor power is suitable for this vehicle.

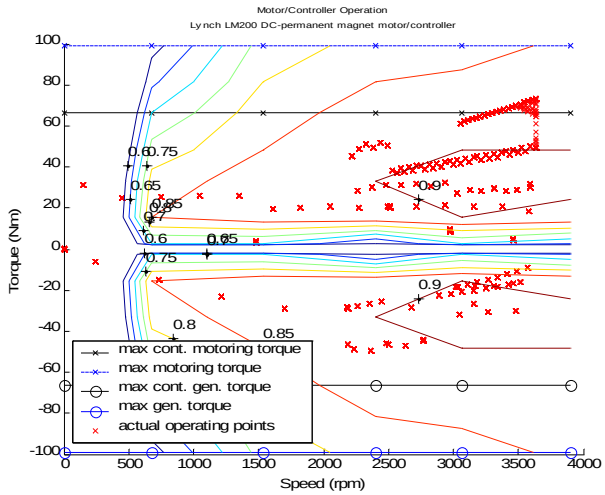

Fig. 3 Propulsion Motor/Controller Efficiency Map with Operating Pointsin EUDC driving cycle

Engine/generator requirements:

The average power determines the engine/generator power requirement in this series HEV concept. Cruising at 112 $^{km}/_{h}$, the maximum velocity on UK highways, without gradient is assumed to define the average power. The continuous generator output power requirement is:

$$P_{gen,cont} = P_{mot}(0\%,112\,{}^{km}/_{h}) \approx 16.5kW$$

The chosen electric motor, used as a generator is also a scaled up version of the Lynch LM200 with a scaling factor of 1.7. The electric output power is 17 kW with an estimated efficiency of 85% the mechanical input power is 20 kW. This is the minimum continuous engine power requirement.

$$P_{engine,cont} \approx 20kW$$

This vehicle concept is designed for urban driving with mainly short trips. The generator and engine aim to increase versatility and Peace-of-Mind for the driver: no need to think and worry about battery state-of-charge. Thus, the engine is designed to run only rarely and only when noise, vibrations and emissions play a minor role. A cheap, small, lightweight engine can be chosen. For example, a 350 cc four-stroke engine size is sufficient to produce 20 kW. In this study, the Advisor SI-30 engine is chosen and scaled down to 20 kW for simulation purpose. Fig. 4 shows that in this engine, the maximum power point equals to the maximum torque point with good efficiency at this point as well.

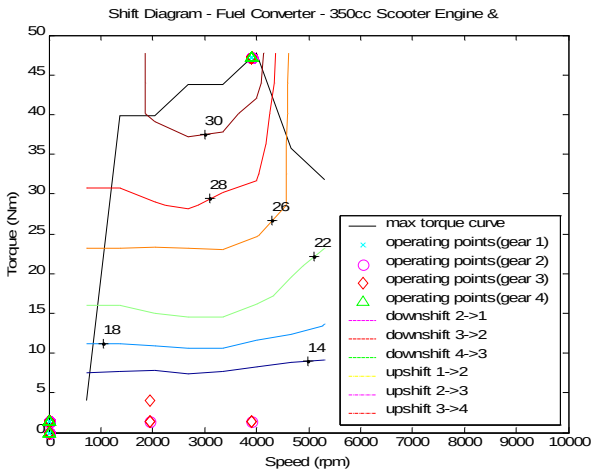

Fig. 4 Engine Efficiency Map with Operating Point

Energy storage requirements:

There are two main energy storage requirements: Available energy and maximum power. The available energy should be sufficient for 60 km urban traffic in pure electric driving mode. The average velocity in cities is about 30 $^{km}/_{h}$. In simplified calculation, we assume an average of 50 $^{km}/_{h}$ for taking the frequent starts and stops into account. The motor power to propel the vehicle at this speed is:

$$P_{mot}(0\%,50\,{}^{km}/_{h}) \approx 2.7kW$$

Assuming a drivetrain efficiency of about 60%, the required energy storage capacity is at least:

$$E_{storage,\min} = \frac{60km}{50\,km/h} \cdot \frac{2.7kW}{0.6} \approx 5.4kWh$$

The battery power should be sufficient to boost the propulsion motor to its highest power, when the generator runs. Maximum motor power is 1.5 times continuous motor power.

$$P_{storage,\max} = 1.5 \cdot P_{mot,cont} - P_{gen,cont} \approx 22kW$$

Most modern lithium-ion batteries are capable of discharging currents that equal to 5 times the rated capacity. However, in order to achieve full performance even after some degradation or in cold conditions, we have assumed a maximum discharge of 3C (3 times the rated capacity). The energy storage capacity is determined by this requirement:

$$E_{storage} = \frac{P_{storage,\max}}{3} \cdot h \approx 7.5kWh$$

A Li-Ion battery has been chosen to keep the battery size and mass low. Li-Ion batteries also provide very good efficiency and good cycle life. Purchase cost is becoming very competitive (400 US$/kWh). A comparatively low voltage of 72V, but high capacity of 110Ah provides the required power and energy. Li-Ion batteries essentially need single cell observation. A smaller cell number in a series connection has fewer problems with cell-imbalances and requires less expensive battery management systems. Fig. 5 shows the chosen battery with a mass of 60 kg and a comparable lead-acid battery with about 250 kg in front of our current test-bed vehicle.

Fig. 5 Li-Ion and comparable lead-acid battery

Gear ratio requirements:

With most motors and also for highly efficient power electronics and low-voltage batteries, it will be required to have different gear ratios in order to allow for maximum speed of 120 km/h on the one hand and good gradeability of 20% on the other. Table 1 summarises the gear ratio calculations:

TABLE I
GEAR RATIOS AND PERFORMANCE

	1st gear	2nd gear	3rd gear	4th gear
Max. speed	36 km/h	60 km/h	100 km/h	120 km/h
Max. grade	20%	11%	4%	1.7%
Total ratio	10.5	6.3	3.8	3.2
Purpose	Hill climbing	Urban driving	Extra-urban	Motorway

The vehicle can be driven in 2nd gear only without changing gears in urban driving cycle. This means good acceleration and comfortable, smooth driving. The gearbox loss characteristics are taken from the TX_VW file that was part of the simulation package (ADVISOR 2002). The wheel information like losses and rolling-radius are taken from the WH_SMCAR file (ADVISOR). Fig. 6 shows the gear ratio changing when accelerating from 0 … 120 km/h. The strategy is to shift into next gear when maximum motor speed is nearly reached. The motor is most efficient at high speeds as shown in fig. 3 but still remains quiet.

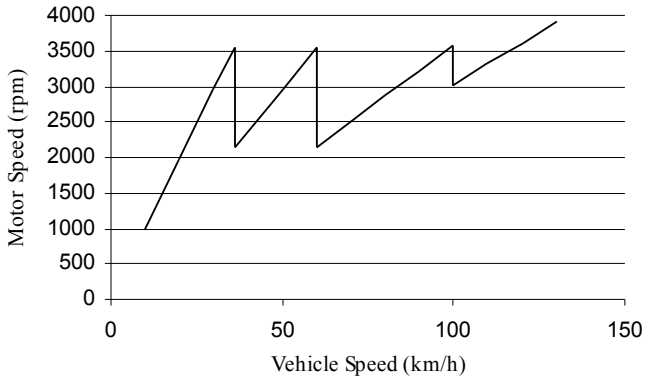

Fig. 6 Gear-shifting: Motor Speed over Vehicle Speed

IV. Simulation

The above calculations helped estimating component specifications. Components and the vehicle have been modelled in ADVISOR 2002 package in order to assess whether such a vehicle may meet the requirements. ADVISOR is a backward-facing vehicle simulation package based on Matlab/Simulink. Vehicle, drivetrain configuration and components can be modeled and run through different standard or purpose-build driving cycles. Different results like loss plots, operating points versus time, operating points in efficiency maps, all sorts of model-variables versus time and average values can be visualized.

Simulation results can be summarized as follows:

1. Maximum **velocity** of 120 km/h can be achieved. Average speed of 112 km/h can be achieved sustainably without battery depletion.

2. The **acceleration** results are presented in comparison to the Advisor results for the inbuilt model of the Toyota PriusI HEV. Our model HEV will undertake this simulation test in full-power hybrid mode with the engine/generator switched on.

TABLE II
ACCELERATION IN COMPARISON WITH TOYOTA PRIUS I

Test	Toyota PriusI	Simulated HEV
0 – 50 km/h	5.8 s	5.1 s
50 – 100 km/h	10.4 s	12.4 s
Max. acceleration	3.4 m/s^2	3.6 m/s^2

Table 2 shows, that this type of HEV can achieve very good acceleration in urban driving, even better than a Toyota Prius. In extra urban driving, the acceleration is still acceptable.

3. **Gradients** of 4% can be achieved at 100 $^{km}/_{h}$ with maximum cargo over long duration. 4% at maximum speed for short duration is possible.

4. **Acceleration** in urban driving is sufficient to follow ECE-15 driving cycle in pure electric mode and in 2nd gear without gear shifting.

5. The **fuel consumption** in 180 km extra urban driving (26 EUDC cycles) is 3.6 $^{l}/_{100km}$ fuel equivalent. In urban driving (ECE-15) the Advisor result is 1.1 $^{l}/_{100km}$ fuel equivalent. With an average charger efficiency of 80% this is less than 1.4 $^{l}/_{100km}$. The total fuel consumption (20% EUDC 80% ECE) in combined consumption is about 1.8 $^{l}/_{100km}$ compared to the 7.3 $^{l}/_{100km}$ of the same vehicle but with internal combustion engine (Daewo Matiz).

6. The pure electric **range** in urban driving is 89 km (ECE-15) of which are 70 km in a very good battery efficiency region. The hybrid mode range is limited by the fuel tank capacity only.

7. The total vehicle **mass** is 779 kg compared to the 778 kg of the original Daewoo Matiz.

8. **Cost** has not been modelled and simulated, but the concept tries to keep it as low as possible. The extra-urban driving cycle (EUDC) showed that average power need is only about 7 kW. Reducing the engine/generator power to a level of about 10 kW could further decrease cost and extra urban fuel consumption, but will lead to battery depletion mode when running at full speed over long periods of time.

V. Conclusions

This paper shows, how some simple initial calculation based on off-the-shelve components and typical vehicle characteristics together with initial (rough) modelling and simulation can help assessing drivetrains for their potential and suitability. Further and more sophisticated modelling and simulation will be required to provide better estimates of specifications and performance. However, within the broad range of hybrid drivetrain options and flavours, it is possible to identify sensible drivetrains in the way demonstrated here.

This paper also demonstrates that using electric propulsion in vehicles can reduce energy consumption and other impacts like noise or local air-pollution without increasing vehicle mass or decreasing versatility and comfort. The only restriction is to limit the maximum speed to a reasonable value that equals to national speed limits in most cases anyway and does not compromise the acceleration. It is shown that the series hybrid electric drivetrain concept makes sense in this type of vehicle, where the average power requirement is low. The fuel economy is about 4 times better than in a comparable vehicle and the comfort is increased without sacrificing performance, versatility, safety or affordability. Environmental impacts like noise and exhaust pipe emissions are decreased.

References

[1] ACEA (European Automobile Manufacturers Association), „*Monitoring of ACEA's commitment on CO_2 emission reductions from passenger cars*“, Final Report, www.acea.be, 2003.

[2] A. Palmer and B. Hartley, *The business environment*, 4th ed., McGraw-Hill, 2001.

[3] A. Schafer and D. G. Victor, „*The future mobility of the world population“, Transportation Research Part A: Policy and Practice,* vol. 34, no. 3, pp. 171-205, April 2000.

[4] Eurostat, *„Panorama of transport“,*Eurostat, ISBN 92-828-7149-5, 1999.

[5] Eurostat, *„Transport and environment“,*Eurostat, ISBN 92-894-1190-2, 2001.

[6] Y. Yang, M. Parten, J. Berg, and T. Maxwell, *„Modelling and control of a hybrid electric vehicle“, IEEE Veh. Tech. Conference,* pp. 2095-2100, 2000.

[7] F. A. Wyczalek, *„Market mature 1998 hybrid electric vehicles“, IEEE Aerospace and Electronic Systems Magazine,* vol. 14, no. 3, pp. 41-44, March 1999.

[8] H. Kleine and U. Stimming, „*Fuel-cells: function, types, systems“* (translated from German), in Fuel-cells: funtion – state of development – applications, Technical Academy Esslingen (Germany), 2001, pp. 11-15.

[9] Society of Motor Manufacturers and Traders (SMMT), *„The future fuels report“,* SMMT, 2002.

[10] G. Gutmann, *„Hybrid electric vehicles and electrochemical storage systems - a technology push-pull couple“, Journal of Power Sources,* vol. 84, no. 2, pp. 275-279, 1999.

[11] A. Kalberlah, „Hybrid electric drivetrains for road vehicles“ (translated from German), in Electric Vehicles (translated from German), pp. 133-149, expert Verlag, ISBN 3-8169-1075-0.

[12] H. K. Chung, *„Rechargeable Solid State Chromium-Fluorine-Lithium Electric Battery“,* United States Patent and Trademark Office, Patent No. 6,686,096, Feb. 2004.

[13] T. C. Moore, *„Tools and Strategies for Hybrid-Electric Drivesystem Optimization“,* Society of Automotive Engineers, no.961660, pp. 49-66, 1996.

[14] R. Bady and J.-W. Biermann, „HEV – structures and future developments*“,* Technical Academy Esslingen (Germany), 2000.

[15] D. J. Thompson, „*The drive-by test“,* Lecture notes: N3-Automotive Engineering II, University of Southampton, 2002.

[16] H.-D. Lee, S.-K. Sul, H.-S. Cho and J.-M. Lee, *„Advanced gear-shifting and clutching strategy for a parallel-hybrid vehicle“, IEEE Industry Applications Magazine,* vol. 6, no. 6, pp. 26-32, 2000.

B1:

"Large Lithium-Ion Batteries: a Review"

EMA2006, Exhibition and Conference at
the University of Aschaffenburg, Germany

[27]

Seminar lecture paper

Large Lithium-Ion Batteries – a Review

Dennis Doerffel[1], Suleiman Abu Sharkh[2]

[1]REAPsystems Ltd, 61A Ivy Road, Southampton SO17 2JP, UK.
dennis@reapsystems.co.uk , Tel/Fax: +44-2380-556516 (Corresponding Author)

[2]University of Southampton, SES, Highfield, Southampton SO17 1BJ, UK.
suleiman@soton.ac.uk , Tel: +44-2380-59-3397

Introduction

Lithium-ion batteries have been extremely successful in the portable equipment markets such as laptops and mobile phones. Currently, the lithium-ion battery technology is transitioning from small cells to large size batteries for a range of applications. Existing systems can be significantly enhanced using this lightweight battery technology and new innovative products can be launched. A better understanding of lithium-ion technology is key know-how for any forward-looking company that works or wants to work with large battery applications. Knowing more about these batteries and understanding how they work and what is required in order to operate them, will help designing safer, smaller, lighter, better performing, longer-lasting products with higher customer acceptance and at lower cost. It will help reducing the time and number of iterations during prototyping and design and hence reduce the time to market. Costly tests, time consuming “wrong” strategic / tactical decisions or even dangerous designs can be avoided by better understanding the lithium-ion battery technology.

This paper will provide a suitable “entry point”. It brings the reader up to speed with the most essential understanding and it will guide the way into the world of lithium-ion battery technology. The paper will touch the most relevant topics including performance comparisons with other battery technologies, the lithium-ion working principle, behaviour and specific characteristics, safety issues, ageing, electronic protection and management requirements as well as a short overview of different battery management implementations and options for cell equalisation. Advantages, disadvantages and issues will be discussed and linked to the fundamental working principles.

Background Information on Lithium-Ion Batteries

Lithium-ion batteries dominate the market for most portable products such as mobile phones, laptop computers, etc. The great success of the lithium-ion battery is mainly due to their significant advantages in terms of performance.

Performance Comparison

Performance is always relative to many other attributes. The most common way for comparing the performance of energy storage solutions is to use the Ragone plot. In such plots, one performance attribute on the first axis is always related to another important performance attribute on the second axis. The first illustration shows the specific energy in Wh/kg over the energy density in Wh/litre for several different energy storage technologies.

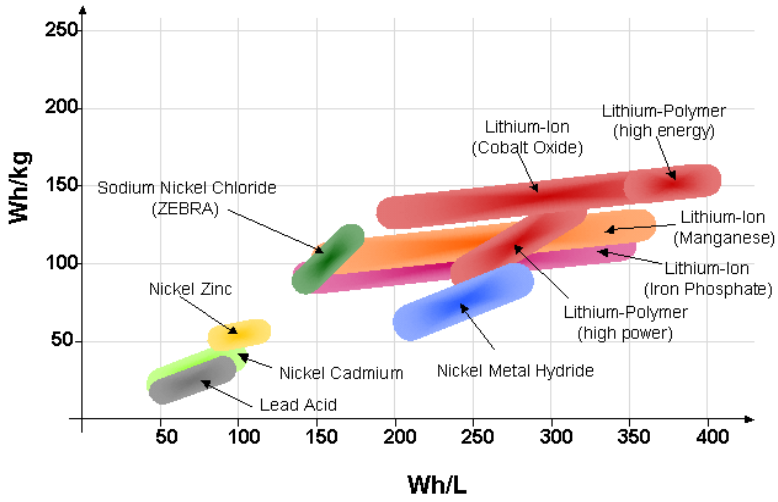

Illustration 1: Energy storage performance of different technologies

This illustration shows clearly, that the family of lithium-ion cells provides much smaller size and much lower weight for a given stored energy if compared with the other most common battery technologies. In particular, size and weight are up to 4 times reduced if compared with the most common battery type, the lead-acid battery.

Following, we will use the term lithium-ion cell in order to represent the whole family of lithium-ion cells. Terms such as lithium-iron, lithium-polymer, lithium-phosphate, etc. will only be used in order to specify a particular type of lithium-ion cells.

Many engineers are aware, that lithium-ion batteries are very good at storing energy. However, there is still a fair “knowledge-gap” regarding the power-capabilities of lithium-ion cells. Many people consider them as not very powerful. The second illustration is another very common Ragone plot, which shows the specific energy over specific power for several energy storage technologies including fuel-cells and combustion engines.

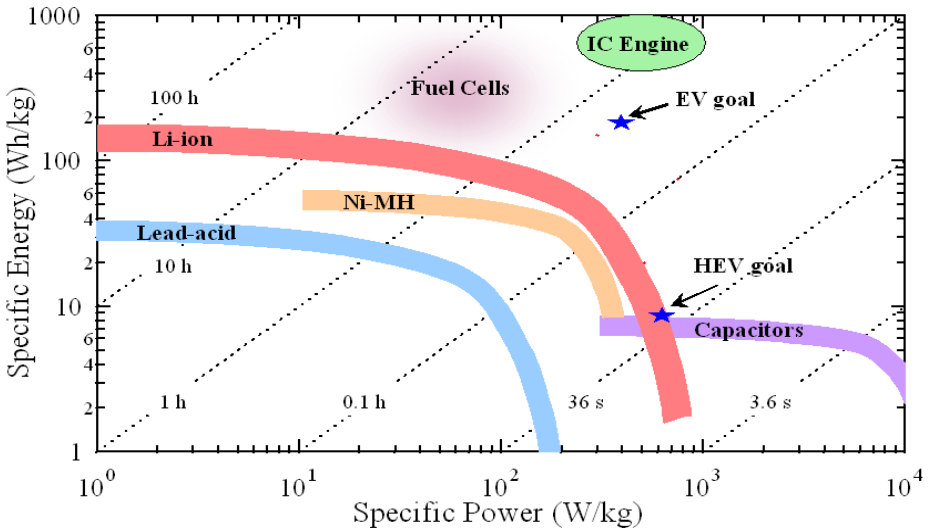

Illustration 2: Ragone plot for different energy storage solutions (Berkeley Electrochemical Research Council Ref: Venkat Srinivasan and John Newman: http://berc.lbl.gov/venkat/Ragone-construction.pps.)

Firstly, it is obvious, that the lithium-ion technology performs better than lead-acid or nickel-metal hydride (NiMH) cells in terms of both, energy and power for a given battery weight. This means, that lithium-ion cells exhibit very good power performance. This however depends on the internal construction. It can also clearly be seen, that for very

high power requirement, capacitors make more sense than battery technology in terms of electrochemical energy storage technology – but the energy storage capabilities of capacitors are very limited. However, this graph only compares two attributes. Other attributes, such as volume, cost and “special attributes” have to be considered as well when making choices. We will discuss a few “special attributes” later.

The graph also shows the performance characteristics of fuel cells and combustion engines. However, both of them are energy converters and the energy storage has to be treated separately. In the above case, a typical amount of stored energy (fuel + fuel tank) has been considered for this particular application (e.g. 60 litres of petrol in a car) in order to derive the overall specific energy / specific power performance of the energy storage + converter device. The result will vary significantly for other applications and is also dependent on the type of power that is required on the output (e.g. mechanical or electrical). However, this estimate is sufficiently good for demonstrating that combustion engines are much better in this comparison. It also demonstrates that fuel cells perform well for storing energy, but may require battery backup or capacitor backup for providing short term power. Again, cost, size and other attributes cannot be displayed in such Ragone plots at the same time, but need to be considered.

The Ragone plot in illustration 2 shows a typical characteristic of all batteries, which is in contrast to the behaviour of other types of energy storage, e.g. in liquid fuels: The available energy decreases rapidly when drawing very high power. This is mainly due to the significant voltage drop and hence power loss when drawing very high currents.

The Construction and Working Principle

It is important to picture the construction and understand the fundamentals of the working principle in order to use battery technologies effectively and appropriately. The construction of a typical lithium-ion cell is illustrated in our third illustration:

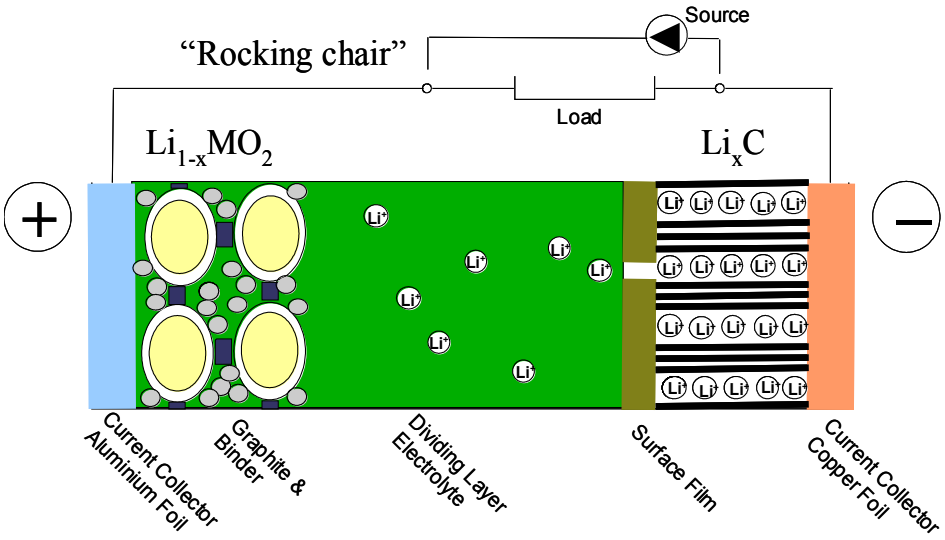

Illustration 3: Model of the construction of a lithium-ion cell

Illustration 3 shows a model of the most important structural features of a lithium-ion cell. From left to right, one can see the current collector and the active material of the positive electrode, then the electrolyte and dividing layer (separator) and on the right the active material and current collector of the negative electrode.

Due to the high voltage of a lithium-ion cell (nominal 3.6V), the choice of materials for the current collectors is very limited: The positive electrode consists of aluminium and the negative electrode is made of copper. Usually, the terminal material is the same as the electrode material in order to avoid potential differences and risk of corrosion inside the cells. In any case, making reliable and long-lasting connections, especially to the aluminium electrode / terminal can pose some challenges.

The electrolyte is an organic solvent with a lithium based salt in solution. The electrolyte is electronically non-conductive, but solves and transports lithium-ions. There is a range of different suitable solvents for lithium-ion cells. Frequently, two to four different solvents are mixed in certain proportions and additives may be added in order to “engineer” the desired characteristics. Currently, the formulation is optimised for a general broad use. However, the formulation could be optimised for certain applications (e.g. high temperatures in UPS systems).

During charging, the lithium-ions move through the electrolyte from the positive to the negative electrode. During discharging they move in the opposite direction. They do not form a solid phase of lithium-metal and go back in solution. No metal lithium is formed at any stage during the process. The ions just move back and forth – hence, amongst electro-chemists, lithium-ion cells are also called “rocking-chair”. The reaction kinetics in lithium-ion cells are much faster than in lead-acid batteries, but the moveability of the ions in the electrolyte is comparatively slow. This is why early lithium-ion cells were not particular powerful. However, nowadays, the paths through the electrolyte are kept very short and hence, high power is available. This is achieved by utilising a thin fleece in which the electrolyte is absorbed. Alternatively, the electrolyte is contained in a polymer. This separator allows the active materials to be very close together.

Both electrodes consists of many small particles as shown for the positive electrode in illustration 3. The particles here are a lithium-metal-oxide and are “glued” together and to the current collector using a binder. A conductive filler (e.g. Graphite) is used to increase the conductivity between the particles. The negative electrode looks very similar, except that the conductive filler is not required, because the particles consist of conductive material themselves (e.g. graphite, coke). Performance is increased by controlling the particle size and keeping them small in order to increase the surface area and reduce the travelling distances for the lithium-ions inside the particles. Nano-technology is the key-word for the ultimate control of this process.

The particles on both electrodes are covered with a surface film , which is called solid-electrolyte-interphase (SEI) as indicated on the right hand side of illustration 3. The left hand side in fact shows one of those particles with its SEI zoomed in. Again both electrodes look very similar. During charging / discharging, the lithium-ions travel through the electrolyte, then between the particles, through the SEI into the solid particles. Entering the solid particles is called intercalation. The active material (particles) may contain no or up to a certain saturation limit of lithium-ions, which can almost freely move inside the layers of the particles – just like in a liquid solution. This is why the active material containing intercalated lithium-ions is also called solid-solution.

Comparison of Specific Behaviour

We have already mentioned a few quantifiable battery attributes, such as energy, power, weight, size and cost. These are quite easily comparable. However, most energy storage solution exhibit a range of “special attributes”, which may be specific to a certain technology and which cannot always be quantified. Many of these attributes are very important for the day-to-day use of the energy storage solution and should hence be taken into account when selecting a certain technology solution. A few “special attributes” of the most common battery technologies shall be mentioned here and compared with the lithium-ion technology.

Most batteries are labelled with their nominal capacity in Ah. However, Peukert has studied an effect for lead acid batteries in 1899, which showed that the available capacity heavily depends on the discharge rate. Usually, the nominal capacity applies to a five hour discharge with a constant current. In many applications, the discharge rate is much higher, in which case the available capacity decreases heavily. We have further investigated this effect [1] and we found that this effect makes it very hard to predict the remaining capacity of a lead-acid battery during a discharge with varying currents. Also, we found that this effect does not exist for lithium-ion cells. The available capacity does not decrease significantly with higher discharge rates as shown in illustration 4.

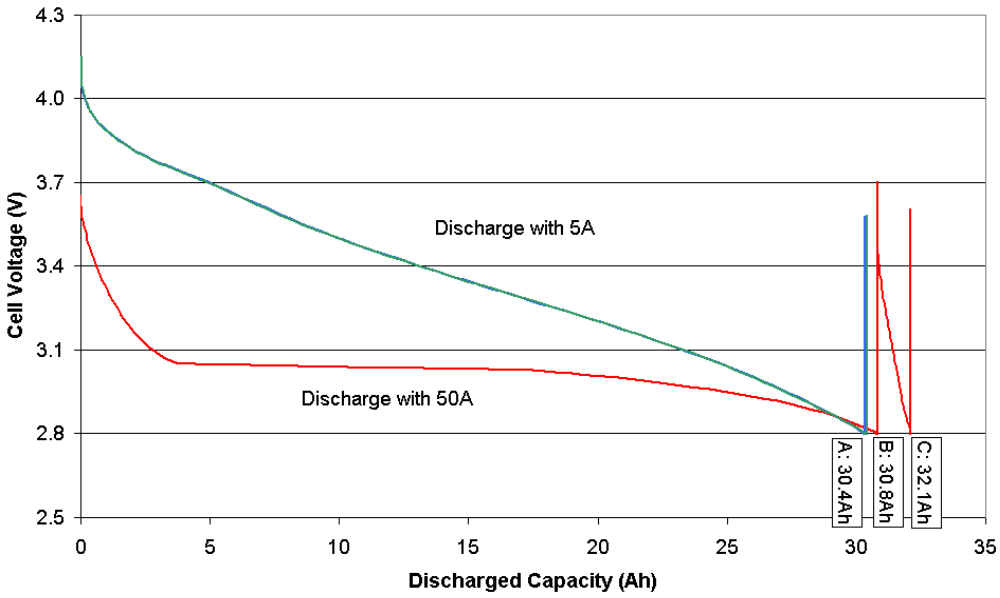

*Illustration 4: Discharge curve of a **lithium-ion cell** using two different discharge rates.*

Another well-known effect is the “memory-effect” of nickel-cadmium (NiCd) cells, which also slightly applies to NiMH cells. If a NiCd cell is not fully discharged from time to time, it appears to “remember” this lowest state of charge which it had during those cycles: after a while, it will not be able to provide sufficient power below this state of charge any more. NiCd cells therefore require a full discharge from time to time. This is very user-unfriendly for many applications (in particular power-tools).

Lead-acid batteries exhibit the opposite behaviour. They will start performing worse if kept in low-charge regions for too long times. In cyclic applications, undercharge is what kills the lead-acid battery and it is important to provide lead-acid batteries with a full charge as often as possible. Charging currents should be as high as practical, charging voltages should be high and opportunity charges should be applied wherever possible. However, in

stand-by applications where the battery is kept fully charged all the time, such as in uninterruptible power supplies, the opposite problems becomes more evident: The cells will die due to corrosion or dry-out, which is a result of gassing. In these cases, the charging voltage should not be too high. Getting it “just right” becomes a challenge, especially, when trying to manage a high voltage pack with several cells in series connection.

Lithium-ion cells do not exhibit any of the above characteristics. Basically, they can be stored or used in any state of charge and they can be recharged whenever suitable. However, they should not be kept at very high state of charge and very high temperatures, as this will increase the thickness of the SEI (see illustration 3). The ionic conductivity of the SEI is not very good and the travelling through that SEI is one of the major rate limiting steps. Increasing it means loss of performance.

Some types of batteries suffer from a sudden death when reaching their end of llife. Flooded lead-acid batteries for example can suffer from internal short-circuit after a certain cycle life, which will cause them to stop working altogether and almost without warning. Lithium-ion cells are subject to a monotonous and predictable ageing: The capacity and the performance will decrease slowly over time and cycles without any surprises. The most important ageing processes will be explained later.

Compatibility with Existing and Well-known Battery Technologies

The 12V block lead-acid battery is a very common battery type. Many components are designed to work with the typical voltage range of those batteries. Lithium-ion cells however exhibit a nominal voltage of 3.6V and hence, it is not possible to obtain exactly the same voltage: Three lithium-ion cells in series provide 10.8V nominal and four cells provide 14.4V. There may be a problem finding a suitable matching voltage when trying to use lithium-ion cells. However, the nominal voltage should not be the only value under consideration. The following illustration compares the total voltage swing as well as the most important voltage levels for a lead-acid battery and three or four lithium-ion cells connected in series.

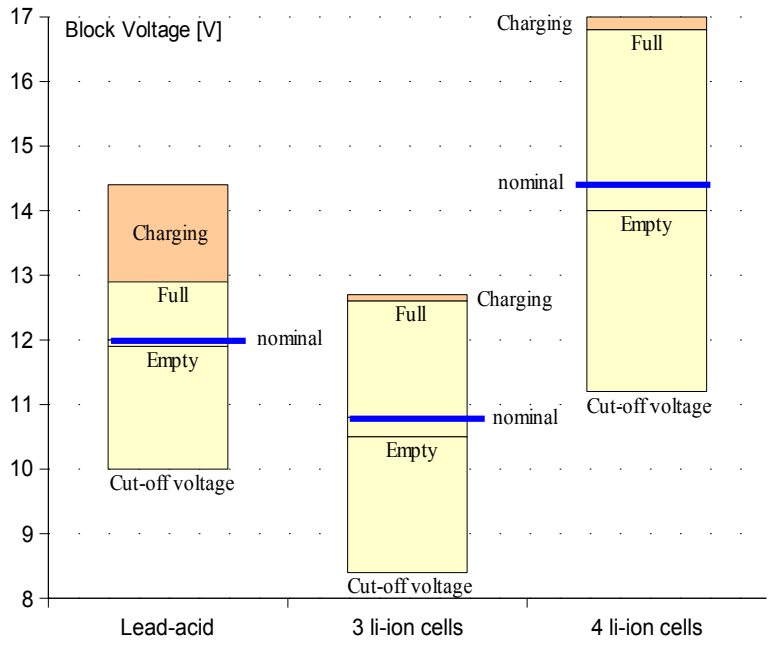

Illustration 5: Typical voltage ranges of a 12V lead-acid battery block compared with three or four lithium-ion cells that are connected in series.

The most important voltage levels to be considered are (from bottom to top): The cut-off voltage, which is the minimum permitted voltage level during discharging. The next voltage level is the “empty” voltage, which is the voltage of an empty battery in equilibrium. Equilibrium means that there is no charging or discharging current and that the cell voltage has reached a stable value. The next voltage level is the nominal voltage and then the “full” voltage, which is the voltage of a full battery in equilibrium. Finally, the top voltage is the maximum voltage at the end of charging.

It can be seen that the voltage levels very much differ between the three solutions. No exactly matching lithium-ion solution can be found for a 12V lead-acid battery block. Lithium-ions have a different voltage swing characteristic. The relative total voltage swing is about the same as for the lead-acid, but the voltage swing during discharging is much higher for the lithium-ion cell if compared with the lead-acid. This is because the lead-acid exhibits a high voltage swing just during charging, whereas the lithium ion doesn't. This can be of importance for applications, where the discharging components are not connected during charging.

However, the problem of matching voltages becomes less of an issue at higher battery voltages. E.g. a battery with 10 x 12V lead-acid blocks in series can be matched quite nicely with 33 lithium-ion cell in series.

Examples of Other Important Battery Characteristics

There are many more important characteristics, which should be considered when choosing the energy storage solution. Go through all of them in great detail would be out of scope for this paper. However, we will briefly mention a few more characteristics, where the lithium-ion technology performs differently:

- Many battery types exhibit some issues with heat. They degrade rapidly at elevated temperatures and some heat up significantly during discharging or charging, especially towards the end of charging - effective cooling may be required. Lithium-ion cells are very efficient and they do not heat-up as much. There are no side-reactions by design and hence they do not heat up at all towards the end of charging. In fact, the thermodynamics make them cool down slightly during charging.
- Batteries with water-based electrolytes may freeze and the case may crack at very low temperatures. This is a well-known problem for fully discharged lead-acid batteries with low acid concentration. The organic solvent in lithium-ion cells does not freeze at low temperatures.
- The performance of some batteries becomes very poor at low temperatures. It is difficult to make general statements about low-temperature performance of lithium-ion cells. However, it is possible to make and buy modern lithium-polymer cells with very good performance at low temperatures.
- Lead-acid batteries tend to produce hydrogen gas towards the end of charging. Hydrogen is explosive even in tiny concentrations and this is why there are several regulations and good practices about the ventilation and explosion protection when using lead-acid batteries in various applications. Lithium-ion cells are fully sealed and there is no gassing, hence no risk of explosions.
- Lead-acid batteries and NiCd batteries are quite robust towards over-charging and deep discharging (abuse tolerant). Depending on the level and duration of abuse, they may not suffer significantly. Lithium-ion cells are slightly more sensitive to abuse conditions. Heavy abuse may cause dangerous situations such as fire.

- For some battery types, it is fairly difficult to determine the remaining capacity during usage (fuel-gauge): lead-acid batteries suffer from the Peukert-effect and NiMH batteries exhibit a significant voltage hysteresis between charging and discharging. Further on, it is fairly difficult to determine the end of charge with NiMH cells. Lithium-ion cells have none of these problems and the coulomb efficiency is 100%. Hence, simpler and more robust state of charge algorithms can be used.
- Lithium-polymer cells are fully sealed and contain no compressible volume. They can be used under very high pressure without any pressure hull and without any loss of performance.

Of course, this is not an exhaustive list and explanation of all attributes and characteristics. Others are e.g. cost, which are currently much higher for the lithium-ion cells, but will come down with volume production. Also, lead-acid batteries are a well-known and mature technology, whereas the behaviour and issues with lithium-ion cells are not commonly known amongst system designers. However, the greatest issue with lithium-ion technology is the safety and this is why we have dedicated a separate section to this topic.

Safety

Lithium-metal provides a high voltage potential and this is why the lithium-ion cell exhibits such a high terminal voltage of 3.6V. This in return is the reason for the high energy density of the cells. The high terminal voltage prohibits the use of water-based electrolytes, because electrolysis would occur – an organic solvent is used instead. This organic solvent has advantages, because it does not freeze at low temperatures. However, all these advantages cause the main disadvantages regarding safety at the same time: Lithium metal is highly reactive and cannot be extinguished with water; high energy densities and high power densities usually equal higher safety risks; and the organic solvent is flammable. Fortunately, there are various working principles, making those cells intrinsically safer than it appears at a first glance.

Firstly, there is no metallic lithium inside lithium-ion batteries. Various lithium-metal batteries have been researched and tried, but for safety reasons, the lithium-ion cell has evolved from those early and sometimes dangerous trials. Since there is no highly reactive lithium-metal inside lithium-ion cells, they are intrinsically much safer than these early predecessors. Lithium metal may be plated on the negative electrode if the cells are being overcharged. However, usually this plated lithium-metal instantly reacts with the electrolyte and just increases harmlessly the SEI layer. However, this reaction may produce sufficient heat in order to start a thermal runaway in case the plating occurred at a high rate, e.g. when overcharging the cell with a high current.

Fortunately, the separator exhibits a shut-down behaviour, which means that it stops the lithium-ions from moving through it once the temperature inside the cell rises to a certain level. This will stop the overcharging and hence further reactions. Unfortunately, the separator will break down, if the process has sufficient thermal momentum and the temperature keeps rising despite the shut-down. When breaking down, the separator will loose its integrity and may allow the positive and the negative electrode to touch each other. This would cause a rapid and exothermic reaction, the solvent will ignite which will lead to more heat generation and even faster reactions. A safety vent will open and prevent the build-up of dangerous pressure inside the cell. The cell will not explode but catch fire. The heat of the fire will cause other cells next to the burning cell to catch fire as well. The positive side of things here is that unlike with burning liquids, the fire will be contained within the battery and not spill out. Reversing polarity with high currents can cause a similar scenario.

For those reasons it is important to prevent every single cell in a pack from entering any of the above abuse conditions. Electronic protection and management will be discussed in the following chapter. Dangerous abuse conditions may also arise from either mechanical impact, from faulty cells or due to growth of dendrites, which could penetrate the separator and cause local internal short-circuits. However, cell manufacturers and independent institutes perform various mechanical and electrical tests and subject the cells to abuse conditions in order to assess the safety of the cell design. Dendrite growth and separator penetration cannot normally generate sufficient local heat for starting a thermal runaway. Low cell voltages or 0V at the cell terminals are indications for internal short-circuits and should not be ignored. Rapid charging should be prohibited in such cases in order to prevent sufficient local heat generation inside the cell. This is usually a task for the battery protection or management electronics.

It is possible to safely use lithium-ion batteries. Good system design and electronic protection are essential in order to achieve this. Finally, the battery industry and research institutes are constantly working on higher intrinsic safety – just like engineers were working for decades, to make cars, engines, fuel tanks and petrol stations safer.

Ageing

So far, the longevity of the small lithium-ion batteries in most portable applications was not really an issue to the manufacturers or suppliers. However, for large expensive battery packs, ageing and lifetime become a real issue. Unlike lead-acid batteries, where it is fairly well known how long they last in certain applications, ageing of lithium-ion batteries is still fairly poorly researched, mainly due to the fact that large lithium-ion cells were not commonly available. Saft in France, AEA technology in the UK and Gaia in Germany can provide some information for certain usage conditions. However, these information are not based on a huge number of tests, cell designs are still changing faster than those tests could be performed and there is no general “formula” in sight, which puts all conditions into relation with the rate of ageing and also with the requirements of a particular application. For this reason, we cannot give a satisfactory answer on the life of lithium-ion batteries here, but we will explain the most important ageing mechanisms briefly.

The working principle of lead-acid batteries demands ageing, because material goes into solution, is transported and crystals are formed. However, in theory there is no such thing in lithium-ion batteries: lithium-ions just move back and forth, travel through the SEI and intercalate into the electrodes without significant volume change. However, in practice, there are three main ageing processes (not considering any abuse conditions):

1. The SEI grows and lithium is consumed, because the SEI may get damaged when lithium-ions travel through it. The SEI then instantly grows back, but increases its thickness around the original damage. A thicker SEI results in worse performance and the consumption of lithium may eventually result in reduced capacity.
2. Solvent molecules may “co-intercalate” together with the lithium-ions into the host structure and hence damage the surface structure and prevent further intercalation of lithium-ions. This will result in reduced capacity as well as performance loss due to decreased active surface area.
3. Finally, the electrolyte is not totally stable. It decomposes with time. The rate of decomposition depends on temperature, terminal voltage and the mixture of solvents. Generally, highly viscous solvent mixtures will decompose slower, but perform worse. High temperatures and high terminal voltages will accelerate the decomposition process.

The above ageing models are not very well researched yet as mentioned earlier. But it is

rather obvious that low temperatures and lower terminal voltages during storage will prolong battery life.

Protection and Management Requirements for Lithium-Ion Batteries

Electronic protection circuitry is required in order to ensure a safe operation of lithium-ion cells. Firstly, we would like to discuss the essential protection requirements.

Essential Requirements for a Simple Electronic Protection

Exceedingly high currents can lead to high temperatures inside the cell and this may cause thermal runaway. A fuse is the simplest form of protection against high currents. Over-voltage or cell reversal (negative terminal voltage) can cause dangerous situations and need to be prevented for each cell. Hence, every cell voltage needs to be monitored and the protection circuitry needs to be able to disconnect the battery from the load or charging device. In the simplest form, this is achieved by employing two comparators per cell and letting each of them switch a relay off, which disconnects the pack from any connected load or charger in case any of the cells exceeds the maximum allowed cell voltage or if any of the cells goes below the minimum allowed cell voltage. Finally, high temperatures may cause dangerous situations especially during charging. Most manufacturers of lithium-ion cells do not allow charging in case of ambient temperatures exceeding 45 degC. The electronic protection circuitry in its simplest form needs to measure several cell temperatures and disconnect the battery pack from any load or charging circuitry in case any of the temperatures exceeds the maximum limit. The essential functionalities of an electronic protection device are summarised in illustration 6.

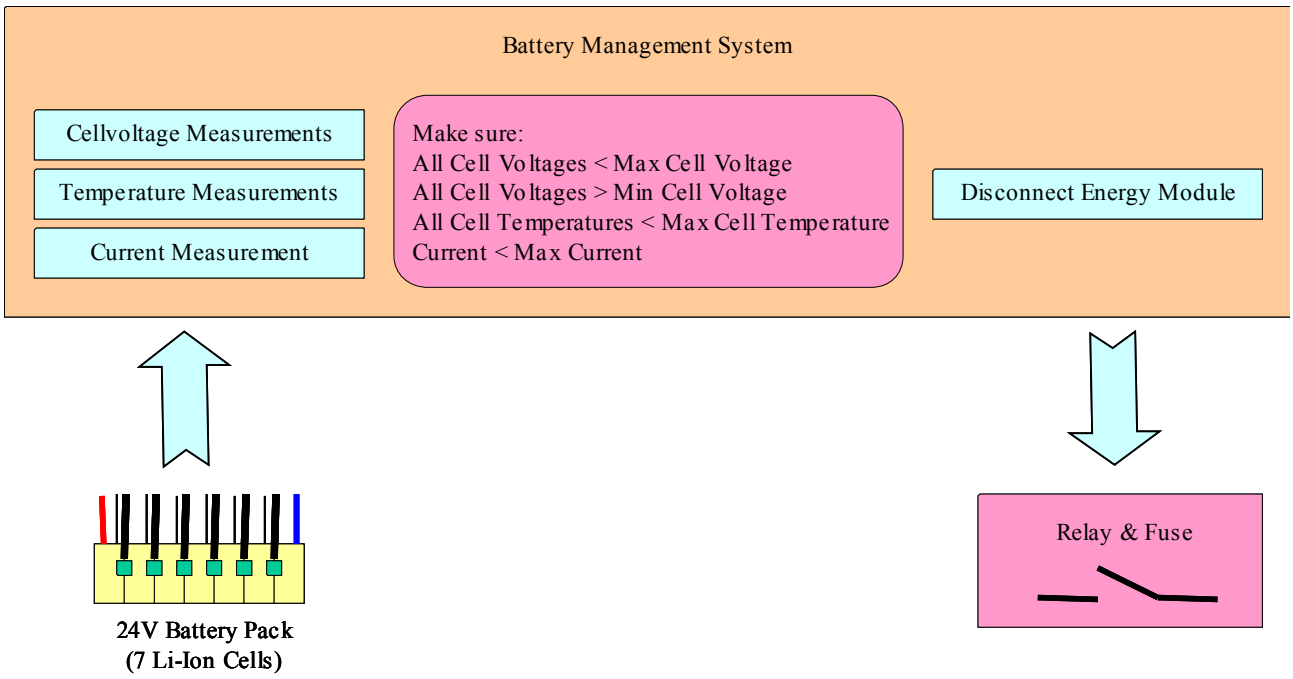

Illustration 6: Essential functionalities of any lithium-ion protection circuitry.

No intelligent control is required for such a simple protection device. However, the behaviour and performance of such a simple protection may not be suitable for all applications nor may this be satisfactory for many users. We will mention a few major disadvantages of such simple protection circuitry:

- The permitted current during discharging is usually higher than the permitted current during charging. Using only one fuse for charging as well as discharging

limits the available discharge current to the maximum allowed charging current.

- The simple protection circuit will disconnect the pack immediately and without warning if any of the monitored values was outside its limit. This is undesirable or even dangerous for many applications. The expected behaviour as known from other battery types without protection electronics is that it should continue to work and the user should feel a decrease of power before it stops delivering energy.
- Some manufacturers provide more sophisticated specifications, such as charging or cut-off voltages that depend on temperature or current. Most of them specify different temperature limits for charging and discharging and usually, there are different current limits for different durations (peak current – continuous current).
- Most battery chemistries can be overcharged without harm. In fact, most batteries must be slightly overcharged in order to equalise several cells that are connected in series. The equalisation is required in order to fully charge all the cells and hence obtain the full capacity of the pack. Lithium-ion cells however must never be overcharged, because there are no side reactions that could absorb the excessive energy. This means, that lithium-ion cells require active equalisation circuitry in order to keep all cells within a pack in a similar state of charge.
- Lithium-ion cells are usually charged until they reach their maximum allowed charging voltage and then the charger should keep this voltage and taper down the current (constant voltage charging phase) until the current drops below a certain limit, at which point the cell is considered fully charged. If several cells are connected in series, it becomes very unlikely, that all cells reach this maximum charging voltage at the same time and since the external charging device has no inside knowledge about individual cell voltages, it would continue charging until the battery protection device disconnects the battery from the charger. However, in such a case, there would be no constant voltage phase and one would not be able to return the full battery capacity. This problem increases with higher charging currents, ageing cells, mismatched cells or if no equalisation was implemented.

Requirements for Simple Battery Management Suitable for a Range of Applications

The above disadvantages of the simple electronic protection translate into a list of requirements that are important for managing the battery in a range of applications to an acceptable standard. Namely, they are:

- Distinguish between charging and discharging current limits.
- Dynamically control discharging and charging based on single cell voltage and temperature measurements instead of just disconnecting the battery from the load or charger. Additionally, one should give an early warning before disconnecting the pack.
- More sophisticated and interdependent or time-dependent cut-off levels.
- Cell equalisation (balancing).

It is still possible to implement these additional functionalities with purely analogue circuitry. However, the circuit will become reasonably complex and difficult to tune for different applications or battery sizes and types. Systems based on micro controllers are not necessarily more expensive nowadays. They are more flexible and probably easier to design in first place. However, there are issues when relying on software for safety functionalities and this usually means that additional hardware protection has to be added, which increases the cost slightly.

Requirements for a Fully Featured Battery Management System

Since a micro controller is probably used anyway, several useful and important features can be added without greatly increasing the cost:

- User information such as raw battery values (temperature, current, voltages), status / problem information or information about state of charge, state of health, state of function, remaining time, etc. can be generated and made available on analogue or digital interfaces, which connect to displays, instruments or other computers.
- Service information can be stored or generated, such as internal cell resistance, problems during the last usage, etc. This is important in order to assess the usage history, e.g. in case of warranty claims.
- The usage can be logged, e.g. total accumulated capacity since the last service, which again is important in case of warranty claims. It also helps learning and understanding the ageing behaviour of the battery.
- Unique battery identification can be implemented, which would be important to prevent fraud.
- More sophisticated, more intelligent or self-learning algorithms can be implemented, e.g. for state of charge calculations, optimum performance or longer life.
- System management functionality can be integrated in some cases and hence save the cost for an additional system controller.
- Parameter spaces can be provided for the user, for service personal or for OEMs, so that they can parametrise the battery system to their requirements and taste.
- Systems in service can be upgraded or updated according to the latest battery knowledge and battery systems can be customised for specific requirements more easily.
- Battery know-how can be separated from electronics know-how. The software can be developed and kept confidential by the battery specialist, whereas the hardware can be developed by electronics design house.
- A range of interfaces or bus-systems can be implemented in order to allow interfacing with other external components using various standards (plug-and-play). E.g. overriding motor controllers or chargers in order to implement dynamical charge / discharge control based on single cell measurements as mentioned earlier.

Illustration 7 shows an example of a sophisticated battery management system using a master-slave architecture.

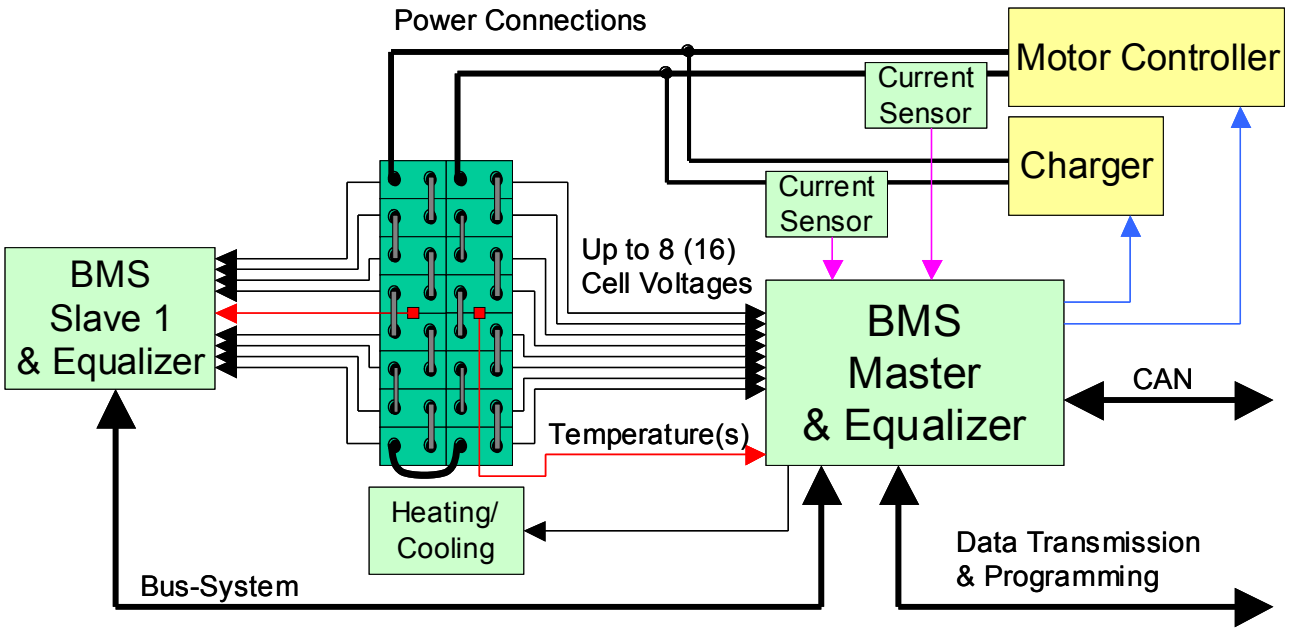

Illustration 7: Example of a sophisticated BMS in master-slave architecture.

Different Approaches for Managing Lithium-Ion Batteries

BMS Architecture

There are various possible BMS architectures in order to fulfil some or all of the aforementioned features and requirements.

- Probably the most obvious architecture is a central BMS module, which measures all the cell voltages, the temperatures and the currents and provides the above functionalities to whatever extent. However, this approach is not very modular, and either it requires one dedicated design for each possible number of managed cells or – if there was only one design – it would be oversized in case it had to manage fewer cells. This solution has even more significant disadvantages when it comes to managing batteries with high voltages or large or distributed batteries. Electrical isolation becomes an issue on the central BMS and would significantly increase the cost. In systems, where the battery is distributed over various locations, the wiring from the BMS to all the parts of the battery becomes an issue. However, for a small number of cells connected within one battery, the central solution can be a sensible option.
- Another possible architecture is one protecting or managing module per cell. The modules can be attached directly to the cell terminals and make each cell “intelligent”. However, in high power and large battery systems, the current requirements usually do not allow having one disconnecting device per cell, because it would become too big, heavy and expensive. This means that all the cell management systems would still have to communicate with each other and with external devices. Each cell will require additional connections for communication and also for analogue safety. A central master module is probably required for sophisticated functionalities ad providing certain bus system standards such as CAN or RS485, making this solution less neat. Finally, due to many different cell shapes and designs, it will not be possible to have “one design for all”. However, there may be specific applications and certain market volumes or cell designs, where this solution is a sensible option.

- The third option is a partly centralised solution, which tries to combine the advantages of the centralised and the decentralised solution. A partly centralised management system will consist of management modules which can independently manage a number of cells. Several of those management modules can be employed for managing higher number of cells. In that case, the independent modules will be communicating on a bus system in order to determine overall battery information and control outputs. One of the modules can act as a master, which connects to external components such as disconnecting relays, charger and motor controller, so that no additional master module would be required. Such a system is shown in the example above (illustration 7). A partly centralised BMS can be designed to suit a range of cell types, cell sizes and cell configurations. The partly centralised option also reduces the bus load for communication thanks to smaller message overheads and this means reduced EMC, power consumption or higher speed, which may be desirable when it comes to closed loop controls.

Different Methods for Cell Equalisation

Cell equalisation is an important and major task for any lithium-ion battery management system. Again, there are three major categories of solutions:

1. Full current shunting allows to shunt the maximum possible charging current “around” each cell, so that a fully charged cell will not receive any further charge whilst other cells that are connected in series with that cell can still receive full charging current. The advantage of this system is that any common charging equipment can be used without any need for communication between the BMS and the charger. However, communication between the cell modules is still required, because the current shunting cannot prevent any cell from exhibiting too low voltages. The shunted current is dissipated as heat and this will be a problem in systems with high-power charging capabilities: large and expensive shunt regulators (e.g. 1kW per cell !) will be required and they will produce significant heat. Finally, the regulation needs to be quite precise and this may be a cost issue if the maximum permitted charging voltage depends on certain factors such as temperature or current or if it was parametrisable.
2. Another type of equaliser can overcome the disadvantages of the above solution. We will call this type “energy distribution”, because rather than dissipating excessive energy. This type of equaliser can take excessive energy from one cell and redistribute it across the other cells where required. This has obvious theoretical advantages over the dissipative type: smaller and less expensive heat-sinks are required if any at all, because only the inefficiencies of the power distribution do contribute to heat generation. Additionally, this equaliser maximises the energy available from the whole pack. The pack would not be limited by the weakest cell. However, redistributing the full discharging currents in a high-power battery requires high power components and will probably not be cost-effective, small and lightweight. However, it finally depends on how the redistribution circuitry exactly works. There are three major implementations of this type of equaliser: one controlled isolating DC/DC per cell working on a common voltage bus; “flying capacitor(s)”; “switched reactor/inductance”. It is not within the scope of this paper to discuss their working principles and advantages / disadvantages. More information can be found in various publications.
3. The third option is to equalise the cells using low-power dissipation. This is the lowest cost option, because the equalisation circuitry can sit on the BMS board and the equalisation currents are small enough so that they can be shunted through the

measurement cables, which are required for single cell voltage measurement anyway. Considering that cell-imbalances in terms of state-of-charge mainly stem from differences in self-discharge rates, small equalisation currents will be sufficient for keeping all cells at the same state of charge. The obvious disadvantages are that the weakest cell determines the performance of the pack and that the BMS needs to be able to control the charger, so that the charging current can be reduced if one of the cells reaches the charging voltage before the others. However, cell variations will become smaller with higher cell production volumes and the advantages of the first two equaliser types will become smaller and will not justify their significantly higher cost.

Conclusions

Lithium-ion batteries can provide significant advantages over almost any other battery technology and they can be used for substituting combustion engines in some applications. They can be used in addition to or instead of fuel-cell technology with the advantage of being available and rechargeable through existing infrastructure right now.

The working principle is relatively simple and the behaviour is straight forward without any of the well-known complications such as sulphation, memory effect and without major pitfalls such as high self-discharge rates. The state of charge can be determined relatively easy and systems can be designed with high user-friendliness.

However, proper system design and electronic battery protection are required in order to assure safe operation. The ageing is not a sudden unexpected process, instead, it occurs at a fairly constant rate. However, there is only little knowledge on the exact ageing behaviour and life-time predictions are currently rarely possible.

A range of essential protection up to “nice-to-have” management requirements have been discussed. Various options and implementations for managing the cells have been pointed out and it has been indicated that some considerations and experience are required for determining an optimal solution for certain applications, cell types and market sizes.

Finally, we have mentioned the three main categories of equaliser solutions and their advantages and disadvantages. We have concluded that the lowest-cost low-power equalisation method is sufficient for keeping lithium-ion cells balanced.

About the Authors

Dipl.-Ing. Dennis Doerffel obtained his Dipl.-Ing. Degree from the University of the German Forces Hamburg (UniBWHH) in 1995. He was responsible for the purchase and maintenance of automated testing software in the German Army before he discovered his passion for electric vehicles and batteries. He started his PhD project on “Energy Management of Hybrid- and Electric Vehicles” with a focus on testing of large lithium-ion batteries at the University of Southampton in 2001. Since 2003, he is the founder and technical director of REAPsystems Ltd. REAPsystems specialises in designing and providing battery management solutions for large lithium-ion batteries.

Dr. Suleiman Abu-Shark obtained his BEng and PhD degrees from the University of Southampton in 1990 and 1994 respectively. He is a senior lecturer in Control Engineering, Electric Machines, Power Electronics and Electrical Systems. He has also been working on battery systems, battery testing, electric and hybrid electric vehicles and underwater equipment. His passion are integrated underwater thrusters.

B2:

"Rapid Test and Non-linear Model Characterisation of Solid State Lithium-Ion Batteries"

Journal of Power Sources 2004

[1]

Journal paper

Available online at www.sciencedirect.com
SCIENCE DIRECT®
Journal of Power Sources 130 (2004) 266–274
JOURNAL OF POWER SOURCES
www.elsevier.com/locate/jpowsour

Rapid test and non-linear model characterisation of solid-state lithium-ion batteries

Suleiman Abu-Sharkh, Dennis Doerffel*

School of Engineering Science, University of Southampton, Highfield, Southampton SO17 1BJ, UK

Received 1 August 2003; received in revised form 24 November 2003; accepted 1 December 2003

Abstract

This paper describes a rapid test-procedure that can be used to derive parameters of a proposed battery model. The battery model is a non-linear dynamic equivalent circuit model, which is based on Randle's model for electrochemical impedance [J. Power Sources 54 (1995) 393]. The level of sophistication has been selected such that it gives a satisfactory prediction of battery performance, but simple enough to enable on-line identification and adaptation of model parameters based on measurements of terminal voltage, current and temperature during usage. The paper also presents test data for a commercial 100 Ah battery including ageing effects.

Keywords: Rapid test; Lithium-ion batteries; Ageing effects

1. Introduction

High-energy density solid-state lithium-ion batteries are increasingly used in many applications ranging from low-power mobile telephones to high-power traction. The recent availability of high-energy cells has created new opportunities for automotive applications including electric and hybrid electric vehicles, which benefit from the high-energy density of this type of battery [2]. However, despite promising a better performance than lead acid, the younger lithium-ion technology is less well-understood and lacking information about lifetime experience.

A good battery model that relates the terminal voltage to state of charge (SOC), current, temperature and history of usage and incorporates safe operating limits should ideally be available to the designer of the system for the purpose of sizing and for the design of the battery management system that controls the charge and discharge of the battery and provides information to the user about the state of charge state of health and state of function. Ideally, such a model would have an adaptive mechanism that changes model parameters in accordance with the change of behaviour due to lifetime degradation. The parameters of a battery model are normally determined by performing charge and discharge tests under controlled conditions and monitoring terminal voltage, current and temperature.

Several different models exist for batteries. Electrochemical models and equations are normally used to design the battery, mathematical or circuit models are used to simulate battery behaviour and thermal models help designing the thermal management and predicting the thermal power limitations. Many other models are also available and usually a combination of them is required to understand the behaviour of the battery up to the required level. "Thermo Analytics Inc." [3] gives a concise and general overview of available models. Preferably the model should be as simple as possible but precise enough for the given problem, target group or application.

A simple equivalent circuit model comprising an electromotive force (emf), that can be a function of the state of charge, in series with internal resistance, which can be a function of SOC, temperature and history, may not be satisfactory in many applications. Such a model does not represent the dynamic behaviour of the battery, which in many applications is important. A dynamic model of a battery normally contains one *RC* combination like Randle's model [1] or two *RC* combinations as suggested by Gao [4] for a Sony Li-ion cell. However, many of the models published in the literature [1,4,5] assume linearity even though the actual behaviour of the battery is found to be significantly non-linear.

The open-circuit voltage (OCV) is one of the most important parameters of a battery. In a conventional test, this voltage is normally measured as the steady-state open-circuit

* Corresponding author. Tel.: +44-2380-592698; fax: +44-23-8049-3053.
E-mail address: ddoerffel@ses.soton.ac.uk (D. Doerffel).

0378-7753/$ – see front matter © 2004 Elsevier B.V. All rights reserved.
doi:10.1016/j.jpowsour.2003.12.001

terminal voltage at different states of charge. However, for each of state of charge this measurement can take a long time. Preliminary tests on our test candidate have indicated that the steady-state is reached after a time of the order of 24 h. Such a test would take days to perform on a single cell. If the cell chemistry shows a voltage hysteresis between charging and discharging, as it is the case for NiMH batteries for example [6], it would take 20 days in order to determine the OCV. Additional tests are required for determining other battery model parameters like the mentioned *RC* combinations for example. All parameters usually vary with state of charge, temperature, age and history (number and depth of cycle) of the cell not to mention variations between cells due to manufacturing tolerances. These costly time-consuming tests are not suited for in situ parameter identification and they are in contrast with the actual rapid battery development.

This paper describes a rapid test-procedure that can be used to derive parameters of a proposed battery model. The battery model is a non-linear dynamic equivalent circuit model that is based on Randle's model for electrochemical impedance. The level of sophistication has been selected such that it gives a satisfactory prediction of battery performance, but simple enough to enable on-line identification and adaptation of model parameters based on measurements of terminal voltage, current and temperature during usage. The paper also presents test data for a commercial battery.

2. Experimental apparatus

The tests were carried out on a Digatron universal battery tester (UBT) 100-18-6 at the Institute for Power Electronics and Electrical Drives (ISEA) in Aachen, Germany. The UBT 100-18-6 is capable of charging and discharging the battery at a maximum rate of 100 A. It can operate in several modes such as constant-current and constant-voltage. It comprises voltage, current and temperature measurements and a computer interface. Table 1 summarizes the specifications of the UBT.

A high-energy solid-state lithium-ion cell with a capacity of 100 Ah was tested. The cell remained within the battery block during the tests to represent a typical in-vehicle configuration. The test arrangement is shown in Fig. 1. The third cell was chosen for testing, because other cells surround it and this is the worst case in terms of temperature rise during high-current discharge and charge. The battery was placed on a plastic grid to allow for natural air-cooling and for isolating the battery from the "ground" heatsink, so that the cell heats up uniformly during the test. The ambient air temperature was 21 °C during the tests.

Table 1
Specifications of the Digatron UBT 100-18-6 universal battery tester

Maximum discharging current (A)	100
Maximum charging current (A)	100
Voltage range during charging (V)	1–18
Voltage range during discharging (V)	0–15
Error (current measurement) (mA)	±0.5% but not better than ±50
Error (voltage measurement) (mV)	±5
Error (temperature measurement) (K)	±0.1

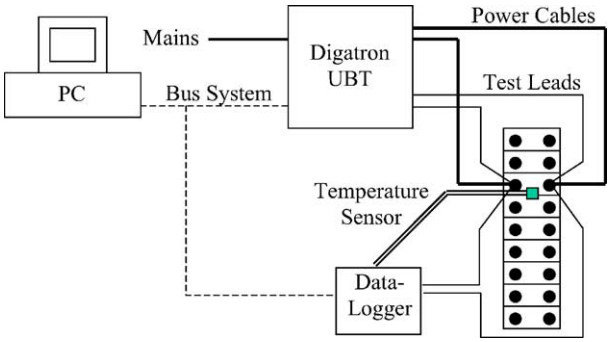

Fig. 1. Arrangement for testing the Li-ion battery on the Digatron battery tester.

The battery tester was connected to the cell using cables with 10-mm^2 cross-section. The test leads for measuring the cell-voltage are separate from the power cables to eliminate errors due to cable voltage drop. A data-logger (Digatron DLP 24C) was used to verify voltage measurement of the battery tester and for measuring cell temperature. The temperature probe was placed between cell three and cell four. The battery tester and the data-logger are connected to a PC through a bus system.

3. Test-procedure

The software "Digatron BTS 600" allows programming the test-procedure and logging data like time, current, voltages, power, temperature, watt-hours and ampere-hours. The sampling time and start/stop criteria can be programmed. Several limits for the battery can be defined separately, so that the tester will stop for safety reasons in case these values are reached.

The tested battery was new and it had to be cycled before starting the test. The behaviour was stable after the first cycle. Fig. 2 shows the first two test cycles. The test starts with a pause of 1 min in order to measure the initial voltage of the cell. The battery is charged with the rated current or less (33 A in our case) till it reaches the maximum charging voltage (4.2 V in our case). Charging continues at this voltage and the current decreases till it reaches the charge-termination current (1.1 A in our case). The manufacturer specifies this as the fully charged condition. After pausing for 1 h, the battery is discharged with a current of 33 A. It is depleted once it reaches 2.8 V at this current. The discharging/charging procedure is repeated a second time after waiting for 1 h. The first cycle assures reaching a certain battery condition. The status of a cell is usually unknown and cycling it once with a defined waiting time before starting

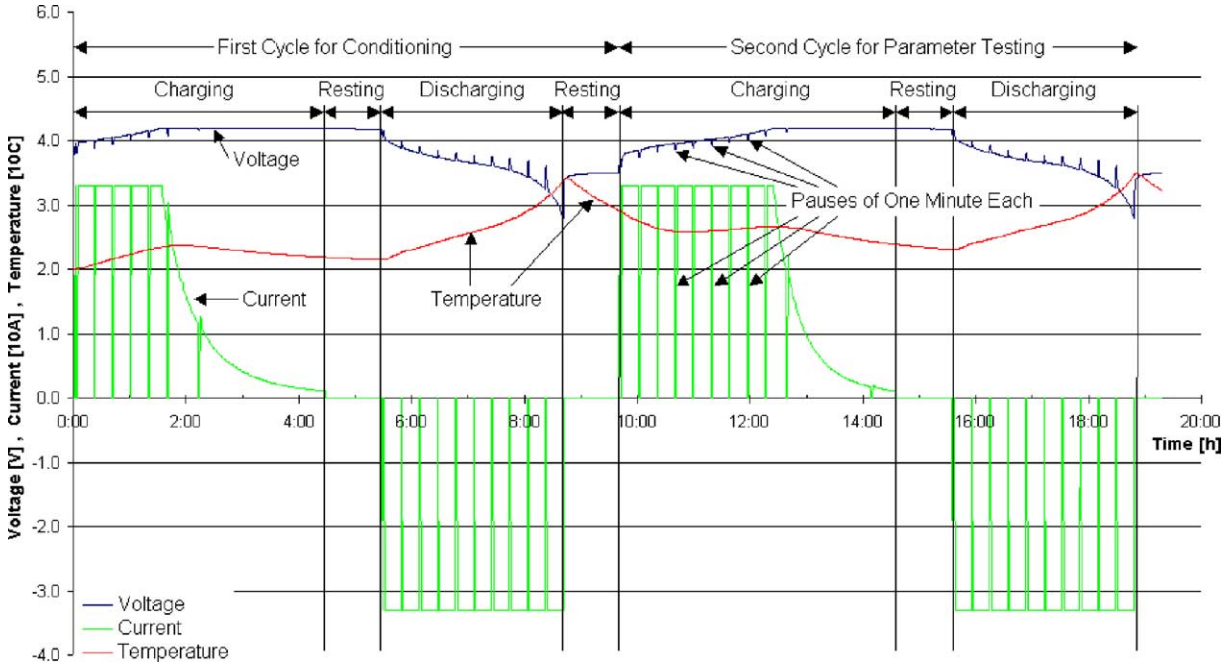

Fig. 2. Typical test curves for a 100 Ah Li-ion battery.

the actual test assures comparable test-conditions. The second cycle is used for determining battery model parameters.

The discharging and the charging process is paused after the first 1 Ah and then every 10 Ah in order to record and analyse the dynamic behaviour of the battery at different SOC. A rest of 1 h is always applied between charging and discharging. This allows the battery to approach equilibrium and to cool down. Measurements are taken every 2 mV change of cell-voltage or additionally every change of 0.5 A change in current (during charging only). This setting keeps the number of data small when no changes occur and takes faster measurement when rapid changes take place. It ensures reliable measurements in constant-current and constant-voltage phases. The measurements of cell-voltage

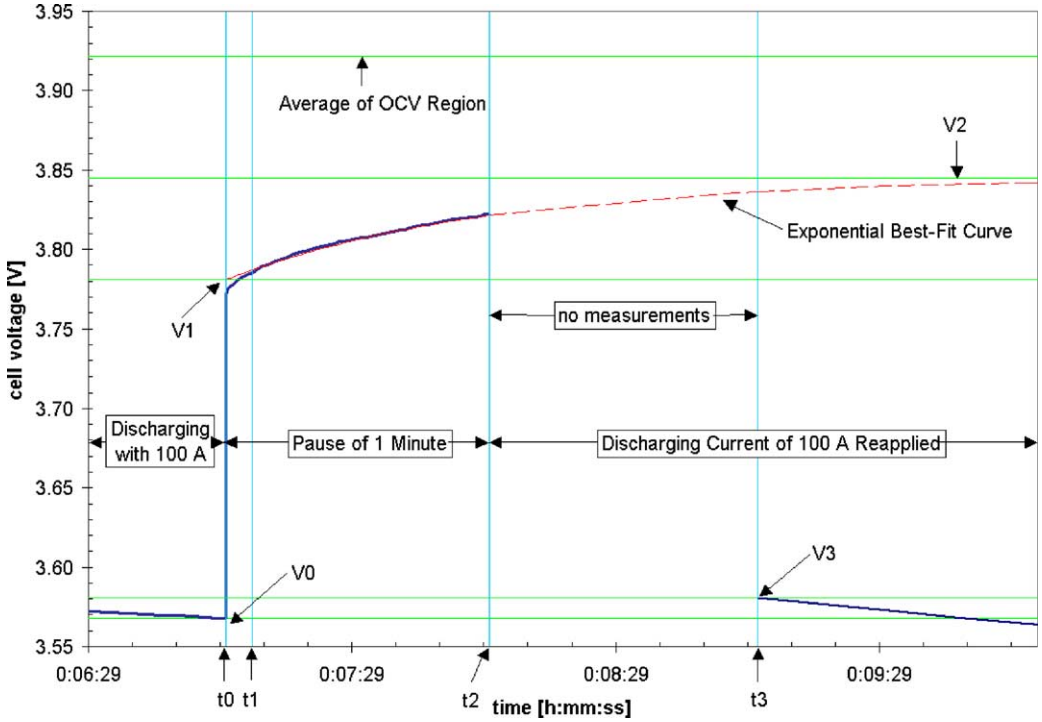

Fig. 3. Dynamic behaviour of cell-voltage when pausing the 100 A discharge current at a SOC of 71 Ah.

(direct), cell-voltage (through data-logger), current and temperature are recorded. Accumulated data like Ah and Wh are also recorded in total (balanced counting), per step and for charging in total and discharging in total.

Fig. 2 shows typical voltage, current and temperature curves that were obtained from these tests. Charging current is shown positive and discharging current is shown negative. The temperature and the current are scaled with a factor of 10 on the *y*-axis. Fig. 3 shows a typical cell-voltage during a discharge pause period (it is an expanded part of a voltage curve in Fig. 2). This figure will be studied in more detail later in this paper.

4. Non-linear dynamic battery model

Fig. 4 shows the proposed equivalent circuit model for the tested solid-state lithium-ion cell during discharge. The model for charging is equivalent to this one, but with the zener-diode the other way round. The OCV or emf is modelled as an ideal voltage source that is a function of the SOC.

R_p models the self-discharge rate, which is related to the electronic conductivity of the electrolyte. This is of interest for predicting the state of charge in case the cell is not used for a long time. It has been suggested that lithium-ion batteries require cell-balancing in order to offset variations in self-discharge rates, because they cannot be equalised based on a small controlled overcharge [7]. These variations in self-discharge rates need to be considered when designing cell-equalisation systems.

The zener-diode and the time-constant of $R_{long}C_{long}$ model a constant-voltage drop, which has been observed during tests. The delay time caused by $R_{long}C_{long}$ is in the order of several hours. Future research has to show whether this part of the model can be related to diffusion limitations in this Li-ion cell with colloidal gel-type electrolyte. The simplicity of this part of the model enables determination of SOC based on terminal voltage measurement. Knowing R_{long} is essential for predicting the behaviour at low-currents like small stand-by loads or equalising currents, because R_{long} is much higher than R_{01} and it determines the voltage drop at low-currents.

The second *RC* combination with R_{12} and C_{12} models the double-layer capacitance and the reaction kinetics. It explains the exponential rise of the terminal voltage between t_1 and t_2 in Fig. 3. It determines the dynamic behaviour of the battery during power bursts, like for example during regenerative braking in vehicles. The time-constant is in the order of 1 min.

R_{01} is the total Ohmic resistances in the cell, like terminal resistances and current collector resistances. The immediate voltage rise between V_0 and V_1 in Fig. 3 is due to this resistor. It is responsible for power-capability, because it causes the biggest share of the total voltage drop at high currents.

5. Analysis of test data—OCV

The following sections discuss the methods used to determine model parameters from the test-procedure shown in Figs. 2 and 3. Two different methods for determining the OCV are investigated. The first method is based on measured values only and the second method makes use of exponential curve fitting and extrapolation.

5.1. First method

To determine the open-circuit voltage of the battery, the results in Fig. 2, are re-plotted as shown in Fig. 5 in which the voltage during the described test-procedure is plotted against the SOC of the battery.

In Fig. 5, the voltage drops at 1 Ah and every 10 Ah that can be seen during charging are caused by the pauses of 1 min as defined in the test-procedure. On discharge the voltage rises during these pauses. All voltages reached during the pauses at different SOC during discharging and charging are connected with the dotted line. These dotted curves for charge and discharge would be expected to be identical, representing the OCV, if the pauses were long enough (of the order of 24 h). However, in this case, they are not identical,

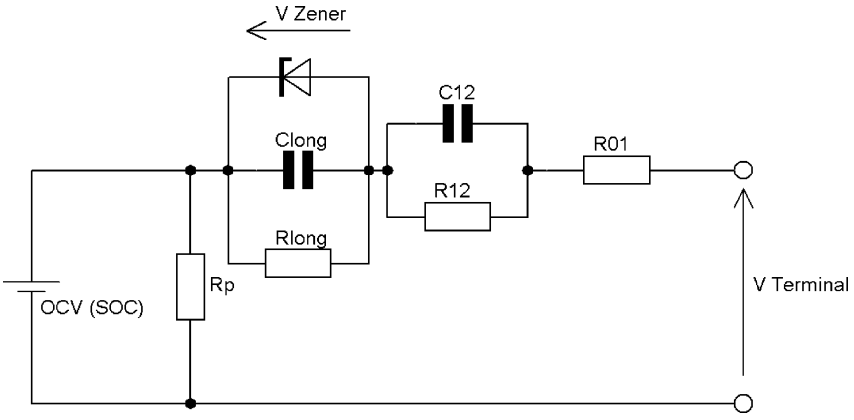

Fig. 4. Proposed equivalent circuit model for the solid-state Li-ion cell during discharge.

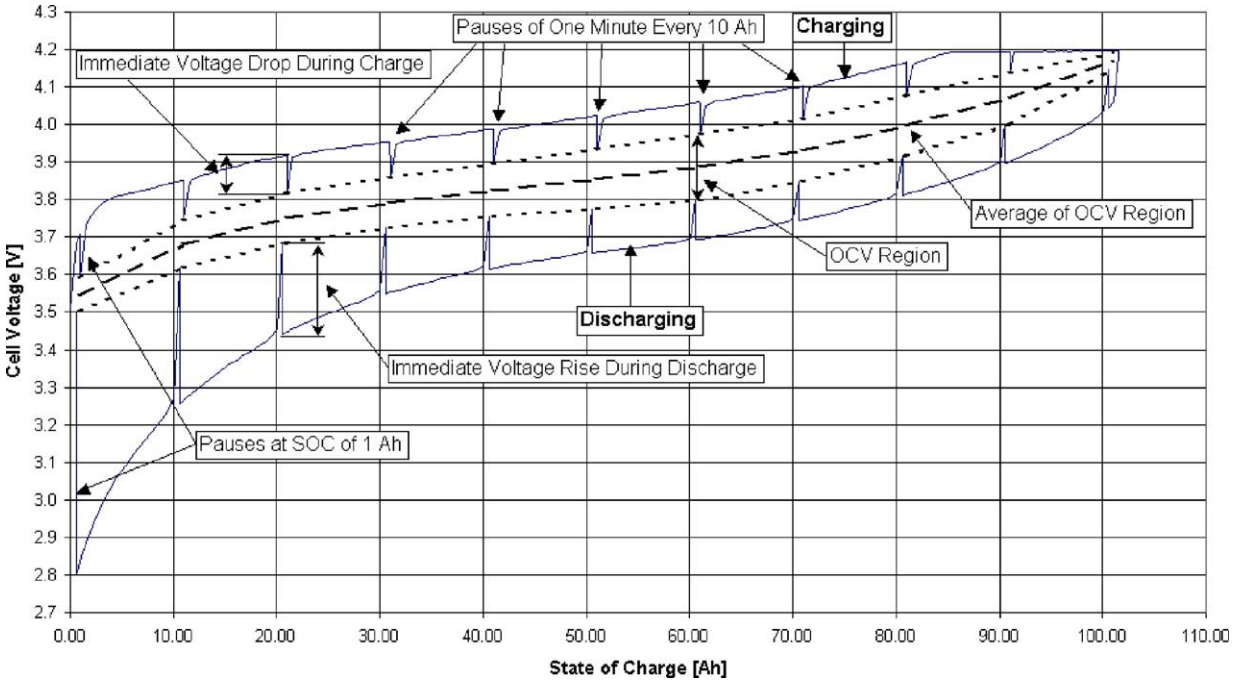

Fig. 5. Cell-voltage vs. SOC during charging and discharging.

which can be explained by the fact that the cell did not reach steady-states during the 1-min pauses. The OCV cannot be measured directly, but it is assumed that the area between the two dotted lines is the region where the OCV can be found. The dashed line shown in Fig. 5 is the mean of the dotted lines. For validation reasons only, the described test has been repeated based on a higher charging and discharging current (100 A instead of 33 A). The same analysis is applied and the resulting dashed mean curve matches the one obtained from the 33 A test with an error of less than ±10 mV or ±1.5% of SOC.

5.2. Second method

This method is based on using the data shown in Fig. 3. The first 30 s in this figure show the cell being discharged with 100 A till time t_0. During this discharge period the cell terminal voltage decreases towards the level of V_0 with decreasing SOC. The load is switched off at t_0 and the voltage rises almost immediately to the level of V_1. During the pause of 1 min between t_0 and t_2 the voltage seems to rise exponentially. The discharging current is reapplied at t_2 and the next measurement is taken 1 min later at t_3 where the voltage has dropped down to V_3.

Fig. 3 shows how an exponential best-fit curve has been laid over the measurement during the pause period. The time between t_0 and t_1 (5 s) has not been taken into account when searching for this best-fit, because the time-constant in the first seconds is much shorter. Good correspondence between the curve-fit and actual measurement data could be found by omitting these first 5 s. The level V_2 is the extrapolated steady-state value of the best-fit exponential curve. It defines the upper limit of the OCV region during charging and it defines the lower limit during discharging. The mean value of V_2 during charging and discharging is the OCV proposed in this second method. The results of different OCV test-methods are presented in Fig. 6 for comparison. The curves for different test-methods and currents are almost indistinguishable, which shows that the two methods produce almost identical results.

In Fig. 6, no measurements were taken at low SOC at 100 A, because the battery tester configuration was not suitable for this test condition. There are slight differences of about ±10 mV between the tests with different currents at SOC of 80 and 90%. The results from the first method and the second method on the other hand are coincident. It is sufficient to make use of the simpler first method for determining OCV. It is not necessary to employ exponential regression as proposed in the second method.

The following paragraphs investigate, whether the OCV results from the rapid method described above agree with results obtained from conventional test-method with long waiting time. A test with a waiting time of 12 h at each SOC level has been carried out. The battery has aged for 1 year and some cycles in an electric vehicle between the proposed test and the conventional test. The total available capacity went down from 101 to 94 Ah under same test conditions. A first analysis was based on a diagram showing the OCV as a function of SOC in Ah. This diagram revealed unsatisfactory results, because of the Ah shift. The diagram in Fig. 7 presents and compares the results using SOC in percentage as *x*-axis.

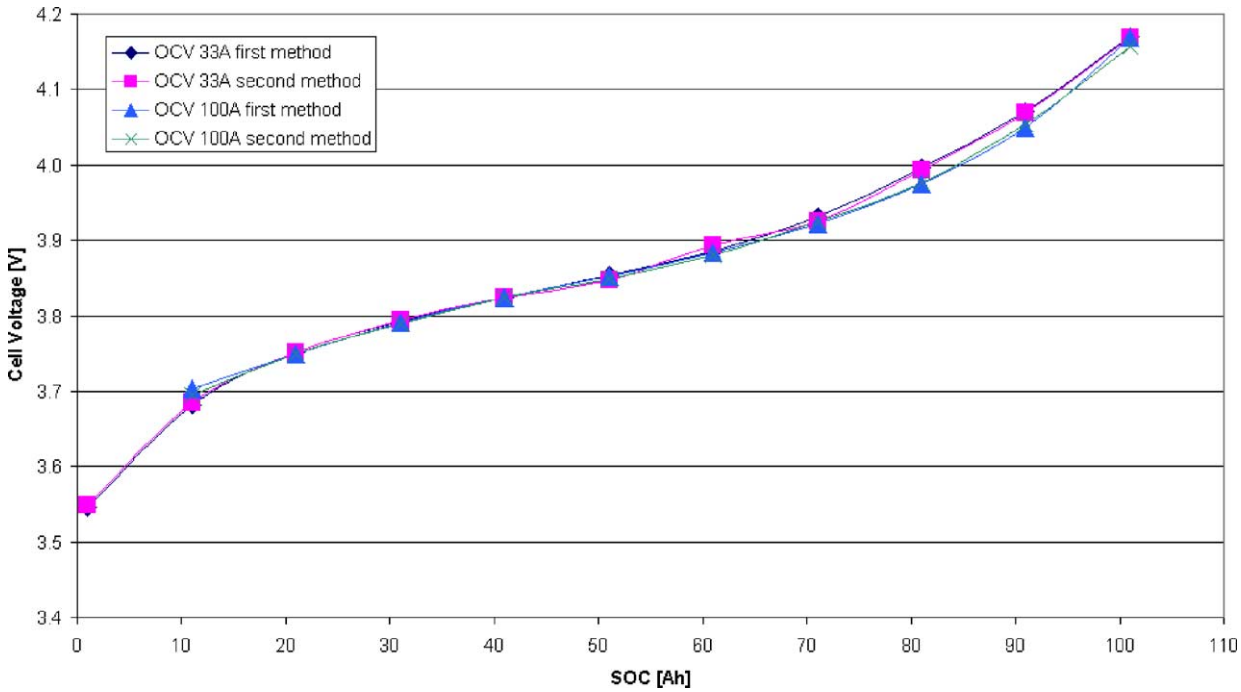

Fig. 6. OCV vs. SOC curves obtained from different methods.

Fig. 7 shows the OCV region obtained from the proposed rapid test. The region is between the top curves obtained during charging and the bottom curves obtained during discharging. The curves between using the same colour and pattern represent the mean values between charging and discharging. The two black curves in the middle represent the OCV results obtained from the long-term test with a waiting time of 12 h. The top one is for charging and the bottom one for discharging. The long-term test has been performed on an aged battery (16 full cycles and 1-year-old), while the rapid test was performed on the same cell when it was new. The rapid test has been repeated just before the long-term

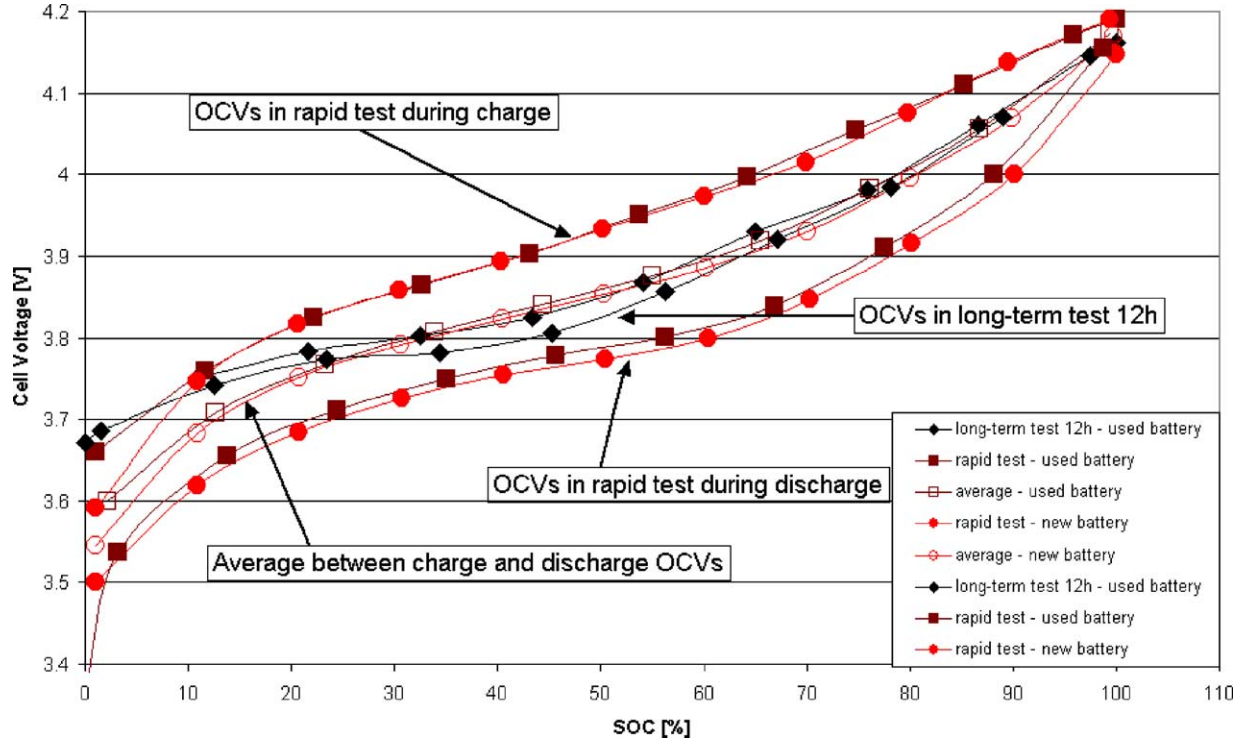

Fig. 7. Comparison of OCV obtained from different tests and different age of battery.

test in order to receive comparable results. The red curve with the dots represents the test with the new battery and the brown curve with the squares represents the used battery.

It can be seen that the battery age has only marginal influence on the shape of the OCV curves if plotted against the SOC expressed in percentage. The two curves obtained from the long-term test do not match between charging and discharging. This reveals that even a waiting time of 12 h is not sufficient to fully reach equilibrium. The OCV results from the proposed rapid test-method match the results from the long-term test reasonably well between 20 and 100% SOC. They are lower at SOC levels below 20%. This can be explained by the short waiting time between discharging in the first cycle and charging in the test cycle as shown in Fig. 2. Another factor is that during discharge, concentration gradients build up by, which cannot be offset during the first minutes of charging due to slow mass transport in the gelled electrolyte and voltage drop is more noticeable at low (local) SOC thanks to the reaction kinetics. This problem is not noticeable at full charge, because the current reaches small values at the end of charge, whereas current remains high during discharge till cell-voltage is 2.8 V.

This paragraph has shown, that the proposed rapid method is suitable for determining the OCV between 20 and 100% SOC. The first simpler method is sufficient for OCV determination, whereas the following paragraph will rely on the second method using exponential extrapolation in order to determine dynamic model parameters.

6. Analysis of test data—dynamic behaviour

The following paragraphs investigate the dynamic behaviour of the cell. The battery model parameters will be determined based on the test explained earlier. The battery was naturally cooled, and therefore, the cell temperature was not constant. It was varying as shown in Fig. 2. This will enable us to make some qualitative statements on the temperature dependency of model parameters.

With reference to Fig. 3, the instantaneous voltage rise when the discharging stops is defined as:

$$\Delta V_{01} = |V_1 - V_0|$$

It is assumed that this immediate voltage drop can be related to the internal Ohmic resistance R_{01} of the battery. This resistance can be calculated for charging and for discharging at various SOC, based on the following equation:

$$R_{01} = \frac{\Delta V_{01}}{|I|}$$

Fig. 8 shows the result of this analysis. The two top curves show the resistance R_{01} during discharging as a function of SOC. One is obtained from the 33 A test and the other from the 100 A test. The two other curves show the equivalent but during charging. In general, the resistance is lower at higher currents. The charge resistance is lower than the discharge resistance.

Similarly, the other resistances in the circuit model can be determined using the following equations:

$$\Delta V_{12} = |V_2 - V_1|$$

$$R_{12} = \frac{\Delta V_{12}}{|I|}$$

Fig. 9 shows the resistance R_{12} as a function of SOC during discharging and charging with 33 and 100 A. The scale on the *y*-axis is the same as in Fig. 8 for better comparison. The curves are almost indistinguishable in this scale and

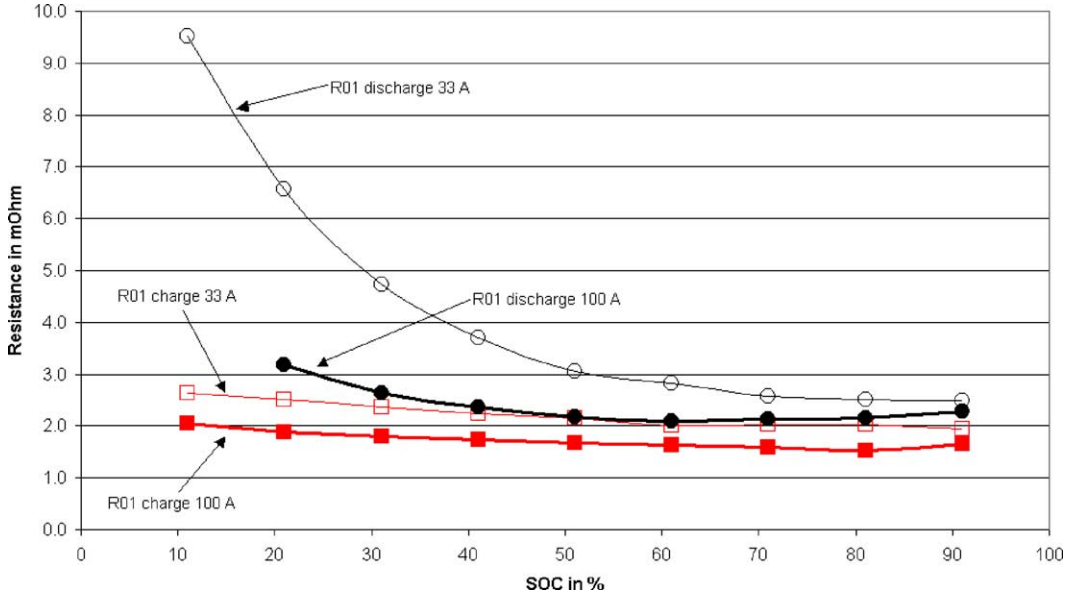

Fig. 8. Internal resistance R_{01} as a function of SOC during charging and discharging obtained from different tests (temperature not constant).

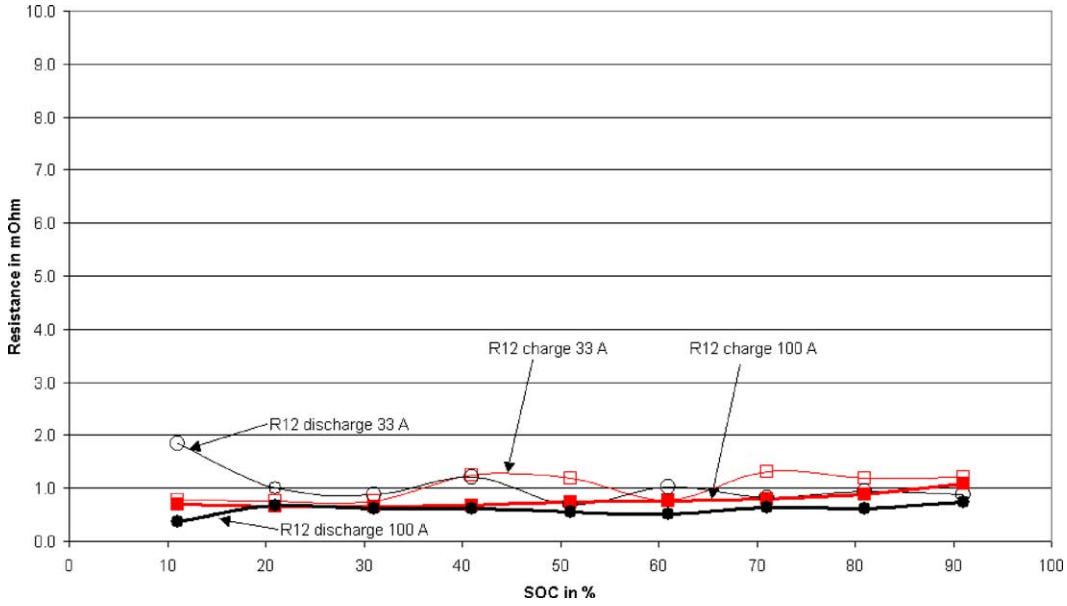

Fig. 9. Internal resistance R_{12} as a function of SOC during charging and discharging with 33 and 100 A (temperature not constant).

remain almost constant throughout different SOCs if compared with the generally higher values of R_{01} in Fig. 8. The results do not show any significant trend within the SOC range or any significant dependency on the current. Resistance during charging and discharging are similar. The temperature varied between 23 and 45 °C during tests, but R_{12} shows no relation to these temperature changes. In conclusion, R_{12} can be called constant if compared with R_{01}. The calculated mean value of R_{12} is 0.869 mΩ with a standard deviation of 0.277 mΩ.

The last analysis focuses on the voltage difference between V_2 and the average of the OCV region. The average of the OCV region will be called OCV in the following text. Though the graph in Fig. 3 suggests that the cell-voltage approaches level V_2, additional tests have revealed that it actually approaches OCV, if waited for long enough.

Fig. 10 shows the level V_2 for charging and discharging, at 33 and 100 A and the OCV over SOC. It reveals that the level of V_2 is independent on the current. The difference between V_2 and OCV for SOC levels between 10 and 90% is a constant 68 mV measured with a standard deviation of 12 mV. This difference is the same for charging and discharging and shows no relation to the temperature changes during tests. It is sensible to model this voltage drop with a zener-diode instead of using a resistor, because the voltage drop is constant and not proportional to the current.

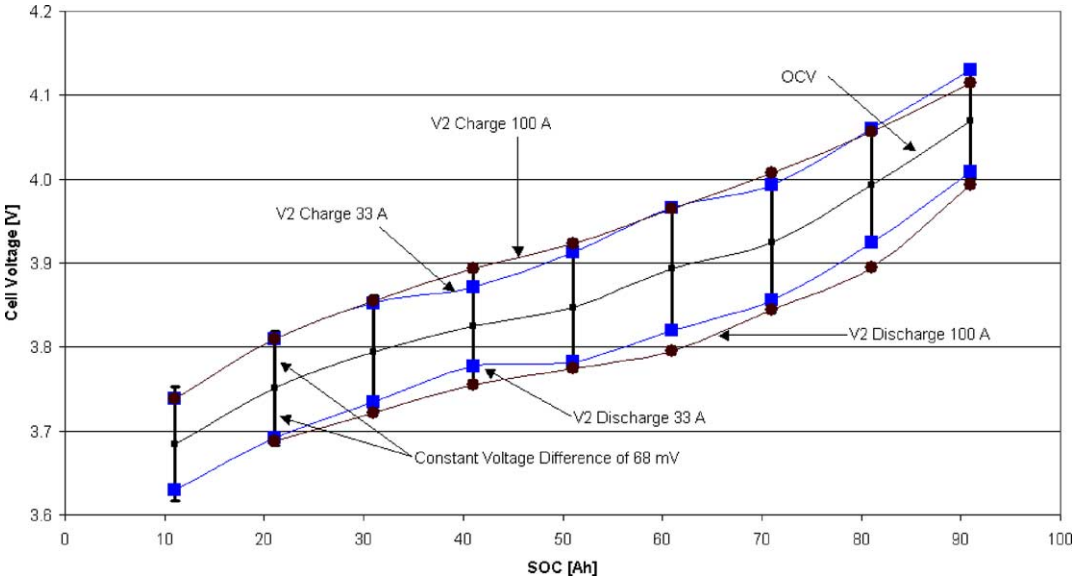

Fig. 10. V_2 during charge and discharge at 33 and at 100 A and OCV over SOC.

7. Discussion and conclusions

A non-linear dynamic equivalent electrical circuit model for a high-energy lithium-ion battery has been presented. The dynamic behaviour is modelled using two *RC* combinations and the non-linearity is modelled using a zener-diode. The value of the zener-diode is constant between 10 and 90% SOC, it is independent of the temperature and ageing did not show an effect to it so far (1 year and 16 cycles). The deviation of the results is acceptable. One *RC* combination represents a very long time-constant in the order of several hours. This is related to the constant-voltage drop of the zener-diode. The second *RC* combination represents another time-constant in the order of minutes. The voltage drop related to this time-constant is proportional to the current and is modelled with the resistor R_{12}. This resistor is almost constant between 10 and 90% SOC and similar between charging and discharging. It is independent on the temperature, but the deviation of the results is quite high. This suggests that the model or the test require improvements. On the other hand R_{12} values are small if compared with voltage drops due to R_{01} and the zener-diode. This means that the deviation has a small impact on the overall model. The immediate voltage drop has been modelled with the resistor R_{01}. R_{01} is not constant over the SOC range, nor is it constant with the current. It is likely that it is temperature dependent as well. R_{01} and the dependencies require further testing and analysis. Fortunately R_{01} can be measured using fast methods like impedance spectroscopy [1]. On the other hand, the actual model will require look-up tables or multi-dimensional functions or graphs to determine R_{01} as a function of current, temperature and age. This is not ideal and the model may require improvement in order to get simpler dependencies. The self-discharge rate is modelled with R_p, which has not been determined yet. The OCV is represented as a function of the SOC. It appears to be independent on the age of the battery.

A rapid test-method has been presented. It helps determining the parameters of the model except the self-discharge rate R_p in less than 19 h per cell. The OCV can be determined with reasonable accuracy between 20 and 100% SOC without waiting for equilibrium. Waiting times of less than 1 min are sufficient if the average between charging and discharging is taken. The OCV at levels below 20% SOC cannot be determined using this method. The proposed test-method reduces the time for testing from almost 20 days to less than 19 h per cell. Further investigations are required to determine the dynamic behaviour not only after stopping the current but also when applying a current. The resistor R_{long} needs to be determined by additional tests, because it is of interest for small currents and equalisation requirements. The capacitors do not need to be determined. The time-constants are sufficient for most applications. It is sufficient to know whether they are in the order of seconds, minutes, hours or days and this can extracted from the proposed test-method.

Future work will focus on validating the proposed battery model by applying different test-methods such as impedance spectroscopy and by comparing different analysis such as Nyquist plots and Lissajous plots. The model will then be assessed by comparing simulation results with in-vehicle testing, before it can be implemented for in-vehicle life-time assessment that aims to reveal parameter dependencies on age, cycles and temperature. Once the model is valid and applicable, the test-procedures can be optimised.

Acknowledgements

The authors would like to thank Institute for Power Electronics and Electrical Machines (ISEA, Aachen, Germany) for using their battery tester, also S. Buller and O. Bohlen from ISEA for help with the testers and Professor Alan Ward and Professor Honor Ward for proof-reading.

References

[1] P. Baudry, M. Neri, M. Gueguen, G. Lonchampt, J. Power Sources 54 (1995) 393–396.
[2] D. Doerffel, S. Abu-Sharkh, in: Proceedings of 19th Electric Vehicle Symposium, 2002, EVAAP (Electric Vehicle Association of Asia Pacific).
[3] Thermo_Analytics_Inc. (available from: http://www.thermoanalytics.com) accessed on 1 June 2003.
[4] L. Gao, IEEE Trans. Components Packag. Technol. 25 (2002) 495–505.
[5] Y.-S. Lee, J. Wang, T.-Y. Kuo, in: Proceedings of 19th Electric Vehicle Symposium, 2002, EVAAP (Electric Vehicle Association of Asia Pacific).
[6] C.G. Motloch, G. Hunt, J.R. Belt, C.K. Ashton, G.H. Cole, T.J. Miller, C. Coates, H.S. Tataria, G.E. Lucas, T.Q. Duong, J.A. Barnes, R.A. Sutula, in: Proceedings of 19th Electric Vehicle Symposium, 2002, EVAAP (Electric Vehicle Association of Asia Pacific).
[7] S.W. Moore, J. Schneider, in: Proceedings of SAE Technical Paper Series, 2001, http://www.SAE.org (Society of Automotive Engineers).

B3:

"Performance of Lithium Polymer Cells at High Hydrostatic Pressure",
14^{th} UUST
(Unmanned Underwater Systems Technology) Conference, 2005

[65]

Conference paper

PERFORMANCE OF LITHIUM-POLYMER CELLS AT HIGH HYDROSTATIC PRESSURE

K. Rutherford[*a], D. Doerffel[a]

[a]*School of Engineering Sciences, University of Southampton, Highfield, Southampton, SO17 1BJ, UK*

Abstract

Lithium polymer cells are an attractive energy source for underwater vehicles due to their high specific energy and possible operation at hydrostatic pressure. Their behaviour at pressures experienced in the deep ocean is of particular concern to designers. This paper presents test results that show how the voltage during discharge is affected by temperatures between 4°C and 28°C, and pressures of 0.1 MPa and 60 MPa. A simple non-linear equivalent circuit to model the internal resistance of the cell is shown and the effect of temperature on resistance is found. The main conclusions are that lithium polymer cells can operate at 60 MPa, and their performance is similar to that at 0.1 Mpa. Underwater cold temperature and high current reduce the performance of the cell more than high pressure.

Keywords: Lithium polymer batteries, AUV, high pressure, equivalent circuit.

* Corresponding author. Tel: +44 (0)2380-596004 Fax: +44 (0)2380-596149; E-mail address: K.Rutherford@soton.ac.uk

Nomenclature

C_{12}	Double layer capacitance	F
C_{long}	Diffusion capacitance	F
I_C	Charge current	A
I_D	Discharge current	A
Q_0	Rated capacity of a cell at full charge	Ah
R_{01}	Total ohmic resistance	Ω
R_{12}	Charge transfer resistance on discharge	Ω
R_{Long}	Diffusion resistance	Ω
R_P	Self discharge resistance	Ω
S_B	Battery specific energy	Wh kg^{-1}
SOC	State of charge	%
S_S	System specific energy	Wh kg^{-1}
V_0	Voltage at beginning of pause in discharge	V
V_1	Voltage at the end of instantaneous voltage rise	V
V_2	Voltage after 900 seconds of pause.	V

1. Introduction

The motivation for this study was to investigate a potential power source for use within battery-powered autonomous underwater vehicles (AUVs), in particular AUVs that dive deep, to over 5000 m. The Southampton Oceanography Centre's Autosub AUV has operated with batteries assembled from manganese alkaline 'D' size primary cells since 1998, completing over 300 missions for marine science [1]. In the current design, the batteries, made up from up to 5000 cells, are housed in four carbon fibre reinforced plastic tubes, rated to an operating depth of 1600 m [2]. The longest mission to date has been 253 km, limited by the energy that was available [3]. As reliability of the vehicles' systems has improved over the last six years the mission endurance becomes limited by the energy available on board rather than by system failures. AUVs are subject to the limitations of terrestrial electric vehicles, but have additional constraints, such as the need to design for near neutral buoyancy, while providing sufficient energy for missions. Autosub requires over 150 MJ for a 250 Km mission, with typically 500 W in propulsion and 500 W in control system and sensors. In turn, choice of power source affects the mass, shape, performance, and cost of operation of the vehicle.

To date, most AUVs use batteries as their power source. These batteries are usually enclosed within pressure vessels, providing dry space at one atmosphere pressure. However, Stevenson and Graham [4] show that the mass to displacement ratio of pressure vessels increases with diving depth. There is an increasing mass penalty in providing space at one atmosphere for the energy system as a whole (batteries and pressure vessel) for deep diving vehicles.

As a consequence, especially for deep diving vehicles, the option to remove the need for the pressure vessels by operating the batteries at ambient pressure would prove highly advantageous [5]. The batteries would displace their own volume of water, reducing the mass of buoyancy required to float the battery system.

However, not all cell chemistries or forms of construction are amenable to operation at ambient pressures of up to 60 MPa (6000 m water depth). Pressure compensated lead-acid cells are in routine use within instruments and vehicles used in the deep sea, for example the valve-regulated Seabattery [6]. However, their specific energy is low (e.g. 21 Wh kg^{-1} for the 12V 48Ah Seabattery). One candidate cell chemistry with a high specific energy and a form of construction expected to be tolerant to pressure is the lithium-polymer cell (e.g.194 Wh Kg^{-1} for the Kokam SLPB526495 [7]).

As yet, there appears to be no open-literature papers on the performance of lithium-polymer cells at high pressure.

This paper reports the results of experiments to evaluate the electrical and mechanical performance of one type of lithium-polymer pouch cells (Kokam SLPB526495 cells rated at 3.27 Ah [7]) under hydrostatic pressure, with a view towards their use in a new deep-diving AUV Autosub-6000.

Cells were first tested at atmospheric pressure and at ambient temperature. This established typical cell capacity and discharge performance, and provided the parameters of a simple equivalent circuit model used previously for lithium-ion cells by AbuSharkh and Doerffel [8]. Furthermore this data provided a reference to compare the performance and characteristics of cells tested at high pressure (60 MPa) or at low temperature (4˚C), typical of the deep ocean. Due to practical constraints it was not possible to alter the temperature of the pressure vessel, preventing the determination of cell performance at the combination of low temperature and high pressure.

2. Methods.

2.1 Test procedures

The experiments under pressure were made within a water-filled cylindrical pressure vessel. The cell was placed within deformable bags filled with oil to ensure electrical insulation and isobaric pressure. The cell was tested with a Digatron universal battery tester as described by Doerffel and Abu Sharkh [8]. The temperature was measured with a thermistor attached to the cell terminal. The same cell was used for the atmospheric pressure tests at 18°C and the tests at 60MPa. A separate cell had to be wired up to test the differing temperature effects.

For reasons of safety, the initial survival test pressurised one cell only to 60 MPa for 1 hour. On depressurisation, the cell was inspected for signs of damage and its terminal and on load voltages checked. These tests showed that this type of lithium-polymer cells would be able to survive the test procedure physically and electrically. Further tests where conducted where batches of 50 cells were pressurised for a total of 12 cycles and then tested electrically, zero failures gave additional confidence that the cells would be suitable for use in pressure compensated batteries.

The electrical test cycle consisted of a full charge with a current of 1 A, until the terminal voltage reached 4.2 V. Charging then continued at this voltage until the current fell below 0.327 A. At this point the cell was considered to be fully charged (100%) SOC. During charging, pauses for 15 minutes were inserted after each 0.327 Ah of charge, representing 10% SOC increase.

During discharge the current was held at a constant value. The cell was considered to be discharged when the on-load voltage reached 3V, above the absolute minimum of 2.5 V as recommended by manufacturer [7]. During discharge pauses of 15 minutes at 0.327Ah intervals meant the peaks in the voltage recovery would align, easing the calculation of OCV using the procedure suggested in [8]. The cell was allowed to rest for 2 hours after a discharge, or at least 4 hours after a charge, to allow the cell to reach close to equilibrium state

One cell, chosen as reference, underwent electrical cycles at 26°C and atmospheric pressure to establish baseline charge discharge characteristics and capacity (section 3.1). Further tests varied the temperature of the air surrounding the cell and the current drawn during discharge at

atmospheric pressure (section 3.1) and at 60 MPa (section 3.2)

A simple method was used to calculate state of charge (SOC), which assumes each cell was fully charged before the start of each test, and that subsequent cycles charged to the same point. Q_o is assumed to be the nominal cell capacity of 3.27 Ah.

$$SOC(t) = 100\frac{Q_o - \int_0^t I_D(t)dt}{Q_o} \quad (1)$$

2.2 Derivation of the equivalent circuit parameters

As well as determining any effect of hydrostatic pressure on capacity, experiments sought to identify any changes in the internal resistance of the cell. The equivalent circuit of the cell is modelled as a simple linear passive network (Fig. 1) based on a Randles configuration. As this representation does not account for complex nonlinearities, the circuit parameters are functions of temperature, current, state of charge and perhaps pressure.

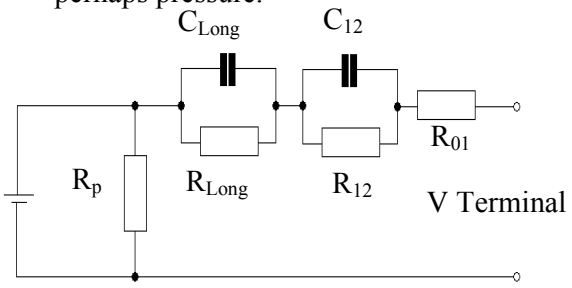

Fig. 1. Equivalent circuit model for the lithium-polymer cells during discharge.

With the exception of R_p, circuit parameters were estimated from discharge test measurements. R_{01} was obtained from: $R_{01} = |V_1\text{-}V_o|/I$ (Fig 2.). This is an instantaneous measurement, and although the equipment was set to a high sampling rate it is likely that the value of V_1 includes the beginning of the kinetic overpotential. The first second of discharge is assumed to be the instantaneous voltage drop though it is likely that, after 100ms or so, the kinetic over potential and double layer capacitance have an effect. The kinetic overpotential is affected by temperature and in turn affects the voltage (Tafel equation). The time constant is small so this should have limited effect over these scales.. In the equivalent circuit of Fig. 1, the voltage rise from V_1 to V_2 (Fig 2.) is described by a double exponential:

$$V(t) = V_1 + iR_{12}(1 - e^{-\frac{t}{R_{12}C_{12}}}) + iR_{Long}(1 - e^{-\frac{t}{R_{Long}C_{Long}}}) \quad (2)$$

These values were estimated from the data using a least squares procedure in Maple (version 9) to minimise the difference between V(t) as modelled using equation 2 and the actual data. R_{12} and C_{12} were determined from the first 300 s of the voltage rise after each pause (Fig. 2). The least squares procedure took these values and then estimated R_{long} and C_{long}. R_{12} and C_{12} found from the 15 minute pauses at the end of each 10% discharge (typically 87 mΩ and 11494 F) were significantly less than those estimated from the 2 hour pause at the end of the discharge cycle (e.g. 130 mΩ and 16026 F at 4˚C and one atmosphere). Causes for this are discussed in section 3.1. Alternative battery model options are available as given by [10], though this requires many parameters that cannot be found from the limited information available from these tests. Non-linear elements have been considered, and initial tests are encouraging. These have not been utilised here as they require high resolution tests of recovery voltage as a function of time, which has not been possible with the Digatron machine as its sampling rate is limited.

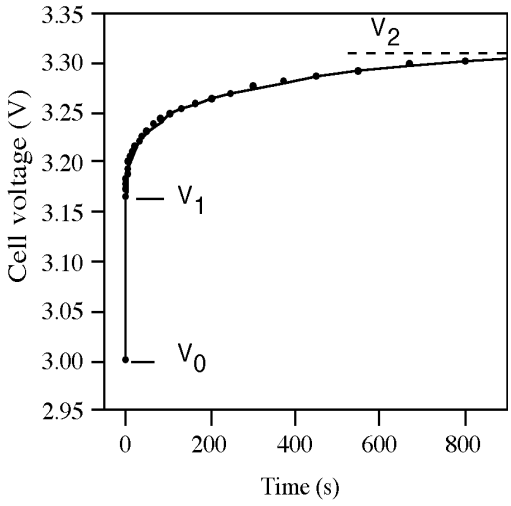

Fig. 2. Voltage-time graph of the reference cell with load of 1 A removed at T=0 showing the voltage points used to estimate the equivalent circuit parameters.

3. Analysis of Results

3.1 Electrical performance at atmospheric pressure

The cell voltage against SOC for a discharge and charge current of 1 A is shown in Fig. 3. with 15 minute pauses at intervals of $Q_0/10$. If the cell voltage reached equilibrium within each pause, then the off load voltage during discharge would be equal to the off load voltage during charge. That is not the case in these tests, for example Fig. 4 shows an enlargement graph of the data from Fig. 3. around the pause at 60% SOC.

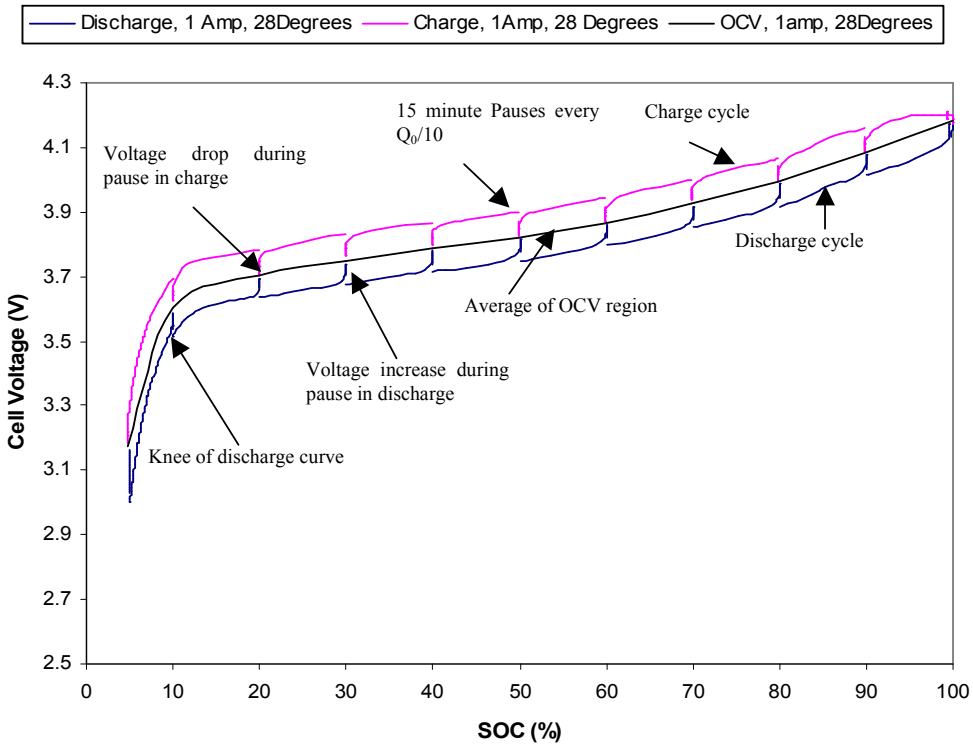

Fig. 3. Cell Voltage with state of charge during charge and discharge at 1A at a mean temperature of 28 °C at one atmosphere.

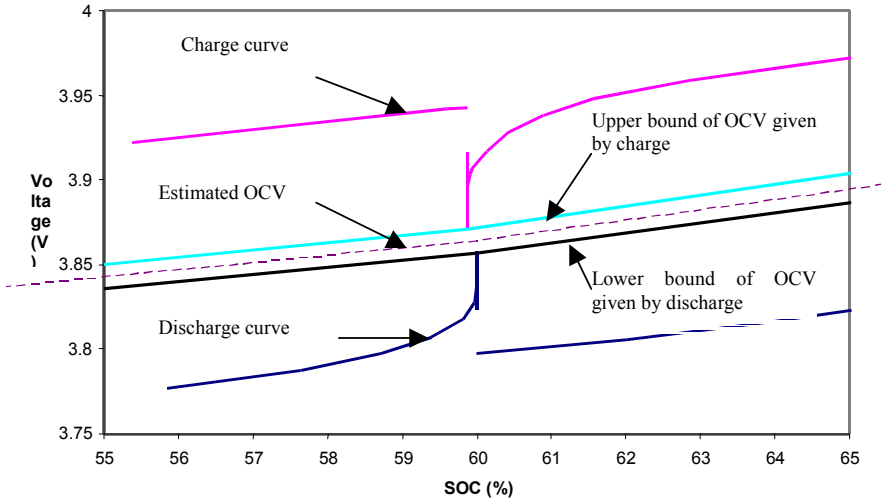

Fig. 4. Cell Voltage at 60% SOC, 1 A and mean temperature of 28 ° C showing upper and lower limits of OCV.

The gap between the cell voltages at the end of discharge and charge pauses was 14 mV. The equilibrium OCV would lie in this region. By taking the mean of the upper and lower bounds shown in Fig. 4 an estimate of the cell OCV against SOC can be made as suggested in [8], which presented experimental evidence to support this approach.

At low SOC levels, there are likely to be some electrochemical affects within the cell that will cause the OCV to be underestimated. During discharge concentration gradients of lithium ions can form at the anode or cathode, which the subsequent charging process then has to reverse. At low SOC these gradients have accumulated over the whole discharge, and so the time to offset them is increased. The end of discharge of a lithium-ion cell is determined by either reaction partners being locally depleted and/or reaction products being locally saturated, which – according to the Nernst equation - leads to a sharp decrease in the equilibrium potential of the cell. This is observed as a knee in the discharge curve and means that small changes in concentration can exhibit large changes in the cell voltage. This amplifies the effect of accumulated concentration gradients at the end of discharge. Hence, the above method for determining the OCV is likely to produce underestimated OCV at low SOC. This effect also occurs at the end of charging but it is not significant here, because the charging current tapers down at the end of charge, which would reduce the concentration gradients.

Fig. 5 shows the discharge curves for tests done at 1 A at three temperatures. All battery types experience a drop in performance with decreasing temperature [11], and this also is the case with lithium polymer cells. A discharge at 1 A still provided at least 90% of cell nominal capacity at 28°C through to 4°C. Discharge at 3.27 A provided 90% nominal capacity at 22°C yet only 65% at 4°C. A discharge at 6.5 A and 23°C still produced 85% nominal capacity, yet only 17% at 3°C.

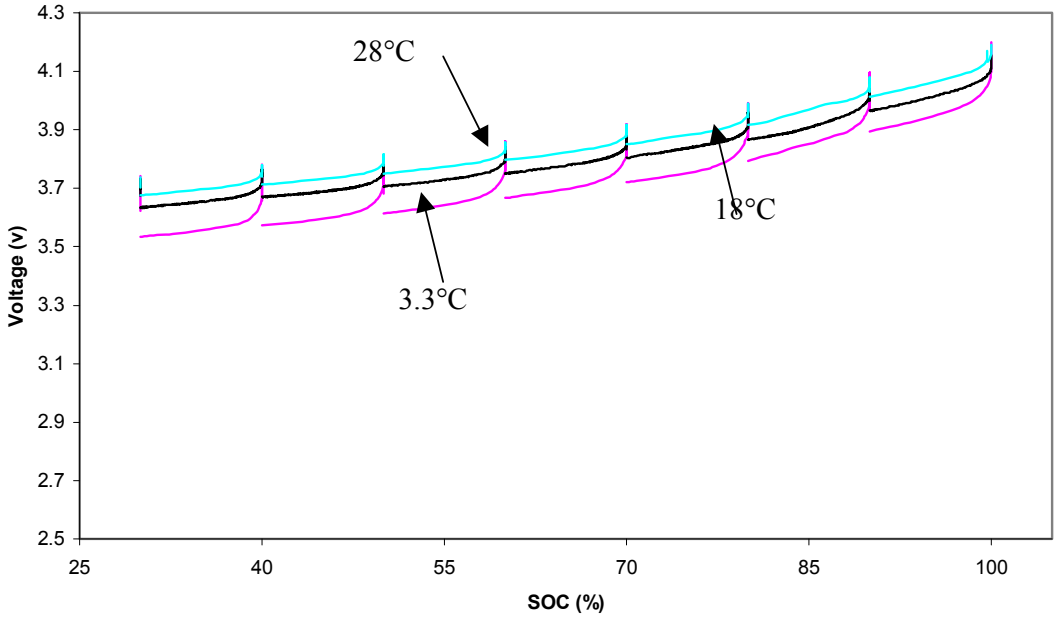

Fig. 5. Discharge curves for 1 Amp, at 28, 18, and 3.3 °C compared to SOC

After a pause the voltage rises to almost the same point at all temperatures (Fig. 5), though the estimated OCV is not quite the same. The Nernst equation in [11] shows that the equilibrium voltage is affected by a temperature coefficient, though this does not seem to be significant as the cell recovered, given 900 seconds, to the same voltage irrespective of temperature.

The drop from V_2 to the on-load voltage at the beginning of each discharge period in Fig. 7 is much larger than observed for the same current load in Fig. 6, implying an increase in R_{01} at the lower temperature. The increase of ohmic resistance (immediate voltage drop) is due to the decrease of ionic conductivity in the polymer electrolyte [12]. The increasing gradient of the discharge curve with increasing current draw is evidence of higher internal resistance R_{12} and will be explored in section 3.3. At 60% SOC, the total voltage drop at 3.27 A and 22°C is 249 mV, while at 4˚C and 3.27 A the voltage drop increases to 783mV.

The exact capacity removed from the cell is influenced by the 'knee' of the discharge curve (Fig. 3.). The cell capacity is almost fully exhausted after this knee is reached during discharge. The voltage drops quickly and only little capacity can be discharged before the cut-off voltage is reached as shown in the low current discharge in Fig 7. Fig 7 also shows that this knee is not yet reached when discharging at high currents and at a low temperature (4°C). The reason for smaller capacities obtained in these tests is not that the cell capacity is exhausted (depletion of reactants or saturation of reaction products), but that simply the cut-off voltage is reached prematurely due to high voltage drops, probably as a result of poor ionic conductivity of the polymer electrolyte.

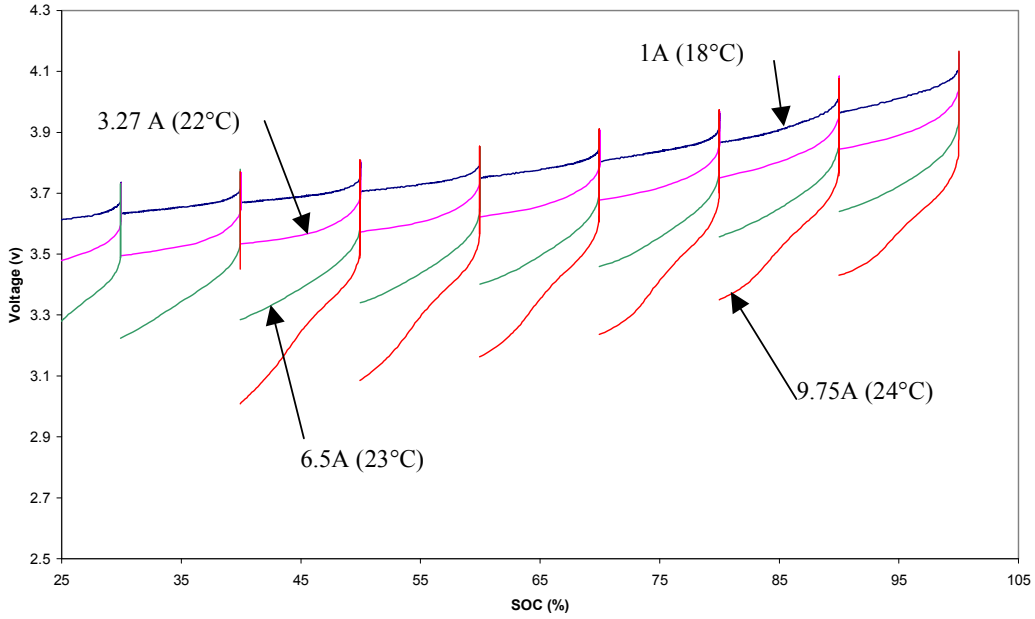

Fig. 6. Cell voltage with SOC at 1, 3.27, 6.5 and 9.75 Amp discharge between 18 and 24° C and at one atmosphere pressure.

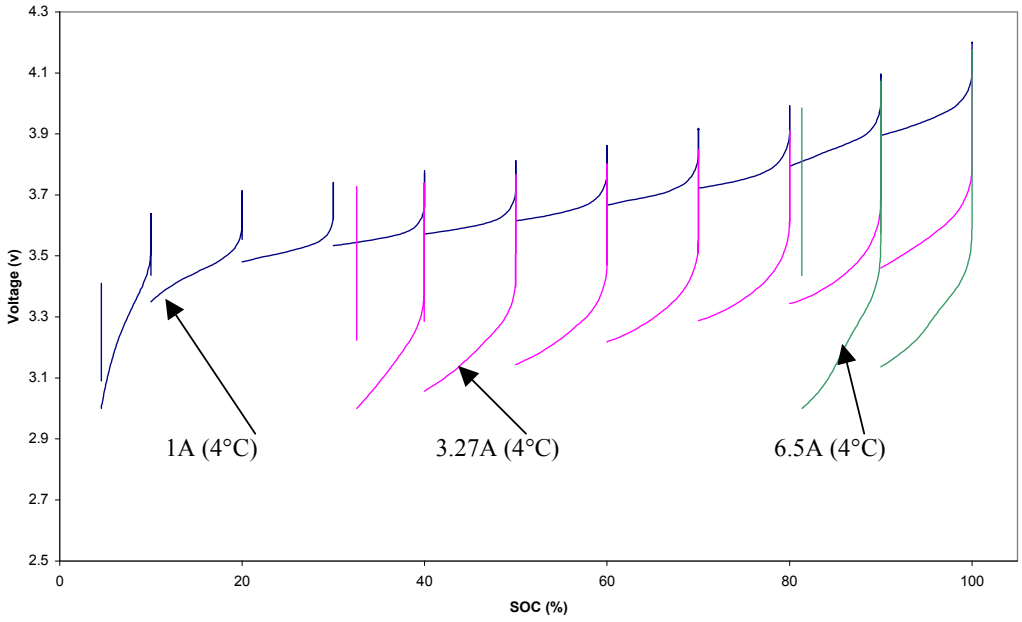

Fig. 7. Cell voltage with SOC during discharge at 1, 3.27 and 6.5 Amps, at 4° C and atmosphere pressure

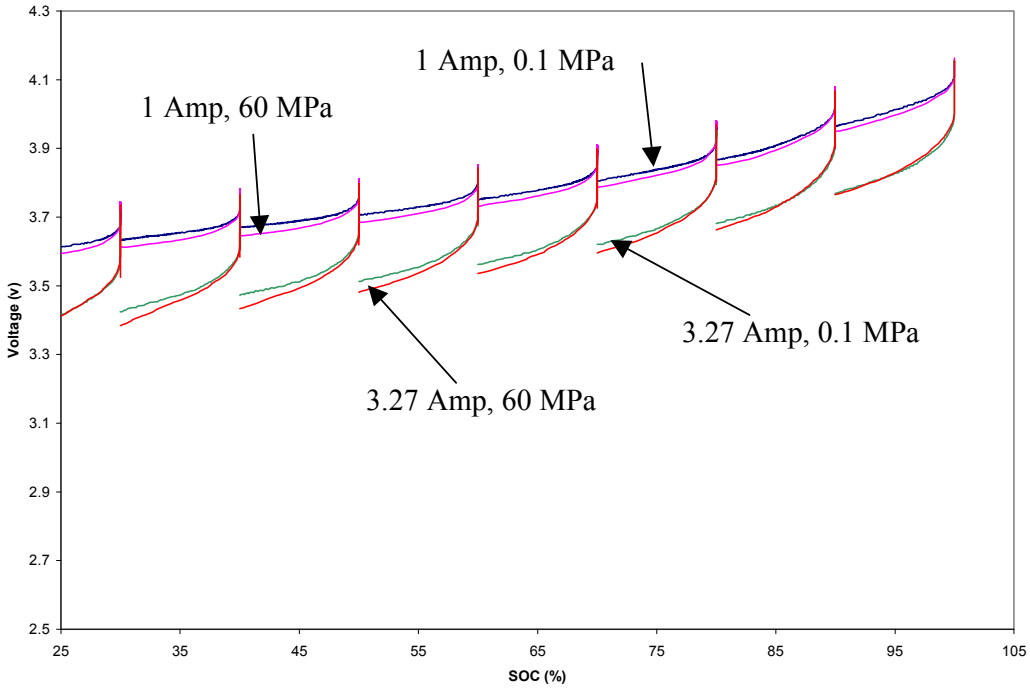

Fig. 8. Cell voltage with SOC during discharge at 1 and 3.27 A, 1 and 60 MPa at 18°C

3.2 Electrical performance at high pressure

Fig. 8 shows the voltage during discharge of tests at 1 and 3.27 A load, and at pressures of 0.1 and 60 MPa. The voltage at the end of each pause, V_2 is the same for each load at 0.1 MPa and at 60 MPa, however the discharge curve has a larger gradient when at pressure, evidence of a higher R_{12}, this will be explored in section 3.3.

Comparisons of capacity drawn from cells under 60 MPa pressure and those in atmospheric conditions have been made. At 1 A load, the capacity of the cell is 90%, slightly lower than at 60 Mpa, 91%, however an error of $\pm$ 1% is not unlikely. At 3.27 A the 60 MPa capacity is 92%, 6% higher than at 0.1 MPa, 86%, which is unlikely to be an error. This would suggest that the electrochemistry of the cell is more efficient at high pressure, though as the internal resistances are greater, this is improbable. Higher efficiency of a cell at 60 MPa would have to be repeated many times to gain confidence of this.

3.3 Equivalent circuit parameters and verification

Fig. 9 shows the estimated equivalent circuit parameters R_{01}, R_{12} and C_{12} as a function of SOC at mean temperatures of 28˚C and 4 ˚C at 0.1 MPa and at 60 MPa when discharged at 1 A. The estimated error in the calculation of the resistances is 1 mΩ and 50 F for the capacitance. The ohmic resistance R_{01} changes in both magnitude and behaviour as a function of SOC and temperature. At 28˚C R_{01} varied little with SOC, increasing from 25-26

mΩ at 100% - 30% SOC to 27-31 mΩ at 20% SOC and below. In contrast, the minimum R_{01} at 4˚C was 89 mΩ, with a rise to 164 mΩ as the cell approached 5% SOC. This ohmic voltage rise should not vary with temperature, but as discussed above in section 2.3, it is likely that this value includes a fraction of the charge transfer resistance, and so is more noticeable at 4°C.. At 60 MPa (Temperature 18˚C) the minimum R_{01} of 49 mΩ was at 90% SOC, with a rise to 71 mΩ as cell approached 5% SOC. These values are 5 – 11 mΩ larger than those found for the cell at atmospheric pressure at the same temperature.

The charge transfer resistance R_{12} behaved differently. The estimates at 0.1 MPa and 60 MPa showed higher resistances at 90% and 5% SOC than at intermediate points. At 28˚C and 0.1 MPa, R_{12} was greater than R_{01} while at 4˚C R_{12} was less than R_{01} except at 90% SOC. Also at 18˚C 60 MPa R_{12} exceeded R_{01} at 90% SOC, although not at 10% SOC and lower. Again the estimates of R_{12} at 60 MPa exceeded those at 1 bar, this time by 7-12 mΩ (except at 20% SOC where the difference of 1 mΩ is within the expected error).

Estimates of the double layer capacitance C_{12} showed lower values at the lower temperature, and highest near 50% SOC. Here tests at 18°C and 28°C have approximately the same values of C_{12}, though at pressure C_{12} could have a lower value, but still have the same curve shape.

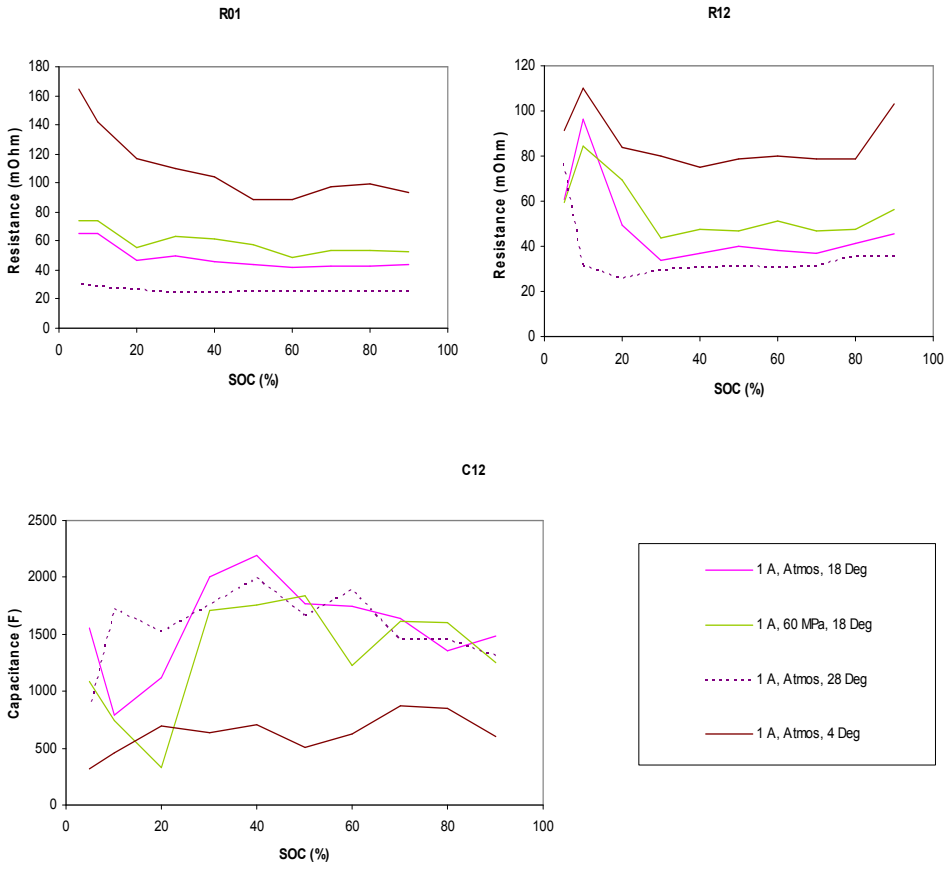

Fig. 9 Estimated Equivalent Circuit parameters R_{01} , R_{12} and C_{12} for cycles at 1 Amp and varying temperature and pressure.

The first minute of the recovery period will include the double layer capacitance, included in the Tafel equation and represented by C12, and though this value is useful for the simulating, it is not an accurate representation of the electrochemistry. The increases in resistance with pressure may also be explained by error in separating ohmic resistance and overpotentials. For the deep ocean application the cells would be far more affected by the reduction of temperature from the ocean surface to 6000 m than for the increase in pressure from 0.1 to 60 MPa. There is a small increase of resistance at pressure, but were the current draw to be kept small, the cell would still produce more than 90% of its rated capacity.

5. Conclusions

Lithium solid-polymer cells have been shown to survive repeated pressurisation to 60 MPa with no external physical failure, electrical failure, or significant degradation to on and off load voltage when returned to 0.1 MPa. This assumes isobaric conditions when these cells are housed in oil-filled pouches. As a consequence the cells have been found suitable for pressure-balanced operation within deep-diving underwater vehicles.

Cell charge capacity has been estimated as a function of temperature and current load at atmospheric pressure, and then compared to capacity at 60 MPa. There was no statistical difference in capacity at 18˚C and 1 A load (C/3) between tests at atmospheric pressure and at 60 MPa. However, at 3.27 A (1C) the capacity at 60 MPa was ~5% above that at atmospheric pressure. This increase may be the result of testing methods used, higher sampling rate tests will be needed to investigate this with more electrochemical analysis.

Analysis of charge and discharge voltage data enabled the parameters of a simple equivalent circuit model to be estimated as a function of temperature, state of charge and pressure. Temperature had a greater effect than pressure on the values of the equivalent circuit parameters. On average, the values of R_{01} and R_{12} at 60 MPa were higher, by 5-11 mΩ at atmospheric pressure at the same temperature, while cooling the cells from 18˚C to 4˚C increased R_{01} by ~60 mΩ and R_{12} by ~40 mΩ.

The equivalent circuit parameters described in this paper, will enable a model of the cell to be created, in order to then produce a fuel gauge algorithm. This algorithm would be able to predict capacity and terminal voltage based on current load, temperature and pressure. By incorporating the capacitive as well as resistive elements of the equivalent circuit within the fuel gauge algorithm the full effect could be predicted of high power pulsed loads, such as sonar transmitters or variation in AUV thrust. Improved realism in the on-board fuel gauge and battery simulator would contribute towards better utilisation and reliability of an autonomous underwater vehicle. Further work could be directed towards assessing and modelling degradation of lithium-polymer cells that have been subject to pressure cycles.

6. Acknowledgements.

The Authors would like to thank Andrew Staszkiewicz for his patience and operation of the pressure vessel.

7. References.

[1] N.W. Millard and 26 others, Multidisciplinary ocean science applications of an AUV: The Autosub science missions programme. In: Griffiths, G. (Ed.), The technology and applications of autonomous underwater vehicles. Taylor and Francis, London, 2003, pp. 139-159.

[2] P. Stevenson, G. Griffiths, A.T. Webb, The experience and limitations of using manganese alkaline primary cells in a large operational AUV. Proc. AUV 2002: A workshop on AUV energy systems, IEEE, Piscataway, 2002, pp. 27-34.

[3] G. Griffiths, G., A. Knap, T. Dickey, The Autonomous Vehicle Validation Experiment, Sea Technology, 41(2) (2000) 35-43.

[4] P. Stevenson, D. Graham, Advanced materials and their influence on the structural design of AUVs, In: Griffiths, G. (Ed.), The technology and applications of autonomous underwater vehicles, Taylor and Francis, 2003, pp. 77-92.

[5] G Griffiths, J Jamieson, S Mitchell, K Rutherford, Energy storage for long endurance AUVs. Proc. ATUV conference, IMarEST, London, 16-17 March 2004. pp. 8-16.

[6] http://www.deepsea.com/seabatry.html#summary accessed on 29 September 2004.

[7] http://www.kokam.com/product/battery_main.html accessed on 20th July 2004.

[8] S. Abu-Sharkh, D. Doerffel, Rapid test and non-linear model characterisation of solid-state lithium-ion batteries. J. Power Sources, 130 (2004) 266-274.

[9] H.Jan Bergveld, W.S.Kruijt, P.H.L.Notten, Battery Management Systems: Design by modelling, Kluwer Academic Publishers, Dordrecht, 2002.

[10] D.Lyndon, T.B.Reddy (Eds)., Handbook of Batteries, third ed., McGraw-Hill, New York, 2002, pp. 22.18

[11] G.M.Ehrlich, in: D.Lyndon, T.B.Reddy (Eds)., Handbook of Batteries, third ed., McGraw-Hill, New York, 2002, pp. 35.26

[12] http://vtb.engr.sc.edu/ last accessed on 25/02/05

[13] J. J. Hong, Lithium secondary cell and method of fabricating the same, .US Patent No. US6,423,449, 2002.

B4:

"Efficient Testing and Evaluation Methods for Faster Market Introduction of Large Lithium-Ion Batteries"

AABC 2005 in Honolulu, Hawaii

[25]

Conference paper

Efficient Testing and Evaluation Methods for Faster Market Introduction of Large Lithium-Ion Batteries

Dennis Doerffel[1], Suleiman Abu Sharkh[2]

1 REAPsystems Ltd., 61A Ivy Road, Southampton SO17 2JP, UK +442380556516, info@reapsystems.co.uk
2 School of Engineering Sciences, University of Southampton, Highfield, Southampton SO17 1BJ, UK +442380593397, Suleiman@soton.ac.uk

Abstract

The paper proposes a rapid cost effective test procedure for characterising large lithium-ion batteries. This procedure involves a series of full charge and full discharge tests with short pauses during these charge and discharge cycles. Such tests are shown to be useful in determining the open circuit voltage and circuit parameters of the battery, as well as battery degradation. However, it is shown that a sophisticated design of experiment is required for these tests to be meaningful. This usually involves gaining information using carefully planned preliminary tests. The reader is taken through an example of such a process. The above tests provide a preliminary picture of the characteristics of a battery, which can be improved further based on in-situ measurements of battery parameters in niche applications.

Introduction

Li-Ion batteries are the key energy storage technology for hybrid- and electric vehicles. Several characteristics seem to make them the ideal choice, such as: high cell voltage, high energy density, high specific energy, good efficiency, low self-discharge, maintenance free, no banned materials and no memory effect [1]. Some cell designs even achieve outstanding power density and specific power [2]. Major disadvantages currently are: requirement for a battery management system with individual cell monitoring, some safety concerns, high initial battery cost, poorer recyclability compared to lead-acid, no long-term experience with larger cells and the associated risk with implementing and using less mature technology.

Testing, understanding their behaviour and gaining experience are required for a wider market introduction of large lithium-ion batteries. One needs to quantify the trade-offs between initial cost, calendar life, cycle life, available energy and performance characteristics, most of which depend on temperature and usage patterns. This is not an easy task, which becomes even more important and more difficult due to the rapid development of new cell designs and chemistry flavours. Additionally, testing packs of large lithium-ion cells is a somewhat different task if compared with testing small single cells. The cost for testing large cells increases dramatically due to several reasons: higher cost of cells, higher power demand for testing, higher safety requirements, more space required and possibly some weight issues. Test results with smaller cells cannot necessarily be scaled up to larger cells [3] for example due to different temperature gradients inside the cell. Additionally, a battery consisting of several tens or hundreds of cells behaves quite differently if compared with a single cell.

This paper presents an alternative faster and more cost-effective approach to the task

of testing and evaluating. Specially designed laboratory experiments investigate the typical behaviour and then determine performance characteristics at different temperatures and currents, measure degradation and evaluate the test methods at the same time. The resources required for these tests are modest. Statistically meaningful results for a larger number of cells are obtained through field experiments, which can be performed in niche markets.

We will also address several issues, which we found to be important for gaining meaningful results. These issues and our proposed procedures for coping with these issues are specific to the tested specimen. However, the methods are presented in a generic way, so that this paper can be used as a template for testing other batteries.

Test Materials and Methods

The laboratory tests were carried out on a Digatron universal battery tester (UBT). A PC was connected through an RS-485 interface. The errors of the tester are shown in table 1.

Current	± 0.5 % but not better than ± 25 mA
Voltage	± 5 mV
Temperature	± 0.1 K

Table 1: Measurement Errors of the Battery Tester

The tested specimens were high-energy lithium-ion cells with capacities of either 50 Ah or 100 Ah per cell. The tests were carried out in a temperature-controlled cabinet with temperatures between -15°C and 45°C. The cells were surrounded by air and hence, the cell temperature was not kept constant; it naturally heated up and cooled down during tests.

Temperature plays an important role for the performance, aging and safety of lithium-ion cells [4]. Ideally, the temperature would be measured inside the cell, but measurements inside sealed cells from a series production are usually not viable. However, it is essential to estimate the temperature inside the cell as accurately as possible. The current collectors are much more thermally conductive than the active material, electrolyte and – in our case – the PP case. Hence measuring at the terminal provides the best approximation to internal temperature.

The temperature was logged during tests together with current and cell voltage. The data logger was set up for taking measurements every 2 mV in change of cell voltage or alternatively every change of 0.5 A in current (during charging only) – whichever occurred first. With this setting rather than logging at fixed time intervals, the number of data can be kept small when no changes occur and high sampling rates are achieved when rapid changes take place. This setting ensures reliable measurements in constant current phases as well as in constant voltage phases.

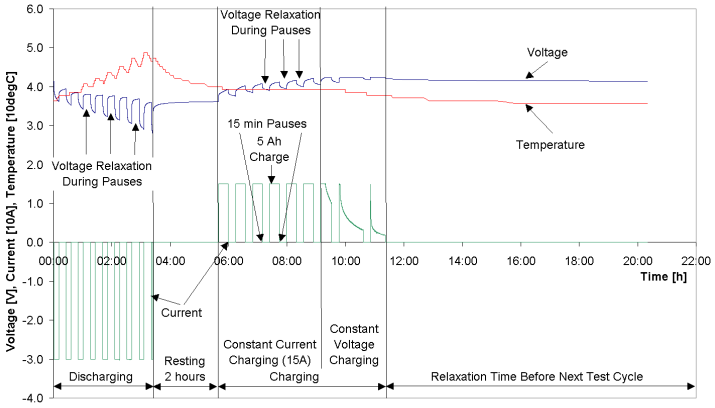

Figure 1: Typical Test Cycle

Figure 1 shows voltage, current and temperature during a typical test cycle. The cycle started with discharging, followed by a resting period of 2 hours, followed by charging. The cell was then left to rest in order to reach equilibrium before the next cycle. During discharging and charging, the current was paused for 15 minutes after every 5 Ah (about 10% for the 50 Ah cell) change of SOC in order to measure the OCV and analyse the step response behaviour. The step response behaviour can be used for determining equivalent circuit model parameters [5]. For smaller cells, one would usually use impedance spectroscopy, but for large or very large cells, it is more economical to use the step response technique.

Preliminary Test Cycles

Most battery chemistries and designs require some initial cycles, before reaching stable behaviour. These cycles were performed using the typical test cycle shown in figure 1 in order to "get a feel" for the performance and behaviour of the tested cell type. In the following paragraphs, we will highlight some important features of the behaviour of our particular test specimen. Other cell designs will show different features, but we would like to emphasize, that these preliminary test cycles could be very important for designing the main series of tests and for obtaining meaningful results.

End of Charge Determination

Our typical test cycle started with discharging and finished with charging, so that the next test cycle could always start with a fully charged cell after a resting period. The charging procedure used in these preliminary test cycles was a CC-CV charging. Following the manufacturers recommendations, the constant charging voltage was 4.2 V (temperature independent) and the cell should have been fully charged when the current reached 0.01C (temperature independent). However, the preliminary tests indicated clearly that this charging regime would not charge the cells equally full. The SOC after charging with the above charging regime significantly depended on temperature.

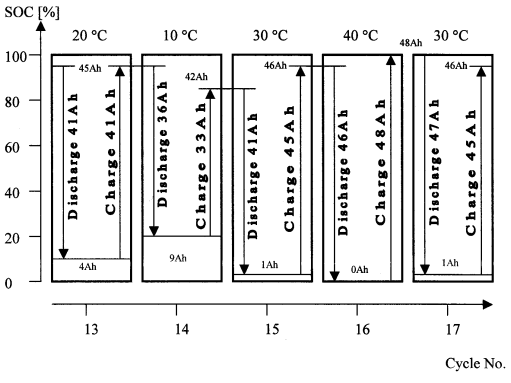

Figure 2: SOC, charged and discharged capacities in preliminary test cycles

Figure 2 shows the charged and discharged capacities in some preliminary test cycles. It can be seen, how those relate to the state of charge at the end of discharge and at the end of charge. The state of the cell at the end of each cycle depended on the temperature during that cycle. The state of the cell at the start of the following cycle depended on the preceding cycle. This is unacceptable for a comprehensive series of test cycles, because one cannot rely on Ah counting alone for determining the state of charge throughout a series of tests. Ah drift may occur and a reference condition is required for setting the Ah counting to a defined value. Ideally every test would be independent from its predecessor and successor.

Additional tests were performed in order to find an end of charge determination method, so that the above requirement of independent cycles and reference conditions could be met: The first test determined the end of charge voltage as a function of temperature. Subsequently, the end of charge current was determined as a function of temperature.

End of Charge Voltage (EOCV)

The temperature dependency of the EOCV has been neglected by the simple end of charge determination as suggested by the manufacturer. Our approach is to determine the temperature dependency of the OCV after a full charge and use the same slope for the EOCV. The cell was fully charged and left to rest in order to reach equilibrium. We found that it was very important, to let the cell reach true equilibrium first, before performing this test. In our case we waited several weeks between charging and performing the test. The OCV and the cell temperature were logged during the test while slowly increasing the temperature in a temperature control cabinet.

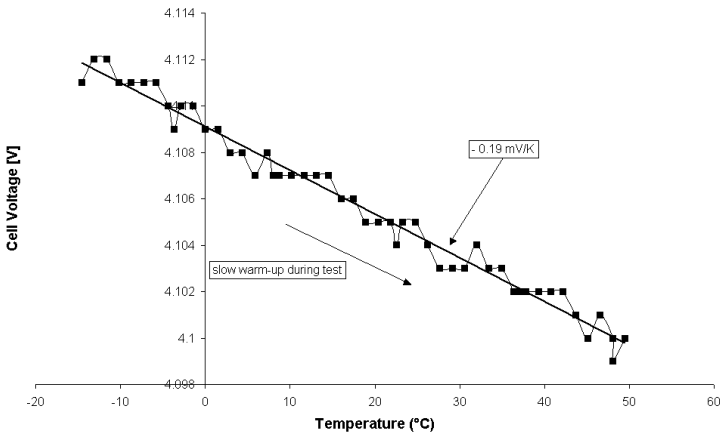

Figure 3: OCV of a fully charged cell as a function of temperature after a waiting time of several weeks

Figure 3 shows the results of this test. The temperature dependency of the tested specimen is linear with a slope of – 0.19 mV/K. This is a total of 11.4 mV over the whole range of temperatures during the main tests. Considering the error of the voltage measurement as stated in table 1, this is a very small voltage change. Most battery management systems would face problems implementing this dependency in a sensible way.

End of Charge Current (EOCC)

The temperature dependency as found above was implemented for the EOCV in the main series of tests. It was still uncertain, whether this alone would assure an equal state of charge at the end of charge regardless the temperature. The EOCC needs to be determined as a function of temperature as well. The following paragraphs will suggest and evaluate a method for determining this dependency as part of the main series of tests itself. This reduces the time and cost involved with an additional dedicated test.

Test cycles as shown in figure 1 were performed at different temperatures and different currents. The experiments at several conditions were repeated in order to detect and quantify the effects of degradation during testing. The most typical condition was chosen as the reference condition (25 °C and 15 A).

The end of charge at this reference condition was determined by the EOCV and a suitable EOCC (0.01C in this case). Lithium-Ion cells do not have any significant capacity consuming side reactions, so that one can expect to recharge always the same amount of capacity as has been discharged before. Hence, Coulomb counting was used to determine the end of charge at all conditions other than the reference condition – with some exceptions as will be explained later. The current at the end of charge using this method is the EOCC at that particular temperature. The result is shown in figure 4.

Figure 4 shows no EOCC values at temperatures below 15 °C. This is because the recharging times went up unacceptably for these temperatures using this method. More than 24 hours would have been required in order to recharge the discharged capacity at 5°C. Instead, a different method is suggested here: The charging was interrupted after acceptable charging times. The cell was than heated up to the reference temperature before charging was continued using the reference end of charge detection method (EOCV-EOCC) rather than Coulomb counting.

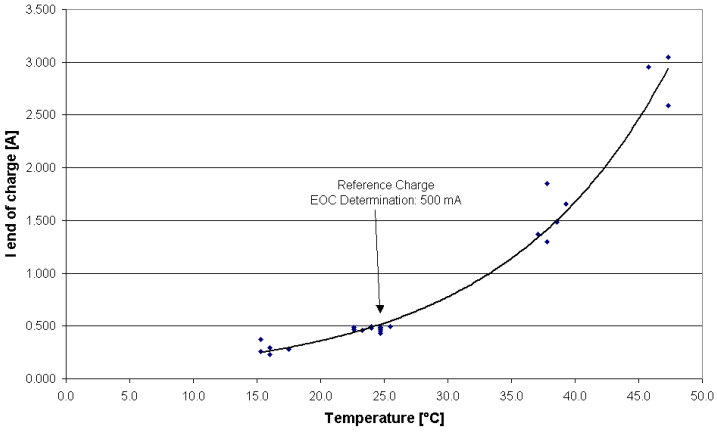

Figure 4: EOCC as a function of temperature for reaching an equal SOC at the end of charge

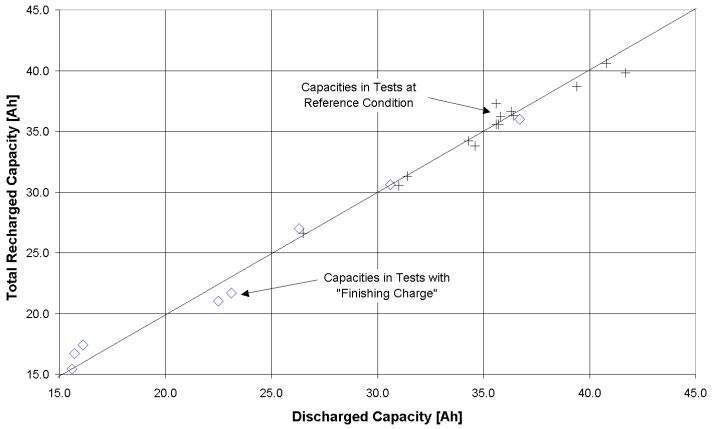

Figure 5: Evaluation of the EOCC determination method by comparing discharged and recharged capacities.

Side reactions and offset errors or errors due to resolution in the current measurement can cause a drift in the Coulomb counting method, especially when applied throughout a long series of tests. Test cycles at reference conditions are repeated frequently between the tests at other conditions in order to prevent drift.

However, Coulomb counting was used as well for the tests at reference condition and for the charging at lower temperatures (also ending at reference conditions), so that the suggested method could be evaluated. Figure 5 shows the comparison of discharged and recharged capacities for all the tests where the end of charged is determined by EOCC rather than coulomb counting. The correlation between charged and recharged capacities is an indicator for the validity of the suggested method.

Determination of OCV as a function of SOC

The aim of finding an appropriate end of charge determination method is to achieve independence between test cycles and to be able to measure cell performance parameters at well-defined and comparable states of charge. The method suggested above is viable but requires a high level of attention. The OCV is an indicator for the state of charge for some cell chemistries and designs and hence we have evaluated its value for our test specimen. Our preliminary tests have indicated that the tested specimen requires extremely long relaxation times for reaching true equilibrium. We will show later that even relaxation times of 96 hours are not sufficient for reaching true equilibrium. This means that a conventional test for determining the OCV as a function of SOC would take several weeks. The following paragraphs investigate a quick method for determining the OCV as a function of SOC.

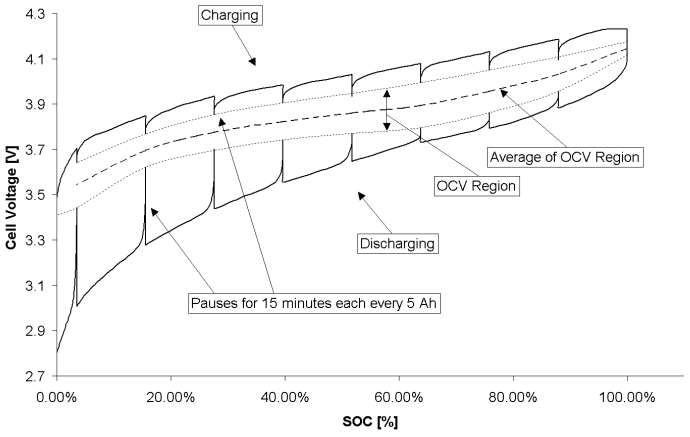

Figure 6: Voltage during a typical test cycle, plotted against the state of charge measured in % of total available capacity.

Figure 6 shows the voltage during a

typical test cycle when plotted over the SOC in percent. The top curve represents charging and the bottom curve represents discharging. The voltage at the end of the relaxation pauses during charging are connected with a dotted line and this apparent equilibrium curve is significantly higher than the apparent equilibrium curve obtained during discharging (bottom dotted line).

Let us assume, that the true equilibrium voltage would be somewhere between these dotted lines, or – in particular – would be equal to the average voltage of these two values. In order to prove or reject this hypothesis we compared the result from this method with the result obtained with a conventional method with long waiting times.

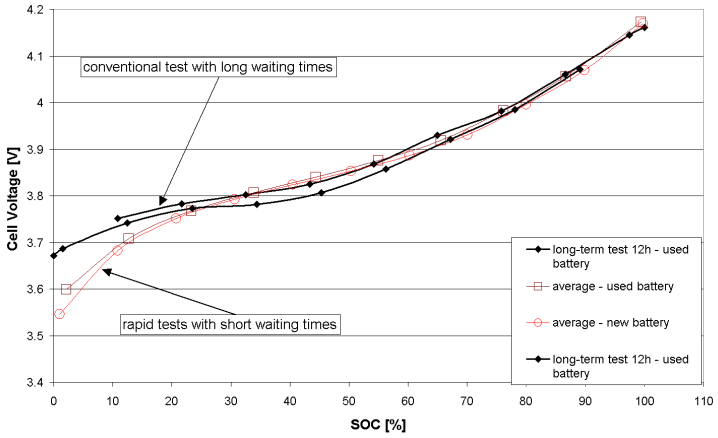

Figure 7: OCV as a function of SOC obtained from different test methods

Figure 7 shows the OCV as a function of SOC obtained from the two different tests. Additionally, the result from the conventional test with long waiting times is shown for an aged cell. This helps evaluating, whether the OCV(SOC) dependency varies significantly with aging. It can be seen, that the rapid test method provides acceptable results apart from the low state of charge region of 20% or less remaining capacity. Though the capacity degraded significantly during the tests, the dependency of OCV(SOC) does not vary significantly between the new and the aged cell.

Charge / Discharge Hysteresis

Figures 7 reveals that the apparent equilibrium voltage during charge is higher than the apparent equilibrium voltage during discharge despite the long waiting times in the conventional test for determining the OCV(SOC) relationship. This suggests that there might be a hysteresis even in the true equilibrium voltage as has been found for NiMH cells [6] and also suggested for some lithium-ion cells [7]. It is important to investigate, whether there is any hysteresis and also to quantify it, because any significant hysteresis would make the determination of SOC from the OCV very difficult, especially if the OCV(SOC) curve is very flat.

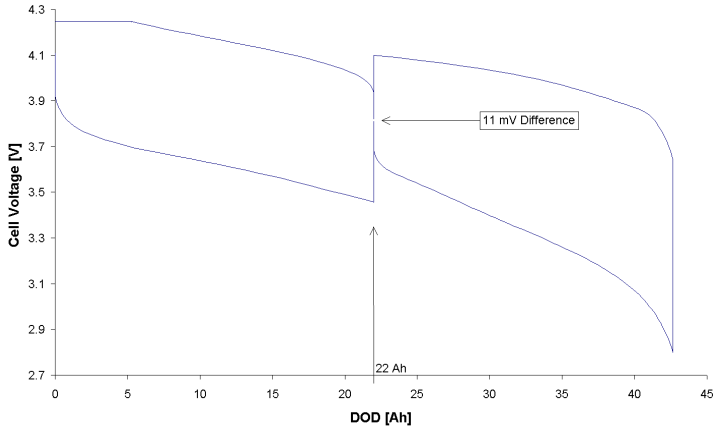

Figure 8: Hysteresis test at 35 ºC with 48 hours waiting time

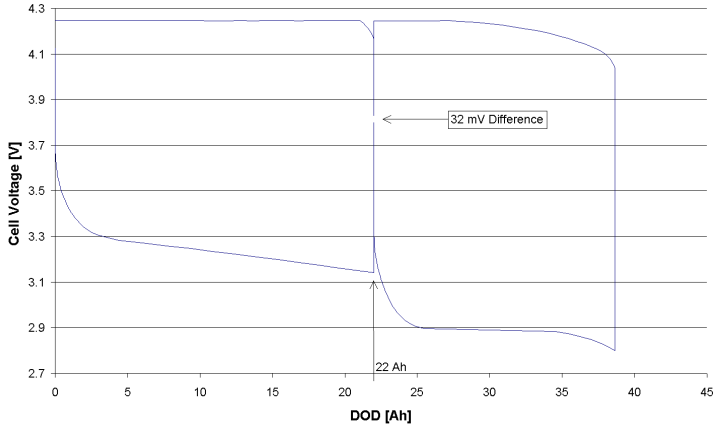

Figure 9: Hysteresis test at 5 ºC with 96 hours waiting time

The following test was performed in order to investigate and measure the hysteresis: A fully charged cell was discharged to about 50% of its capacity and left to rest for 48 hours. 50% of the capacity was chosen, because the preliminary tests revealed, that the OCV(SOC) is most flat around this state and any hysteresis would have the most significant impact on the SOC determination. After the rest, the discharge was continued until the cell reached its end of discharge voltage. Then the cell was recharged to the same state of charge where the waiting time was applied during the discharge and left to rest for 48 hours again. Finally, the cell was fully recharged. The result is shown in figure 8. Despite the waiting time of 48 hours, there is still a significant OCV difference of 11 mV between charging and discharging. This difference equates to an uncertainty of about 3% in SOC. However, the speed of relaxation depends significantly on temperature. The test above was performed at 35 ºC. The result of the same test performed at 5 ºC and with a waiting time of 96 hours is shown in figure 9. The difference between charging and discharging is 32 mV. This is almost 3 times larger than at the higher temperature despite the fact, that the waiting time was twice as long. The difference of 32 mV equates to about 9% difference in SOC.

Figure 8 reveals a significant performance increase after the waiting times. The voltage during discharge after the waiting time is significantly higher than before the waiting time – even though the state of charge is lower. This behaviour can be explained with the relaxation of concentration gradients. However, the behaviour at the lower temperature as shown in figure 9 reveals the opposite characteristic: The performance during discharge after the waiting time is significantly poorer than before the waiting time. This can be explained with temperature changes: The cell heats up during discharge and performs better. It cools down in the long waiting time of 96 hours and performs worse.

Optimal waiting times between test cycles

Figures 8 and 9 have revealed that the waiting time can significantly affect the performance of a cell. It is important that the preceding test cycle in a series of test cycles does not influence the behaviour of the following test cycle. Hence, the waiting time should be as long as possible in order to approach true equilibrium as close as possible. However, the tests above have revealed that this can take several days and such long waiting times are unacceptable for efficient testing. We suggest performing several typical test cycles with different waiting times between each other in order to determine suitable waiting time ranges.

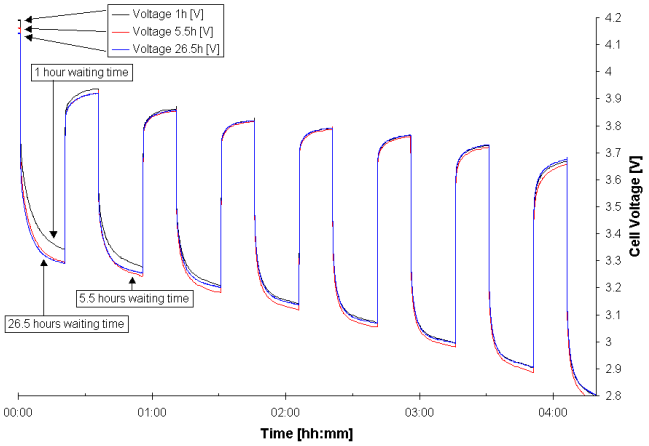

Figure 10: Voltage during typical test but with different waiting times between the tests

Figure 10 shows the result of such a waiting time test. Three typical test cycles were performed with three different waiting times between each other: 1 hour, 5.5 hours and 26.5 hours. A significant performance difference can be seen when waiting only one hour if compared with waiting for 5.5 hours. This difference is significant for the first 20% of discharge capacity. However, the difference when waiting for 26.5 hours if compared with waiting for 5.5 hours is insignificant. As a result of this test, we were using waiting times between 5.5 hours and 26.5 hours in our test series for this specific test specimen.

Cell Degradation During Testing

The type of cell that was used for testing showed degradation during preliminary tests [5]. Four different measures were built into the design of experiment in order to cope with degradation during the tests:

1. The test conditions were chosen randomly in order to minimise systematic errors.
2. One test condition was chosen as a reference. It was performed from time to time, so that the degradation can be quantified and eliminated during later analysis.
3. The test conditions at the beginning of the series of tests were repeated at the end, so that the degradation elimination method can be verified.
4. Most batteries show a high performance variation during the first cycles. The tested cell was cycled several times before starting the actual series of tests in order to minimise this problem.

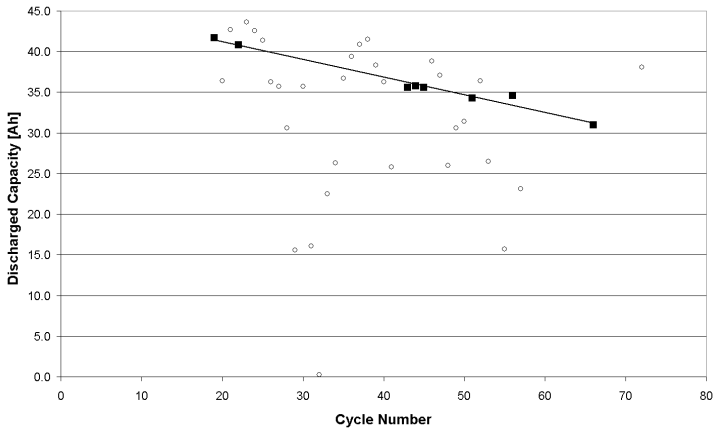

Figure 11: Discharged capacities during the series of test cycles, showing the degradation in capacity (black: reference test cycles, white: other test cycles).

Figure 11 shows the discharged capacities in the test cycles under different test conditions. The reference test conditions are highlighted, they allow us to quantify the degradation by drawing a linear regression line as shown in figure 11. Any qualitative or quantitative statement would be difficult without these reference cycles.

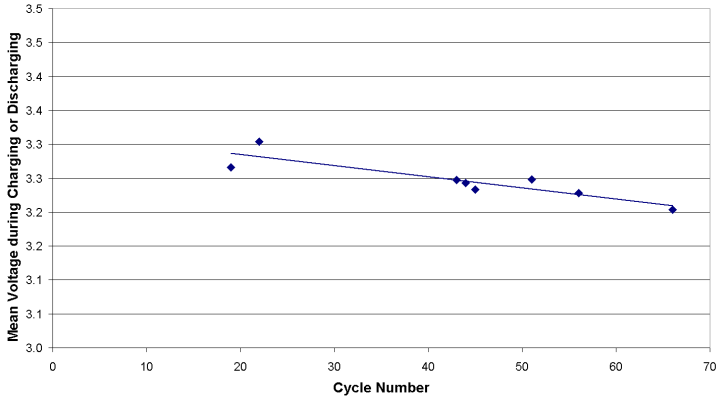

Figure 12: Mean voltage during discharging for all reference test cycles.

Cell degradation can also become visible in terms of performance decrease rather than capacity decrease. Figure 12 shows the decrease of the mean voltage during discharging for all reference test cycles. The mean voltage during discharge is a good indicator for overall changes in the performance characteristics of a cell.

Field Testing and Evaluation Methods

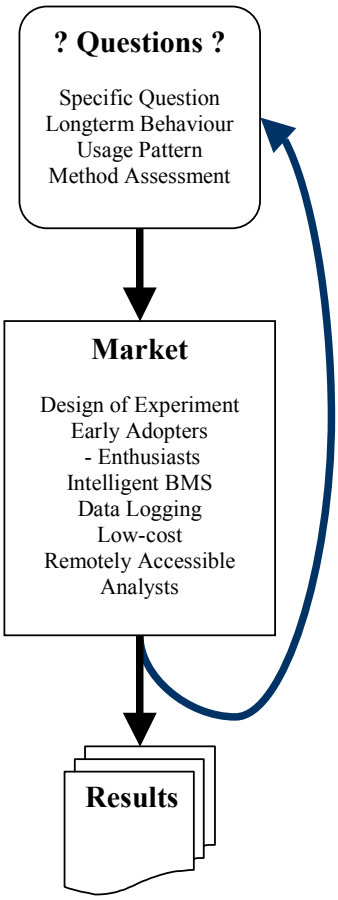

Figure 13: Field Testing and Evaluation Process

The tests above were performed using one or two cells. This helps understanding the performance behaviour of this particular cell only and the degradation behaviour is tested for one specific usage pattern only. Several cells in a battery string however will show variations in performance and the degradation depends on the usage pattern.

Investigating these issues with conventional laboratory tests would be very time consuming and field testing with a small fleet would provide only very little variation in usage patterns. Both methods are expensive. Figure 13 suggests how these issues can be investigated much more cost and time effective: Experiments are designed into intelligent BMS with data logging facilities and the product is launched in niche markets using early adopters or enthusiasts.

This approach requires a low-cost BMS with data logging facility and remote access and scientific analysts are required for designing the experiment and producing meaningful results from the logged data. In many cases, the results will lead to further questions, which can be fed into a similar process. The product evolves as it diffuses into larger markets.

This process may also be used for answering specific questions, such as whether the above end of charge determination method is viable throughout the life of the battery. It can be used for assessing certain methods, such as SOC determination methods or cell balancing methods and it can be used for gathering usage patterns.

Discussion & Conclusions

This paper has shown several battery characteristics that are not necessarily expected before testing:

The end of charge is strongly temperature dependent and neglecting this fact causes large errors in SOC during testing (up to 20%). Additional careful tests are required for determining a consistent end of charge during testing.

Relaxation takes very long for the tested cell. Additional tests are required for optimising the waiting time between test-cycles.

The pauses in the proposed test cycle let the cell cool down and relax. Relaxation can increase performance in some cases and cooling down can decrease the performance in other circumstances. It is important to design the tests (type of cooling, length and frequencies of relaxation times) as close as possible to the potential usage pattern in the application.

This emphasizes the importance of performing some preliminary tests and carefully

examining their results before designing the series of test cycles. The paper has shown, that our proposed typical test cycle is viable, provided that a reference test cycle is performed from time to time: OCV(SOC) curves, EOCC reference points, performance characteristics and model parameters can be obtained and their changes with degradation can be monitored with a minimum of resources.

The paper has shown, that the OCV(SOC) curve can be obtained from the proposed test cycles. This curve is essential for determining the model parameters during the test. However, the OCV is of limited use for determining the state of charge during testing, because it is difficult to determine due to the long relaxation times. Coulomb counting is used instead and reference cycles prevent SOC drift and help detecting degradation.

The performance of lithium-ion cells can vary significantly with the usage pattern. Not only the discharge history and the state of health but also the future usage pattern are important when trying to estimate the remaining energy. Our proposed field-testing method can help learning about usage patterns in different applications. The proposed field-testing method is also useful for investigating long-term behaviour, analysing cell differences, assessing different methods (SOC determination, equalisation, etc.) or for investigating specific questions such as whether the obtained EOCC is suitable throughout the life of a battery.

References

[1] D. Linden and T. B. Reddy, Handbook of Batteries, 3rd ed: McGraw-Hill, 2002.

[2] GAIA, "45 Ah HP-602050 Lithium Ion Cell," vol. 2005: GAIA Advanced Lithium Battery Systems, 2004.

[3] R. Spotnitz, "Scale-Up of Lithium-Ion Cells and Batteries," in Advances in Li-Ion Batteries, W. A. van Schalkwijk and B. Scrosati, Eds. New York: Kluwer Academic / Plenum Publishers, 2002, pp. 433 - 457.

[4] M. Salomon, H.-p. Lin, E. J. Plichta, and M. Hendrickson, "Temperature Effects on Li-Ion Cell Performance," in Advances in Li-Ion Batteries, W. A. van Schalkwijk and B. Scrosati, Eds. New York: Kluwer Academic / Plenum Publishers, 2002, pp. 309 - 344.

[5] S. Abu-Sharkh and D. Doerffel, "Rapid test and non-linear model characterisation of solid-state lithium-ion batteries," Journal of Power Sources, vol. 130, pp. 266-274, 2004.

[6] C. G. Motloch, G. Hunt, J. R. Belt, C. K. Ashton, G. H. Cole, T. J. Miller, C. Coates, H. S. Tataria, G. E. Lucas, T. Q. Duong, J. A. Barnes, and R. A. Sutula, "Implications of NiMH Hysteresis on HEV Battery Testing and Performance," presented at 19th Electric Vehicle Symposium, Busan, Korea, 2002.

[7] H. J. Bergveld, W. S. Kruijt, and P. H. L. Notten, Battery Management Systems - Design by Modelling, vol. 1. Eindhoven: Kluwer Academic Publishers, 2002.

Abbreviations and Terminology

BMS = Battery management
SOC = state of charge
DOD = depth of discharge
OCV = open circuit voltage
EOCV = end of charge voltage
EOCC = end of charge current
CC-CV charging = constant current charging followed by constant voltage charging at the EOCV after reaching the EOCV
Current: aa.bbC (e.g. 0.01C): way of expressing a current relative to the nominal capacity C of an energy storage cell. I = aa.bb x C / h

B5:

"A critical review of using the Peukert equation for determining the remaining capacity of lead-acid and lithium-ion batteries"

Journal of Power Sources 2006

[26]

Journal paper

Available online at www.sciencedirect.com
SCIENCE DIRECT
Journal of Power Sources 155 (2006) 395–400
JOURNAL OF POWER SOURCES
www.elsevier.com/locate/jpowsour

Short communication

A critical review of using the Peukert equation for determining the remaining capacity of lead-acid and lithium-ion batteries

Dennis Doerffel *, Suleiman Abu Sharkh [1]

School of Engineering Sciences, University of Southampton, Highfield, Southampton SO17 1BJ, UK

Received 6 October 2004; received in revised form 22 April 2005; accepted 26 April 2005
Available online 23 June 2005

Abstract

In many applications it is essential to predict the remaining capacity of a battery reliably, accurately and simply. Several existing techniques for predicting the remaining capacity of a lead-acid battery discharged with a variable current are based on variants of Peukert's empirical equation, which relates the available capacity to a constant discharge current. This paper presents a critical review of these techniques in the light of experimental tests that were carried out on two lead-acid commercial batteries. The relevance of these Peukert's equation based techniques to lithium-ion batteries is also discussed in the light of tests carried on a lithium-ion power battery. The basic conclusion of the paper is that Peukert's equation cannot be used to predict the state of charge of a battery accurately unless it is discharged at a constant current and constant temperature.

Keywords: Battery testing; State-of-charge; Modelling; Lead-acid battery; Lithium-ion battery

1. Introduction

Prediction of state-of-charge (SOC) of a battery is vital in many applications. Many scientists and engineers [1–8] base their methods for SOC prediction on Peukert's equation [9], which relates the available capacity of a lead-acid battery to discharge rate, for a constant current discharge. As the discharge current in most applications is variable, several methods were proposed [1–8,11] to adapt Peukert's equation to a variable current discharge. However, upon closer examination, these techniques can be shown (see later sections) to produce different and sometimes confusing results regarding the state of charge of a battery.

This paper presents a review of Peukert's findings based on the original paper that was published in 1897 [9] in the light of tests carried out on two commercial lead-acid batteries. The alternative techniques proposed in the literature for using variants of Peukert's empirical equation to predict the state of charge of a lead-acid battery discharged with a variable current are then critically reviewed. The paper also discusses the relevance of Peukert's findings and those techniques to lithium-ion batteries in the light of tests on a commercial lithium-ion battery.

2. A review of Peukert's findings

Peukert performed constant current discharge tests on several different lead-acid batteries from different manufacturers. He found that a simple equation was sufficient to put capacity and discharge rate into relation for all lead-acid batteries [9]:

$$I^{\mathrm{pc}}t = \text{constant} \quad (1)$$

where I is the discharge current, t the maximum discharge time and pc is the "Peukert coefficient" (usually between 1 and 2) unique to a battery of a certain make and model.

* Corresponding author. Tel.: +44 2380 59 2896.
E-mail addresses: d.a.doerffel@soton.ac.uk (D. Doerffel), s.m.abu-sharkh@soton.ac.uk (S.A. Sharkh).
[1] Tel.: +44 2380 59 3397; fax: +44 2380 59 3053.

0378-7753/$ – see front matter © 2005 Elsevier B.V. All rights reserved.
doi:10.1016/j.jpowsour.2005.04.030

A Peukert-coefficient of pc = 1, for example, means that the accessible total capacity of that battery does not depend on the discharge rate, which is not true for real lead-acid batteries which usually have a pc > 1. This simple equation enables the calculation of the available discharge time for a given battery with a certain Peukert coefficient discharged with a constant current load.

Most battery manufacturers specify the capacity of their batteries for a certain discharge time of n (h), for example, $C_n = 100$ Ah [10]. This means that the battery will deliver 100 Ah if discharged at such a rate that the discharge time is n hours. Using this example, if $n = 20$ (h), the rate would be $I_{20} = 5$ A. The Peukert equation can be used for calculating the available capacity C_{n1} at a different discharge rate I_{n1} using the following equation which is derived in Appendix A:

$$C_{n1} = C_n \left(\frac{I_n}{I_{n1}} \right)^{\mathrm{pc}-1} \quad (2)$$

The total discharge time will be $n1$ h. Peukert found that pc was about 1.47 on average for available lead-acid batteries at that time. Modern batteries have better coefficients. This means that the available capacity at a constant discharge current becomes less if the discharge rate increases. The loss of capacity at a high discharge rate was explained by Peukert to be due to "a poorer utilisation of the electrode surface". However, based on latest research [14–16], the loss of capacity at a high discharge rate can be explained to be due to a decrease of the number of active centres in the positive active material and a rapid increase in the resistance of the interface between the grid and the lead dioxide active material.

Peukert's equation should be interpreted with care. It should not be understood to mean that when a battery is discharged fully at a certain high current discharge rate that it is completely empty. In fact it is well-known that a seemingly empty battery discharged at a high current will still have some available capacity at a lower discharge current [10], [12]. In fact [10] suggests that if a battery was discharged at successively decreasing rates, the total Ah capacity obtained from a battery will be the same as that obtained from using a constant low current discharge. However, this paper presents results that suggest that there is a net loss of available capacity when a battery is discharged at a high rate, followed by successive low discharge rates compared to a battery discharged at a low current rate from the start.

3. Experiments

Battery discharge tests at specified rates as described in the following sections are carried out on three specimens which are an aged 12 V 65 Ah sealed lead-acid battery (battery BLA1), a new sealed lead-acid with 17.2 Ah (battery BLA2) and an aged 50 Ah lithium-ion cell (battery Blion). All tests are carried out at room temperature using a commercial battery tester. Before a test the cells are fully charged as recommended by the manufacturers.

3.1. Lead-acid battery tests

In the first set of tests, a typical test consisted of two test sections. In the first section, the test specimen is fully discharged at a high rate I_{high}. After a waiting time, t_{wait} it is further discharged with a small current I_{low}. After fully recharging, in the second test section, the same cell is discharged with the low rate I_{low} from the beginning. The waiting time t_{wait} after the first high-rate discharging is 6 h, so that the total discharge time in the second test section is similar to the discharge time in the first test section. The aim is to minimise the impact of mass-transportation limitations [11] and to give time for the hydration of active centres in the positive electrode—see, [16]. This whole test is repeated four times with identical charging algorithms and identical waiting times between charging and discharging and between the tests and between the test sections. The charged and discharged Ahs are counted separately throughout all tests.

Fig. 1 shows the battery voltage versus depth of discharge (DOD) for the BLA1 lead-acid battery. Two out of four tests are shown for clarity; the other tests produce almost identical results. The two upper-right curves represent two cycles of the second test section: the discharges at a small current of 5 A from the beginning. The discharge ends at point C with 67.6 Ah discharged in total. The voltages relax to 11.58 V in point F after 1 h. Both curves are almost identical. This demonstrates the good repeatability of the test.

The two lower curves represent two cycles of the first test section: the discharges start with a high current of 50 A until the cut-off voltage of 10.0 V is reached at point A. A discharge of 44.2 Ah occurs up to this point. Within the resting period of 6 h, the voltage relaxes to 12.13 V (point D). Following this stage is the next continuous discharge at a lower rate of 5 A until the battery reaches the cut-off voltage again at point B, having now discharged a total of 64.3 Ah. The voltages relax up to 11.71 V at point E in the subsequent pause of 1 h. Again, both curves are almost identical, demonstrating good repeatability.

The BLA2 sealed lead-acid battery is tested in the same way in order to find out whether the behaviour is unique to a certain battery design or whether it may be general to the lead-acid chemistry. Fig. 2 shows the test results with the BLA2 sealed lead-acid battery. The test undertaken is generally the same as the tests with the BLA1 battery. However, the battery is discharged to different cut-off voltages, depending on the discharge current and following the recommendations of the manufacturer. Additionally, four different discharge rates are tested instead of only two, and the highest discharge rate is 40 times higher than the lowest, instead of being only 10 times higher.

Figs. 1 and 2 confirm the well-known fact [10] that a battery fully discharged at a high current rate can be discharged further at a lower current rate. However, they also reveal that

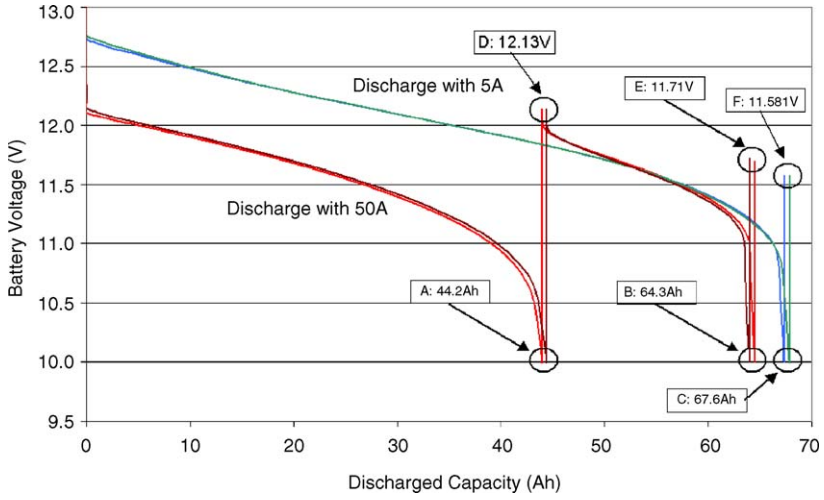

Fig. 1. First set of discharge tests on a 65 Ah sealed lead-acid battery BLA1 (black and white).

there is a net loss of Ah capacity that is caused by discharging the battery at a high rate first before the low current discharge.

A second set of tests was also carried out on the batteries as shown in Fig. 3. The test procedure is very similar to the previous test. The only difference is that another discharging at the same high rate is performed after the waiting time of 6 h and before the subsequent discharge at the lower rate.

The tests in Fig. 3 present evident that a battery can be discharged further at the same rate when it is left to rest. This may be explained according to [14,15], to be due to the reformation of the hydrated gel zones in the electrode active centres during the waiting period. However, there is still a net loss of capacity compared to the low current discharge rate case, which is similar to that in Figs. 1 and 2. This net loss of capacity may be explained according [14–16] to be due to stoichiometric changes in the interface between the grid and the lead dioxide active mass at high current discharge which leads to an increase in the resistance of the interface and hence a net loss of capacity when the battery is further discharged at the low rate.

3.2. Lithium-ion battery tests

Equivalent tests to those described in Figs. 1 and 2 were carried out on a large high-energy lithium-ion cell (Blion) with 50 Ah capacity. Fig. 4 shows the results with an aged 50 Ah high-energy lithium-ion cell. The top graphs show the cell voltage versus depth of discharge. The cell was discharged with a high rate of 50 A till the cut-off voltage of 2.8 V is reached at point B. After a waiting time of 6 h, it was further discharged with a small current of 5 A till the cut-off voltage is reached at point C. This is compared with a discharge at the lower current of 5 A from the beginning till the cut-off voltage is reached in point A. The bottom graphs in Fig. 4 show the cell temperatures during the same tests. The procedures are repeated three times each time yielding very similar curves; however, in order to achieve better readability, not all of the test results are presented in Fig. 4.

Fig. 4 reveals that for the tested large high-energy lithium-ion cell, the dischargeable capacities are between 30 and 32 Ah in all tests regardless the discharge rate. This can be

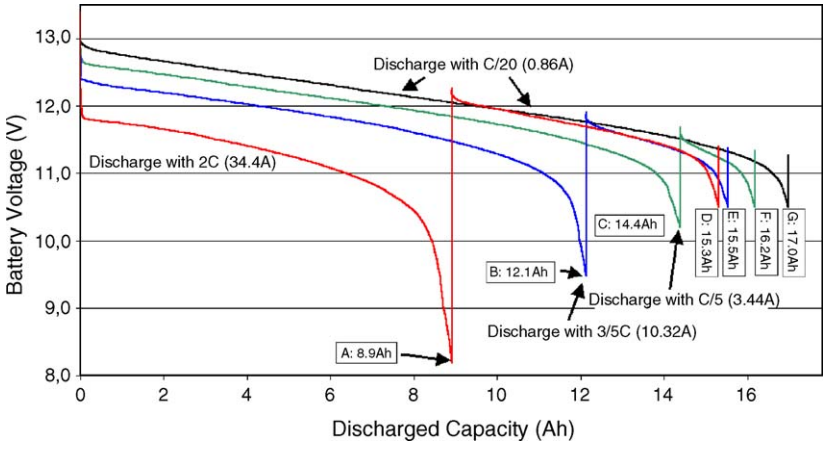

Fig. 2. Discharge tests on a 17 Ah sealed lead-acid battery BLA2 (black and white).

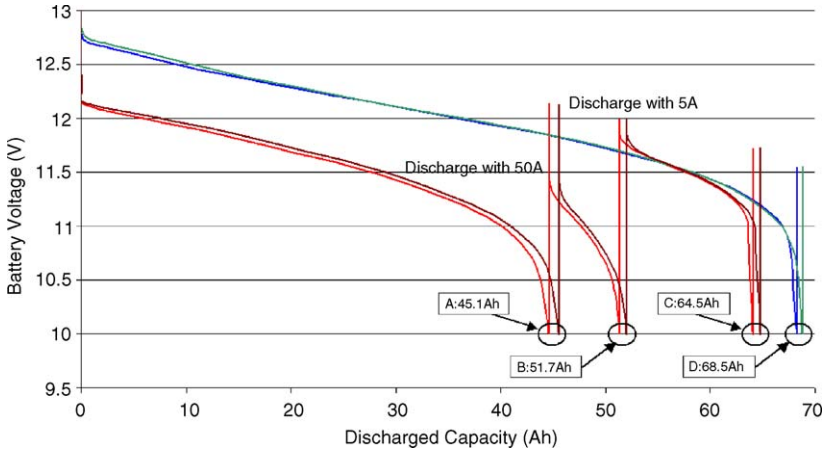

Fig. 3. Second set of discharge tests on a 65 Ah sealed lead-acid battery BLA1 (black and white).

explained with the rise in cell temperature to almost 55 °C during the continuous high rate discharge, which is known to enhance the performance of a lithium-ion cell. In contrast, the temperature at low rate discharge stays at about 25 °C as shown in Fig. 4. If the battery is discharged at a high current, while the battery temperature is maintained at 25 °C, then it is expected that the available capacity will be reduced. Clearly, the battery temperature rise, which is a function of

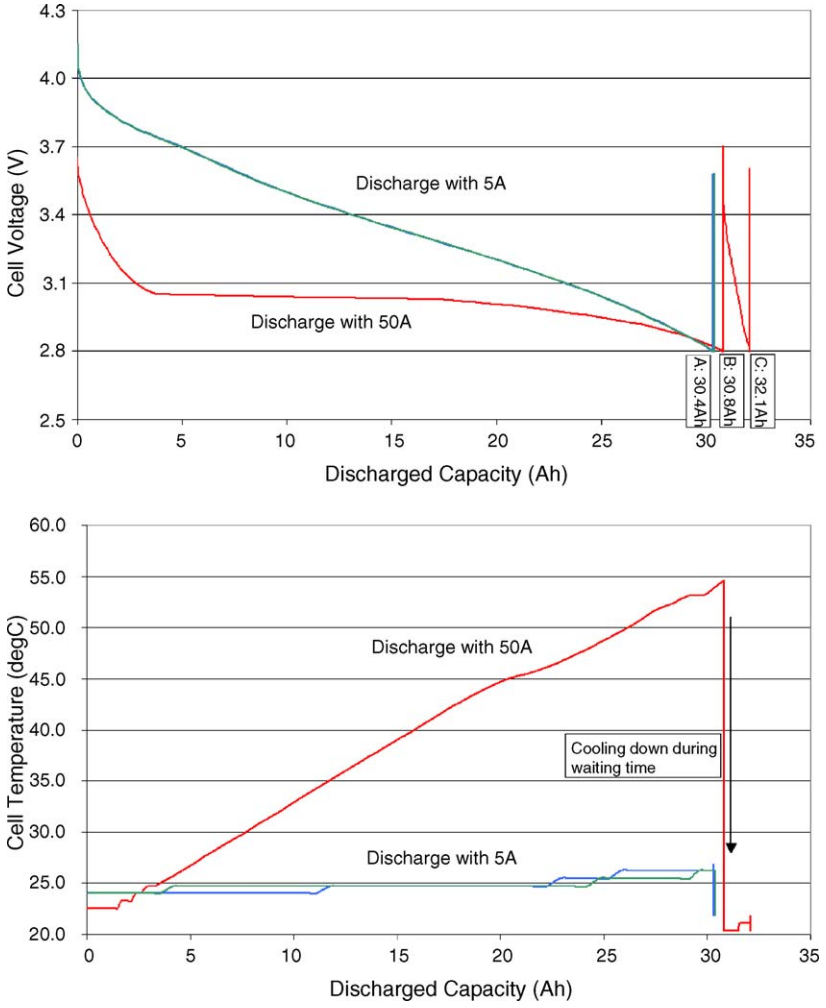

Fig. 4. Cell voltage and temperature during the "Passivation test" on a lithium-ion cell Blion (black and white).

environmental conditions and discharge duty cycle and the design of the battery, is an important factor that should be taken into account when making estimates of the remaining capacity in this type of battery.

4. Review of techniques using Peukert's equation to calculate remaining capacity

As mentioned earlier, many researchers developed techniques adapting Peukert's equation to estimate the remaining capacity in a battery when discharged using a variable current. For example [2–5,7], apply the Peukert equation to varying currents by basically calculating an "effective discharge current" $I_{\text{effective}}$ based on Peukert's equation:

$$I_{\text{effective}} = I\left(\frac{I}{I_{\text{nominal}}}\right)^{\text{pc}-1} \tag{3}$$

In this equation, I is the actual current and I_{nominal} is the nominal current for which the nominal capacity is given by the manufacturer. The "effectively discharged capacity" is then calculated by numerical integration of this effective current over time:

$$C_{\text{dch,effective}} = \sum (I_{\text{effective}}\,\Delta t) \tag{4}$$

The remaining capacity is then determined by subtracting this effectively discharged capacity from the nominal capacity:

$$C_{\text{remaining}} = C_{\text{nominal}} - C_{\text{dch,effective}} \tag{5}$$

These methods would determine zero remaining capacity after a "full" discharge at a high current (point A in Fig. 1). However, our tests reveal that the battery can still deliver a small amount of capacity at the same current after a waiting time. A substantial capacity may be discharged at a lower current.

Other methods [1,6] set I in Eq. (3) to be the average discharge current (usually during the last 5 min) to calculate an effective current, which multiplied by the total discharge time to calculate the discharged capacity so far. Eq. (5) is then used to calculate the remaining capacity. However, the "fuel-gauge" based on this method would show inconsistent results: when no current is drawn the remaining capacity would go slowly up with time, and it would go down steeply when drawing high currents, which might confuse the user. Like the effective current method, the average current technique tends to underestimate the remaining capacity in a battery.

For lithium-ion batteries, the remaining capacity estimation method should significantly take into account the temperature of the battery, which is a function of the load duty cycle, battery design and environmental conditions. The Peukert equation is not applicable.

5. Conclusions

Test results were presented which show that a seemingly fully discharged (at a high rate) lead-acid battery may be discharged further after a period of rest, which allows the active centres in the electrodes to recover (hydrate). However, if a battery is discharged at a high rate followed by discharge at a lower rate, the capacity obtained will be less than that obtained from the battery if it was discharged from the start at a low rate. This is thought to be due to chemical and structural changes in the active material grid interface that occur during a high current discharge, which increases the resistance of the interface, thus leading to a net loss of capacity.

The capacity obtained from a lithium-ion battery is strongly dependent on temperature, which is in turns dependent on the rate of discharge. At a high current discharge rate, the temperature of the battery may increase considerably, thus increasing the available capacity.

Peukert's equation is strictly applicable to batteries discharged at constant temperature and constant discharge current. When applied to a battery with a variable discharge rate and changing operating temperature using average or effective current, it generally results in an underestimation of the remaining capacity.

Acknowledgement

We would like to thank Simon Barnes for the support with the battery tester.

Appendix A. Derivation of Eq. (2)

From (1)

$$I_n^{\text{pc}} t_n = I_{n1}^{\text{pc}} t_{n1} \tag{A1}$$

The above equation can be written as

$$I_n t_n I_n^{\text{pc}-1} = I_{n1} t_{n1} I_{n1}^{\text{pc}-1} \tag{A2}$$

Substituting $I_n t_n = C_n$ and $I_{n1} t_{n1} = C_{n1}$ yields

$$C_n I_n^{\text{pc}-1} = C_{n1} I_{n1}^{\text{pc}-1} \tag{A3}$$

which can be arranged to yield Eq. (2).

References

[1] R.Y. Ying, United States Patent and Trademark Office, Patent No. 6,646,419 (2003).
[2] R.L. Proctor, G.A. Ure, W.L. Merkes, J. Young, H. Richard, S.H. Kahle, United States Patent and Trademark Office, Patent No. 5,656,919 (1997).
[3] T. Atwater, United States Patent and Trademark Office, Patent No. 5,640,150 (1997).
[4] P. Singh, J. Fennie, United States Patent and Trademark Office, Patent No. 6,011,379 (2000).

[5] T. Atwater, R.M. Dratler, United States Patent and Trademark Office, Patent No. 5,372,898 (1994).
[6] V. Johnson, M. Keyser, Center for Transportation Technologies and Systems National Renewable Energy Laboratory, 1999 (available from: http://www.ctts.nrel.gov/analysis/documents/hawker_validation.html#Capacity%20Tests).
[7] J.R. Bumby, P.H. Clarke, I. Forster, Forster IEE Proceedings 132 Pt.A (5) (1985).
[8] Thermo Analytics Inc. HEVSim Technical Manual on Battery Modeling, 2001 (available from: http://www.thermoanalytics.com/support/publications/batterymodelsdoc.html).
[9] W. Peukert, Elektrotechnische Zeitschrift 20 (1997) 20–21.
[10] D. Linden, Handbook of Batteries, McDraw-Hill Handbooks, 2002, pp. 3.1–3.24.
[11] J.H. Aylor, A. Thieme, B.W. Johnson, IEEE Trans. Ind. Electron. 39 (1992) 398–409.
[12] M. Doyle, J. Newman, J. Reimers, J. Power Sources 52 (1994) 211–216.
[14] D. Pavlov, J. Power Sources 53 (1995) 9–21.
[15] D. Pavlov, G. Petkova, J. Electrochem. Soc. 149 (5) (2002) A644–A653.
[16] D. Pavlov, G. Petkova, J. Electrochem. Soc. 149 (5) (2002) A654–A661.

List of References

[1] Abu Sharkh, S. and Doerffel, D. (2004) Rapid test and non-linear model characterisation of solid-state lithium-ion batteries. Journal of Power Sources, 130 (1-2), 266-274.

[2] ACEA (1999) A 35 million tonnes CO2 Kyoto contribution to date, Report, Brussels: ACEA.

[3] ACEA (2003) ACEA Car Parc 1991-2001, Report, Brussels: ACEA (Source: ANFAC).

[4] ACEA (2003) Monitoring of ACEA's Commitment on CO2 Emission Reductions from Passenger Cars - Final Report, Report, Brussels: ACEA.

[5] Alzieu, J., et al. (1997) Improvement of intelligent battery controller: state-of-charge indicator and associated functions. Journal of Power Sources, 67 (1-2), 157-161.

[6] Anderman, M. (2005) Overview of Large Battery Markets and Opportunities for Lithium Ion Batteries. IN: Advanced Automotive Battery Conference, Honolulu, Hawaii June 13-17, 2005.

[7] Aurbach, D. (2002) The Role of Surface Films on Electrodes in Li-Ion Batteries IN: van Schalkwijk, W. A. and Scrosati, B. Advances in Li-Ion Batteries, New York: Kluwer Academic / Plenum Publishers, 7 - 77.

[8] Bady, R. and Biermann, J.-W. (2000) HEV - structures and future developments. IN: TAE Electric Vehicles, Esslingen, 4.

[9] Barsoukov, E., et al. (2002) A novel impedance spectrometer based on carrier function Laplace-transform of the response to arbitrary excitation. Journal of Electroanalytical Chemistry, 536 (1-2), 109-122.

[10] Baudry, P., et al. (1995) Electro-thermal modelling of polymer lithium batteries for starting period and pulse power. Journal of Power Sources, 54 (54), 393 - 396.

[11] Bergveld, H. J., et al. (2002) Battery Management Systems - Design by Modelling Eindhoven: Kluwer Academic Publishers.

[12] Blomgren, G. E. (1999) Electrolytes for advanced batteries. Journal of Power Sources, 81-82.

[13] Boughtwood, M. (2007) Electric Hybrid Drive. electric & hybrid vehicle technology international, 107-108.

[14] Broussely, M. (2002) Aging Mechanisms and Calendar-Life Predictions in Lithium-Ion Batteries IN: van Schalkwijk, W. A. and Scrosati, B. Advances in Li-Ion Batteries, New York: Kluwer Academic / Plenum Publishers, 393 - 432.

[15] BSI (1991) Glossary of Electrotechnical, power, telecommunication, electronics, lighting and colour terms - Part 2: Terms particular to power engineering - Group 17: Secondary cells and batteries, BS 4727-2:Group 17:1992 IEC 50(486):1991.

[16] BSI (1997) Secondary cells and batteries containing alkaline or non-acidic electrolytes - Guide to the designation of current in alkaline secondary cell and battery standards, BS EN 61434:1997 IEC 61434:1996.

[17] Carcone, J. A. (2002) Portable Sealed Nickel-Cadmium Batteries IN: Linden, D. and Reddy, T. B. Handbook of batteries, New York: Mc Graw Hill, 28.1 - 28.35.

[18] (CENELC), E. C. f. E. S. (2001) EN 50272-2: Safety requirements for secondary batteries and battery installations.

[19] Chung, H. K. (2004) Rechargeable Solid State Chromium-Fluorine-Lithium Electric Battery, Patent No.: 6,686,096. Shenzhen (CN): New Billion Investments Limited.

[20] Crompton, T. R. (2000) Battery Reference Book 3rd ed. Oxford: Reed Educational and Professional Publishing Ltd.

[21] Crosse, J. (2001) Audi beats the 3-litre barrier. Automotive Engineer.

[22] Daewoo Cars Ltd (2002) Matiz Hertfordshire: Daewoo.

[23] Doerffel, D. (2002) Peace of Mind Drivetrain for Hybrid Electric Vehicles. IN: Britain's Younger Engineers at the House of Commons (SET for Britain), London 09.12.2002.

[24] Doerffel, D. (2003). Peace-of-Mind Series Hybrid Electric Vehicle Drivetrain Transfer Thesis (MPhil), University of Southampton.

[25] Doerffel, D. and Abu Sharkh, S. (2005) Efficient Testing and Evaluation Methods for Faster Market Introduction of Large Lithium-Ion Batteries. IN: Advanced Automotive Battery Conference 2005 and First Large Lithium-Ion Battery Technology and Applications Symposium, Honolulu, HawaiiAABC,

[26] Doerffel, D. and Abu Sharkh, S. (2006) A critical review of using the Peukert equation for determining the remaining capacity of lead-acid and lithium-ion batteries. Journal of Power Sources, 155 (2), 395 - 400.

[27] Doerffel, D. and Abu Sharkh, S. (2006) Large Lithium-Ion Batteries - a Review. IN: Electric Vehicle Exhibition (EMA 2006), Aschaffenburg (Germany) 14.10.2006. 15.

[28] Doerffel, D. and Abu-Sharkh, S. (2002) Performance Evaluation of a Low Cost Series Hybrid Electric Vehicle. IN: 19th Electric Vehicle Symposium, Busan, Korea,

[29] Doerffel, D. and Abu-Sharkh, S. (2006) System modeling and Simulation as a Tool for Developing a Vision for Future Hybrid Electric Vehicle Drivetrain Configurations. IN: VPPC2006, Windsor, UK,

[30] Ehrlich, G. M. (2002) Lithium-Ion Batteries IN: Linden, D. and Reddy, T. B. Handbook of batteries, New York: Mc Graw Hill, 35.1-35.94.

[31] Ehsani, M. and Holtzapple, M. (2006) A Vision of Sustainable Fuel and Vehicle Technologies. IN: Vehicle Power and Propulsion Conference (VPPC), Windsor (UK),

[32] eurostat (1999) Panorama of transport - Statistical overview of road, rail and inland waterway transport in the Eurpean Union Luxembourg.

[33] eurostat (2001) Transport and environment - Statistics for the transport and environment reporting mechanism (TERM) for the European Union Luxembourg.

[34] Fletcher, R. (2001) LYNCH electric motor: Lynch Motor Company Ltd.

[35] Foxon, T., et al. (2005) Transforming policy processes to promote sustainable innovation: some guiding principles. A report for policy-makers., Report, London: Imperial College London.

[36] Funabiki, A., et al. (1999) Nucleation and phase-boundary movement upon stage transformation in lithium–graphite intercalation compounds. Electrochimica Acta, 45 (6), 865-871.

[37] Gao, L., et al. (2002) Dynamic Lithium-Ion Battery Model for System Simulation. IEEE Transactions on Components and Packaging Technologies, 25 (No.3).

[38] Goodenough, J. B. (2002) Oxide Cathodes IN: van Schalkwijk, W. A. and Scrosati, B. Advances in Li-Ion Batteries, New York: Kluwer Academic / Plenum Publishers, 135 - 154.

[39] Gutmann, G. (1999) Hybrid electric vehicles and electrochemical storage systems - a technology push-pull couple. Journal of Power Sources, 84 (2), 275 - 279.

[40] Harrison, L.-A. and Doerffel, D. (2003) Life Cycle Impacts and Sustainability Considerations for Alternative and Conventional Vehicles. IN: SAE 2003 World Congress & Exhibition, Ann Arbor 11.03.2003.

[41] Harrison, L.-A. and Doerffel, D. (2003) Sustainable Future Transportation. IN: 2003 SAE International Future Transportation Technology Conference, Costa Mesa, California USA 23.-25.06.2003.

[42] Heinemann, D. and Naunin, D. (2000) BattMobil IV. IN: EVS-17, Montreal, Canada October 2002.

[43] Jana, K. (2000) Genesis Application Manual 5 th: Hawker Energy.

[44] Kalberlah, A. (1994) Elektro-Hybridantriebe fuer Strassenfahrzeuge Elektrische Strassenfahrzeuge, Berlin: expert Verlag, 133 - 149.

[45] Keim, T. A. (2006) Requirements for a Revolution in Automotive Technology (Keynote Presentation). IN: Vehicle Power and Propulsion Conference (VPPC), Windsor, UK 06.-08.09.2006.

[46] Kim, K., et al. (2005) High Power Li-ion Battery Technologies and Their Applications. IN: Advanced Automotive Battery Conference, Honolulu, Hawaii 13.-17.06.2005.

[47] Kleine, H. and Stimming, U. (2001) Brennstoffzellen: Funktion, Typen, Systeme (Fuel-Cells: function, types, systems) TAE-Seminar: Brennstoffzellen: Funktion - Entwicklungsstand - Einsatz (Fuel-Cells: function - state of development - applications), Esslingen (Germany), 11 - 15.

[48] Kutkut, N. H. (2000) Prolong the life of series battery strings with individual battery equalizers. electric & hybrid vehicle technology international, 116 - 121.

[49] Lee, H.-D., et al. (2000) Advanced gear-shifting and clutching strategy for a parallel-hybrid vehicle. IEEE Industry Applications Magazine, 6 (6), 26 - 32.

[50] Li, J., et al. (2001) Studies on the cycle life of commercial lithium ion batteries during rapid charge-discharge cycling. Journal of Power Sources, 102 (1-2), 294-301.

[51] Linden, D. (2002) Basic Concepts IN: Linden, D. and Reddy, T. B. Handbook of batteries, New York: Mc Graw Hill, 1.3 - 1.18.

[52] Linden, D. (2002) Factors affecting battery performance Handbook of Batteries: McDraw-Hill Handbooks, 3.1-3.24.

[53] Linden, D. (2002) Secondary Batteries - Introduction Handbook of Batteries: McDraw-Hill Handbooks, 22.3 - 22.24.

[54] Linden, D. and Magnusen, D. (2002) Portable Sealed Nickel-Metal Hydride Batteries IN: Linden, D. and Reddy, T. B. Handbook of batteries, New York: Mc Graw Hill, 29.1 - 29.35.

[55] Linden, D. and Reddy, T. B. (2002) Handbook of Batteries 3rd: McGraw-Hill.

[56] Moore, T. C. (1996) Tools and Strategies for Hybrid-Electric Drivesystem Optimization. SAE, 49-66.

[57] Motloch, C. G., et al. (2002) Implications of NiMH Hysteresis on HEV Battery Testing and Performance. IN: 19th Electric Vehicle Symposium, Busan, Korea 19.-23.10.2002.

[58] Nagasubramanian, G., et al. (1999) Electrical and electrochemical performance characteristics of large capacity lithium-ion cells. Journal of Power Sources, 80, 116-118.

[59] Naunin, D. (2000) Technology-innovations by battery-powered, fuel-cell-powered and hybrid- electric vehicles Esslingen.

[60] NREL (2002) ADVISOR (Advanced Vehicle Simulator) 2002: National Renewable Energy Laboratory (NREL).

[61] Ogumi, Z. and Inaba, M. (2002) Carbon Anodes IN: van Schalkwijk, W. A. and Scrosati, B. Advances in Li-Ion Batteries, New York: Kluwer Academic / Plenum Publishers, 79 - 101.

[62] Palmer, A. and Hartley, B. (2001) The Business Environment 4th Maidenhead: McGraw - Hill Higher Education.

[63] Peukert, W. (1897) On the dependency of the discharge capacity versus discharge rate for lead-acid batteries. Elektrotechnische Zeitschrift, 20, 20 - 21.

[64] Reddy, T. B. and Hossain, S. (2002) Rechargeable Lithium Batteries (Ambient Temperature) IN: Linden, D. and Reddy, T. B. Handbook of batteries, New York: Mc Graw Hill, 34.1 - 34.62.

[65] Rutherford, K. and Doerffel, D. (2005) Performance of Lithium-Polymer Cells at High Hydrostatic Pressure. IN: Unmanned Untethered Submersible Technology (UUST), Durham, USA 22.-24.08.2005.

[66] Salkind, A. J., et al. (2002) Lead-Acid Batteries IN: Linden, D. and Reddy, T. B. Handbook of batteries, New York: Mc Graw Hill, 23.1 - 23.88.

[67] Salomon, M., et al. (2002) Temperature Effects on Li-Ion Cell Performance IN: van Schalkwijk, W. A. and Scrosati, B. Advances in Li-Ion Batteries, New York: Kluwer Academic / Plenum Publishers, 309 - 344.

[68] Schafer, A. and Victor, D. G. (2000) The future mobility of the world population. Transportation Research Part A: Policy and Practice, 34 (3), 171-205.

[69] Schipman, J. and Lebourg, A. (2001) KANGOO ELECT'ROAD: Description of the Kangoo Fitted with a Range Extender. IN: EVS-18, Berlin, Germany 20.-24.10.2001.

[70] SMMT (2002) The Future Fuels Report, Report, London: Society of Motor Manufacturers and Traders (SMMT).

[71] Spotnitz, R. (2002) Scale-Up of Lithium-Ion Cells and Batteries IN: van Schalkwijk, W. A. and Scrosati, B. Advances in Li-Ion Batteries, New York: Kluwer Academic / Plenum Publishers, 433 - 457.

[72] Srinivasan, V. and Newman, J. (year unknown) A Model-based Comparison of Various Li-ion Chemistries Available from: http://berc.lbl.gov/venkat/Ragone-construction.pps [Accessed 21.01.2007].

[73] Strattan, R. D. (1998) The Evolving Role of Electric and Hybrid Electric Vehicles. IN: Frontiers of Power Conference 1998. XI-1 - XI-4.

[74] Thermo_Analytics_Inc. (2001) Battery Modeling Available from: http://www.thermoanalytics.com/support/publications/batterymodelsdoc.html [Accessed 01.06.2003].

[75] Thomas, K. E., et al. (2002) Mathematical Modeling of Lithium Batteries IN: van Schalkwijk, W. A. and Scrosati, B. Advances in Li-Ion Batteries, New York: Kluwer Academic / Plenum Publishers, 345 - 392.

[76] Thompson, D. (2002) The drive-by test. Lecture Notes N3 University of Southampton.

[77] ThunderSky (2002) Thunder Sky Solid State Cr-F-Li Battery Instruction Manual.

[78] Wang, X. and Stuart, T. (2002) Charge Measurement Circuit for Electric Vehicle Batteries. IEEE Transactions on Aerospace and Electronic Systems, 38 (4), 1201 - 1209.

[79] Wenzl, H. (1999) Batterietechnik (Optimierung der Anwendung - Betriebsfuehrung - Systemintegration), Technology of Batteries (Optimization of Application - Usage - Integration) + additions from Seminar at TAE (21.05.2001) Renningen-Malmsheim: expert verlag.

[80] Wyczalek, F. A. (1999) Market Mature 1998 Hybrid Electric Vehicles. IEEE Aerospace and Electronic Systems Magazine, 14 (3), 41-44.

[81] Yamaki, J.-i. (2002) Liquid Electrolytes IN: van Schalkwijk, W. A. and Scrosati, B. Advances in Li-Ion Batteries, New York: Kluwer Academic / Plenum Publishers, 155 - 183.

[82] Yang, Y., et al. (2000) Modeling and Control of a Hybrid Electric Vehicle. IN: IEEE Vehicular Technology Conference, Tokyo Spring 2000. 2095-2100.